Site U1406[1]

R.D. Norris, P.A. Wilson, P. Blum, A. Fehr, C. Agnini, A. Bornemann, S. Boulila, P.R. Bown, C. Cournede, O. Friedrich, A.K. Ghosh, C.J. Hollis, P.M. Hull, K. Jo, C.K. Junium, M. Kaneko, D. Liebrand, P.C. Lippert, Z. Liu, H. Matsui, K. Moriya, H. Nishi, B.N. Opdyke, D. Penman, B. Romans, H.D. Scher, P. Sexton, H. Takagi, S.K. Turner, J.H. Whiteside, T. Yamaguchi, and Y. Yamamoto[2]

Chapter contents

[1] Norris, R.D., Wilson, P.A., Blum, P., Fehr, A., Agnini, C., Bornemann, A., Boulila, S., Bown, P.R., Cournede, C., Friedrich, O., Ghosh, A.K., Hollis, C.J., Hull, P.M., Jo, K., Junium, C.K., Kaneko, M., Liebrand, D., Lippert, P.C., Liu, Z., Matsui, H., Moriya, K., Nishi, H., Opdyke, B.N., Penman, D., Romans, B., Scher, H.D., Sexton, P., Takagi, H., Turner, S.K., Whiteside, J.H., Yamaguchi, T., and Yamamoto, Y., 2014. Site U1406. *In* Norris, R.D., Wilson, P.A., Blum, P., and the Expedition 342 Scientists, *Proc. IODP,* 342: College Station, TX (Integrated Ocean Drilling Program). doi:10.2204/iodp.proc.342.107.2014
[2] **Expedition 342 Scientists' addresses.**

Background and objectives

Integrated Ocean Drilling Program (IODP) Site U1406 (proposed Site JA-6A; 40°21.0′N, 51°39.0′W; 3798.9 m water depth) is a mid-depth site (~3300 meters below sea level [mbsl] paleodepth at 50 Ma) (Tucholke and Vogt, 1979) in the middle of the Expedition 342 Paleogene Newfoundland sediment drifts depth transect (Fig. **F1**). The site is positioned to capture a record of sedimentation >1.1 km shallower than the largely sub–carbonate compensation depth (CCD) record drilled at Site U1403 (Figs. **F2, F3, F4**). The location above the average late Paleogene CCD should be sensitive to both increases and decreases in carbonate burial, whether these reflect variations in dissolution related to changes in the CCD, changes in carbonate production, or variations in background noncarbonate sedimentation. Our primary scientific objectives for drilling Site U1406 were

- To reconstruct the mid-depth CCD in a primarily carbonate-dominated record;
- To obtain records of the Oligocene–Miocene and Eocene–Oligocene transition (EOT) events in carbonate-rich sediments that host abundant foraminifers suitable to the construction of geochemical climate records;
- To evaluate the history of deep water and possible northern hemisphere glaciation on sediment chemistry, grain size, and provenance; and
- To evaluate biological evolution during Paleogene climate transitions.

The primarily calcareous sequence expected at Site U1406 should record changes in ocean alkalinity and carbonate production. Sites U1403–U1405 were mainly positioned to capture large-amplitude CCD deepening events such as the carbonate budget "overshoots" that are thought to be associated with the most extreme climate perturbations of the Cenozoic, such as those involved with the Cretaceous/Paleogene (K/Pg) boundary, the Paleocene/Eocene Thermal Maximum (PETM), and the EOT (see the **"Site U1403"** and **"Site U1404"** chapters [Norris et al., 2014b, 2014c]). These events were expected to be recorded at deepwater sites as stratigraphically thin intervals of calcareous sediment in otherwise noncalcareous sediment. In contrast, transient shoaling of the CCD in generally carbonate-rich sequences should be recorded at Site U1406 by decreases in carbonate preservation and decreasing carbonate content relative to clay or biosiliceous sedi-

doi:10.2204/iodp.proc.342.107.2014

ment. As a mid-depth site on the Newfoundland depth transect, Site U1406 should have few intervals in which the sediment is 100% carbonate, but also few intervals in which no carbonate appears in the record. Carbonate content is expected to be generally higher at sites in shallower water depth, such as the majority of the sites located on Southeast Newfoundland Ridge.

The high carbonate contents anticipated in sediment at Site U1406 should permit the construction of detailed stable isotope records and calcareous microfossil biostratigraphy that can be tied by physical property records and magnetochronology to Sites U1403–U1405 further downslope. Ties between sites on J-Anomaly Ridge will allow the isotope stratigraphy and biochronology developed for Site U1406 to be extended to the entire lower half of the depth transect. Stable isotope records are likely to be developed for Sites U1404 and U1405 for intervals of good carbonate preservation in, for example, the early Miocene–Oligocene and the EOT, and it should be possible to match them with more complete Site U1406 records. In addition, coring at Site U1404 also recovered a partial record of carbonate burial events in the late Eocene and late middle Eocene. Our aim is to match these carbonate-rich intervals across all of the J-Anomaly sites in which they occur to create an orbital-resolution record of fluctuations in ocean chemistry and deepwater origins. Coupled with provenance and grain size studies of the sediments, we should also be able to identify times of deposition of lithic fragments and test competing hypotheses for the onset and development of extensive northern hemisphere ice sheets (see the **"Site U1403"** and **"Site U1404"** chapters [Norris et al., 2014b, 2014c]).

Site U1406 was proposed as a replacement for proposed Site JA-5A. This substitution was made to avoid drilling a large thickness of Miocene sediment such as that encountered at Sites U1404 and U1405. Instead, Site U1406 was proposed to drill directly through an outcropping of the basal part of the acoustically uniform, largely transparent seismic sequence that was expected to be mostly of Oligocene to early Eocene age, based on prior drilling of nearby Deep Sea Drilling Project (DSDP) Site 384 and previous Expedition 342 sites. One piece of gray silt recovered from the Site 384 drill bit after drilling operations were terminated contained a moderately preserved upper Miocene assemblage (*Discoaster quinqueramus* Zone) and must have originated somewhere within the uncored upper 50 m of the sedimentary section (Tucholke and Vogt, 1979). Spot coring of the sequence below indicated a sequence of middle Eocene to Cretaceous pelagic ooze and chalk overlying Lower Cretaceous reef sediment and basalt (Tucholke and Vogt, 1979). The exact seismic expression of Site 384 is not entirely clear because Leg 43 drilled in the vicinity of a single-channel *Glomar Challenger* seismic line of low quality and could only report that the line was "near" the drill site. Expedition 342 single-channel seismic lines show a reflector package that broadly resembles the *Glomar Challenger* line and suggests that Site 384 was drilled on the edge of the transparent acoustic unit before penetrating a lower Eocene, Paleocene, and Cretaceous succession of chert and chalk that is represented by a package of relatively dense reflectors. Therefore, we interpret the lowermost 50 m of the transparent acoustic unit at Site U1406 to be of middle Eocene and early Eocene age. We conclude that Site U1406 will provide an expanded record of primarily calcareous ooze and chalk of rough age-equivalence to sites in deeper water on J-Anomaly Ridge. In particular, Site U1406 should provide a carbonate-rich record through the middle to late Eocene as a counterpart to the largely sub-CCD record drilled through this interval at Site U1404. Site U1406 will thereby improve age- and water-depth control on the behavior of the CCD in the North Atlantic during this key interval of the Cenozoic when the CCD in the equatorial Pacific was at its most dynamic (Lyle, Wilson, Janecek, et al., 2002; Pälike et al., 2012).

Operations

All times are local ship time (UTC – 2.5 h). See Table **T1** for coring summary.

Hole U1406A summary

Latitude: 40°20.9992′N
Longitude: 51°38.9994′W
Water depth below sea level (m): 3814.8
Date started: 1435 h, 30 June 2012
Date finished: 1920 h, 2 July 2012
Time on hole (days): 2.2
Seafloor depth (m drilling depth below rig floor [DRF]): 3826.3
Seafloor depth estimation method: mudline core
Rig floor to sea level (m): 11.5
Penetration depth (m drilling depth below seafloor [DSF]): 283.3
Cored interval (m): 283.3
Recovered length (m): 267.3
Recovery (%): 94
Total cores (number): 34
Advanced piston corer (APC) cores (number): 25
Extended core barrel (XCB) cores (number): 9
Drilling system: 11 7/16 inch APC/XCB bit with 136.00 m bottom-hole assembly (BHA)

Objective: core from seafloor to ~250 m DSF or until science objectives are met.
Result: target reached; objectives met.

Hole U1406B summary

Latitude: 40°20.9995′N
Longitude: 51°38.9851′W
Water depth below sea level (m): 3813.7
Date started: 1920 h, 2 July 2012
Date finished: 1435 h, 4 July 2012
Time on hole (days): 1.8
Seafloor depth (m DRF): 3825.2
Seafloor depth estimation method: mudline core
Rig floor to sea level (m): 11.5
Penetration depth (m DSF): 253.6
Cored interval (m): 253.6
Recovered length (m): 241.34
Recovery (%): 95
Total cores (number): 30
APC cores (number): 22
XCB cores (number): 8
Drilling system: 11⅞ inch APC/XCB bit with 136.00 m BHA
Objective: core from seafloor to ~250 m DSF
Result: target reached; objectives met

Hole U1406C summary

Latitude: 40°20.9892′N
Longitude: 51°38.9853′W
Water depth below sea level (m): 3813.0
Date started: 1435 h, 4 July 2012
Date finished: 1600 h, 6 July 2012
Time on hole (days): 2.1
Seafloor depth (m DRF): 3824.6
Seafloor depth estimation method: mudline core
Rig floor to sea level (m): 11.6
Penetration depth (m DSF): 241.4
Cored interval (m): 236.4
Recovered length (m): 223.02
Recovery (%): 94
Drilled interval (m): 5
Drilled interval (number): 2
Total cores (number): 27
APC cores (number): 17
XCB cores (number): 10
Drilling system: 11⅞ inch APC/XCB bit with 136.00 m BHA
Objective: repeat cored sequence from Hole U1406B
Result: target reached; objectives met

Description

The vessel arrived at Site U1406 after a 14.9 nmi transit from Site U1405, which was made in dynamic positioning mode at a speed of 1.4 kt with the drill pipe suspended below the vessel. The vessel stabilized over Site U1406 at 1435 h on 30 June 2012. The plan for this site called for drilling three holes to a depth of ~250 m DSF. Holes U1406A, U1406B, and U1406C were successfully cored to a depth of 283.3, 253.6, and 241.4 m DSF, respectively, without any significant problems. The total time spent at Site U1406 was 145.5 h (6.1 days).

Hole U1406A coring

The calculated precision depth recorder depth for the site was 3810.4 m DRF. Two water cores were shot before the mudline was recovered, establishing seafloor depth at 3826.3 m DRF (3814.8 mbsl). Hole U1406A was spudded at 1950 h on 30 June, and Cores 342-U1406A-1H through 25H were retrieved using nonmagnetic core barrels for all cores and the FlexIT core orientation tool on the first 17 cores. The first partial stroke was experienced with Core 16H, and the APC was advanced by recovery for this and subsequent cores. The XCB was deployed for Cores 26X through 34X to a total depth of 283.3 m DSF. The seafloor was cleared at 1920 h on 2 July, ending Hole U1406A. Overall core recovery for Hole U1406A was 267.30 m for the 283.3 m interval cored (94% recovery). The total time spent on Hole U1406A was 52.75 h.

Hole U1406B coring

The vessel was offset 20 m east. Hole U1406B was spudded at 2055 h on 2 July, and a 6.5 m mudline core established seafloor depth at 3825.2 m DRF (3813.7 mbsl). Cores 342-U1406B-1H through 22H were retrieved from the seafloor to 188.8 m DSF using nonmagnetic core barrels and the FlexIT core orientation tool. The XCB was deployed for Cores 23X through 30X to a total depth of 253.6 m DSF. The seafloor was cleared at 1435 h on 4 July, ending Hole U1406B. Recovery for Hole U1406B was 241.34 m over the 253.6 m cored (95% recovery). The total time spent on Hole U1406B was 43.25 h.

Hole U1406C coring

The vessel was offset 20 m south. Hole U1406C was spudded at 1630 h on 4 July, and a 9.4 m mudline core established seafloor depth at 3824.6 m DRF (3813.0 mbsl). Cores 342-U1406C-1H through 18H were recovered from the seafloor to 161.4 m DSF using nonmagnetic core barrels. Core orientation was not performed in Hole U1406C. The XCB was deployed to a final depth at 241.4 m DSF. Two intervals were drilled without coring (2 and 3 m) in an attempt to cover coring gaps in the previous two holes. The seafloor was cleared at 0500 h on 6 July.

After clearing the seafloor, the drill string was tripped to the surface. The BHA was set back in the derrick with the exception of the lower seal bore drill collar plus subs. Schlumberger logging tools were then rigged up to conduct a pass-through check on the lower portion of the BHA. At the conclusion of the test, the remaining BHA components were secured. The drill floor was secured at 1600 h on 6 July, ending Hole U1406C.

The acoustic positioning beacon was recovered, and the vessel began the move to Site U1405 to recover the beacon left behind there. The total time spent on Hole U1406C was 49.5 h.

Lithostratigraphy

Coring in Holes U1406A–U1406C recovered a sedimentary succession of deep-sea pelagic sediment of Pleistocene to middle Eocene age, comprising four lithostratigraphic units (Figs. **F5, F6, F7, F8, F9, F10;** Table **T2**). Unit I is ~2 m thick and composed of Pleistocene brown foraminiferal sand and nannofossil ooze with manganese nodules. Unit II is brown, transitioning downhole to a green Oligocene to Miocene nannofossil ooze that occurs in a ~180 m thick sequence and contains abundant diatoms and/or radiolarians in some intervals. Unit III is a ~40 m interval of alternating carbonate-rich nannofossil ooze, clay-rich nannofossil ooze, and clay of earliest Oligocene to middle Eocene age. Unit IV is also largely composed of nannofossil ooze and marks the downhole transition from reduced to oxidized sediment that is middle Eocene to Paleocene in age. Sand-sized lithoclasts are found in the >63 µm size fraction in Site U1406 sediment, particularly in sediment of Miocene and Oligocene age.

Lithostratigraphic units and boundaries are defined by changes in lithology (as identified by visual core description and smear slide observations), physical properties, color reflectance (L*, a*, and b*), and biogenic content (calcium carbonate and silica) (Fig. **F5**). The lithologic differences observed between units are primarily attributable to varying abundances of nannofossils, diatoms, radiolarians, and foraminifers (Figs. **F8, F9, F10**). Lithologic descriptions are based on sediment recovered from Hole U1406A and supplemented with observations from the two shorter holes, U1406B and U1406C. The Unit II/III boundary is defined by a transition from ooze to chalk. As the ooze–chalk transition is a broad zone, we have tied the lithostratigraphic Unit II/III boundary to a magnetic susceptibility peak in the middle of this lithologic transformation. This unit boundary falls in nannofossil Zone NP22 and planktonic foraminifer Zone O1 (see **"Biostratigraphy"**).

The Unit III/IV boundary is marked by a distinct color change that reflects redox conditions in the sediment and may be related to lower productivity in Unit IV when compared to younger parts of the sedimentary record.

Unit I

Intervals: 342-U1406A-1H-1, 0 cm, to 1H-2, 111 cm; 342-U1406B-1H-1, 0 cm, to 1H-2, 112 cm; 342-U1406C-1H-1, 0 cm, to 1H-2, 10 cm

Depths: Hole U1406A = 0–2.61 meters below seafloor (mbsf); Hole U1406B = 0–2.62 mbsf; Hole U1406C = 0–1.60 mbsf

Age: Pleistocene

Lithology: foraminiferal sand and nannofossil ooze

Unit I is a 2.61 m thick succession of sediment encountered in all three holes at Site U1406 (Fig. **F6A**). This thin unit in Core 342-U1406A-1H is composed of pale brown (10YR 6/3) and light brown (7.5YR 6/4) nannofossil foraminiferal ooze with clay and "foraminiferal sand" that occurs downhole to interval 342-U1406A-1H-2, 111 cm. Bioturbation is extensive to complete with no discrete burrows. Unit I contains abundant sand-sized foraminifers throughout as well as manganese nodules and ice-rafted clastic material that includes sand- to pebble-sized clasts. The lithologies range from high-grade metamorphic rocks and granodiorites to dolomites and limestones.

Unit II

Intervals: 342-U1406A-1H-2, 111 cm, through 21H-3, 91 cm; 342-U1406B-1H-2, 112 cm, through 21H-2, 120 cm; 342-U1406C-1H-2, 10 cm, through 21X-6, 107 cm

Depths: Hole U1406A = 2.61–184.86 mbsf; Hole U1406B = 2.62–181.12 mbsf; Hole U1406C = 1.60–184.57 mbsf

Age: Oligocene to Miocene

Lithology: nannofossil ooze

Unit II is a ~180 m thick succession of dominantly nannofossil ooze (Figs. **F5, F6B, F6C**). The top of the unit is defined by homogeneous, light yellow (2.5Y 8/2) and light greenish gray (10GY 7/1) clayey nannofossil ooze with foraminifers. At Section 342-U1406A-3H-1, 98 cm, sediment color distinctly changes from light yellow to light greenish gray. This sediment color change likely reflects sedimentary redox conditions and is not associated with a change in lithology (Fig. **F5**). The vast majority of Unit II is composed of light greenish gray (10GY 7/1) nannofossil ooze with common 1 cm thick green layers of disseminated glauconite and chlorite. Bioturbation traces are slightly darker light greenish

gray (10Y 6/1) and result in subtle mottling of the core surface. Sulfide blebs (1–2 cm in diameter) are present throughout Unit II.

Unit III

Intervals: 342-U1406A-21H-3, 91 cm, through 29X-2, 0 cm; 342-U1406B-21H-2, 120 cm, through 29X-6, 10 cm; 342-U1406C-21X-6, 0 cm, through 28X-CC, 27 cm

Depths: Hole U1406A = 184.86–243.40 mbsf; Hole U1406B = 181.12–243.50 mbsf; Hole U1406C = 184.57–229.19 mbsf

Age: middle Eocene–early Oligocene

Lithology: nannofossil chalk

The top of Unit III is defined as the transition from ooze to chalk, which occurs within nannofossil Zone NP22 in the lower Oligocene in Holes U1406B and U1406C. Hole U1406A undergoes the transition to chalk deeper in the core than Holes U1406B and U1406C, so a tie was picked based on the magnetic susceptibility peak in Hole U1406A (184.86 mbsf). Unit III is 50–60 m thick and composed of light grayish (10Y 7/1) nannofossil chalk with foraminifers; the latter are visible macroscopically. The chalk is slightly bioturbated and mottled. Section 342-U1406A-27X-3 contains centimeter-scale laminated beds that display indications of low-angle cross lamination. Native copper metallogenic phases were observed in thin veins and as single crystals in interval 342-U1406A-27X-1, 80–120 cm. Biscuiting is common throughout Unit III.

Unit IV

Intervals: 342-U1406A-29X-2, 0 cm, through 34X-CC, 28 cm; 342-U1406B-29X-6, 10 cm, through 30X-CC, 25 cm

Depths: Hole U1406A = 243.40–281.05 mbsf; Hole U1406B = 243.50–254.83 mbsf

Age: Paleocene to middle Eocene

Lithology: nannofossil chalk with foraminifers and nannofossil chalk with radiolarians

Lithostratigraphic Unit IV is distinguished by a color change from light grayish nannofossil chalk (10Y 7/1) in Unit III to pale brown (10YR 6/3) nannofossil chalk with foraminifers and nannofossil chalk with radiolarians (Figs. **F5, F6, F7, F8, F9, F10**). The unit is ~38 m thick. Unit IV also contains variable abundances of radiolarians and/or calcareous nannofossils. Centimeter- to decimeter-scale color variation in various shades of light grayish brown (10YR 8/1 to 10YR 8/2) occurs through most of the unit and is the result of differential bioturbation intensity and, in some cases, of diagenesis. The diagenesis results in two important features, gray sulfide precipitation and green chlorite with glauconite bands. These bands, commonly characterized by diffuse margins, are recognized as the result of an early diagenetic phenomenon because of their crosscutting relationship with sedimentary structures such as burrows (Fig. **F12** in the "Site U1408" chapter [Norris et al., 2014e). Foraminiferal tests are macroscopically visible, and radiolarians are also concentrated in certain intervals. The sediment is moderately to slightly mottled, resulting from bioturbation. Cores drilled with the XCB are significantly disturbed in places (biscuiting and fracturing).

Lithostratigraphic unit summary

Carbonate content in Site U1406 sediment is generally moderate (typically ~40 wt% $CaCO_3$; Fig. **F5**), suggesting that the site was positioned above the CCD for much of its Cenozoic history. No distinct lithostratigraphic boundary is associated with the Oligocene/Miocene chronostratigraphic boundary. At ~199 mbsf in Hole U1406A, just above the Eocene/Oligocene boundary, we observed a peak in carbonate concentration, presumably reflecting a deepening and overshoot of the CCD (see **"Background and objectives"** and a similar signal at Site U1404). The sedimentary succession at Site U1406 also records a number of carbonate content increases or "events" in middle to upper Eocene strata, including an a peak of 90 wt% $CaCO_3$ at 250.45 mbsf, during the middle Eocene (46.29 Ma) nannofossil Subzone NP15a (see **"Biostratigraphy"**).

Oligocene–Miocene transition

The Oligocene–Miocene transition was recovered in a moderately carbonate rich interval in Holes U1406A, U1406B, and U1406C at 81.16, 82.48, and 75.71 mbsf, respectively (Fig. **F11**). The Oligocene/Miocene boundary is approximated by the first occurrence and last occurrence datums of the nannofossil taxon *Sphenolithus delphix* and defined by the base of Chron C6Cn2n. The Oligocene/Miocene boundary zone does not stand out from the underlying and overlying sediment in terms of physical properties such as color or carbonate content (Fig. **F11**). Color is relatively uniform greenish gray (10GY 6/1 to 10GY 7/1), and carbonate content varies between 30 and 50 wt% at 60–100 mbsf in Hole U1406A.

Eocene–Oligocene transition

The EOT was recovered in a carbonate-rich interval in Holes U1406A, U1406B, and U1406C at ~199, ~198, and ~195 mbsf, respectively. These depths are approximate because the EOT is transitional rather

than a boundary and occurs midway through nannofossil Zone NP21 near the top of Chron C13r. Lithologic expressions of this interval relative to underlying and overlying sediments are less pronounced than at the deeper water Site U1404, where background levels of carbonate accumulation are lower (Fig. F12). Upper Eocene sediments below the Eocene/Oligocene boundary are composed of very uniform, light greenish gray (10Y 7/1) nannofossil ooze with a carbonate content close to 50 wt%. Slight mottling as a result of moderate bioturbation occurs throughout these sediments. In Hole U1406A, the EOT (199.33–190.44 mbsf) is composed of greenish gray (5GY 6/1) nannofossil ooze. The slightly darker, light greenish gray regions (typically ~1 interval per section) display more visible bioturbation. Disseminated sulfide blebs (10Y 3/1) occur throughout. Post-EOT Oligocene sediment (above 190.44 mbsf in Hole U1406A) typically has a carbonate content of 40 wt% (Fig. F12).

Carbonate content reaches a peak value (~80 wt%) in calcareous nannofossil Zone NP21 and Chron C13n (Fig. F12) and coincides stratigraphically with the lightest colored sediments recovered at Site U1404. Color reflectance and carbonate content are broadly correlated with one another in Hole U1406A. Magnetic susceptibility, a*, and b* reach peaks in the earliest Oligocene (Core 342-U1406A-23H) (Fig. F5).

Stratigraphically above this early Oligocene peak in magnetic susceptibility, color reflectance and calcium carbonate drop to a sustained low.

Sand-sized lithic grains

Sand-sized (>63 µm) grains were observed above the Eocene/Oligocene boundary at Site U1406. These grains consist mostly of angular quartz within the 63–150 µm sieve size fraction. Rock fragments also occur but are rare. In general, the composition of the sand-sized grains resembles those observed at Site U1404 in time-correlative strata (Fig. F13).

Deepwater authigenic glauconite

Sediment in Units II and III includes green layers that we interpret to contain mostly glauconite and chlorite. We hypothesize that these layers represent diagenetic layers that form on an oxidation/reduction boundary tens of centimeters deep in the sediment when sedimentation rate slows (Figs. F6C, F13).

Copper veins

Section 342-U1406A-28X-3 contains an occurrence of native copper associated with a minor fracture (Fig. F14). Copper is found both as grains in the sediment and as vein fill in Cores 342-U1406A-27X and 342-U1406B-28X. Native copper is very rarely seen in pelagic sediments, though it has been reported previously (Dickens et al., 1995). The presence of copper was confirmed by X-ray diffraction. Vein fills of copper are up to centimeters in length, whereas the grains are hundreds of micrometers across. The grains are clearly euhedral, and the crystal shapes are consistent with native copper. Unlike the copper reported by Dickens et al. (1995), no "halos" surround the copper occurrence; however, blue inclusions of azurite [$Cu_3(CO_3)_2(OH)_2$] can be seen in Figure F14 associated with the vein fill. The copper found at Site U1406 on J-Anomaly Ridge was recovered from ~230 mbsf, whereas the copper reported by Dickens et al. (1995) was found between ~500 and 800 mbsf at Ocean Drilling Program (ODP) Leg 145 Site 884.

Biostratigraphy

Coring at Site U1406 recovered a 281 m thick sequence of Pleistocene to middle Paleocene nannofossil ooze with varying amounts of clay and biosiliceous material (mainly radiolarians). Nannofossils and planktonic and benthic foraminifers are generally present throughout. Radiolarians are present in the lower Miocene–upper Oligocene and in the middle Eocene–upper Paleocene but are absent from the ~105 m thick interval spanning the EOT (Cores 342-U1406A-15H through 28X). The lower Miocene to middle Eocene succession appears to be stratigraphically complete at the resolution of shipboard biostratigraphy, but a significant hiatus is apparent between the middle Eocene and uppermost Paleocene. Sedimentation rates are relatively consistent around ~3 cm/k.y. for the lower Miocene to upper middle Eocene but are lower (~0.5 cm/k.y.) through the lower middle Eocene and the Paleocene.

The uppermost brown foraminifer sandy clay and nannofossil ooze (Cores 342-U1406A-1H through 2H; 0–2.25 mbsf) contain nannofossils and planktonic foraminifers that indicate Pleistocene ages (nannofossil Zones NN18–NN19). From 2.25 mbsf, nannofossils, planktonic foraminifers, and radiolarians provide a well-defined biostratigraphy indicating upper lower Miocene to middle Eocene sediment. A major unconformity at 255.30 mbsf is inferred to span the entire lower Eocene and uppermost Paleocene, including the PETM. Below this unconformity, a complete succession of uppermost to middle Paleocene microfossil zones was identified. Benthic foraminifers are generally rare (the "present" category) but increase in abundance in upper Eocene to upper

Oligocene sediment (Cores 342-U1406A-13H through 26X; 113.20–221.74 mbsf). Benthic foraminifer preservation is generally good to very good.

Below the Pleistocene veneer, a complete sequence of nannofossil zones from Zone NN4 to NP15 (upper middle Miocene to middle Eocene) and then from Zone NP9 to NP5 (upper to middle Paleocene) is apparent. The three radiolarian-rich intervals are assigned to Zones RN3–RP21, RP11–RP12, and RP6–RP7. The planktonic foraminifer zones from Subzone PT1a (Pleistocene), Zones M4–E7 (lower Miocene to upper Eocene), and Zones P5–P4 (Paleocene) are recognized.

An integrated calcareous and siliceous microfossil biozonation is shown in Figure **F15.** Datum and zonal determinations from nannofossils, planktonic foraminifers, and radiolarians are in close agreement. An age-depth plot including biostratigraphic and paleomagnetic datums is shown in Figure **F23.** A summary of calcareous and siliceous microfossil abundances and preservation is given in Figure **F16.**

Calcareous nannofossils

Calcareous nannofossil biostratigraphy is based on analysis of core catcher and additional working section half samples from Holes U1406A and U1406B. Depth positions and age estimates of biostratigraphic marker events are shown in Table **T3.** Calcareous nannofossil occurrence data are shown in Table **T4.** Note that the distribution chart is based on shipboard study only and is, therefore, biased toward age-diagnostic species.

At Site U1406, the preservation of calcareous nannofossils is generally moderate and good. The uppermost sediment in Hole U1406A contains abundant nannofossils indicative of Pleistocene Zones NN19 and NN18, as indicated by the presence of *Pseudoemiliania lacunosa* in Sample 342-U1406A-1H-1, 75 cm (0.75 mbsf), the top of *Discoaster brouweri* in Sample 1H-2, 75 cm (2.26 mbsf), and the absence of *Discoaster pentaradiatus*.

The interval from Sample 342-U1406A-1H-3, 75 cm, to 30X-CC (3.76–254.68 mbsf) contains abundant calcareous nannofossils ascribed to upper lower Miocene to middle Eocene Zones NN4–NNP14. All primary zonal marker species are present and listed in Table **T3.** The Oligocene/Miocene boundary is approximated by the top of the short-ranging species *Sphenolithus delphix* and the top of *Sphenolithus capricornutus,* which are both identified in Sample 342-U1406A-9H-5, 88 cm (79.72 mbsf). The Eocene/Oligocene boundary falls within nannofossil Zone NP21, which is identified by the top of *Coccolithus formosus* and top of *Discoaster saipanensis* in Samples 342-U1406A-21H-CC (191.51 mbsf) and 22H-CC (199.29 mbsf), respectively. Carbonate is continuously present across the boundary interval and through the upper to middle Eocene section, and preservation of calcareous nannofossils is good and moderate to good. The base of *Dictyococcites bisectus* occurs in Sample 342-U1406A-28X-1, 100 cm (233.41 mbsf), and equates with a level just prior to the Middle Eocene Climatic Optimum (Fornaciari et al., 2010). Middle Eocene nannofossil preservation deteriorates slightly below 245.11 mbsf through Zones NP14 and NP15, and the presence of *Chiphragmalithus* spp. is evidence of lower Eocene reworking in the lower half of Core 342-U1406A-29X (Sections 342-U1406A-29X-5 through 29X-CC). The oldest Eocene at this site is tentatively assigned at the upper part of Zone NP13 based on the absence of *Tribrachiatus orthostylus, Nannotetrina* spp., or any specimens ascribable to *Discoaster sublodoensis* and the co-occurrence of *Coccolithus crassus, Discoaster lodoensis, Discoaster kuepperi,* and *Zygrhablithus bijugatus.* A hiatus between Cores 342-U1406A-30X and 31X represents a roughly 7 m.y. interval, with nannofossil Zones NP13 and NP9 identified above and below. Moderate to good nannofossil preservation is seen in the Paleocene section, and Zones NP9–NP5 are identified based on the occurrence of base *Discoaster multiradiatus* in Sample 342-U1406A-32X-2, 34 cm (262.84 mbsf), the base of *Heliolithus riedelii* in Sample 32X-CC (267.19 mbsf), the base of *Discoaster mohleri* in Sample 33X-CC (278.63 mbsf), the base of *Heliolithus kleinpellii* in Sample 34X-1, 83 cm (279.43 mbsf), and the presence of *Fasciculithus tympaniformis* in the lowermost sample (34X-CC; 281.03 mbsf).

Radiolarians

Radiolarian biostratigraphy is based on analysis of all core catcher samples from Hole U1406A and selected section samples from Cores 342-U1406A-29X through 33X. No samples from Hole U1406B were examined. Radiolarians are absent from uppermost Sample 342-U1406A-1H-CC (6.23 mbsf) but are abundant to common and of good to moderate preservation in Sections 342-U1406A-2H-CC through 15H-CC (16.04–139.68 mbsf). Below this radiolarian-rich interval, radiolarians are absent over a ~100 m thick interval that encompasses the Eocene/Oligocene boundary (Samples 342-U1406A-16H-CC through 28X-CC; 148.04–242.30 mbsf). Middle Eocene radiolarians are common in underlying interval 342-U1406A-29X-3, 20–22 cm, through 29X-4, 16–18 cm (245.11–246.57 mbsf), but are rare and poorly preserved in Sample 30X-CC (254.68 mbsf). Nannofossil evidence suggests that a significant hiatus is situated between Cores 342-U1406A-30X and 31X

and that sediment below Section 342-U1406A-30X-CC is of Paleocene age. Radiolarians are abundant and well preserved in this Paleocene interval. Depth positions and age estimates of biostratigraphic marker events are shown in Table **T5,** and radiolarian distribution is shown in Table **T6.** Note that the distribution chart is based on shipboard study only and is, therefore, biased toward age-diagnostic species.

Sample 342-U1406A-1H-CC (6.23 mbsf) is barren of radiolarians. Radiolarians are abundant and well preserved from Sample 342-U1404A-2H-CC through 10H-CC (16.04–91.65 mbsf), and the assemblages can be correlated to lower Miocene–uppermost Oligocene radiolarian Zones RN3–RP22. In contrast to Sites U1404 and U1405, diatoms are relatively rare in the lower Miocene–upper Oligocene at Site U1406. Sections 342-U1406A-2H-CC through 3H-CC (16.04–25.49 mbsf) are assigned to Zone RN3 based on the range overlap of *Lychnocanoma elongata* and *Dorcadospyris dentata*. Sections 342-U1406A-4H-CC through 5H-CC (35.07–44.43 mbsf) are assigned to Zone RN2 based on the primary marker for the base of the zone, the top of *Theocyrtis annosa,* in Sample 342-U1406A-5H-CC (44.43 mbsf). Another key datum, the top of *Dorcadospyris ateuchus,* occurs in Sample 4H-CC (35.07 mbsf). Sections 342-U1406A-6H-CC through 8H-CC (53.93–72.63 mbsf) are assigned to Zone RN1 based on the primary datum for the base of the zone, the base of *Cyrtocapsella tetrapera,* in Sample 8H-CC (72.63 mbsf). Sections 342-U1406A-9H-CC through 10H-CC (82.64–91.65 mbsf) are assigned to Zone RP22 based on the primary datum for the base of the zone, the base of *L. elongata,* in Sample 10H-CC (91.65 mbsf). Sections 342-U1406A-11H-CC through 13H-7 (101.52–120.06 mbsf) are assigned to recently defined Subzone RP21b (Kamikuri et al., 2012) based on the primary datum for the base of the zone, the base of *Lychnocanoma apadora,* in Section 13H-7 (120.06 mbsf). Sections 342-U1406A-14H-CC through 15H-CC (128.55–139.68 mbsf) are assigned to Subzone RP21a (Kamikuri et al., 2012) based on the primary datum for the base of the zone, the base of *D. ateuchus,* in Sample 15H-CC (139.68 mbsf).

Samples 342-U1406A-16H-CC through 28X-CC (148.04–242.03 mbsf) are barren of radiolarians. A comparable barren interval spanning the lower Oligocene and upper Eocene was encountered at Site U1404. At Site U1405, the barren interval extends lower into the Eocene to Zone RP12 (~45 Ma), whereas at Site U1404 the barren interval terminated in Zone RP16 (~40 Ma).

Samples 342-U1406A-29X-3, 20–22 cm, through 29X-3, 98–100 cm (245.11–245.89 mbsf), are assigned to Zone RP12 based on the co-occurrence of primary index species *Eusyringium lagena* and *Theocotyle conica,* a species that last occurs at the top of the zone. Sample 342-U1406A-29X-4, 16–18 cm (246.57 mbsf), is assigned to Zone RP11 based on the presence of primary index species *Dictyoprora mongolfieri* and the absence of *E. lagena*. An unconformity is inferred to lie between this interval and Sample 342-U1406A-31X-1, 15–17 cm (255.96 mbsf), which contains a poorly preserved assemblage of late Paleocene or early Eocene age. Nannofossils indicate that Section 342-U1406A-32X-2, 34 cm, through 34X-CC (262.84–281.03 mbsf) is late to middle Paleocene in age, and radiolarians are abundant and well preserved. Samples 342-U1406A-31X-2, 99–101 cm, through 32X-CC (258.30–266.19 mbsf) are assigned to Zone RP7 based on the presence of primary index species *Bekoma bidartensis*. In the absence of other fossil evidence, this interval would be assigned the Eocene part of the zone based on the presence of *Podocyrtis papalis, Theocorys*? *phyzella,* and *Theocorys*? aff. *phyzella* (sensu Sanfilippo and Blome, 2001). These three species first occur directly above or within the PETM at Blake Nose ODP Site 1051 (Sanfilippo and Blome, 2001) and at Mead Stream, New Zealand (Hollis et al. 2005). However, as there is strong evidence from calcareous nannofossils and foraminifers for a Paleocene age, it seems likely that we have sampled an upper Paleocene interval that was absent from Blake Nose and perhaps poorly represented at nearby Site 384, where there is an exceptional record of radiolarians of late and middle Paleocene age (Nishimura, 1992). This implies that there are currently no unequivocal markers to separate Eocene and Paleocene components of Zone RP7, at least in the North Atlantic. The stratigraphically deepest sample examined, Sample 342-U1406A-33X-4, 102–103 cm (275.89 mbsf), is assigned to Zone RP6 based on the presence of primary index species *Bekoma campechensis*.

Planktonic foraminifers

Core catchers and additional samples from working-half sections were examined in Hole U1406A. Samples contained diverse and generally well preserved assemblages of planktonic foraminifers from the lower Miocene through Paleocene. Depth positions and age estimates of biostratigraphic marker events identified are shown in Table **T7.** The stratigraphic distribution of planktonic foraminifers is shown in Table **T8** and Figure **F15.**

The uppermost interval from Sample 342-U1406A-1H-1, 134 cm (1.35 mbsf), contains *Globorotalia truncatulinoides,* indicative of Pleistocene age. Samples 1H-2, 130–132 cm, through 9H-4, 100–102 cm

(2.81–78.22 mbsf), contain diverse and well-preserved lower Miocene assemblages containing the marker species *Praeorbulina glomerosa, Praeorbulina sicana, Catapsydrax dissimilis, Paragloborotalia kugleri,* and *Globoquadrina dehiscens,* indicating a continuous succession at the zonal level from Zone M5 through Subzone M1a. The base of *P. sicana* indicates Zone M5 in Sample 342-U1406A-2H-CC (16.04 mbsf). The top of *C. dissimilis* marks the top of Zone M3 in Sample 3H-CC (25.49 mbsf). The base of *G. dehiscens* in Sample 8H-4, 100–102 cm (68.71 mbsf), denotes the Subzone M1a/M1b boundary. The top and base of *P. kugleri* occur in Samples 5H-6, 100–102 cm (43.21 mbsf), and 9H-4, 100–102 cm (78.22 mbsf), respectively, marking the top of Subzone M1b and base of Subzone M1a. The base of *P. kugleri* has been calibrated to occur just 70 k.y. above the Oligocene/Miocene boundary (23.03 Ma).

Samples 342-U1406A-9H-6, 88–90 cm, through 22H-6, 50–52 cm (81.12–198.97 mbsf), contain abundant and well- to moderately preserved planktonic foraminifers. The base of *Paragloborotalia pseudokugleri* (Sample 342-U1406A-13H-6, 75–77 cm) indicates the base of Zone O7. The bases of Zones O4 and O3 are marked by the base of *Globigerina angulisuturalis* in Sample 342-U1406A-17H-3, 46–48 cm (151.57 mbsf), and the top of *Turborotalia ampliapertura* in Sample 18H-4, 60–62 cm (162.25 mbsf), respectively. The top of *Pseudohastigerina naguewichiensis* occurs in Sample 20H-2, 100–102 cm (175.12 mbsf), marking the top of Zone O1. Although the absence of *Hantkenina* in the upper sediment at Site U1406 means that the Eocene/Oligocene boundary cannot be defined sensu stricto, the evidence from nannofossils and sedimentology indicates that the Eocene/Oligocene boundary occurs between Samples 342-U1406A-22H-6, 50–52 cm, and 22H-CC (198.97–199.29 mbsf).

Relatively diverse planktonic foraminifers of Eocene age occur in Samples 342-U1406A-22H-CC through 30X-CC (199.29–254.67 mbsf), where preservation varies from good to moderate. The tops of *Globigerinatheka semiinvoluta* and *Morozovella crassatus* mark the base of Zones E15 and E14 in Samples 342-U1406A-26X-2, 100–102 cm (220.21 mbsf), and 27X-6, 100–102 cm (231.31 mbsf), respectively. The top of *Acarinina* species, calibrated to 37.75 Ma, occurs in Sample 27X-2, 100–102 cm (225.31 mbsf). The comparatively short (400 k.y.) Zone E12 is not recognized, probably because of the relatively low sedimentation rates (Fig. **F23**). The top of *Guembelitrioides nuttalli* demarcates the base of Zone E11 in Sample 342-U1406A-28X-4, 100–102 cm (237.91 mbsf). The comparatively short (~900 k.y.) Zone E9 is not recognized at Site U1406, again probably because of the low sedimentation rates. The boundary between Zones E8 and E7, marked by the base of *G. nuttalli,* is found in Sample 342-U1406A-29X-2, 50–52 cm (243.91 mbsf).

Below Sample 342-U1406A-30X-CC (254.67 mbsf), planktonic foraminifers indicate sediment of late Paleocene age (Zone P5) indicative of an unconformity spanning the lower Eocene. The top of Zone P4 is in Sample 342-U1406A-31X-3, 10–11 cm (258.91 mbsf). Below Sample 34X-CC (281.25 mbsf), planktonic foraminifers are rare or absent, preventing zonal demarcation.

Benthic foraminifers

Benthic foraminifers were examined semiquantitatively in core catcher samples from Hole U1406A. Additional working section half samples taken from Cores 342-U1406A-2H through 34X were examined for preservation and relative abundance of total benthic foraminifers and individual morphogroups. Benthic foraminifers at this site are rare (the "present" category) relative to total sediment particles >150 µm in the Miocene and Paleocene to middle Eocene and more abundant in the upper Eocene to upper Oligocene (Fig. **F16**).

Preservation of benthic foraminifer tests is generally good to very good except for lithostratigraphic Unit IV, which contains poorly and moderately preserved samples (Fig. **F16**). The occurrences of benthic foraminifers at this site are shown in Tables **T9** and **T10.**

Sections 342-U1406A-1H-CC through 23H-CC (6.20–207.93 mbsf) are dominated by an uppermost Eocene to lower Miocene assemblage of the calcareous taxa *Cassidulina subglobosa, Gyroidinoides* spp., *Pullenia bulloides, Pullenia quinqueloba,* and stilostomellids (including *Stilostomella gracillima, Stilostomella lepidula, Stilostomella subspinosa,* and *Stilostomella* sp.). Agglutinated benthic foraminifers are minor constituents only. Overall, this assemblage shows a high abundance of infaunal taxa, indicating high organic matter flux to the seafloor, comparable to deeper sites at J-Anomaly Ridge (Sites U1404 and U1405).

The lower to upper Eocene sediment from Sections 342-U1406A-25H-CC through 30X-CC (217.60–254.64 mbsf) shows a distinct change in benthic foraminifer assemblages compared to the overlying sediment (Table **T9**). Infaunal taxa are less abundant, and assemblages are mainly characterized by *Cibicidoides subspiratus, Nuttallides truempyi,* and *Oridorsalis umbonatus*, indicating a lower organic matter flux to the seafloor at this time.

Samples 342-U1406A-31X-CC through 34X-CC (260.44–281.03 mbsf) are dominated by a Paleocene assemblage. Abundant calcareous taxa include *Arago-*

nia velascoensis, Bulimina sp., gavelinellids (*Gavelinella beccariiformis, Gavelinella hyphalus,* and *Gavelinella* sp.), *Guttulina* sp., *Gyroidinoides globosus, N. truempyi,* and *Pullenia coryelli.* The agglutinated benthic foraminifer *Gaudryina pyramidata* occurs frequently in these samples (Table T9). Preservation of benthic foraminifer individuals is poor or moderate in these samples, and calcite infill is commonly observed.

Paleomagnetism

We completed a paleomagnetism study of APC and XCB cores from Holes U1406A–U1406C with the primary objective of establishing a magnetostratigraphic age model for the site. The natural remanent magnetization (NRM) of each archive-half section was measured at 2.5 cm intervals before and after demagnetization treatment in a peak alternating field (AF) of 20 mT. Archive-half section measurement data were processed by removing measurements made within 7.5 cm of section ends and from disturbed intervals described in the Laboratory Information Management System database. Cores 342-U1406A-1H through 17H and 342-U1406B-1H through 18H were azimuthally oriented using the FlexIT orientation tool (Table T11); all other cores were not oriented.

We also collected 185 discrete samples from working-half sections to verify the archive-half measurement data and to measure anisotropy of magnetic susceptibility (AMS) and bulk susceptibility of Site U1406 sediment. Discrete samples were collected and stored in 7 cm^3 plastic cubes and were typically taken from the least disturbed region closest to the center of each section in Hole U1406A. Selected samples were subjected to measurements of AMS, including bulk susceptibility, and NRM after 20 mT AF demagnetization. Sixteen samples were further selected for step-wise demagnetization at 10, 20, 30, 40, and 60 mT. All discrete sample data are volume corrected to 7 cm^3.

Results

Downhole paleomagnetism data after 20 mT demagnetization are presented for Holes U1406A, U1406B, and U1406C in Figures F17, F18, and F19, respectively. Similar to paleomagnetism results from Sites U1403, U1404, and U1405 (see "Paleomagnetism" in the "Site U1403," "Site U1404," and "Site U1405" chapters [Norris et al., 2013b, 2013c, 2013d]), section-half measurement data from XCB cores are difficult to interpret because of biscuiting and substantial core disturbance. We chose to interpret only results obtained from APC cores, except for a few cases where XCB core disturbance is remarkably low.

We identified two principal features in the paleomagnetism data at Site U1406. First, a large decrease in magnetic intensity and susceptibility occurs over the uppermost ~10 mbsf followed by a gradual increase downhole below ~60 mbsf, with two notable exceptions at ~180–190 and ~200–210 mbsf. Second, inclination values cluster at ~60° and –30°, a trend associated with clustering of declination values at ~0° and 180°, respectively.

Downhole intensity trends

Magnetic intensity values show distinct downhole changes and trends (Figs. F17, F18, F19). Magnetic intensity decreases from ~10^{-2} to ~10^{-4} A/m over the uppermost ~16 m of sediment at Site U1406. Between ~16 and ~60 mbsf, intensity values remain constant at ~10^{-4} A/m. From ~60 to ~180 mbsf, intensity continues to increase gradually. Below ~180 mbsf, magnetic intensity abruptly increases to ~10^{-3} A/m and in some intervals, as much as ~10^{-2} A/m. The amplitude of intensity variations is greatest in this interval as well. Weak-field magnetic susceptibility shows similar trends.

These magnetic trends generally correspond with lithostratigraphy. Sediment at Site U1406 changes from yellow and brown Pleistocene–Pliocene foraminiferal sand and nannofossil ooze (lithostratigraphic Unit I) to tan nannofossil ooze (Unit II) at ~2 mbsf. Unit II abruptly changes color at 16.70 mbsf in Hole U1406A from tan to green and remains green below this depth, the same depth at which the decreasing trend in magnetic intensity and susceptibility stops. Although shipboard geochemical data were not collected at a resolution sufficient to provide an independent test (see "Geochemistry"), we suggest that the decrease in magnetic intensity in the upper 16 m of Hole U1406A is caused by progressive reductive dissolution of iron oxide. At ~60 mbsf, lithostratigraphic Unit II changes color from dark green to pale green, perhaps attributable to slightly greater carbonate content (Fig. F5; also see "Geochemistry"). The magnetic intensity peak at ~180–190 mbsf corresponds to a change from Unit II to III, and the peak at ~200–210 mbsf corresponds to a transition from tan to brown nannofossil chalk in Core 342-U1406A-23H.

Inclination and declination clustering

Inclination values following 20 mT AF demagnetization often cluster around 60° or –30° (Figs. F17, F18, F19). Inclination clustering is usually associated with declination clustering at ~0° and 180°, respectively.

The approximately –30° inclination is shallow with respect to the reversed polarity value expected at the ~40°N latitude of Site U1406. This shallow bias is readily attributed to a small drilling overprint that remains after 20 mT AF demagnetization. AF demagnetization at 20 mT was more effective at removing the drilling overprint than it was with sediment recovered from Sites U1403 and U1404 but less effective than that at Site U1405. Regardless of the effectiveness of AF treatments between sites, we can utilize the positive and negative polarity clustering behavior to readily identify magnetozones in recovered intervals at Site U1406.

Comparison between pass-through and discrete sample data

AF demagnetization results for the discrete samples are summarized in Table **T12.** Of the 16 samples treated with a peak AF demagnetization field of 60 mT, 7 reveal relatively stable components of magnetization (e.g., Fig. **F20A**). These samples have remanent magnetizations that are strong enough to be measured by the onboard JR-6A spinner magnetometer. The remaining samples typically display NRM intensities that decrease by an order of magnitude following AF demagnetization in a 20 mT field. This behavior indicates that the combination of drilling overprint and magnetic intensity decrease described above has probably obscured the primary magnetic signal in these stratigraphic intervals, similar to results at Sites U1404 and U1405. Nevertheless, these results are useful for verifying the polarity of the 20 mT pass-through paleomagnetism data from the archive-half sections.

In general, paleomagnetism data from archive-half sections and discrete samples from oriented APC core intervals agree well. In contrast, some discrete samples from XCB cores show single stable components that are consistent with the section-half measurement data (e.g., Fig. **F20B**), but others show complex behavior that is not consistent with the section-half measurement data (e.g., Fig. **F20C**). These results suggest that section-half measurement data from XCB-cored intervals should be interpreted with care. A similar conclusion was reached with respect to Site U1403 data.

Magnetostratigraphy

The shipboard downhole results reveal a nearly continuous series of normal and reversed magnetozones between Cores 342-U1406A-2H and 23H (~10–204 mbsf), between Cores 342-U1406B-4H and 20H (~25–178 mbsf), and between Cores 342-U1406C-8H and 23X (~66–201 mbsf). Downhole plots indicate that additional series of magnetozones are recorded higher and possibly lower in the recovered interval in all three holes, but shore-based studies are necessary to identify and fully characterize magnetozones in these intervals and provide independent age control to correlate them to the geomagnetic polarity timescale (GPTS). Magnetozones can be straightforwardly correlated between all three holes, especially between ~65 and ~200 mbsf.

By utilizing radiolarian, foraminifer, and nannofossil biostratigraphic datums from Hole U1406A (see **"Biostratigraphy"**), we can correlate magnetozones to the GPTS. The shipboard magnetostratigraphic age model is based on Hole U1406A, for which we have the most biostratigraphic datums. Extension of this age model to the magnetozonation observed in Holes U1406B and U1406C is contingent on the accuracy of the stratigraphic correlation between holes, which is corroborated by some lithologic horizons and physical property features (see **"Stratigraphic correlation"**). In some key intervals, biostratigraphic datums from each hole provide unambiguous correlation between holes and to the GPTS. Our correlation is presented in Table **T13** and is shown in Figures **F17, F18, F19,** and **F21.**

In Hole U1406A, we correlate the magnetostratigraphy in Core 2H to Chrons C5Dn through C5En. We correlate magnetozones in Core 342-U1406A-3H to Chrons C6n–C6An.1r. Magnetozones in Cores 6H through 9H correlate to Chrons C6AAr.3r–C6Cn.2r. The entire interval of Core 10H is reversed polarity, which we correlate to Chron C6Cr. This correlation implies that Chron C6Cn.3n, which is only 0.062 m.y. long (~0.7 m thick given the 1.2 cm/k.y. average linear sedimentation rate [LSR] implied by the biostratigraphy and overall magnetostratigraphy), is recorded in the core catcher of Core 9H or in the core gap between Cores 9H and 10H. A discontinuous series of magnetozones in Cores 11H, 12H, and 16H can be correlated to Chrons C6Cr–C7n.2n, C7r–C7Ar, and the Chron C8r/C9n boundary, respectively. The entire interval of Core 15H shows reversed polarity, which we interpret to correspond to Chron C8r. Finally, we correlate a discontinuous series of magnetozones in Cores 18H through 23H to Chrons C10r–C15n.

Magnetozone correlations for Hole U1406B and U1406C are generally similar to those for Hole U1406A but do include some notable differences. For example, we are unable to correlate magnetozones in Cores 342-U1406B-2H through 3H to Hole U1406A, and therefore to the GPTS, with confidence. By using biostratigraphic datums from core catchers, however, we have correlated magnetozones in Core 342-U1406B-6H to Chrons C6n.2n–C6AAr.1n. In Hole U1406C, we are unable to correlate magnetozones in

Cores 342-U1406C-2H through 7H to the other two holes with confidence. A strong correlation between magnetozones in Hole U1406C to Hole U1406A and the GTPS is possible because of excellent magnetic behavior in these high-quality XCB cores and additional biostratigraphic datums. Magnetozones in Cores 342-U1406C-22X through 23X correlate to Chrons 12r–C15r. We did not observe the Chron C13n/C13r boundary (33.705 Ma) in any shipboard magnetic data.

The correlations described above provide a shipboard chronostratigraphic framework for interpreting the uppermost late Eocene–middle Miocene sediment drift record at Site U1406. The most salient implications of this age model are summarized as follows.

1. The Oligocene–Miocene transition is dated by the base of Chron C6Cn.2n (23.030 Ma), which we identified in intervals 342-U1406A-9H-5, 55.0–90.0 cm (~81.16 mbsf); 342-U1406B-10H-1, 135.0 cm, through 10H-2, 40.0 cm (~82.48 mbsf); and 342-U1406C-9H-4, 85.0–107.5 cm (~75.71 mbsf).
2. The Eocene–Oligocene transition occurs just prior to the transition from Chron C13r to C13n (33.705 Ma). We did not observe this chron boundary in any core from Site U1406, but we did identify the preceding and following chron boundaries in Holes U1406A and U1406C. The Chron C13r/C15n boundary (34.999 Ma) is between Sections 342-U1406A-23H-3, 120.0 cm, and 23H-4, 37.5 cm (~203.84 mbsf), and between Sections 342-U1406C-23X-2, 85.0 cm, and 23X-2, 110.0 cm (~197.68 mbsf). The Chron C12r/C13n boundary (33.157 Ma) is between Sections 342-U1406A-22H-2, 140.0 cm, and 22H-4, 12.5 cm (194.93 mbsf), and between Sections 342-U1406C-22X-6, 105.0 cm, and 22X-7, 10.0 cm (~193.10 mbsf). We predict that the Chron C13n/C13r boundary is in Core 342-U1406B-24X. Superconducting rock magnetometer data from section halves of this core are very noisy because of the XCB-disturbed nature of this interval. Shore-based paleomagnetism studies on discrete samples coupled with high-resolution stable carbon isotope stratigraphy will help locate this critical chron boundary with confidence.
3. The shipboard magnetostratigraphic age model also indicates at least three hiatuses in Hole U1406A, none of which are longer than ~3 m.y. These hiatuses complicate the magnetostratigraphic correlation between the three holes at Site U1406. The first of these hiatuses occurs within the interval between the lower part of Core 342-U1406A-2H and upper part of Core 3H (~16 mbsf). This interval is also marked by an abrupt step in natural gamma radiation (NGR) (see **"Physical properties"**). Our correlation suggests another hiatus between the bottom of Core 342-U1406A-5H and the top of Core 6H (~46 mbsf), in which we can no longer match the magnetozones to the C6AA chron series on the GPTS. This interval also corresponds to a distinct change in color, porosity, and bulk density (see **"Physical properties"**) and a variety of biostratigraphic datums (see **"Biostratigraphy"**). Finally, we conclude that ~3 m.y. is missing between Cores 342-U1406A-17H and 18H. The top of Core 17H is correlated to Chron C9n, whereas the top of Core 18H is correlated to Chron C11n.1n. This interval is also characterized by a distinct change in NGR values (see **"Physical properties"**). These hiatuses occur at approximately the same time as those observed in the Site U1405 record.

Like the age models for the other sites from J-Anomaly Ridge, the Site U1406 shipboard age model demonstrates slow sedimentation rates (~0.2 cm/k.y.) in the late Eocene and across the EOT. Sedimentation rates gradually increase throughout the Oligocene (~1.1 cm/k.y.) and then rapidly increase just following the Oligocene–Miocene transition (~3.3 cm/k.y.) (Fig. **F23**).

Magnetic susceptibility and anisotropy of magnetic susceptibility

Bulk magnetic susceptibility measured on 101 discrete samples is summarized in Table **T14.** Downhole variation in whole-round magnetic susceptibility (WRMS) and discrete sample magnetic susceptibility (DSMS) for Hole U1406A are shown in Figure **F17.** The WRMS data for Hole U1406A are shown in raw form; they have not been trimmed at section ends or filtered for obvious outliers, so noise in the data probably reflects edge effects or spurious measurements. We multiplied the WRMS data, which are in instrument units, by a factor of 0.577×10^{-5} to convert to approximate SI volume susceptibilities (see **"Paleomagnetism"** in the "Methods" chapter [Norris et al., 2013a]). WRMS and DSMS data agree very well after this conversion, and we attribute small absolute differences to the fact that the conversion factor applied to the WRMS data is not constant downhole because of changes in core diameter and density; only discrete samples provide calibrated susceptibility values in SI units. Both magnetic susceptibility data sets show the same first- and second-order cyclic trends, indicating that these trends are robust features of Site U1406 sediment. Although discrete

samples were collected along each core section from the entire depth of Hole U1406A, we chose to measure only odd-numbered samples.

AMS results for the discrete samples are also summarized in Table T14 and are shown in Figure F22. The eigenvalues associated with the maximum (τ_1), intermediate (τ_2), and minimum (τ_3) magnetic susceptibilities at Site U1406 show prominent downhole trends. Eigenvalues are divergent from the uppermost part of Hole U1406A to ~100 mbsf, with exceptional divergence between ~20 and 80 mbsf. This trend in magnetic fabric is similar to the downhole trends in water content and porosity (see "Physical properties"). From ~100 to 187 mbsf, τ_1 and τ_3 converge and remain relatively invariant. We note a distinct zone of eigenvalue divergence centered at ~200 mbsf. Eigenvalues diverge even more beginning at ~218 mbsf, corresponding to a change from APC to XCB coring technology. These eigenvalue trends are also clearly expressed in the degree of anisotropy, which is greatest in the uppermost 100 m of Hole U1406A. In general, the shape anisotropy is triaxial, although some intervals have strong oblate or prolate fabrics, such as between ~160 and 190 and between ~110 and 120 mbsf, respectively. However, we did not observe a strong depth-dependence in the inclination of the minimum eigenvector (V_3), suggesting that there is not preferred fabric orientation.

Age-depth models and mass accumulation rates

Coring at Site U1406 recovered a 281 m thick sequence of Pleistocene to middle Paleocene nannofossil ooze with varying amounts of clay and biosiliceous material (mainly radiolarians). Sedimentation rates are relatively consistent at ~3 cm/k.y. for the lower Miocene to upper middle Eocene but are lower (~0.5 cm/k.y.) through the lower middle Eocene and the Paleocene. The lower Miocene to middle Eocene succession appears to be stratigraphically complete at the resolution of shipboard biostratigraphy, but a significant hiatus is apparent between the middle Eocene and uppermost Paleocene.

Biostratigraphic and magnetostratigraphic datums from Hole U1406A (Table T15) were compiled to construct an age-depth model for this site (Fig. F23). A selected set of datums (Table T16) was used to create an age-depth correlation and calculate LSRs. Total mass accumulation rate (MAR), carbonate MAR (CAR), and noncarbonate MAR (nCAR) were calculated at 0.2 m.y. intervals using a preliminary shipboard splice rather than the "sampling splice" described in this volume (Table T17; Fig. F24).

Age-depth model

The age-depth model is tied to Pleistocene to lower Miocene nannofossil datums in the upper 10 mbsf. Through the lower Miocene and Oligocene, the paleomagnetic datums are used as the primary tie points for the age-depth correlation. Paleomagnetism and nannofossil datums agree well through this interval. A series of radiolarian and foraminifer datums in the Miocene suggest an alternative correlation and lower LSR, but these are at odds with a cluster of well-constrained nannofossil and paleomagnetism datums at ~17 Ma. The persistence of Chron C10r uphole to 146.99 mbsf indicates that there is a short hiatus in the upper Oligocene (~26–28 Ma). Below this level, the age model is tied to nannofossil and paleomagnetism datums until the lower middle Eocene. Nannofossil and radiolarian datums are the primary tie points for the lower Eocene and Paleocene and delimit a significant hiatus that spans the entire early Eocene, possibly including the Paleocene/Eocene boundary (48–56 Ma).

Linear sedimentation rates

Below the condensed Pleistocene–Miocene interval in the upper 10 mbsf, LSRs in Hole U1406A are highest in the lower Miocene and Oligocene/Miocene boundary interval (up to ~3.0 cm/k.y.), relatively high in the Oligocene to upper middle Eocene and upper Paleocene (0.7–0.8 cm/k.y.), and low in the lower middle Eocene (0.2 cm/k.y.).

Mass accumulation rates

MAR at Site U1406 increases in the upper Paleocene from 0.5 to 1 g/cm^2/k.y., predominantly driven by changes in CAR. MAR is relatively low (0.3 g/cm^2/k.y.) during the middle Eocene and increases to 0.8 g/cm^2/k.y. in the upper middle Eocene. CAR and nCAR are roughly equivalent during this interval, as carbonate content during this interval is close to 50 wt%. MAR increases across the Eocene/Oligocene boundary interval, largely because of increasing rates of noncarbonate accumulation, but is accompanied by increasing carbonate accumulation. Following the hiatus in the upper Oligocene, MAR increases in a double peak spanning the Oligocene/Miocene boundary. In the upper Oligocene, MAR peaks at 2 g/cm^2/k.y., decreases to 1 g/cm^2/k.y. in the uppermost Oligocene, and then peaks at 1.6–2.0 g/cm^2/k.y. in the lowermost Miocene. Following the double peak at

the Oligocene/Miocene boundary, MAR decreases to 0.5 g/cm^2/k.y. in the lower Miocene and then falls to <0.1 g/cm^2/k.y. for the remainder of the sequence.

Geochemistry

The geochemistry program during operations at Site U1406 included

- Analysis of interstitial gas compounds on headspace samples;
- Measurement of minor and trace element concentrations in interstitial water squeezed from whole-round samples from Hole U1406A; and
- Inorganic carbon, total carbon, and total nitrogen determinations of solid sediment samples from multiple holes.

Headspace gas samples

Headspace gas samples for routine safety monitoring were collected at a frequency of one sample per core in Hole U1406A (Table **T18;** Fig. **F25**), usually in the bottom half of each core (i.e., Sections 4, 5, or 6). Methane was the only hydrocarbon detected in measurable amounts. Methane concentrations increase from 1.4 to 3 ppmv in the upper 140 mbsf of Hole U1406A. After reaching peak concentrations at 140 mbsf, methane decreases to 1.6 ppmv between 140 and 290 mbsf.

Interstitial water geochemistry

Thirty interstitial water samples were squeezed from whole-round samples taken at a typical frequency of one per core in Hole U1406A (Table **T19**). Whole-round samples were collected immediately after the cores were sectioned on the catwalk. In some cases, disturbed cores or low recovery precluded whole-round sampling, as in the case with Cores 342-U1406A-24X and 25X, which had no recovery. In other instances, systematic whole-round sampling was temporarily suspended because of the suspected presence of critical lithologies or chronostratigraphic boundaries in the core. For example, we did not sample Cores 342-U1406A-21H and 22H, which contain an expanded lowermost Oligocene sequence (see **"Biostratigraphy"**).

Results

As with Sites U1402–U1405, manual titrations of pH and alkalinity were carried out on Hole U1406A interstitial water samples. Chloride concentration measurements by manual titration were suspended during operations at Site U1406 because results from ion chromatograph measurements of chloride concentration in Hole U1405A were of equivalent precision and accuracy.

The interstitial fluid profiles of sulfate, alkalinity, ammonium, and methane in the upper ~170 m of Hole U1406A reflect typical changes associated with organic carbon cycling (Figs. **F25, F26**). Downhole patterns of pH and alkalinity concentrations in Hole U1406A can be divided into two trends. First, from the top of Hole U1406A to ~180 mbsf, the boundary between Oligocene–Miocene nannofossil ooze of lithostratigraphic Unit II and Eocene–Oligocene nannofossil chalk of Unit III (see **"Lithostratigraphy"**), pH decreases from 7.5 to 7.0 and alkalinity concentrations increase from 3 to 5.8 mM. Second, below 180 mbsf, pH and alkalinity trends reverse, with pH increasing to 7.3 and alkalinity concentrations decreasing to 4 mM. Salinity shows a uniform downhole profile with no substantial inflections.

Interstitial fluid constituents that are sensitive to redox changes resulting from organic matter consumption (e.g., manganese and iron) show significant inflections at 170 mbsf, broadly coincident with the lithostratigraphic Unit II/III boundary and the reversal in pH and alkalinity trends described above. Manganese concentrations increase from 1 to 15 µM at the top of the sediment column at 170 mbsf and then decrease to 0 µM at the base of the recovered sequence. Iron concentrations are low (<2 µM) from 0 to 150 mbsf and then rise rapidly to peak concentrations of 8 µM from 150 to 170 mbsf, corresponding to maximum manganese concentrations. Iron concentrations fall again to <2 µM at 180 mbsf and below.

The downhole patterns of pH, alkalinity, manganese, and iron suggest a diagenetic sequence driven by organic matter consumption that does not progress beyond iron oxide reduction. The typical sequence of electron acceptor use during early diagenesis is manganese followed by iron then sulfate (cf. Berner, 1980). Sulfate concentrations remain relatively high within the depth range where manganese and iron reach their maximum concentrations (~170 mbsf). However, manganese and iron concentrations measured in Hole U1406A are lower than those at Sites U1403–U1405, suggesting that less organic matter has been consumed at Site U1406. Ammonium concentrations, which peak at relatively low values (10 µM at 170 mbsf; Fig. **F26**) compared to Sites U1403–U1405, corroborate this interpretation.

Calcium concentrations in Hole U1406A show an increasing downhole trend in the upper 180 mbsf (lithostratigraphic Units I and II). Below the sampling gap between 180 and 200 mbsf, calcium concentrations increase downhole to a maximum between ~150 and 180 mbsf, corresponding to a

decrease in alkalinity and the lithologic transition from ooze to chalk (see **"Lithostratigraphy"**). Calcium concentrations then slightly decrease below 240 mbsf, the depth that marks the lithostratigraphic Unit III/IV (nannofossil chalk to nannofossil chalk with foraminifers) boundary.

Magnesium concentrations gradually decrease in Hole U1406A within the upper 180 mbsf. Across the sampling gap (180 mbsf), magnesium concentrations drop rapidly from 51 to 46 mM. Below 210 mbsf, the magnesium concentration depth gradient reverses, with magnesium concentrations reaching 49 mM at the bottom of Hole U1406A. Mg/Ca ratios first decrease sharply with depth and then decrease more gradually until becoming roughly constant with depth from 140 to 220 mbsf. Below 220 mbsf, Mg/Ca ratios increase to the bottom of Hole U1406A.

Strontium concentrations increase from 80 to 130 µM in the upper 210 mbsf of Hole U1406A. Below 210 mbsf, the strontium concentration depth gradient reverses and strontium concentrations fall to 100 µM at the bottom of Hole 1406A. Sr/Ca ratios decrease from 7.25 to 6.5 in the upper 70 mbsf of Hole U1406A and then become roughly constant with depth until 180 mbsf, where values sharply increase to 7.5 across the sampling gap and then steadily decrease to 6.5 at the bottom of Hole U1406A.

Potassium concentrations range from 9 to 17 mM and are highly variable with no discernible downhole trends that correspond to lithostratigraphic units.

Discussion

Typically, calcium concentrations in deep-sea sediment interstitial fluids show pronounced systematic increases with increasing depth, whereas magnesium concentrations decrease. A marked discontinuity in the interstitial water chemistry profiles at Site U1406 occurs at the sampling gap between 180 and 200 mbsf. This disparity is associated with an inferred low-porosity chert horizon that appears to serve as an aquiclude (Fig. **F26**) with strong physical control on the transport of dissolved chemical constituents within interstitial water.

The prominent downhole gradients in calcium, magnesium, and strontium concentrations in Hole U1406A point to multiple processes controlling the interstitial fluid chemistry at Site U1406. First, comparison of calcium concentrations from Sites U1403–U1405 suggest that exchange reactions and alteration with the underlying basalt likely play a strong role. Gently sloping concentration gradients in the upper 180 mbsf are diagnostic of deep exchange reactions with basaltic basement and/or volcaniclastic sediment and subsequent diffusion of calcium and magnesium through the sedimentary sequence (Gieskes and Lawrence, 1981). During these reactions, calcium is released into interstitial fluid and magnesium is removed, which appears to be reflected in decreasing Mg/Ca ratios in the upper lithostratigraphic units of Hole U1406A. A potential problem with this interpretation for Site U1406 is that the low-porosity chert horizon at 180–200 mbsf should have acted as an impediment to this exchange. Additionally, the reversal in the trends of calcium, magnesium, Mg/Ca ratio, and several other parameters below the chert interval appears to preclude attributing the gradients in the uppermost 180 m of core to exchange with deep reservoirs such as basaltic basement. The reversal of magnesium below the chert suggests a deep source for magnesium, perhaps seawater or flow through reefal sediments below the drilling depth.

The gradient of calcium concentrations at Site U1403 is the steepest, whereas that of Site U1406 is the weakest among all J-Anomaly Ridge sites. Because water depth is greatest at Site U1403, the variation in these gradients appears to reflect carbonate dissolution controlled by the CCD. Indeed, carbonate content at Site U1403 is lower than at the shallower sites, whereas Site U1406 is characterized by the highest carbonate concentrations. At Site U1406, the decrease in calcium concentration below 200 mbsf corresponds to a decrease in alkalinity and an interval of well-cemented chalk in lithostratigraphic Unit IV, indicating precipitation of carbonate. Carbonate overgrowths on benthic foraminifers in Unit IV (see **"Biostratigraphy"**) are consistent with this interpretation.

Sediment geochemistry

Sediment plugs (5 cm^3) for downhole analysis of sediment elemental geochemistry were taken from Cores 342-U1406A-1H through 34X at an average resolution of one sample per section, adjacent to the moisture and density (MAD) samples (Table **T20**). Additional samples were taken at roughly 40 cm intervals from Cores 342-U1406B-24X through 30X and 342-U1406C-22X and 24X to resolve high-amplitude changes in carbonate contents. Elemental determinations of total organic carbon and total nitrogen were not made on all samples from Holes U1406B and U1406C.

Results

Carbonate content in Site U1406 sediment ranges from 21 to 92 wt% (Fig. **F27**). In lithostratigraphic Unit I (composed of foraminiferal sand and nanno-

fossil ooze), carbonate contents are >50 wt%. Carbonate contents of 40 wt% are typical in the nannofossil ooze of Unit II. Several fluctuations within Unit II where carbonate contents increase to 60 wt% in 5 to 10 m thick intervals are evident. At the base of Unit III, carbonate contents increase to 60 wt% and reach 80 wt% in a discrete interval at ~199 mbsf. In the nannofossil chalk of Unit III, carbonate contents increase to 92 wt% and remain above 70 wt% to the bottom of Hole U1406A.

Total organic carbon, calculated as the difference between total carbon and inorganic carbon, ranges from 0.01 to 0.5 wt%, with many samples falling below detection limit (Table T20). Total nitrogen values generally fall below 0.1 wt%, with slightly lower values at the bottom of Hole U1406A.

Discussion

The prominent increase in carbonate content at 199 mbsf is associated with the Eocene–Oligocene transition (see **"Biostratigraphy"** and **"Paleomagnetism"** for identification criteria). Carbonate concentrations reach their maximum (92 wt% at 250.45 mbsf) at Site U1406 in calcareous nannofossil Zone NP21 (Chron C13n) in middle to upper Eocene strata. This increase is provisionally interpreted to reflect CCD deepening and overshoot events (see **"Background and objectives"**) but could also reflect the onset of sediment drift formation.

Physical properties

We made physical properties measurements on whole-round sections, section halves, and discrete samples from section halves. Gamma ray attenuation (GRA) bulk density, magnetic susceptibility, *P*-wave velocity, and NGR measurements were made on whole-round sections using the Whole-Round Multisensor Logger (WRMSL). Thermal conductivity measurements could not be performed at Site U1406 because of technical problems. Compressional wave velocity on section halves was also measured at a frequency of two in each section (at ~50 and 100 cm) using a *P*-wave caliper. For MAD analyses, one discrete sample was collected in each section (typically at ~35 cm from the top of a section). The Section Half Multisensor Logger was used to measure spectral reflectance and magnetic susceptibility on archive section halves.

Magnetic susceptibility

Whole-round magnetic susceptibility ranges from 0 to 60 IU at Site U1406 (Fig. F28). From the top of the sediment column to ~2 mbsf (lithostratigraphic Unit I; see **"Lithostratigraphy"**), magnetic susceptibility is characterized by high values between 30 and 60 IU. At the contact with underlying Unit II, an abrupt step down to ~5 IU occurs. Throughout Unit II, magnetic susceptibility averages 9 IU and increases gradually downhole to ~20 IU at ~182 mbsf. An isolated peak of up to 25 IU occurs at ~30 mbsf in Holes U1406A–U1406C and corresponds to diffuse dark green beds in the core images. Units III and IV are characterized by larger variations in magnetic susceptibility (from 0 to 50 IU). Three notable peaks appear in Unit III and correlate between all three holes. The first peak, to ~25 IU, occurs at the transition between Units II and III at ~182 mbsf. The second peak, to 50 IU, appears at 205 mbsf. The third peak, to ~26 IU, appears at ~235 mbsf (not recovered in Hole U1406C). This third peak correlates with a darker brown-gray color in intervals 342-U1406A-28X-1, 46 cm, and 342-U1406B-28X-5, 62 cm.

Density and porosity

Two methods were used to evaluate bulk density at Site U1406. The GRA method provided a bulk density estimate from whole-round sections. The MAD method, applied to 191 discrete samples, provided a second, independent measure of bulk density, as well as dry bulk density, grain density, water content, and porosity. Changes in MAD bulk density are consistent with those observed in GRA bulk density records (Fig. F28). MAD density values vary between 1.2 and 1.9 g/cm^3 and are on average <1% lower than the GRA densities in the APC-cored section and 1.6% higher than GRA densities in the XCB-cored interval. These differences are readily explained by the fact that the same core diameter is assumed for the two core types in the GRA calculations when in fact they are not exactly the same.

In lithostratigraphic Unit I, bulk density averages 1.6 g/cm^3, whereas at the top of Unit II at ~2.5 mbsf, bulk density decreases to 1.4 g/cm^3. Bulk density then increases downhole to reach ~1.9 g/cm^3 at ~210 mbsf, a trend typical of compaction. Between 210 mbsf and the bottom of Hole U1406A, bulk density is relatively constant except for two discrete low intervals at 245 and 270 mbsf.

Water content and porosity vary throughout Site U1406 between 25 and 60 wt% and between 50 and 80 vol%, respectively. Lithostratigraphic Unit I shows lower values (~45 wt% water content and 72 vol% porosity) than the top of Unit II (60 wt% water content and 80 vol% porosity). Below 2.5 mbsf, both of these physical properties decrease gradually downhole to 25 wt% and 50 vol% at ~210 mbsf. Some superimposed shifts are observed at 85, 100, 223, 245,

and 270 mbsf; some of these shifts may be associated with stratigraphic hiatuses (see **"Age-depth models and mass accumulation rates"**).

Grain density generally varies between 2.6 and 2.8 g/cm³ throughout Hole U1406A. The upper part of lithostratigraphic Unit II is characterized by higher variability in grain density than the lower part of the unit, with some values as low as 2.3 g/cm³.

P-wave velocity

P-wave velocity from whole-round sections and section halves are generally consistent and have an average offset of ~20 m/s (Fig. **F29**). Overall, *P*-wave velocity gradually increases downhole from 1500 to 1800 m/s. We attribute this trend, which is similar to those observed in bulk density and water content, to downhole compaction. Lithostratigraphic Unit I shows slightly higher values than the top of Unit II. PWL measurements were not performed for most of Units III and IV because sediment rarely filled the liner in these XCB-recovered intervals.

Natural gamma radiation

At Site U1406, NGR values range from 2 to 35 cps and increase downhole to ~230 mbsf (Fig. **F29**). Over this interval, NGR values shift from 18 to 10 cps at the contact between lithostratigraphic Units I and II. In Unit II, NGR values increase from 10 to 35 cps. Units III and IV are characterized by a generally decreasing downhole trend from 30 to 2 cps, with an abrupt decrease to <10 cps over a <20 m interval centered around ~240 mbsf. Throughout the sediment column, distinctive variations are readily correlated between the three holes, with peaks at ~20, 110, 184, and 240 mbsf (see **"Stratigraphic correlation"**).

Color reflectance

Color reflectance was measured on archive section halves from Holes U1406A–U1406C. For Hole U1406C, the standard operating resolution of data acquisition was decreased from 2.5 to 5 cm except for key intervals (e.g., for the EOT at ~200 mbsf, color reflectance was measured every 2.5 cm). Color reflectance parameters a* and b* follow similar trends among all three holes (Fig. **F30**). Four general trends can be defined. In lithostratigraphic Unit I, values vary from 4.5 to 8 for a* and from 7 to 15 for b*. At the contact between Units I and II, a* decreases from 6 to 4.5 and b* increases from 12 to 14. This change in color reflectance values corresponds to the transition from dark brown nannofossil foraminifer ooze to light brown nannofossil ooze (see **"Lithostratigraphy"**). At ~17 mbsf in the upper part of Unit II, a* and b* values decrease abruptly, with a* shifting from 3.3 to –2 and b* from 12 to –1. This decrease corresponds to the transition in sediment color from light yellow to greenish gray, interpreted as change in sedimentary redox conditions in otherwise homogeneous nannofossil ooze (see **"Lithostratigraphy"**). Throughout Units II and III (downhole to ~240 mbsf), a* increases slightly from –2 to 1.5 downhole, whereas b* remains relatively constant with an average of 0. Small but distinctive peaks occur within this interval at 30, 180, and 235 mbsf; magnetic susceptibility data show small peak values in these intervals, as well (Fig. **F28**). At ~245 mbsf in both Holes U1406A and U1406B, a* and b* abruptly increase from 1.5 to 6 and 2 to 10, respectively; this step corresponds to the top of Unit IV. This increase also correlates to increases in magnetic susceptibility and water content, a decrease in bulk density, the transition from greenish gray to grayish brown color, and a substantial increase in radiolarian content (see **"Lithostratigraphy"**).

L* shows similar trends in all three holes (Fig. **F30**). In lithostratigraphic Unit I, L* averages 52. L* fluctuates between 50 and 67 in the top ~14 m of Unit II. Distinctive peaks at 17, 160, 195, and 245 mbsf correlate among all three holes. Some other peaks cannot be traced between all holes. For example, peaks at ~45 and ~90 mbsf in Hole U1406B are not observed in Holes U1406A and U1406C. The subtle variations in L* recorded at Site U1406 appear to correlate with changes in carbonate content (see **"Geochemistry"**).

Stratigraphic correlation

Sampling splice

We constructed a sampling splice for Site U1406 that is continuous downhole to ~235 m core composite depth below seafloor (CCSF). Below ~235 m CCSF, there are two floating splices from ~235 to ~247 m CCSF and ~248 to ~284 m CCSF. Shipboard physical property analysis led to an ambiguous correlation from ~20 to ~175 m CCSF (Fig. **F31**), and we anticipated heavy sampling requests across the EOT from ~220 to ~230 m CCSF, so we scanned archive-half sections from all three holes between ~5 and ~283 m CCSF using the Avaatech X-ray fluorescence (XRF) core scanner at Texas A&M University (Fig. **F32**). The sampling splice is based primarily on XRF core scanning measurements of Ca/Fe, but other elements and physical properties were occasionally used. Tie points in the upper ~20 m CCSF of the splice are tentative and based on shipboard NGR, WRMSL magnetic susceptibility, and color changes present in the core image composites. Future interpretation of XRF core scanning data may lead to adjustments in these

ties. XRF Ca/Fe measurements were crucial for determining tie points below ~20 m CCSF. Real-time correlation was difficult between 20 and 200 m CCSF, where a low Special Task Multisensor Logger (STMSL) magnetic susceptibility signal and ambiguous GRA bulk density data were insufficient to determine the offset between the three holes. Hole U1406A is the deepest hole drilled at this site, with a maximum depth of 281.05 mbsf (313 m CCSF). Holes U1406B and U1406C extend to 254 mbsf (283 m CCSF) and 241 mbsf (268 m CCSF), respectively. Our correlation yields a growth rate of 11% for Hole U1406A and 12% for Holes U1406B and U1406C (Fig. F33), which represent the average increase of the CCSF depth scale relative to each hole's mbsf depth scale. The affine table (Table T21) summarizes the individual offsets assigned to each core drilled.

Correlation during drilling operations

In the upper ~20 m CCSF of the drilled sediment column at Site U1406, distinct changes in sediment color and physical properties allowed the offset of coring gaps between holes. Below this depth, we attempted correlation during drilling operations using magnetic susceptibility and GRA bulk density data collected at 2.5 cm resolution on the STMSL before allowing cores to equilibrate to room temperature. These quickly generated records were difficult to interpret because the magnetic susceptibility signal rarely exceeded the noise level, and GRA bulk density showed few distinctive features. Our experience at previous sites indicated that GRA bulk density might be unreliable on a core-by-core basis as a result of core deformation during drilling and curation. However, an overall increase in GRA bulk density with depth, combined with the top depths reported on the drill floor, provided an indication of the relative offset between holes.

Drilling switched from APC to XCB coring with Core 342-U1406A-26X after zero recovery from the previous two consecutive cores (Core 342-U1406A-24H was a full stroke, and Core 25H was a partial stroke). As a result, the strategy for Hole U1406B was to switch to XCB drilling earlier in an attempt to recover some of the missing ~10 m interval corresponding to Cores 342-U1406A-24H and 25H. Unfortunately, the final APC attempt for Core 342-U1406B-22H was also a partial stroke, and the first XCB coring attempt resulted in poor recovery (13%). In order to recover this interval in Hole U1406C, drilling switched to XCB coring for Core 342-U1406C-20X, and Cores 20X through 24X had excellent recovery with no obviously disturbed intervals (>100% nominal recovery), thereby successfully bridging the unrecovered interval in Holes U1406A and U1406B.

Correlation and splice construction

For stratigraphic correlation and splice construction, we primarily used XRF core scanner Ca/Fe data, which showed significantly clearer features than the available shipboard physical properties. Our correlation and splice is generally consistent with biostratigraphic and paleomagnetic results (see "Biostratigraphy" and "Paleomagnetism").

In the splice table (Table T22), tie points are labeled as tentative if they occur near the top or bottom ~50 cm of a core and/or are not associated with a prominent feature in the available data. These tentative tie points fall in the upper ~20 m CCSF (where we used only physical property data to assign ties) and below ~200 m CCSF. However, we are confident that we have recovered a continuous splice across the Oligocene–Miocene transition from ~67 to 111 m CCSF and a continuous EOT in the interval spanned by Cores 342-U1406A-22H to 324-U1406C-24H from ~215 to ~235 m CCSF.

There is a large disagreement (~15 m) between our correlation and paleomagnetic chron identification for Holes U1406A and U1406C from ~67 to 82 m CCSF. Our correlation in this interval is based on XRF Ca/Fe measurements, which suggests correlation between the bottom of Core 342-U1406A-7H and the top of Core 342-U1406C-7H (Fig. F33A). In contrast, the Chron C6Bn.2n/C6Br reversal is assigned to the bottom of Cores 342-U1406A-7H and 342-U1406C-8H (Table T13). The spacing between chron boundaries in Hole U1406C mbsf depths is consistently smaller than spacing between the same chron boundaries in Hole U1406A and U1406B mbsf depths, suggesting possible differences in the thickness of the same stratigraphic intervals between Hole U1406C compared to Holes U1406A and U1406B. Postcruise XRF core scanning revealed large differences between cores from Holes U1406A and U1406B compared to cores from Hole U1406C between ~65 and ~110 m CCSF and between ~150 and ~190 m CCSF. XRF data indicate the presence of hiatuses in Hole U1406C that do not appear in Holes U1406A and U1406B. These occur between Cores 342-U1406C-6H and 7H and within Core 17H. In order to correct for the latter, we applied a correction to Core 18H rather than break up Core 17H. A number of large overlaps are also apparent between successive cores from Hole U1406C, which we interpret as relatively expanded intervals in Hole U1406C compared to Holes U1406A and U1406B (Fig. F33). The overlapping cores in Hole U1406C on the CCSF

depth scale are solely the result of correlating more expanded cores in Hole U1406C to a splice that is mostly based on more compressed cores from Holes U1406A and U1406B. The drift origin of the sediment package drilled in the upper ~200 m CCSF of this site is likely responsible for the large lateral variability between holes at Site U1406.

As a result of poor recovery for Cores 342-U1406A-24H and 25H and 342-U1406B-25X, only Cores 342-U1406C-24X and 25X recover the interval from ~233 to 241 m CCSF. Core 342-U1406C-24X had ~140% recovery but showed no evidence of disturbance. As a result, we appended Core 342-U1406C-25X below 24X. Based on XRF core scanning, only a small overlap exists between Cores 342-U1406C-25X, 342-U1406B-26X, and 342-U1406A-26X; as a result, the tie point at ~243 m CCSF is tentative (Fig. F31). This correlation is also consistent with biostratigraphy, although the core catcher of Core 342-U1406C-25X belongs to nannofossil Zone NP19/NP20, the core catchers of both Cores 342-U1406A-26X and 342-U1406B-26X belong to Zone NP18 (see "Biostratigraphy"). Finally, we appended Cores 342-U1406A-31X through 34X, which have no equivalent in either Hole U1406B or U1406C, using offsets consistent with the growth rate.

The Site U1406 splice can be used as a sampling guide to recover a single sedimentary sequence, though it is advisable to overlap splice intervals at the tie points by a few decimeters (or more, where splice ties are labeled as tentative).

References

Berner, R.A., 1980. *Early Diagenesis: A Theoretical Approach:* Princeton, NJ (Princeton Univ. Press).

Dickens, G.R., Owen, R.M., and Pedersen, T.F., 1995. Copper mineralization at Site 884 in the North Pacific. *In* Rea, D.K., Basov, I.A., Scholl, D.W., and Allan, J.F. (Eds.), *Proc. ODP, Sci. Results,* 145: College Station, TX (Ocean Drilling Program), 389–397. **doi:10.2973/odp.proc.sr.145.129.1995**

Fornaciari, E., Agnini, C., Catanzariti, R., Rio, D., Bolla, E.M., and Valvasoni, E., 2010. Mid-latitude calcareous nannofossil biostratigraphy and biochronology across the middle to late Eocene transition. *Stratigraphy,* 7(4):229–264. **http://www.micropress.org/micropen2/articles/1/7/94581_articles_article_file_1717.pdf**

Gieskes, J.M., and Lawrence, J.R., 1981. Alteration of volcanic matter in deep-sea sediments: evidence from the chemical composition of interstitial waters from deep sea drilling cores. *Geochim. Cosmochim. Acta,* 45(10):1687–1703. **doi:10.1016/0016-7037(81)90004-1**

Gradstein, F.M., Ogg, J.G., Schmitz, M.D., and Ogg, G.M. (Eds.), 2012. *The Geological Time Scale 2012:* Amsterdam (Elsevier).

Hollis, C.J., Dickens, G.R., Field, B.D., Jones, C.M., and Strong, C.P., 2005. The Paleocene–Eocene transition at Mead Stream, New Zealand: a southern Pacific record of early Cenozoic global change. *Palaeogeogr., Palaeoclimatol., Palaeoecol.,* 215(3–4):313–343. **doi:10.1016/j.palaeo.2004.09.011**

Kamikuri, S., Moore, T.C., Ogane, K., Suzuki, N., Pälike, H., and Nishi, H., 2012. Early Eocene to early Miocene radiolarian biostratigraphy for the low-latitude Pacific Ocean. *Stratigraphy,* 9(1):77–108. **http://www.micropress.org/micropen2/articles/1/7/27546_articles_article_file_1785.pdf**

Kirschvink, J.L., 1980. The least-squares line and plane and the analysis of palaeomagnetic data. *Geophys. J. R. Astron. Soc.,* 62(3):699–718. **doi:10.1111/j.1365-246X.1980.tb02601.x**

Lyle, M., Wilson, P.A., Janecek, T.R., et al., 2002. *Proc. ODP, Init. Repts.,* 199: College Station, TX (Ocean Drilling Program). **doi:10.2973/odp.proc.ir.199.2002**

Nishimura, A., 1992. Paleocene radiolarian biostratigraphy in the northwest Atlantic at Site 384, Leg 43, of the Deep Sea Drilling Project. *Micropaleontology,* 38(4):317–362. **doi:10.2307/1485764**

Norris, R.D., Wilson, P.A., Blum, P., Fehr, A., Agnini, C., Bornemann, A., Boulila, S., Bown, P.R., Cournede, C., Friedrich, O., Ghosh, A.K., Hollis, C.J., Hull, P.M., Jo, K., Junium, C.K., Kaneko, M., Liebrand, D., Lippert, P.C., Liu, Z., Matsui, H., Moriya, K., Nishi, H., Opdyke, B.N., Penman, D., Romans, B., Scher, H.D., Sexton, P., Takagi, H., Turner, S.K., Whiteside, J.H., Yamaguchi, T., and Yamamoto, Y., 2014a. Methods. *In* Norris, R.D., Wilson, P.A., Blum, P., and the Expedition 342 Scientists, *Proc. IODP,* 342: College Station, TX (Integrated Ocean Drilling Program). **doi:10.2204/iodp.proc.342.102.2014**

Norris, R.D., Wilson, P.A., Blum, P., Fehr, A., Agnini, C., Bornemann, A., Boulila, S., Bown, P.R., Cournede, C., Friedrich, O., Ghosh, A.K., Hollis, C.J., Hull, P.M., Jo, K., Junium, C.K., Kaneko, M., Liebrand, D., Lippert, P.C., Liu, Z., Matsui, H., Moriya, K., Nishi, H., Opdyke, B.N., Penman, D., Romans, B., Scher, H.D., Sexton, P., Takagi, H., Turner, S.K., Whiteside, J.H., Yamaguchi, T., and Yamamoto, Y., 2014b. Site U1403. *In* Norris, R.D., Wilson, P.A., Blum, P., and the Expedition 342 Scientists, *Proc. IODP,* 342: College Station, TX (Integrated Ocean Drilling Program). **doi:10.2204/iodp.proc.342.104.2014**

Norris, R.D., Wilson, P.A., Blum, P., Fehr, A., Agnini, C., Bornemann, A., Boulila, S., Bown, P.R., Cournede, C., Friedrich, O., Ghosh, A.K., Hollis, C.J., Hull, P.M., Jo, K., Junium, C.K., Kaneko, M., Liebrand, D., Lippert, P.C., Liu, Z., Matsui, H., Moriya, K., Nishi, H., Opdyke, B.N., Penman, D., Romans, B., Scher, H.D., Sexton, P., Takagi, H., Turner, S.K., Whiteside, J.H., Yamaguchi, T., and Yamamoto, Y., 2014c. Site U1404. *In* Norris, R.D., Wilson, P.A., Blum, P., and the Expedition 342 Scientists,

Proc. IODP, 342: College Station, TX (Integrated Ocean Drilling Program). **doi:10.2204/iodp.proc.342.105.2014**

Norris, R.D., Wilson, P.A., Blum, P., Fehr, A., Agnini, C., Bornemann, A., Boulila, S., Bown, P.R., Cournede, C., Friedrich, O., Ghosh, A.K., Hollis, C.J., Hull, P.M., Jo, K., Junium, C.K., Kaneko, M., Liebrand, D., Lippert, P.C., Liu, Z., Matsui, H., Moriya, K., Nishi, H., Opdyke, B.N., Penman, D., Romans, B., Scher, H.D., Sexton, P., Takagi, H., Turner, S.K., Whiteside, J.H., Yamaguchi, T., and Yamamoto, Y., 2014d. Site U1405. *In* Norris, R.D., Wilson, P.A., Blum, P., and the Expedition 342 Scientists, *Proc. IODP,* 342: College Station, TX (Integrated Ocean Drilling Program). **doi:10.2204/iodp.proc.342.106.2014**

Norris, R.D., Wilson, P.A., Blum, P., Fehr, A., Agnini, C., Bornemann, A., Boulila, S., Bown, P.R., Cournede, C., Friedrich, O., Ghosh, A.K., Hollis, C.J., Hull, P.M., Jo, K., Junium, C.K., Kaneko, M., Liebrand, D., Lippert, P.C., Liu, Z., Matsui, H., Moriya, K., Nishi, H., Opdyke, B.N., Penman, D., Romans, B., Scher, H.D., Sexton, P., Takagi, H., Turner, S.K., Whiteside, J.H., Yamaguchi, T., and Yamamoto, Y., 2014e. Site U1408. *In* Norris, R.D., Wilson, P.A., Blum, P., and the Expedition 342 Scientists, *Proc. IODP,* 342: College Station, TX (Integrated Ocean Drilling Program). **doi:10.2204/iodp.proc.342.109.2014**

Pälike, H., Lyle, M.W., Nishi, H., Raffi, I., Ridgwell, A., Gamage, K., Klaus, A., Acton, G., Anderson, L., Backman, J., Baldauf, J., Beltran, C., Bohaty, S.M., Bown, P., Busch, W., Channell, J.E.T., Chun, C.O.J., Delaney, M., Dewangan, P., Dunkley Jones, T., Edgar, K.M., Evans, H., Fitch, P., Foster, G,L., Gussone, N., Hasegawa, H., Hathorne, E.C., Hayashi, H., Herrle, J.O., Holbourn, A., Hovan, S., Hyeong, K., Iijima, K., Ito, T., Kamikuri, S., Kimoto, K., Kuroda, J., Leon-Rodriguez, L., Malinverno, A., Moore, T.C., Jr., Murphy, B.H., Murphy, D.P., Nakamura, H., Ogane, K., Ohneiser, C., Richter, C., Robinson, R., Rohling, E.J., Romero, O., Sawada, K., Scher, H., Schneider, L., Sluijs, A., Takata, H., Tian, J., Tsujimoto, A., Wade, B.S., Westerhold, T., Wilkens, R., Williams, T., Wilson, P.A., Yamamoto, Y., Yamamoto, S., Yamazaki, T., and Zeebe, R.E., 2012. A Cenozoic record of the equatorial Pacific carbonate compensation depth. *Nature (London, U. K.),* 488(7409):609–614. **doi:10.1038/nature11360**

Sanfilippo, A., and Blome, C.D., 2001. Biostratigraphic implications of mid-latitude Paleocene–Eocene radiolarian faunas from Hole 1051A, ODP Leg 171B, Blake Nose, western North Atlantic. *In* Kroon, D., Norris, R.D., and Klaus, A. (Eds.), *Western North Atlantic Palaeogene and Cretaceous Palaeoceanography.* Geol. Soc. Spec. Publ., 183(1):l85–224. **doi:10.1144/GSL.SP.2001.183.01.10**

Tucholke, B.E., and Vogt, P.R., 1979. Western North Atlantic: sedimentary evolution and aspects of tectonic history. *In* Tucholke, B.E., Vogt, P.R., et al., *Init. Repts. DSDP,* 43: Washington, DC (U.S. Govt. Printing Office), 791–825. **doi:10.2973/dsdp.proc.43.140.1979**

Publication: 3 March 2014
MS 342-107

Figure F1. Bathymetric map of the southwestern end of J-Anomaly Ridge showing location of Site U1406 (red star). Track lines are from a single-channel seismic survey conducted during the KNR179-1 site survey. See Figures F2 and F3 for seismic profiles.

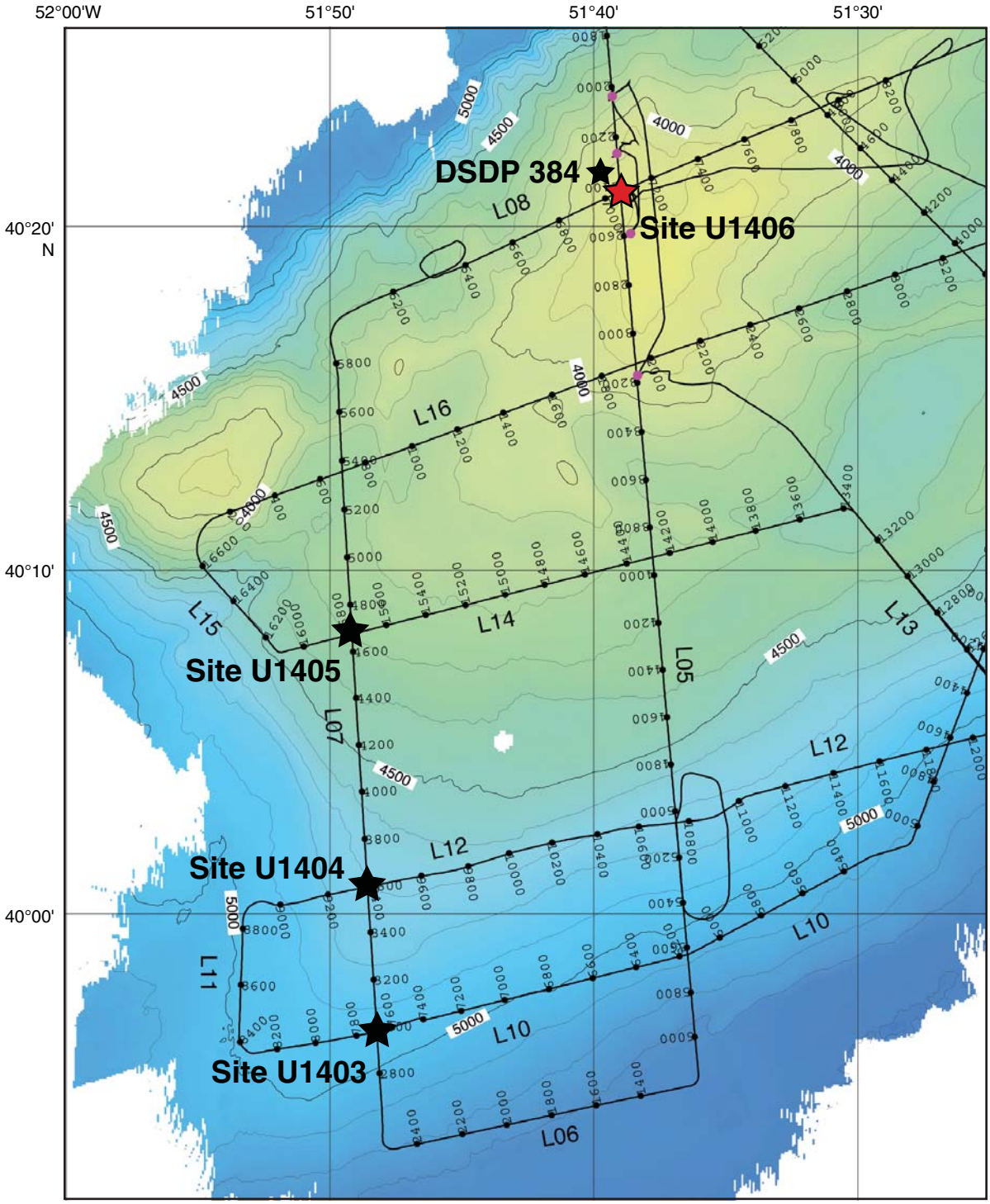

Figure F2. Single-channel seismic KNR179-1 Line 5. This is the north–south dip line crossing Site U1406 (at shotpoint [SP] 3600). White bars represent approximate depths of penetration at Sites U1406 and DSDP 384.

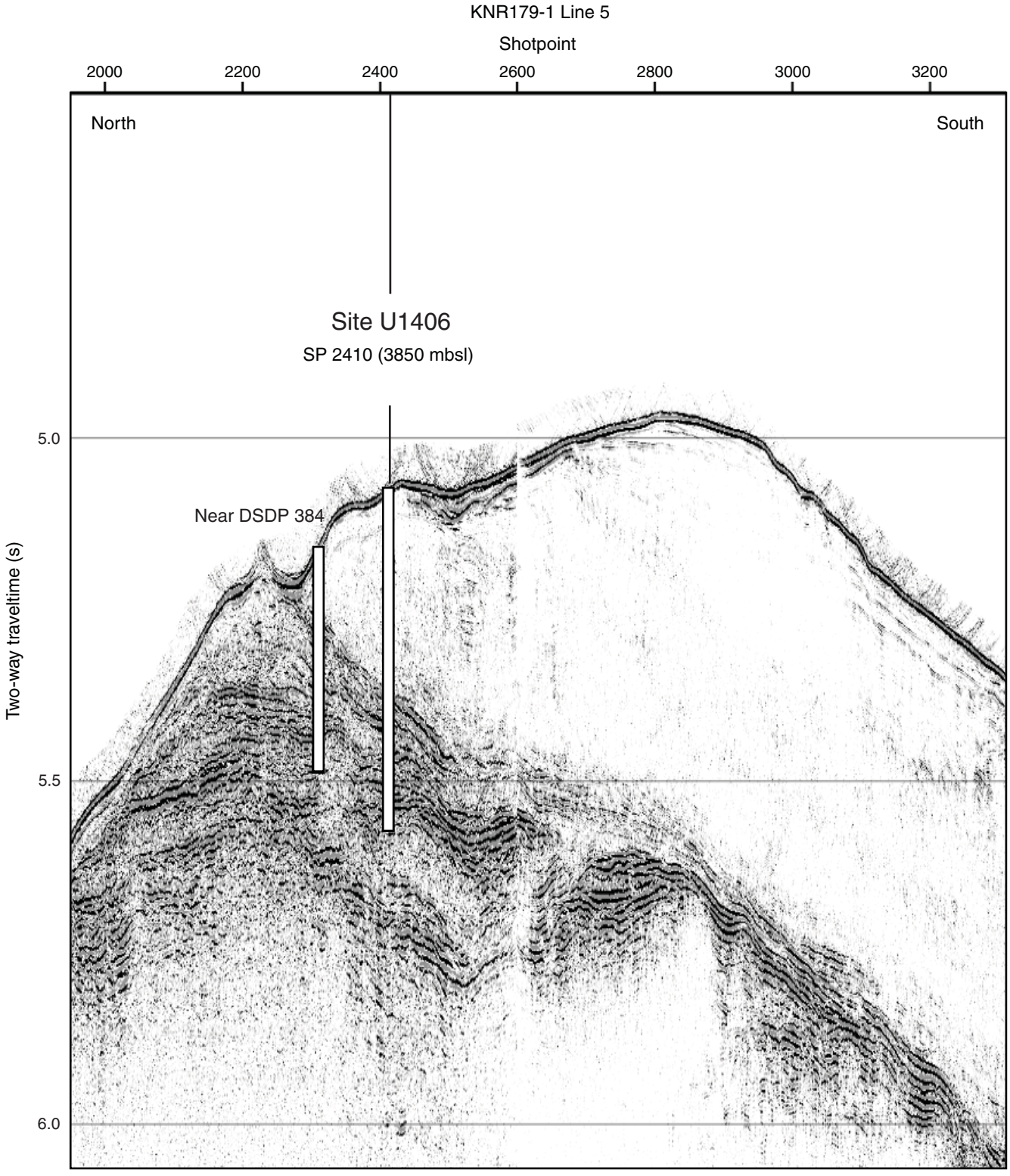

Figure F3. Single-channel seismic KNR179-1 Line 8. This is the northeast–southwest strike line crossing Site U1406 (at shotpoint [SP] 9390). White bars represent approximate depths of penetration at Sites U1406 and DSDP 384.

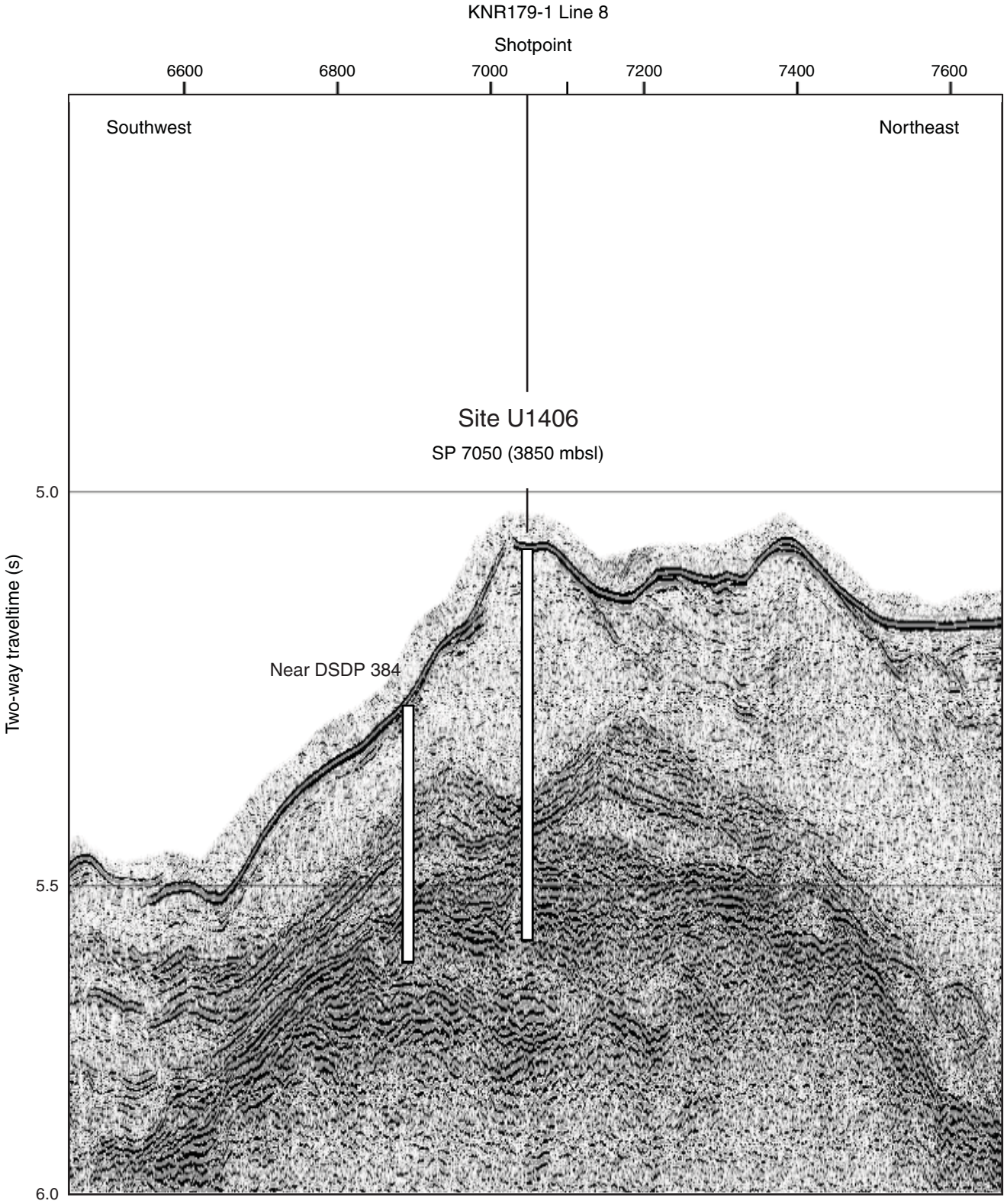

Figure F4. Comparison of acoustic character of single-channel seismic KNR179-1 Lines 5 (top) and 7 (bottom) crossing J-Anomaly Ridge, Site U1403–U1406.

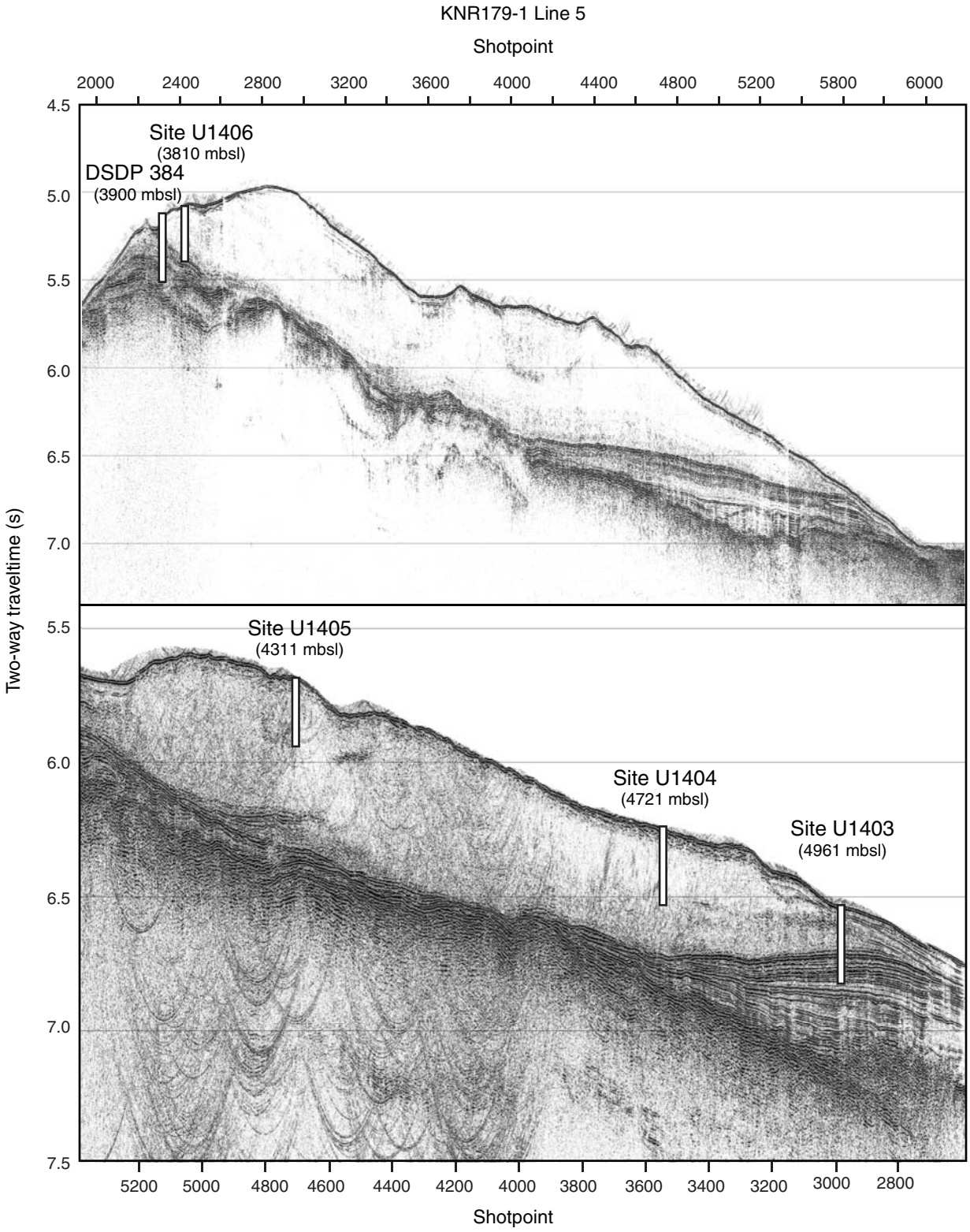

Figure F5. Lithologic summary, Site U1406. Typically the lighter colors in the core image reflect higher carbonate content. At the top of the core, note the tan to green transition in the color data.

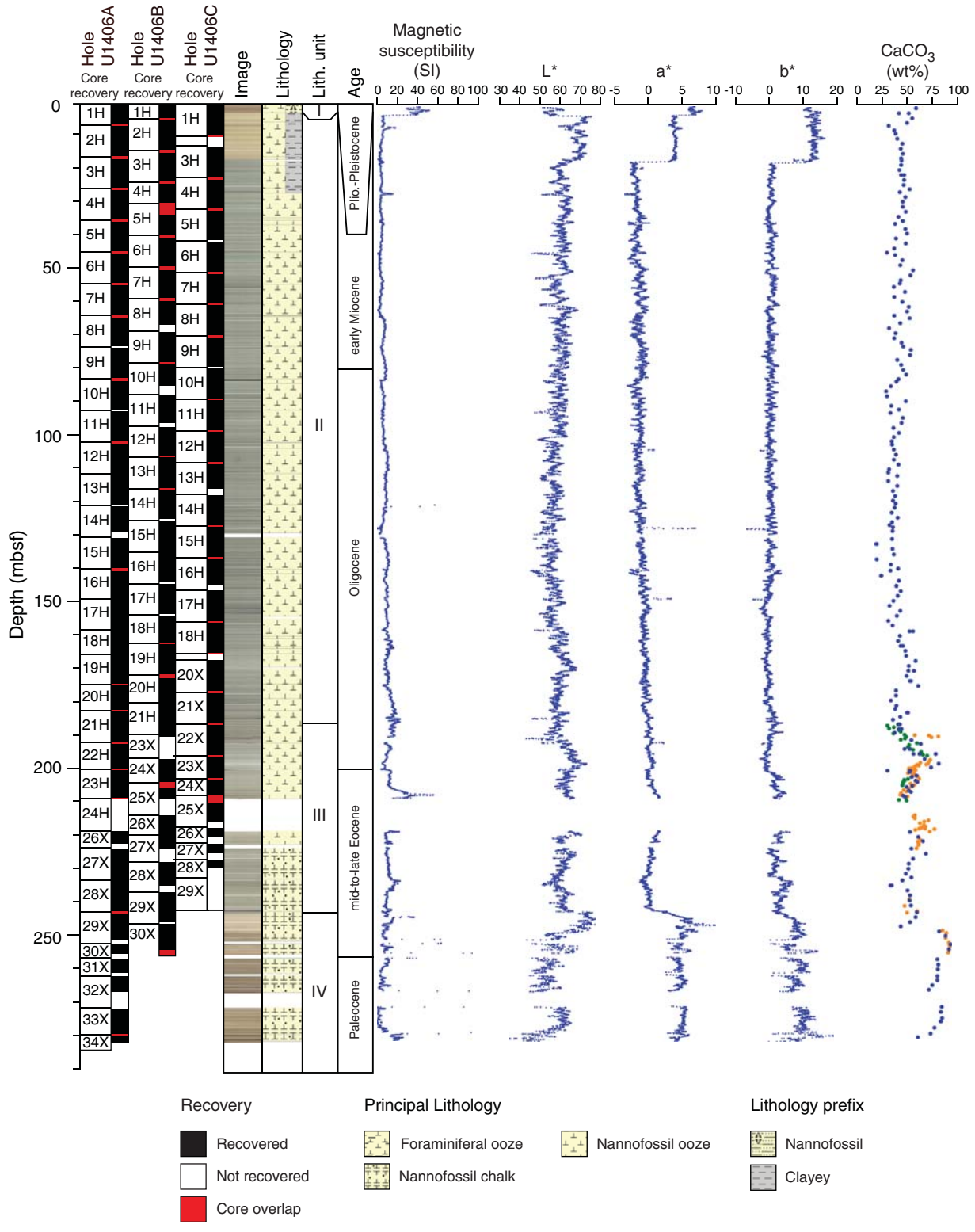

Figure F6. Line scan images of most common lithologies, Site U1406. **A.** Pleistocene foraminiferal sand in nannofossil ooze, Unit I. **B.** Miocene nannofossil ooze, Unit II. **C.** Oligocene nannofossil ooze, Unit II. **D.** Eocene nannofossil chalk, Unit III. **E.** Eocene nannofossil chalk with foraminifers and radiolarians and dark manganese or sulfide blebs, Unit IV.

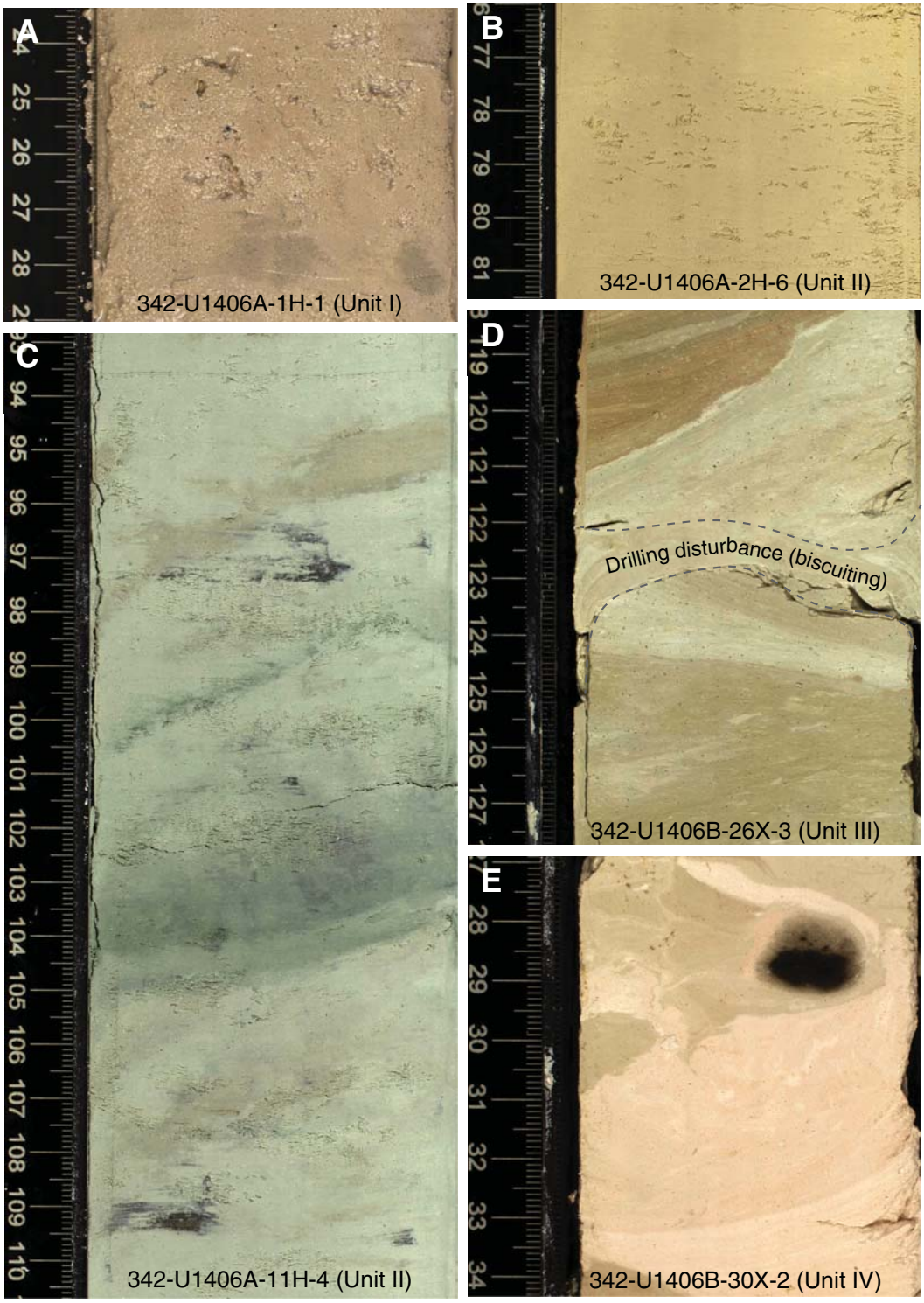

Figure F7. Photomicrographs of smear slides indicating the dominant lithologies of Units I–IV, Site U1406. **A.** Nannofossil foraminiferal ooze, Unit I. **B.** Nannofossil ooze with radiolarians and foraminifers, Unit II. **C.** Nannofossil chalk, Unit III. **D.** Nannofossil chalk with foraminifers, Unit IV.

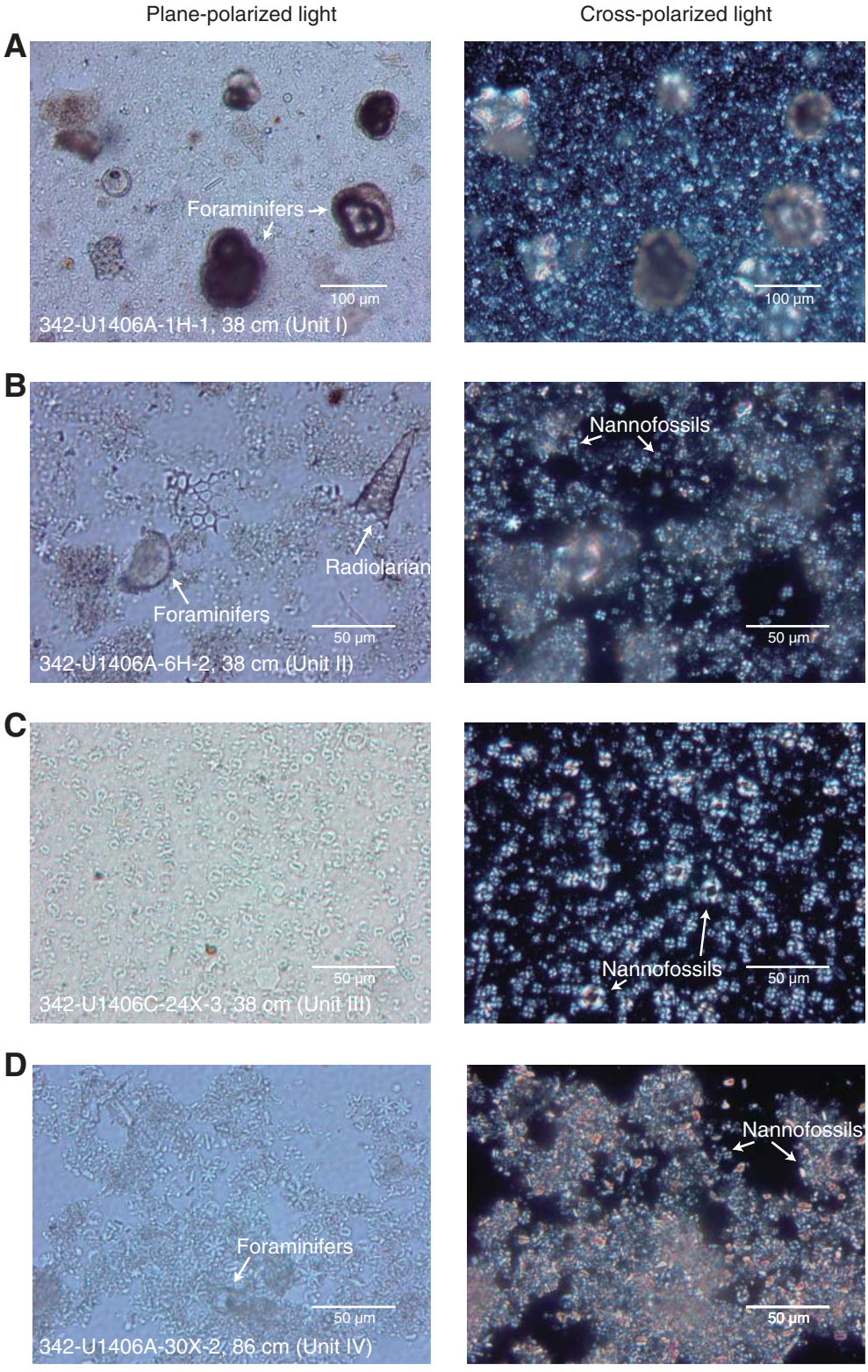

Figure F8. Plots of smear slide results of major biogenic and lithologic components and their relative abundance, Hole U1406A. VA = very abundant, A = abundant, C = common, F = few, P = present.

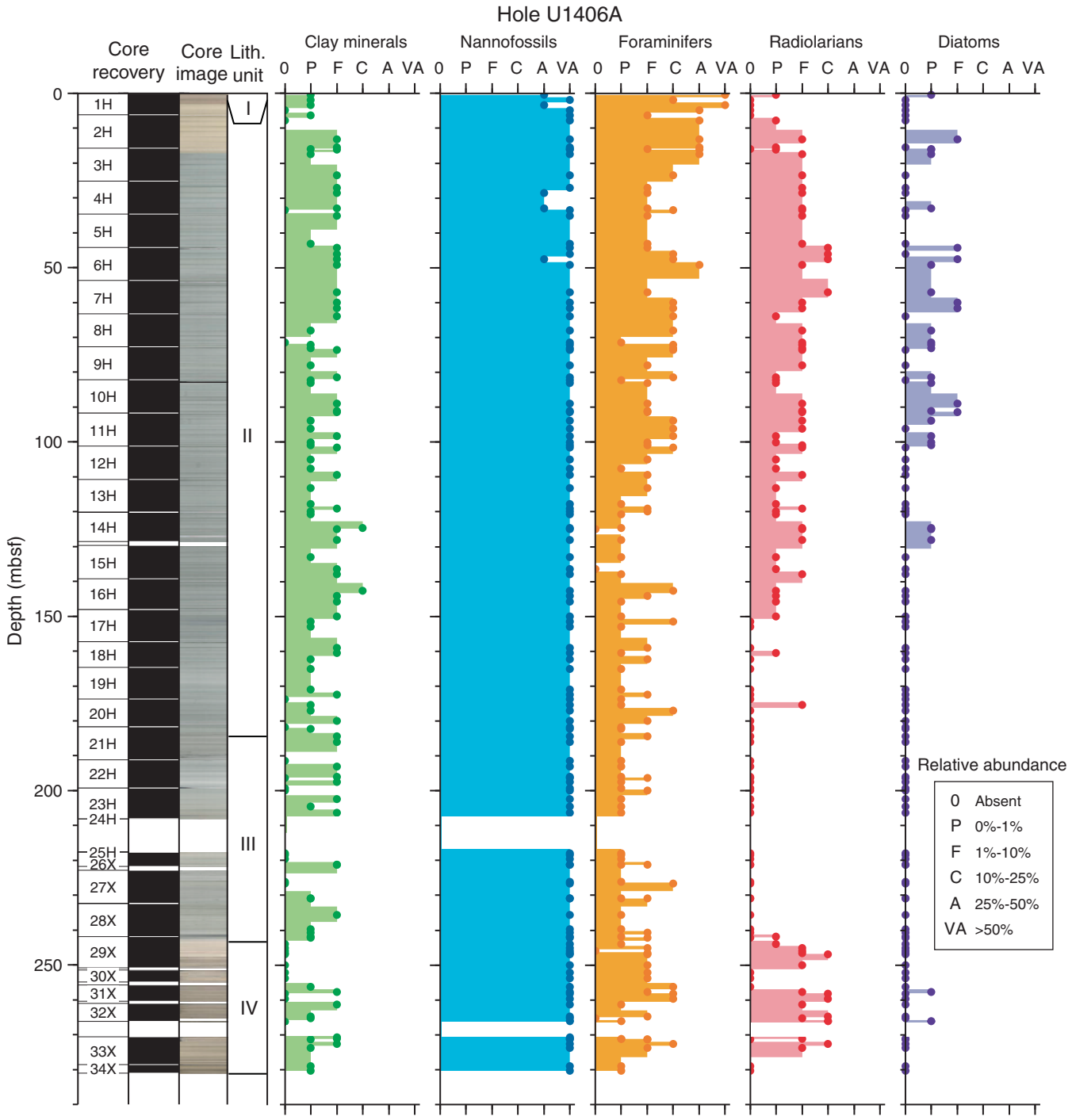

Figure F9. Plots of smear slide results of major biogenic and lithologic components and their relative abundance, Hole U1406B. VA = very abundant, A = abundant, C = common, F = few, P = present.

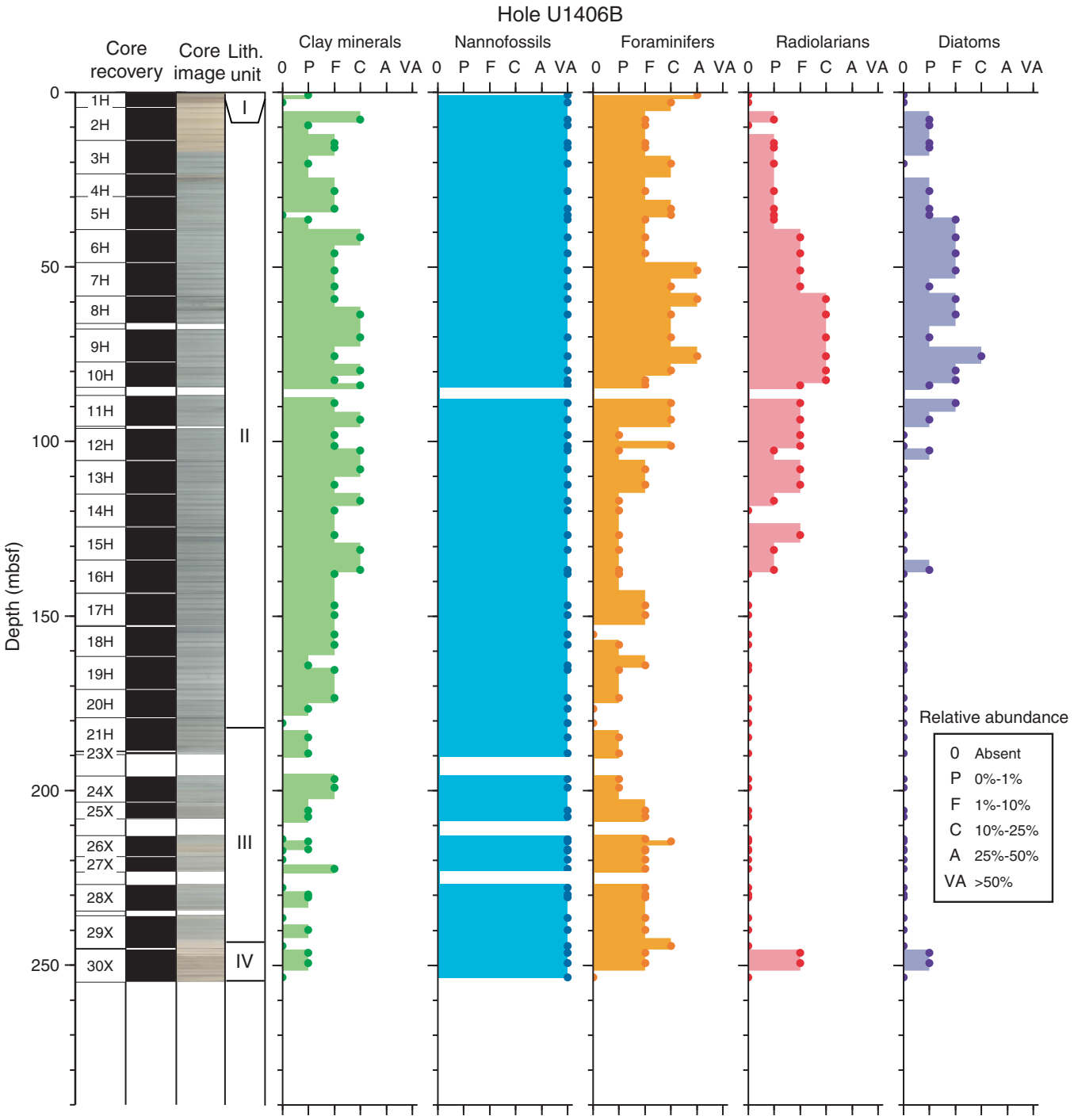

Figure F10. Plots of smear slide results of major biogenic and lithologic components and their relative abundance, Hole U1406C. VA = very abundant, A = abundant, C = common, F = few, P = present.

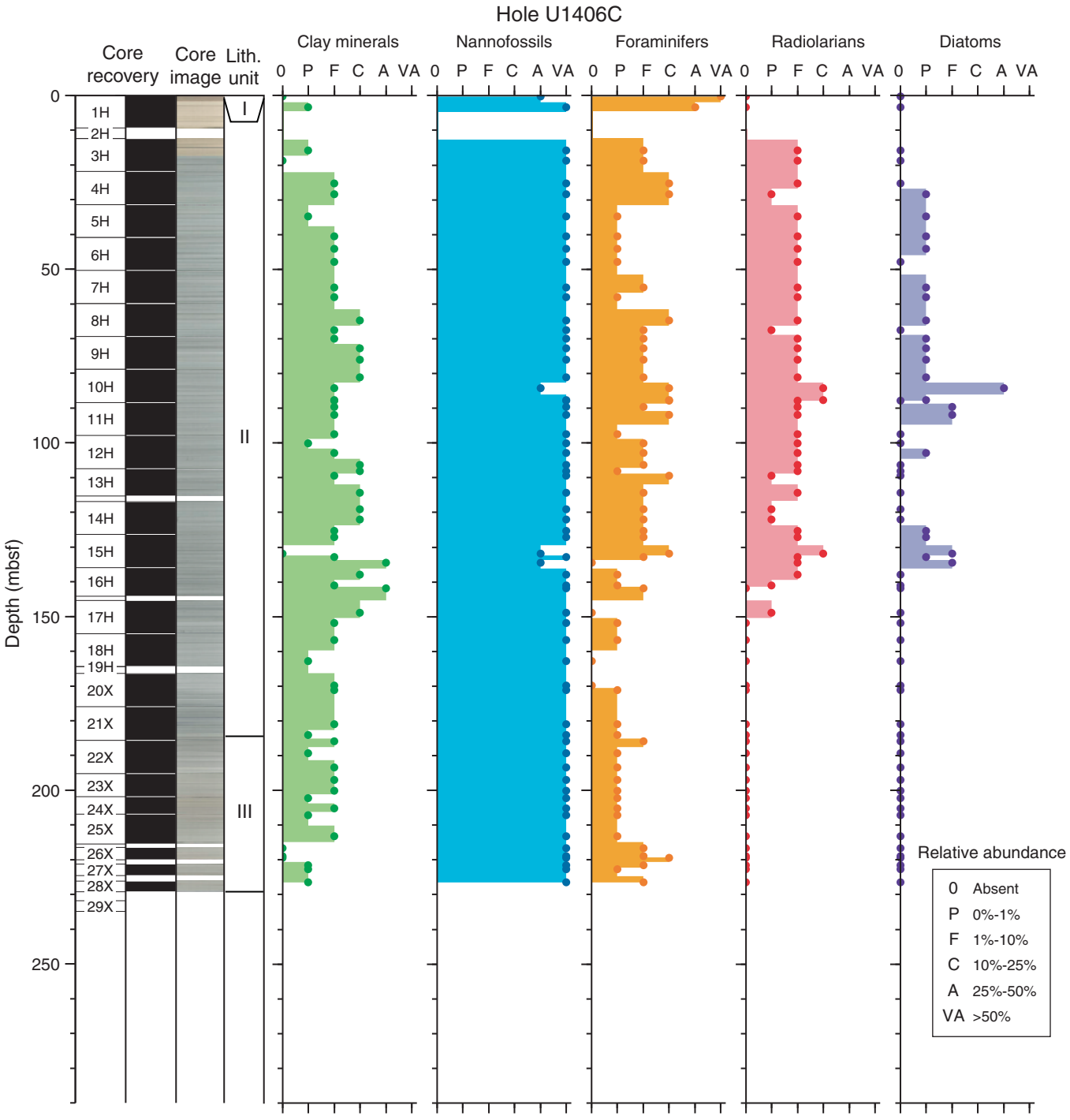

Figure F11. Plot and core images of lithologic expression of the Oligocene–Miocene transition, Site U1406. Red lines indicate splice ties (see **"Stratigraphic correlation"**). The Oligocene/Miocene boundary is approximated by the first occurrence and last occurrence datums of the nannofossil taxon *Sphenolithus delphix* and defined by the base of Chron C6Cn.2n.

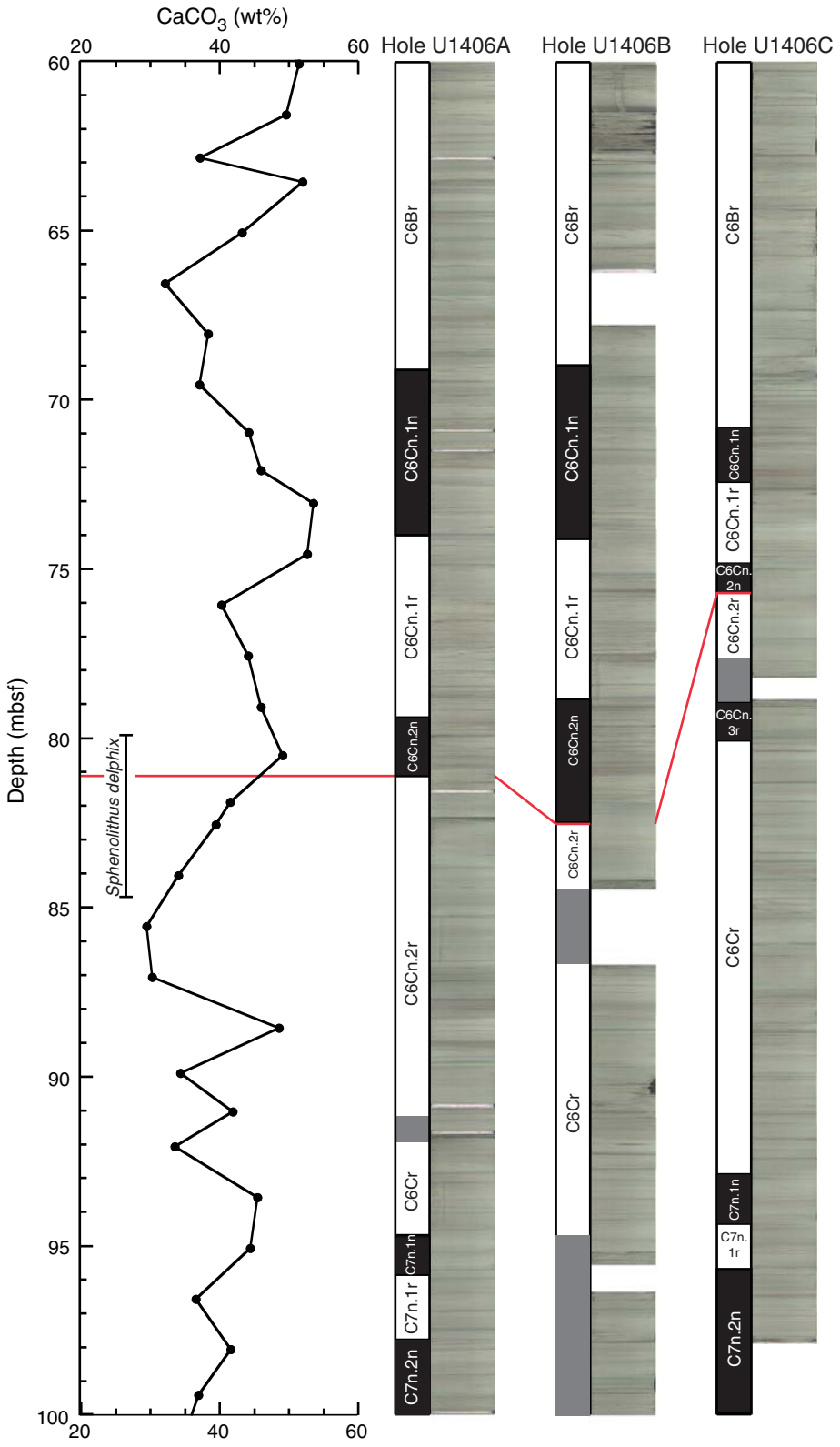

Figure F12. Plots and core images of lithologic expression of the Eocene–Oligocene transition (EOT), Site U1406. The EOT is approximately indicated by yellow shading. **A–D.** Examples of the four major sediment textures.

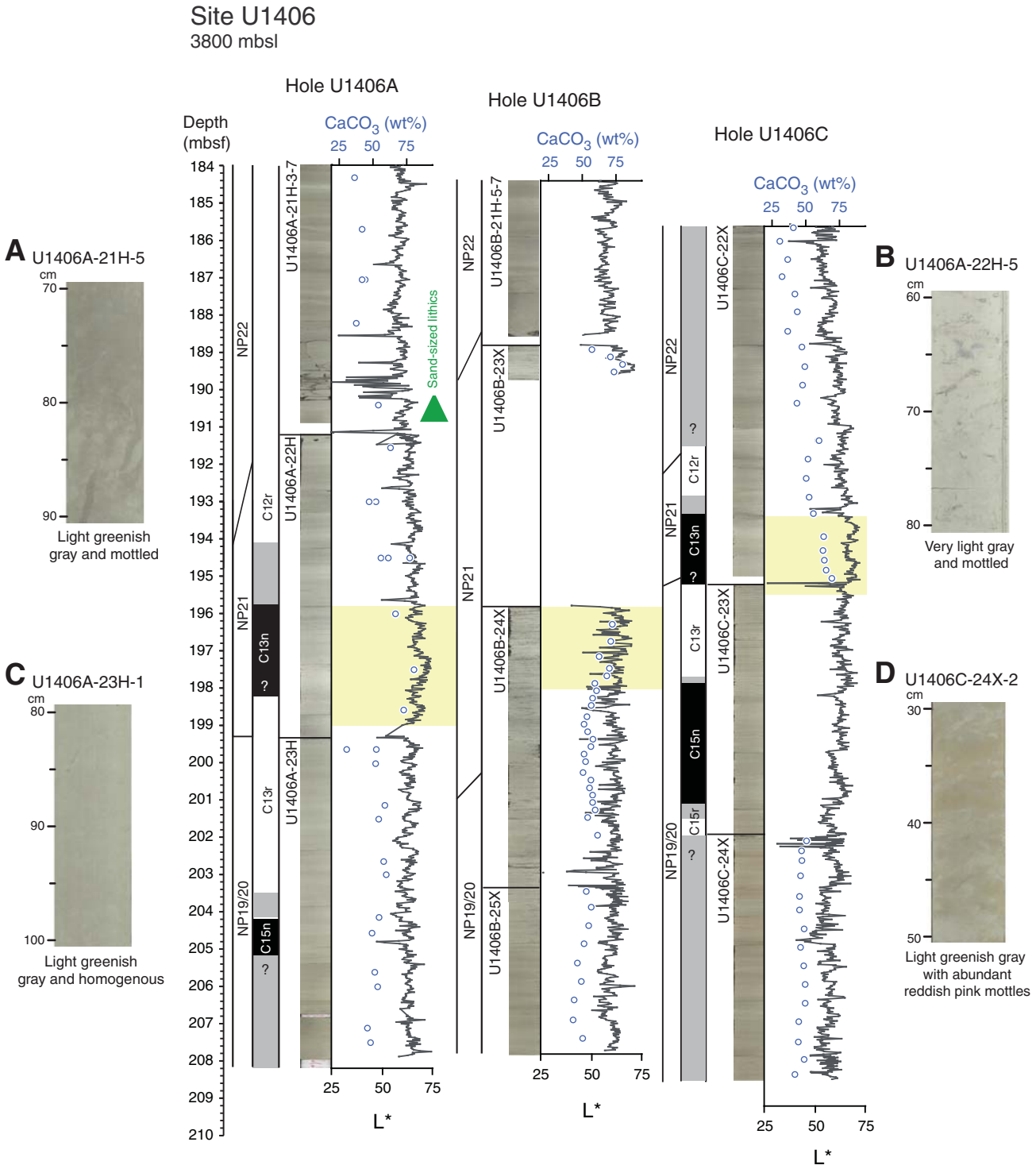

Figure F13. Photomicrographs of sand-sized lithic grains from Oligocene nannofossil Zones NP22–NP23. **A.** Overview of lithic grain types on a picking tray, showing abundant (angular) quartz grains and other mineral phases (Sample 342-U1406A-18H-CC). **B, C.** Sample 342-U1406A-21H-CC; (B) larger rock fragment; (C) yellow quartz grain. **D–I.** Sample 342-U1406A-18H-CC; (D) yellow quartz grain; (E) orange-brown and two transparent highly angular quartz grains with small rock fragment in the lower right corner; (F) pinkish brown quartz; (G) larger red mineral phase; (H) transparent highly angular quartz grains (top) and fish debris (bottom); (I) two transparent highly angular quartz grains.

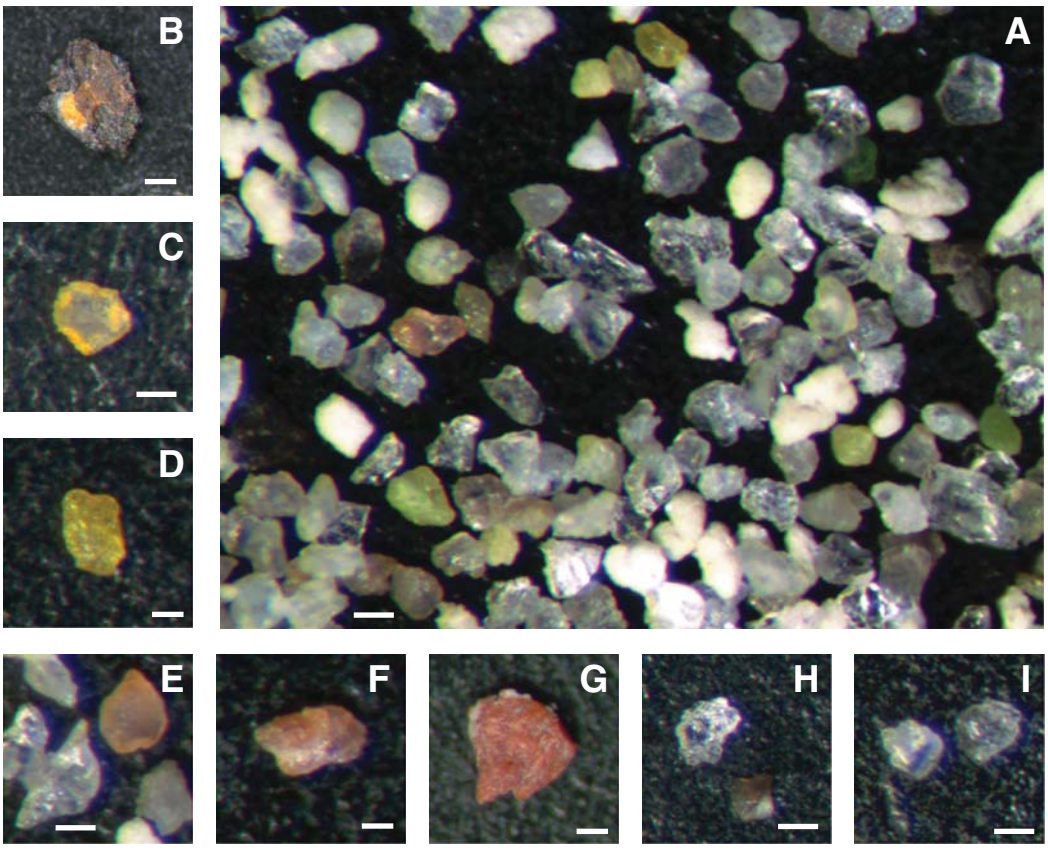

Figure F14. Close-up image of a copper vein (interval 342-U1406B-28X-3, 99–101 cm). Inset is euhedral copper from a smear slide in the same location.

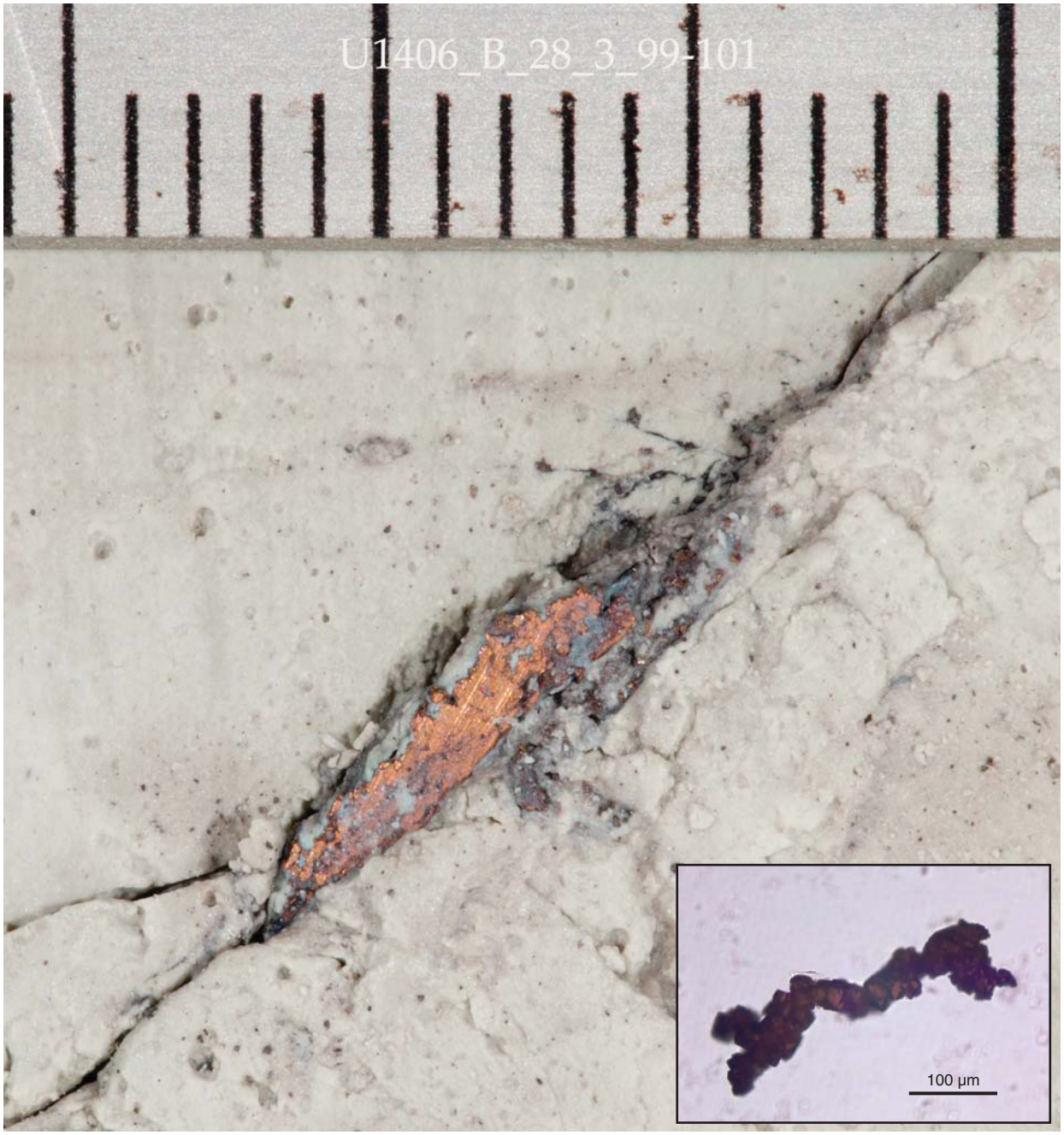

Figure F15. Integrated calcareous and siliceous microfossil biozonation, Site U1406.

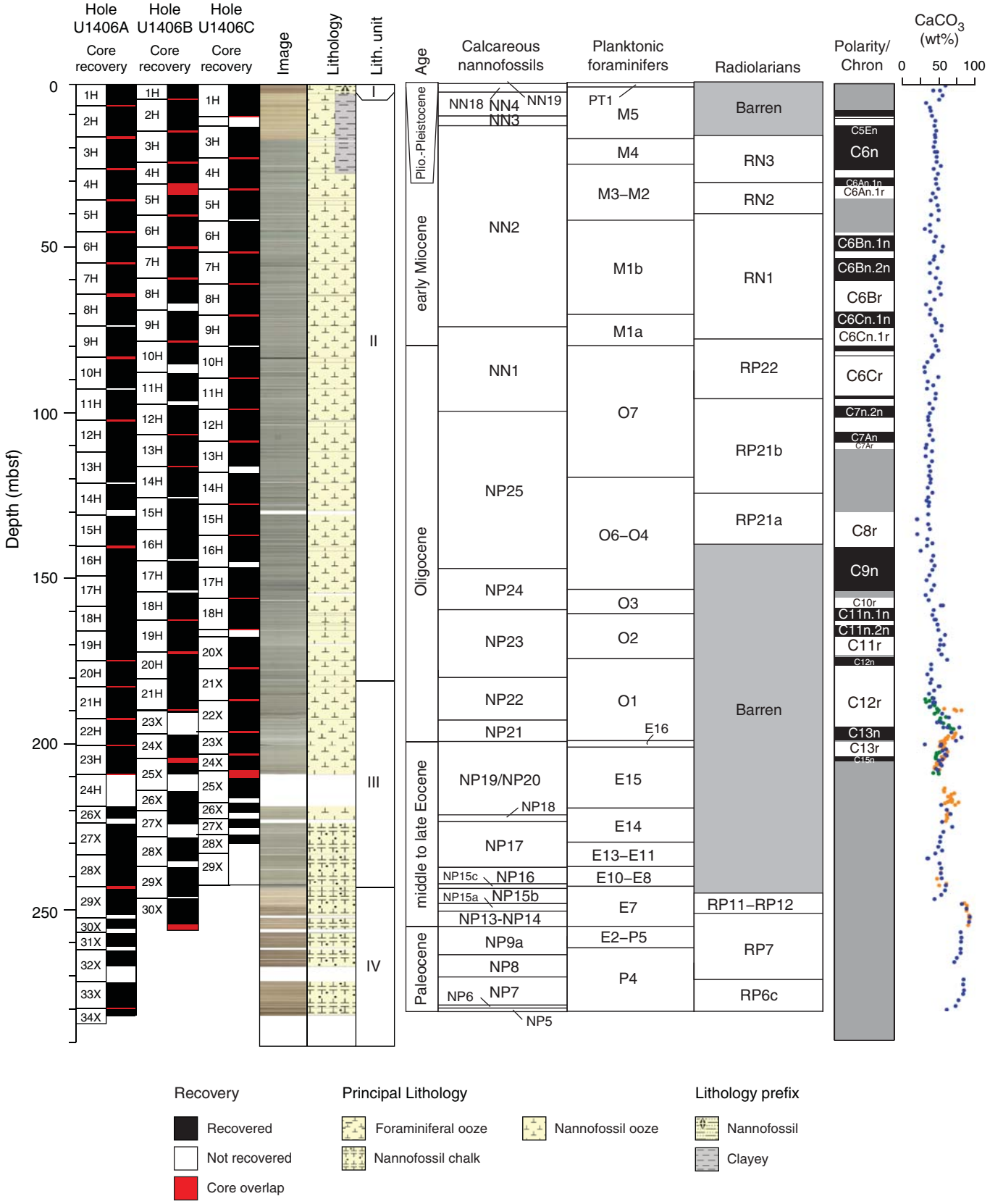

Figure F16. Plots of group abundance and preservation of calcareous and siliceous microfossils, Site U1406. Solid and open symbols represent Holes U1406A and U1406B, respectively. Abundance: B = barren, P = present, R = rare, F = few, C = common, A = abundant, D = dominant. Preservation: P = poor, M = moderate, G = good, VG = very good.

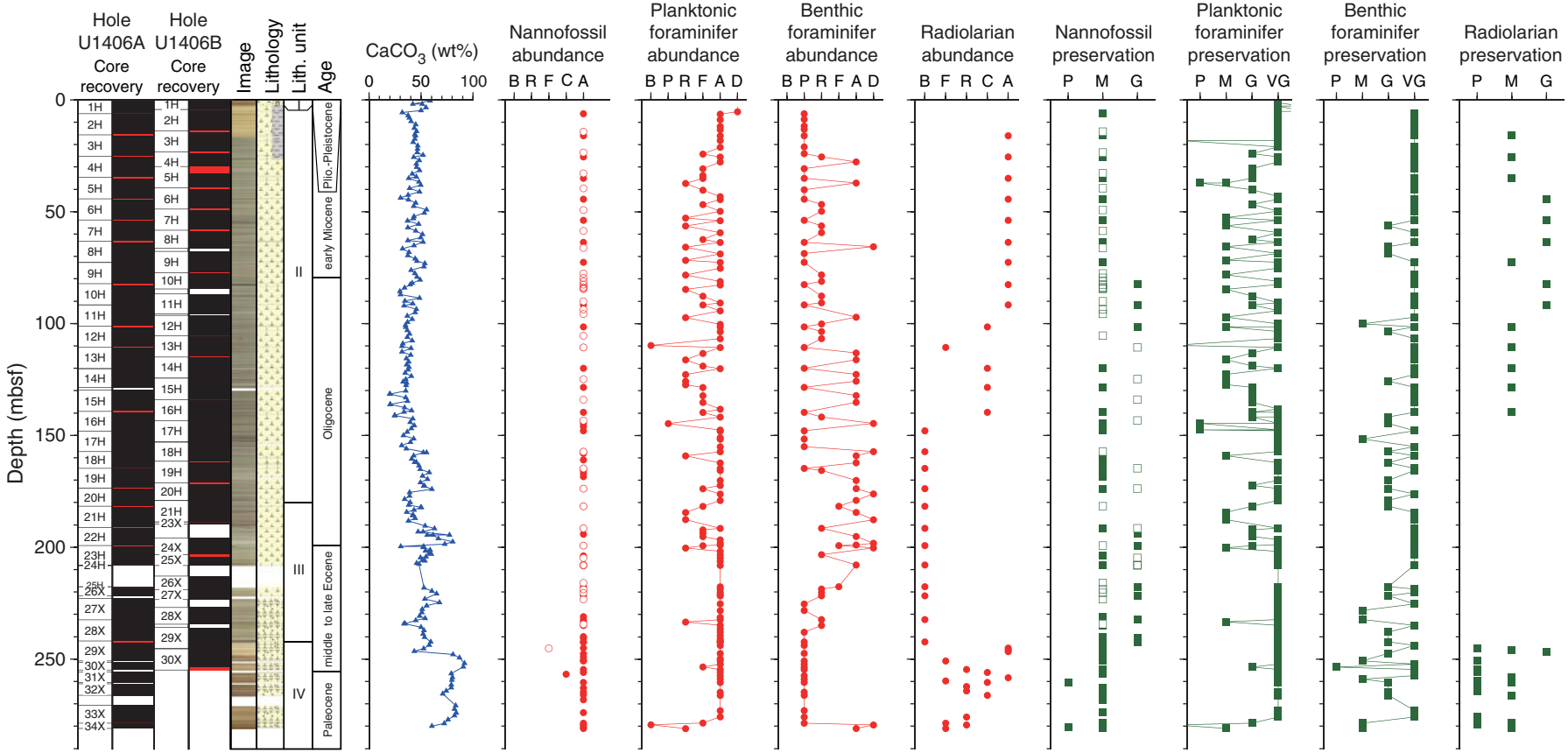

Figure F17. Plots of downhole variation of magnetic susceptibility and paleomagnetism data, Hole U1406A. Magnetization intensity, inclination, and declination are after 20 mT demagnetization. Only oriented advanced piston corer (APC) intervals show directions in geographic coordinates. Directions from all other intervals are shown in sample coordinates. For discrete sample data, if the samples were analyzed by principal component analysis (PCA; Kirschvink, 1980), then directions are shown according to PCA declination and inclination. Otherwise, directions following 20 mT demagnetization are shown. XCB = extended core barrel. Polarity: black = normal chron, white = reversed chron, gray = unidentified interval.

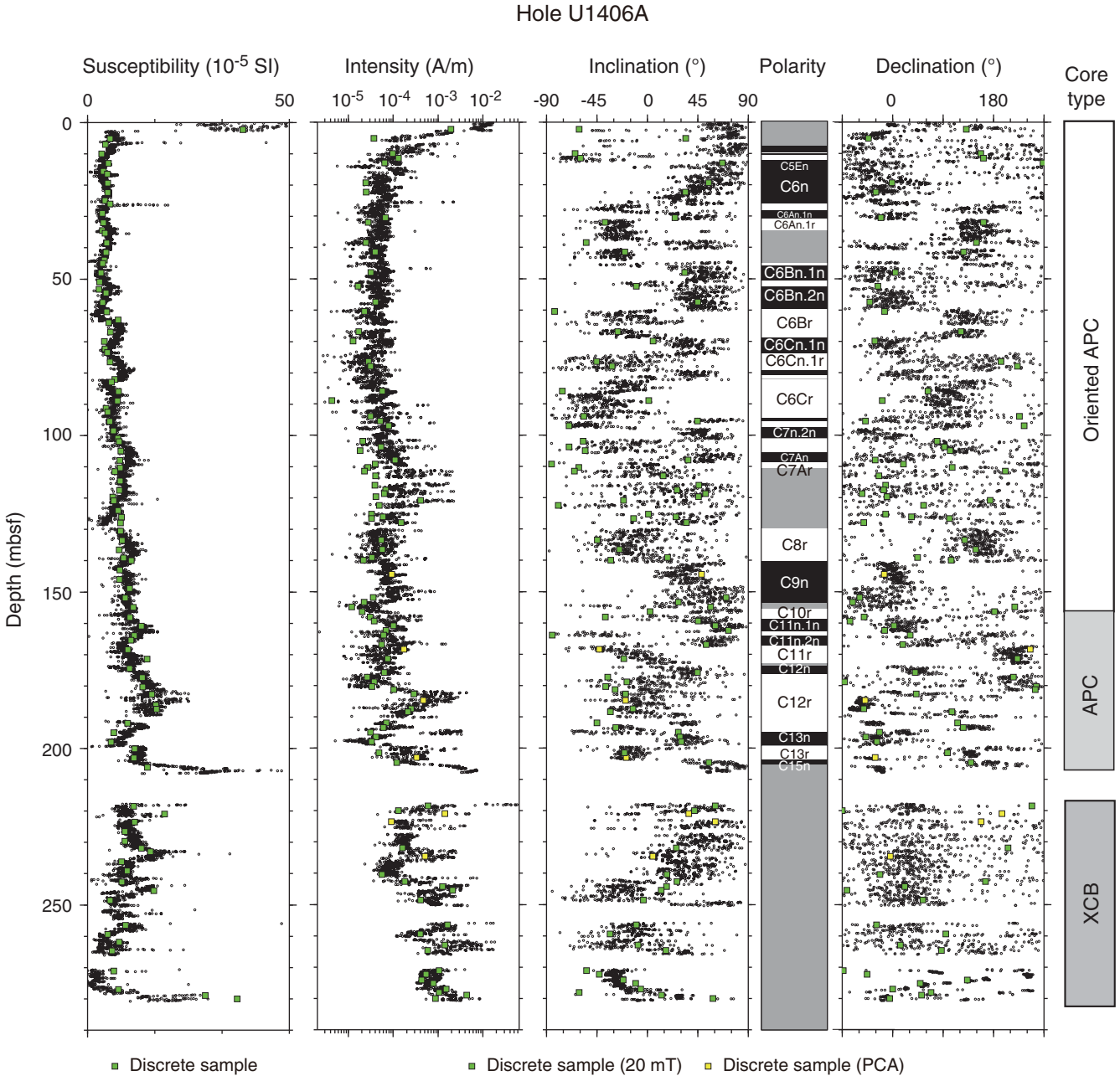

Figure F18. Plots of downhole variation of magnetic susceptibility and paleomagnetism data, Hole U1406B. Magnetization intensity, inclination, and declination are after 20 mT demagnetization. Only oriented advanced piston corer (APC) intervals show directions in geographic coordinates. Directions from all other intervals are shown in sample coordinates. For discrete sample data, if the samples were analyzed by principal component analysis (PCA; Kirschvink, 1980), then directions are shown according to PCA declination and inclination. Otherwise, directions following 20 mT demagnetization are shown. XCB = extended core barrel. Polarity: black = normal chron, white = reversed chron, gray = unidentified interval.

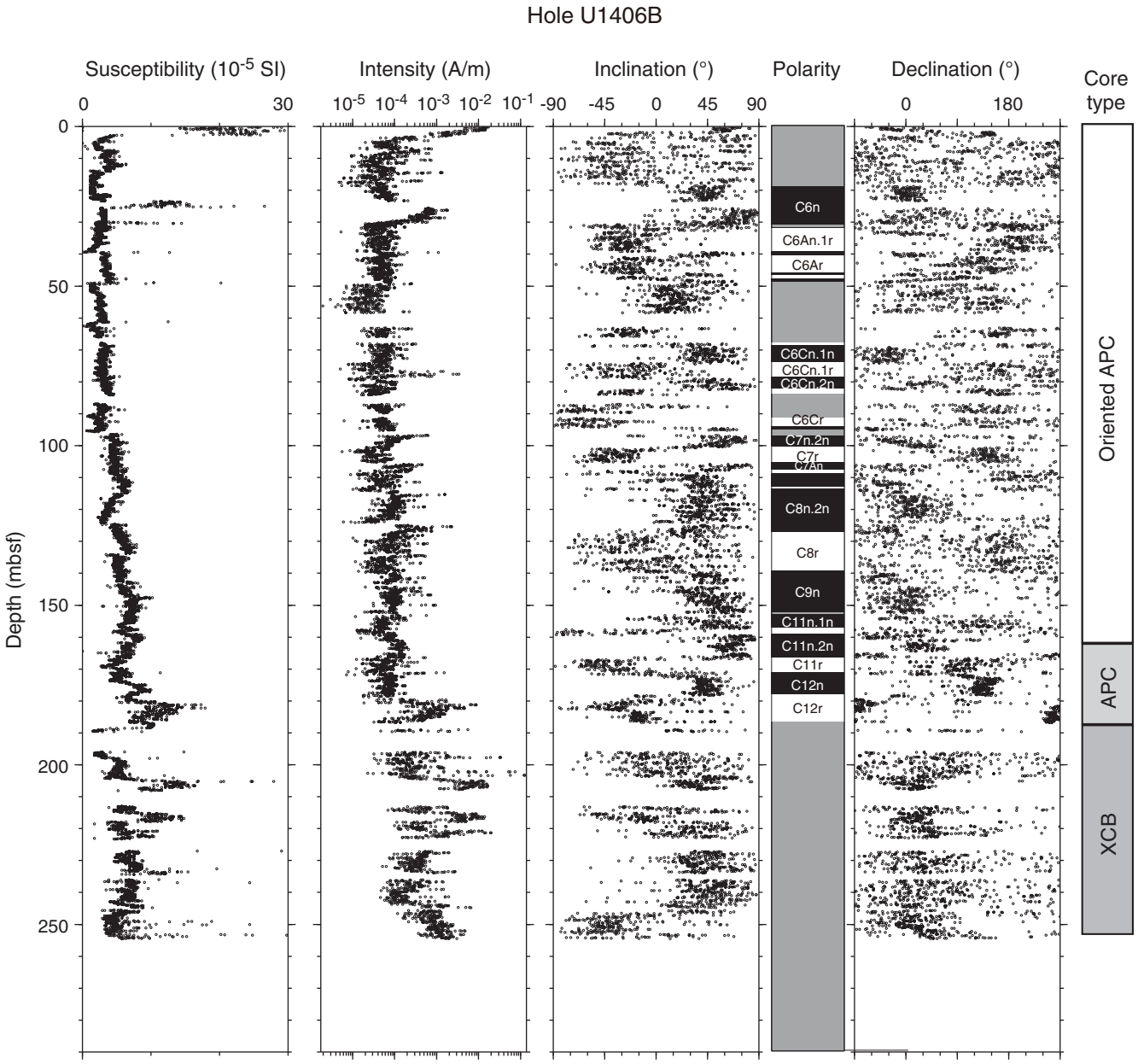

Figure F19. Plots of downhole variation of magnetic susceptibility and paleomagnetism data, Hole U1406C. Magnetization intensity, inclination, and declination are after 20 mT demagnetization. Directions are shown in sample coordinates. APC = advanced piston corer, XCB = extended core barrel. Polarity: black = normal chron, white = reversed chron, gray = unidentified interval.

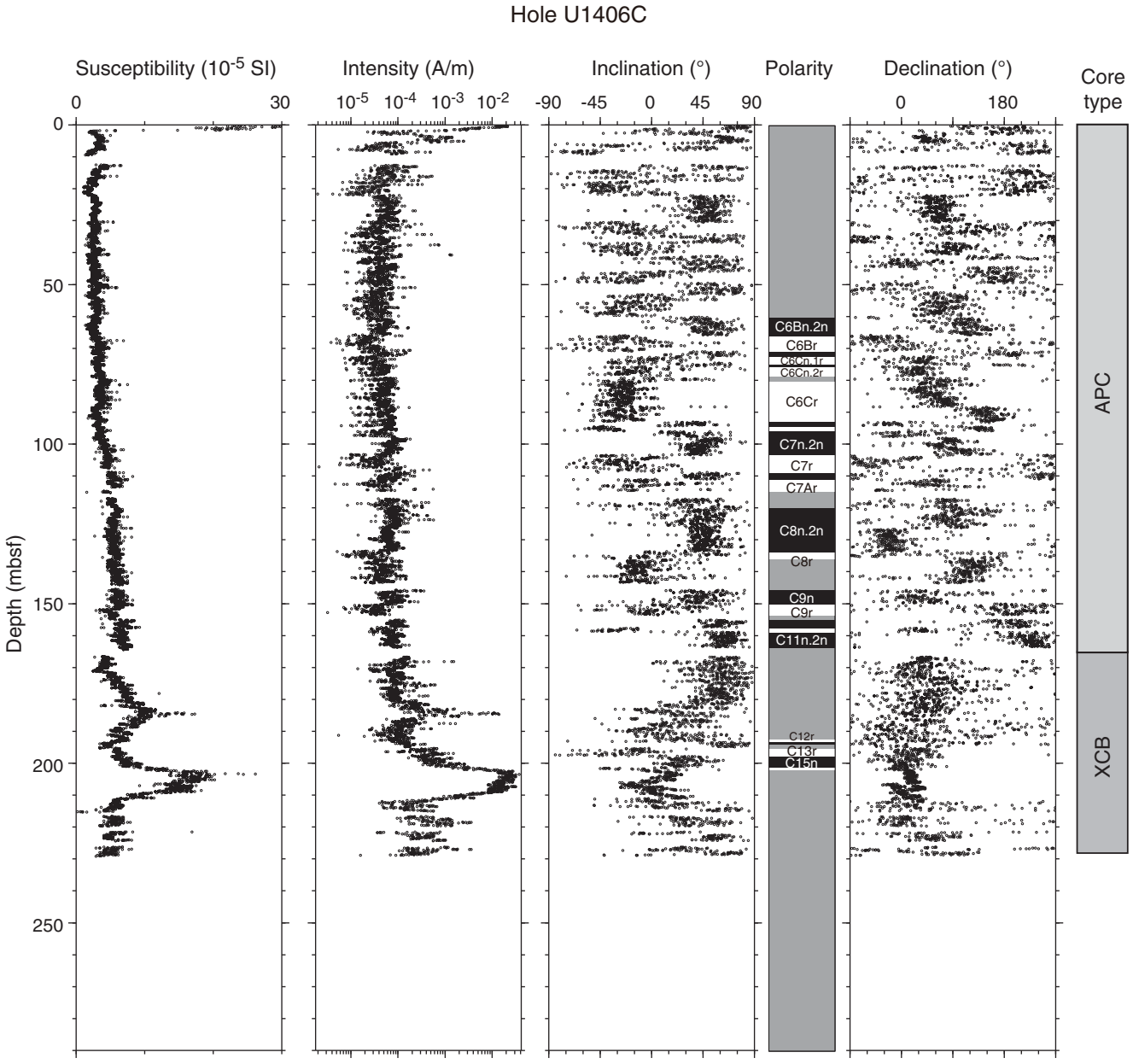

Figure F20. Plots of representative alternating field (AF) demagnetization results for discrete paleomagnetism samples, Site U1406. Upper plots show intensity variation with progressive demagnetization, and lower plots show vector endpoints of paleomagnetism directions on orthogonal vector diagrams (i.e., Zijderveld plots). Vector diagrams indicate reasonably resolved characteristic remanent magnetization (ChRM) directions from the (**A**) advanced piston corer and (**B**) extended core barrel intervals, whereas (**C**) some samples from the XCB intervals show complex behavior. Solid circles = horizontal projections, open circles = vertical projections, gray circles = data not used to calculate the ChRM direction, black dashed line = ChRM direction. Inc = inclination, Dec = declination, MAD = maximum angle of deviation.

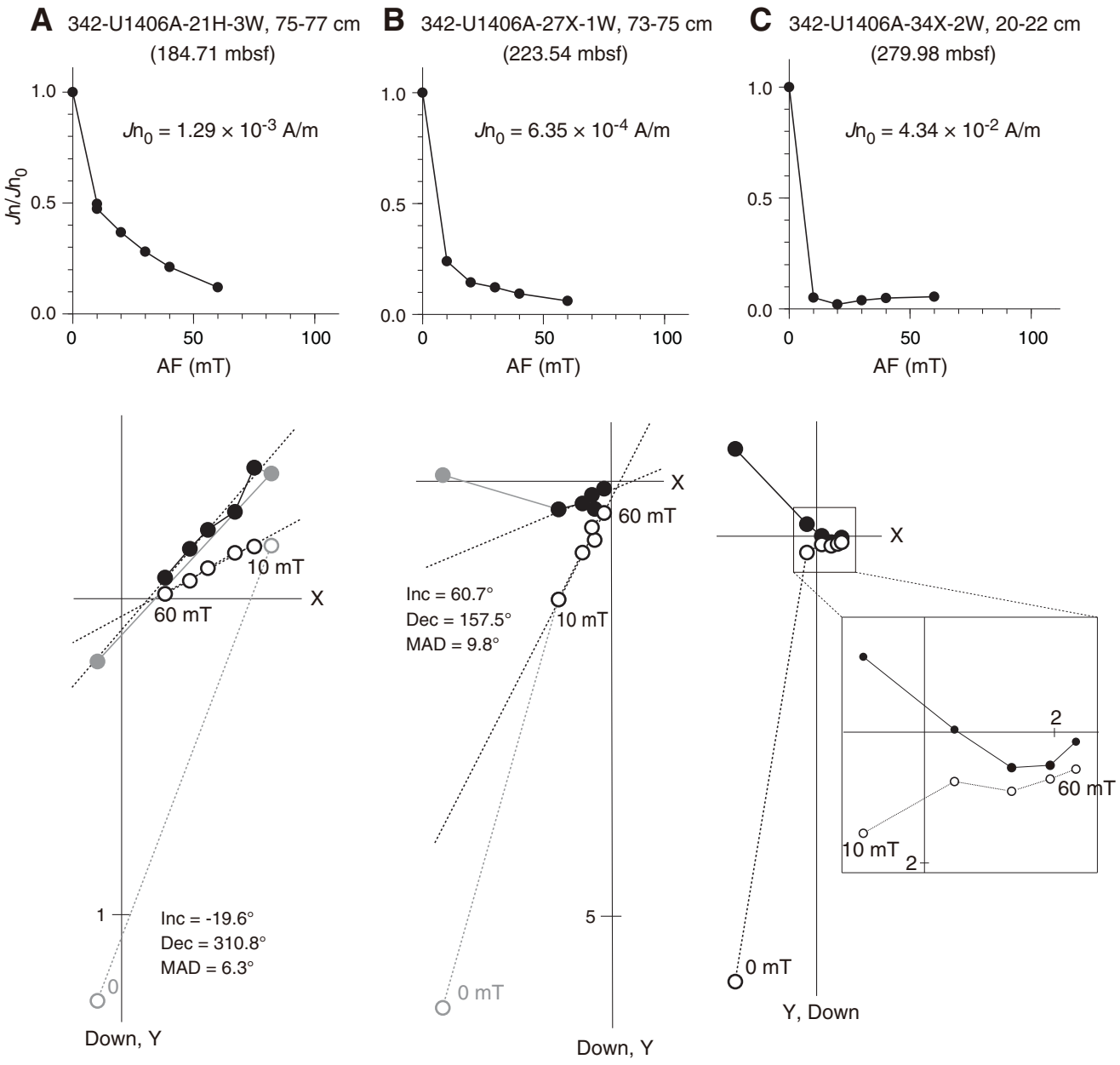

Figure F21. Illustration of magnetostratigraphy, Site U1406. Core recovery: black = recovered core, red = core overlap.

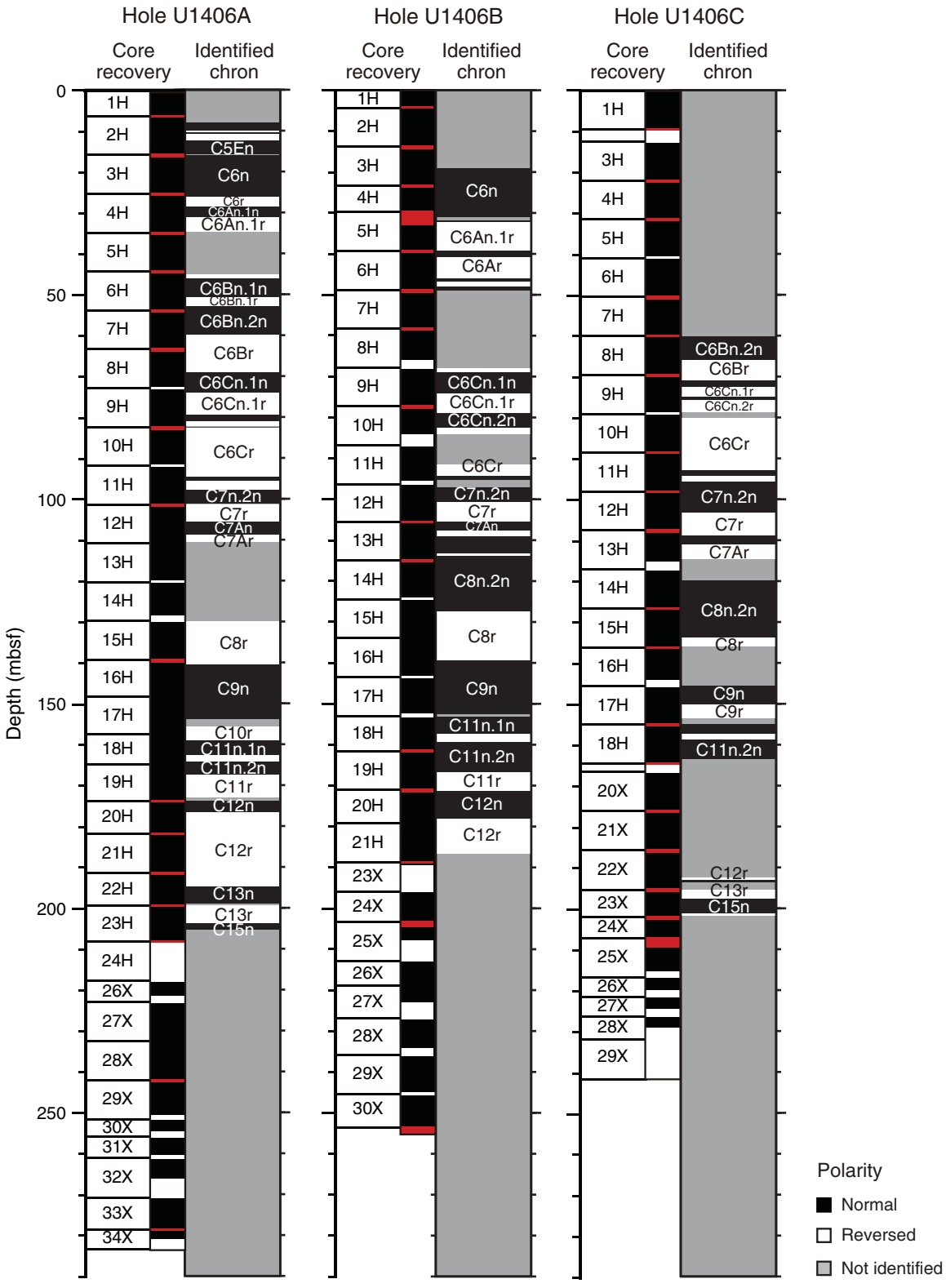

Figure F22. Plots of anisotropy of magnetic susceptibility vs. depth, Hole U1406A. Separation of eigenvalues is related to the shape and degree of the magnetic fabric (see **"Paleomagnetism"** in the "Methods" chapter [Norris et al., 2014a]). For example, if τ_1 and τ_2 are close or indistinguishable but distinct from τ_3, then the bulk fabric is oblate. Lithostratigraphic units are described in **"Lithostratigraphy."** Eigenvalues: τ_1 = maximum, τ_2 = intermediate, τ_3 = minimum. V_3 = minimum eigenvector, P = degree of anisotropy (τ_1/τ_3). APC = advanced piston corer, XCB = extended core barrel.

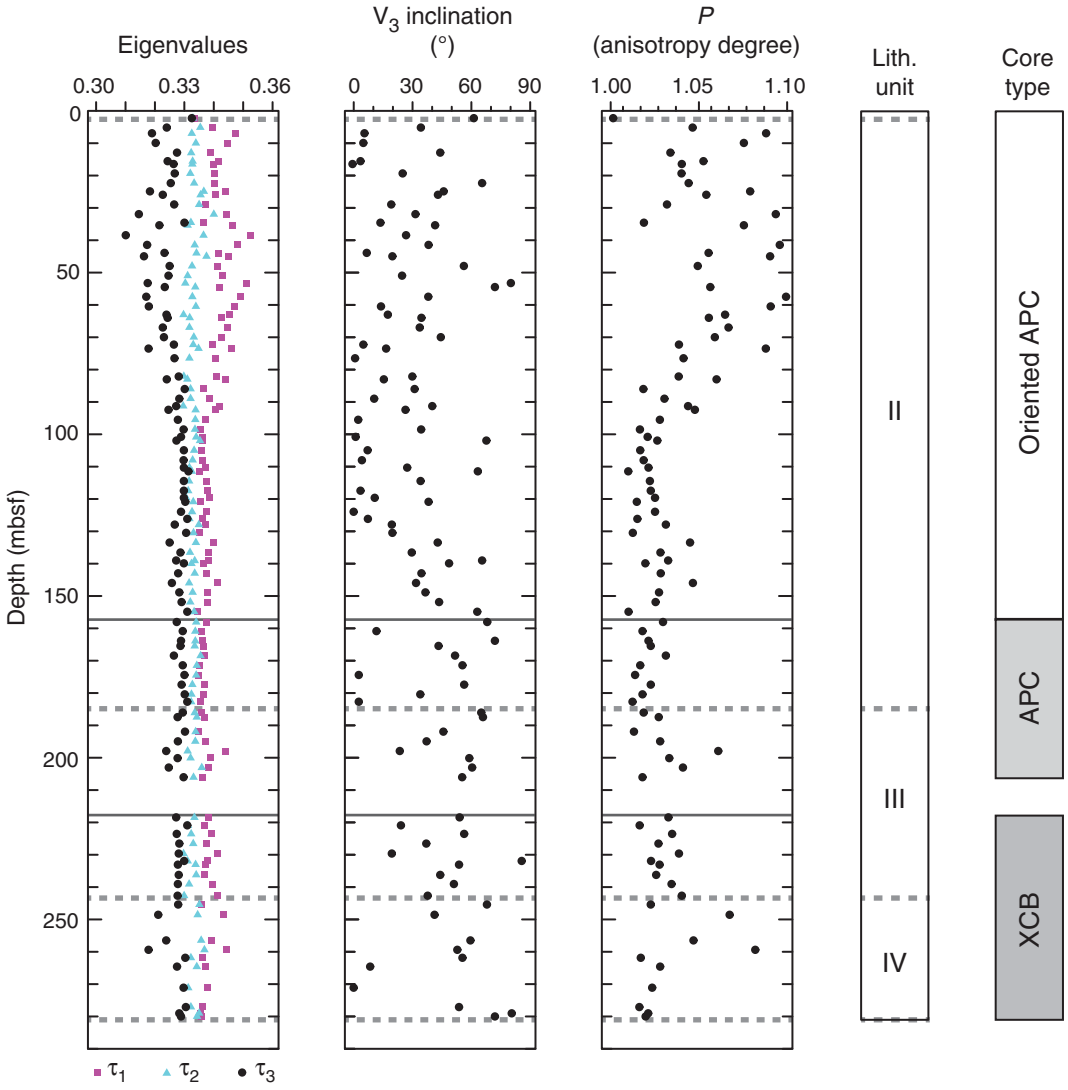

Figure F23. Plot of age-depth model for Hole U1406A showing biostratigraphic and magnetostratigraphic datums. Also shown are estimated linear sedimentation rates for line segments based on the datums listed in Table T16.

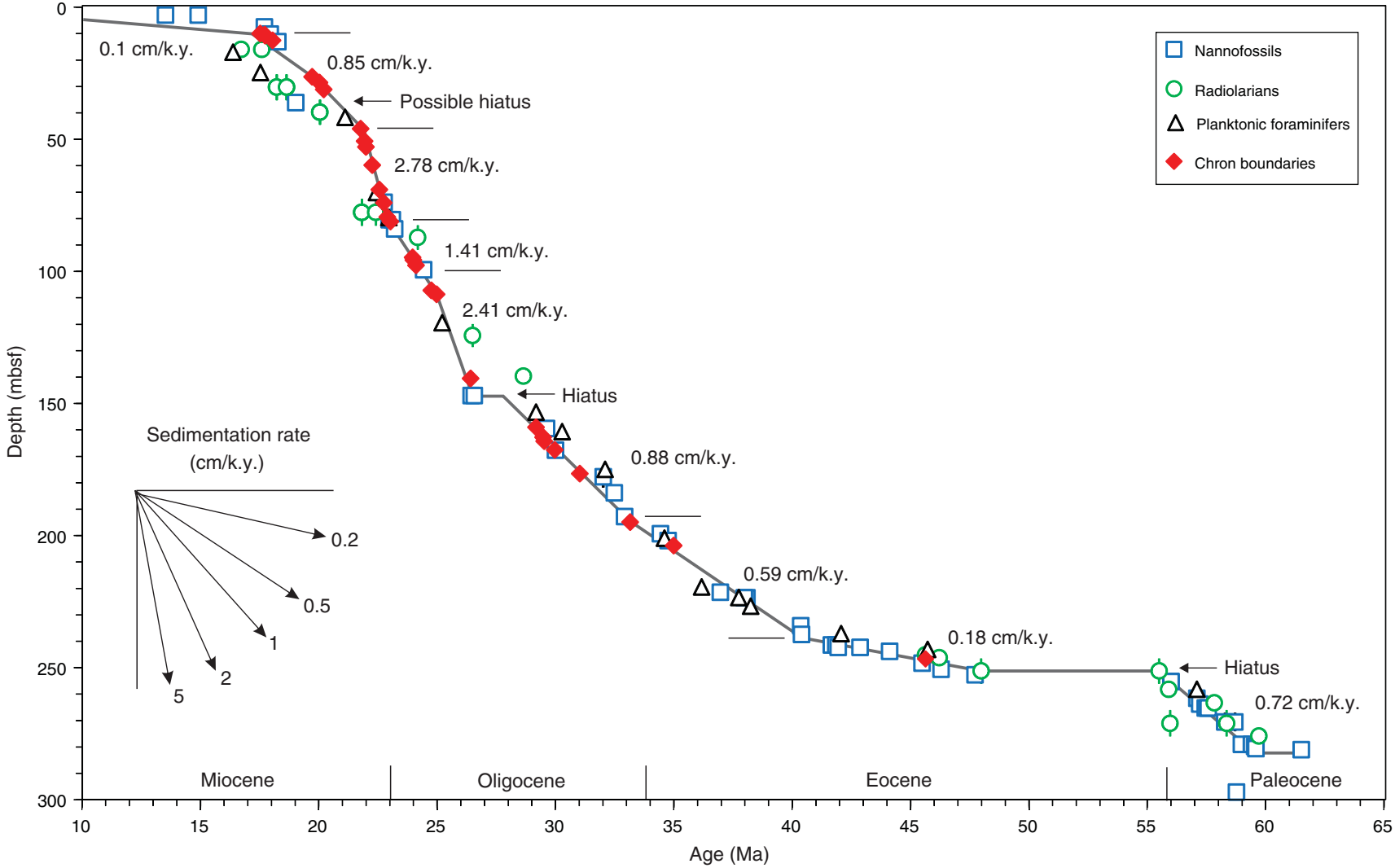

Figure F24. Plots of linear sedimentation rate (LSR), dry bulk density (DBD), carbonate content, and mass accumulation rate (MAR) at 200 k.y. time steps, Hole U1406A. Solid black diamonds show the inflection points in estimated LSR, DBD, and carbonate content. Geologic ages are shown on the GTS2012 timescale (Gradstein et al., 2012). CAR = carbonate mass accumulation rate, nCAR = noncarbonate mass accumulation rate.

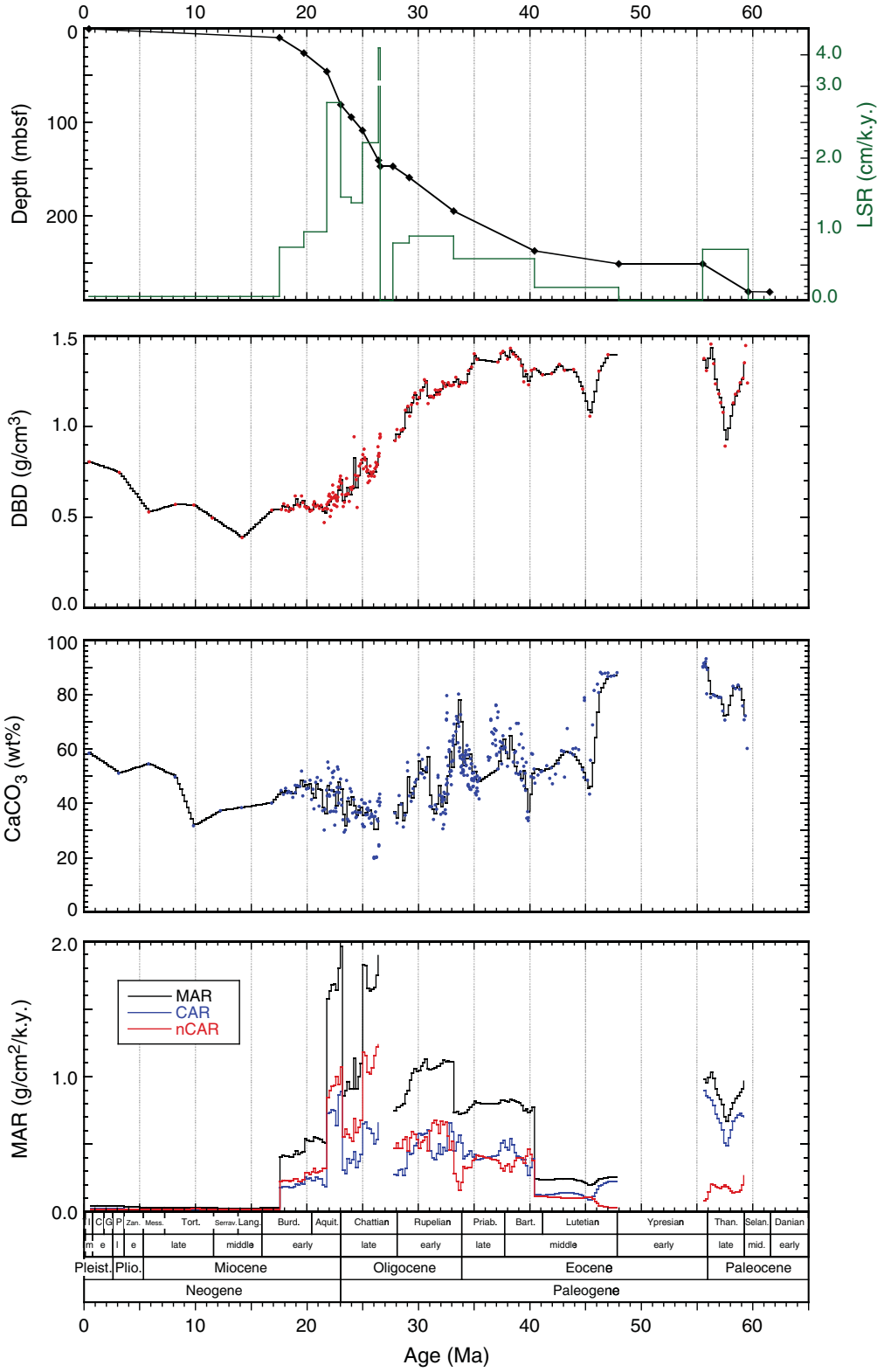

Figure F25. Plot of methane concentrations, Hole U1406A. Lithostratigraphic Unit I is Pleistocene foraminiferal sand and nannofossil ooze, Unit II is Oligocene–Miocene nannofossil ooze, Unit III is middle Eocene–early Oligocene nannofossil chalk, and Unit IV is Paleocene–middle Eocene nannofossil chalk with foraminifers.

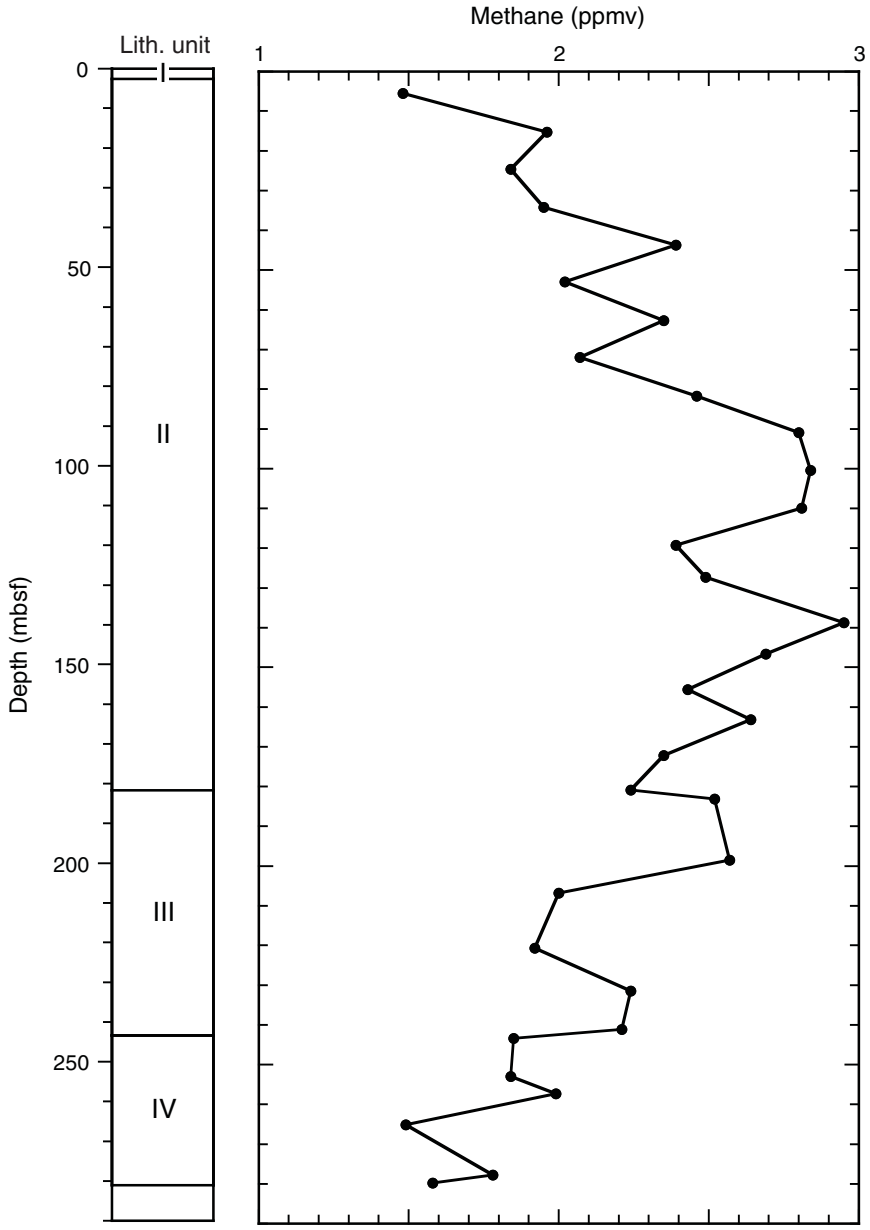

Figure F26. Plots of interstitial water constituent concentrations, Hole U1406A. Solid gray horizontal lines represent the unrecovered chert sequence that appears to act as an aquiclude. Dashed gray lines designate distinct zones of geochemical trends.

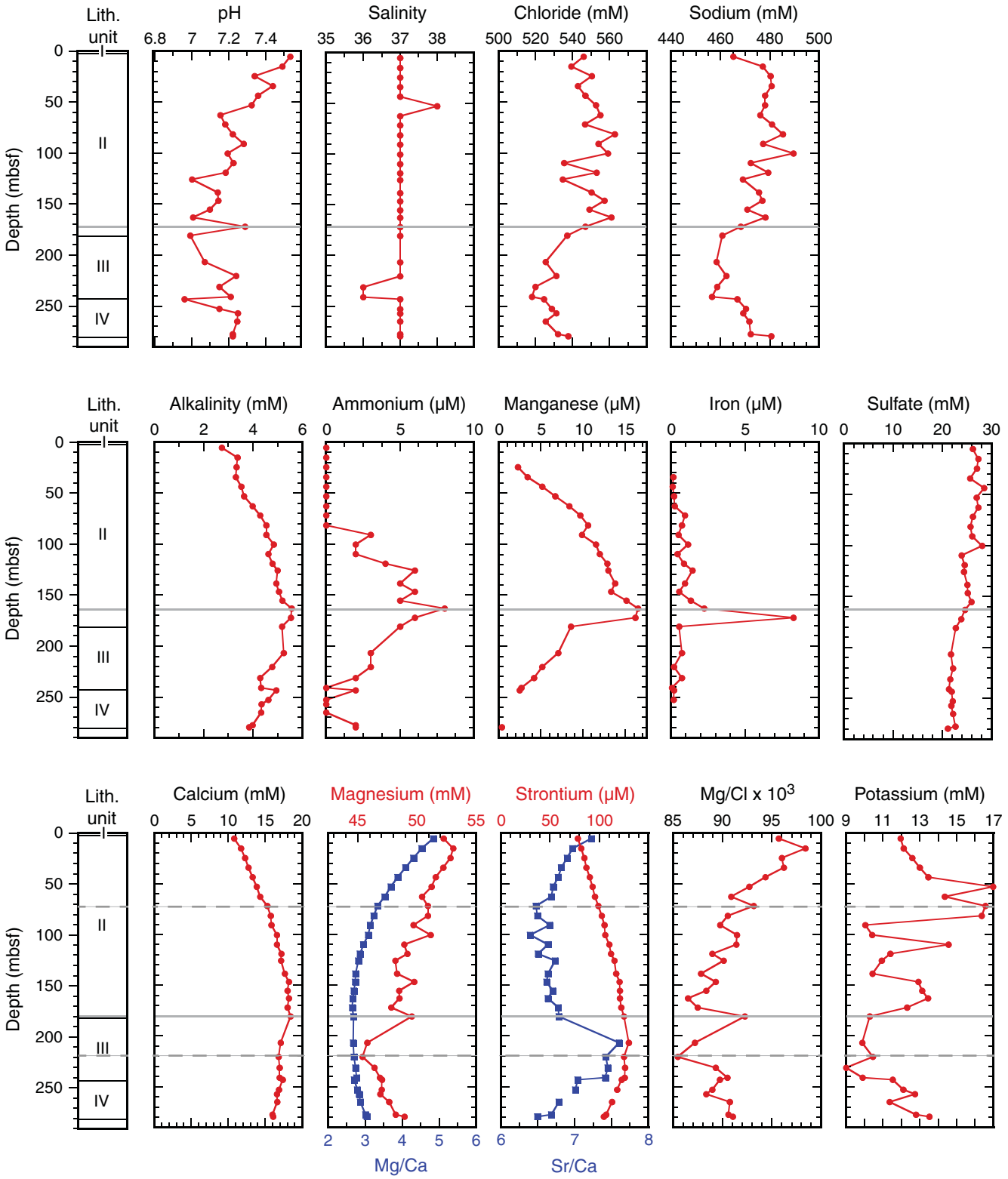

Figure F27. Plots of sedimentary carbonate, total organic carbon (TOC), and total nitrogen contents for Hole U1406A (red) and sedimentary carbonate contents for Holes U1406B (blue) and U1406C (green). Core recovery: black = recovered, white = not recovered, red = overlap.

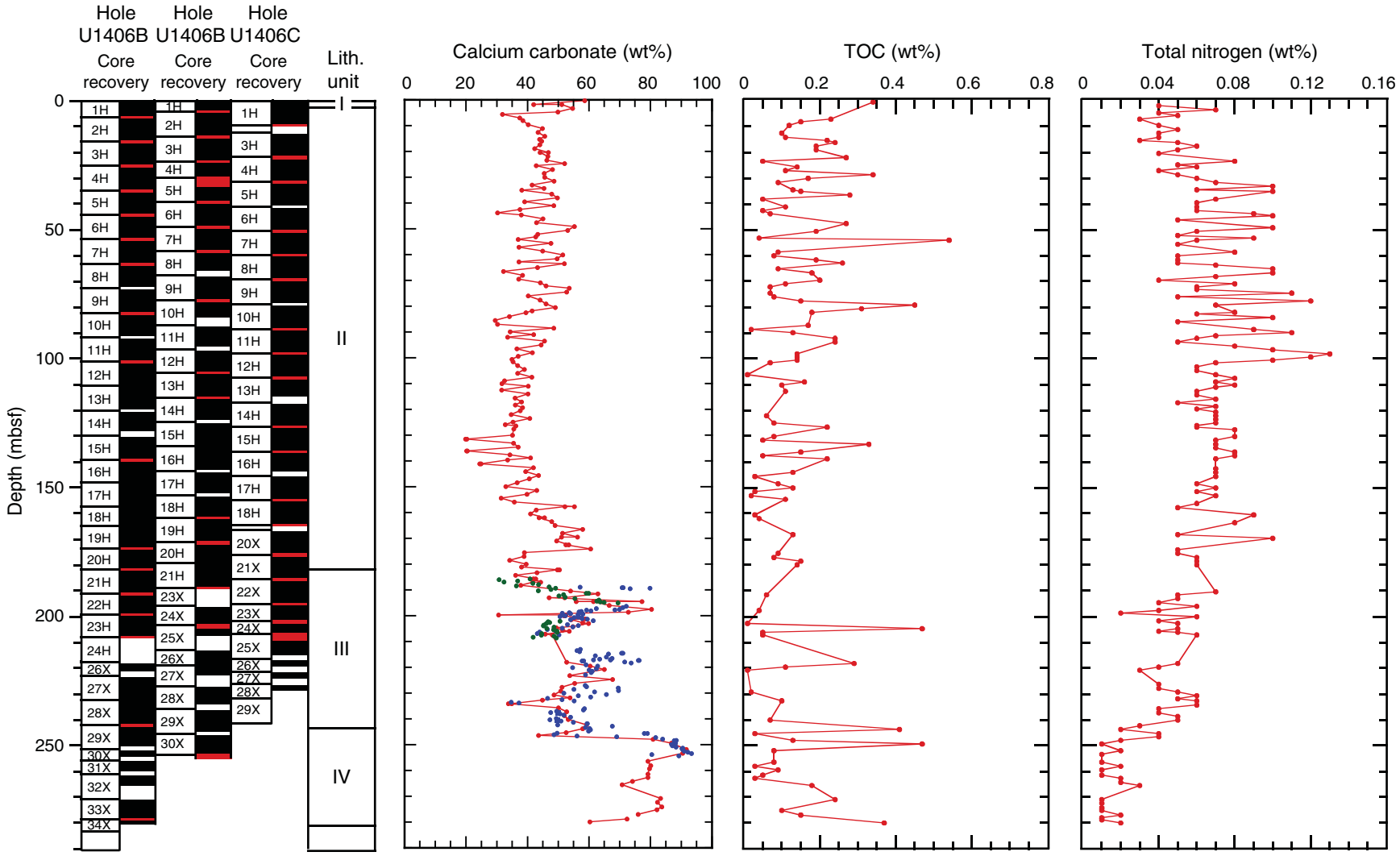

Figure F28. Plots of magnetic susceptibility (MS), bulk density (gray line = GRA density from Whole-Round Multisensor Logger, black circles = moisture and density analysis from discrete samples), porosity, water content, and grain density, Site U1406. Core recovery: black = recovered, white = not recovered, red = overlap. Horizontal gray lines indicate lithostratigraphic unit boundaries (see **"Lithostratigraphy"**). APC = advanced piston corer, DI = drilled interval, XCB = extended core barrel.

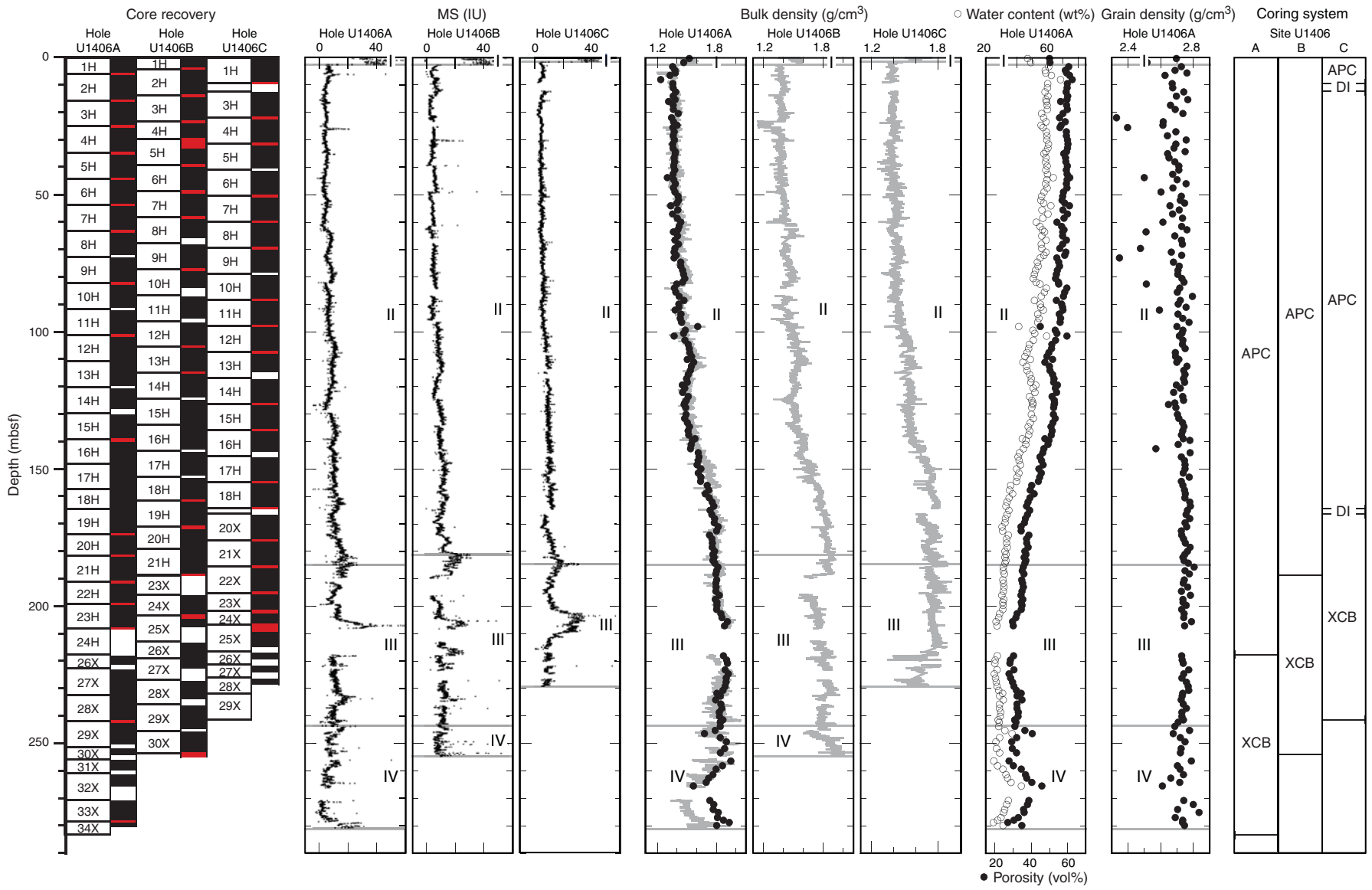

Figure F29. Plots of magnetic susceptibility (MS), *P*-wave velocity (gray line = *P*-wave logger data from whole-round sections, black circles = *P*-wave caliper data from working section halves), and natural gamma radiation (NGR), Site U1406. Core recovery: black = recovered, white = not recovered, red = overlap. Horizontal gray lines indicate lithostratigraphic unit boundaries (see **"Lithostratigraphy"**). APC = advanced piston corer, DI = drilled interval, XCB = extended core barrel.

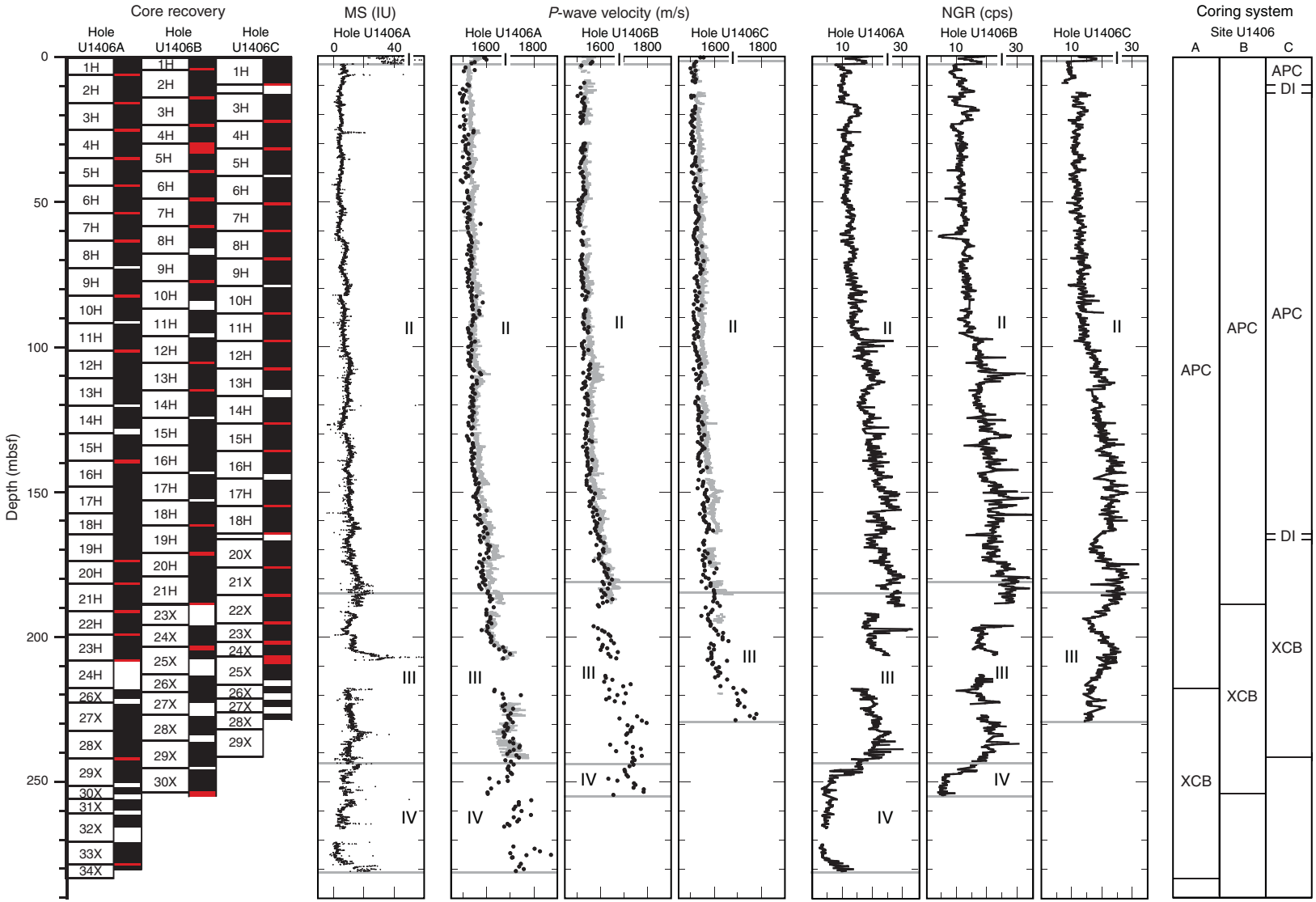

Figure F30. Plots of magnetic susceptibility (MS) and color reflectance (a*, b*, and L*), Site U1406. Core recovery: black = recovered, white = not recovered, red = overlap. Horizontal gray lines indicate lithostratigraphic unit boundaries (see **"Lithostratigraphy"**). APC = advanced piston corer, DI = drilled interval, XCB = extended core barrel.

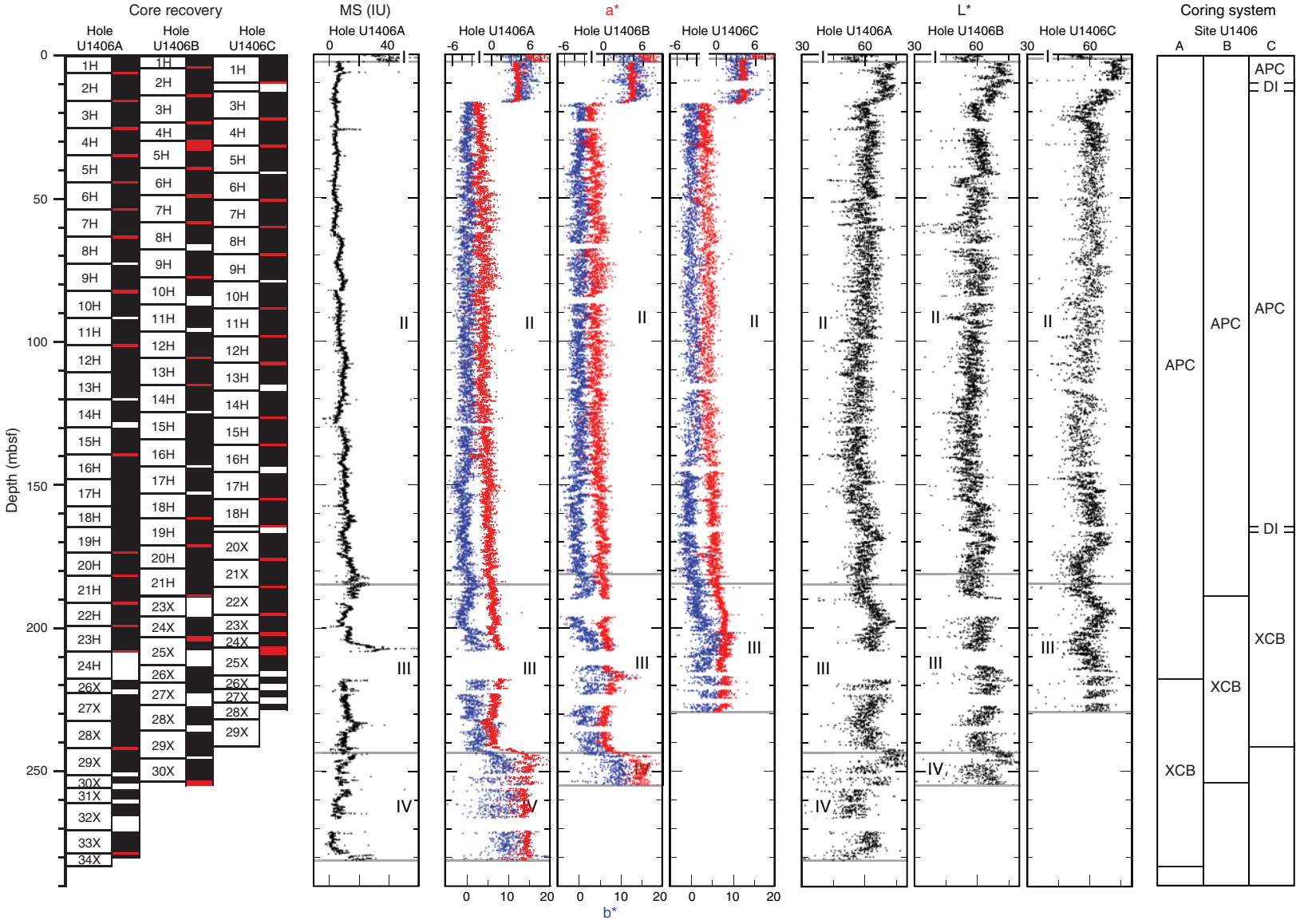

Figure F31. Plots of natural gamma radiation (NGR) data, Site U1406. Top panels show the spliced section for each interval of the splice, and bottom panels show all complete NGR records. Data from Holes U1406B and U1406C are offset by 10 and 20 cps, respectively, to aid visualization. Open circles indicate core tops. **A.** 0–50 m CCSF. (Continued on next six pages.)

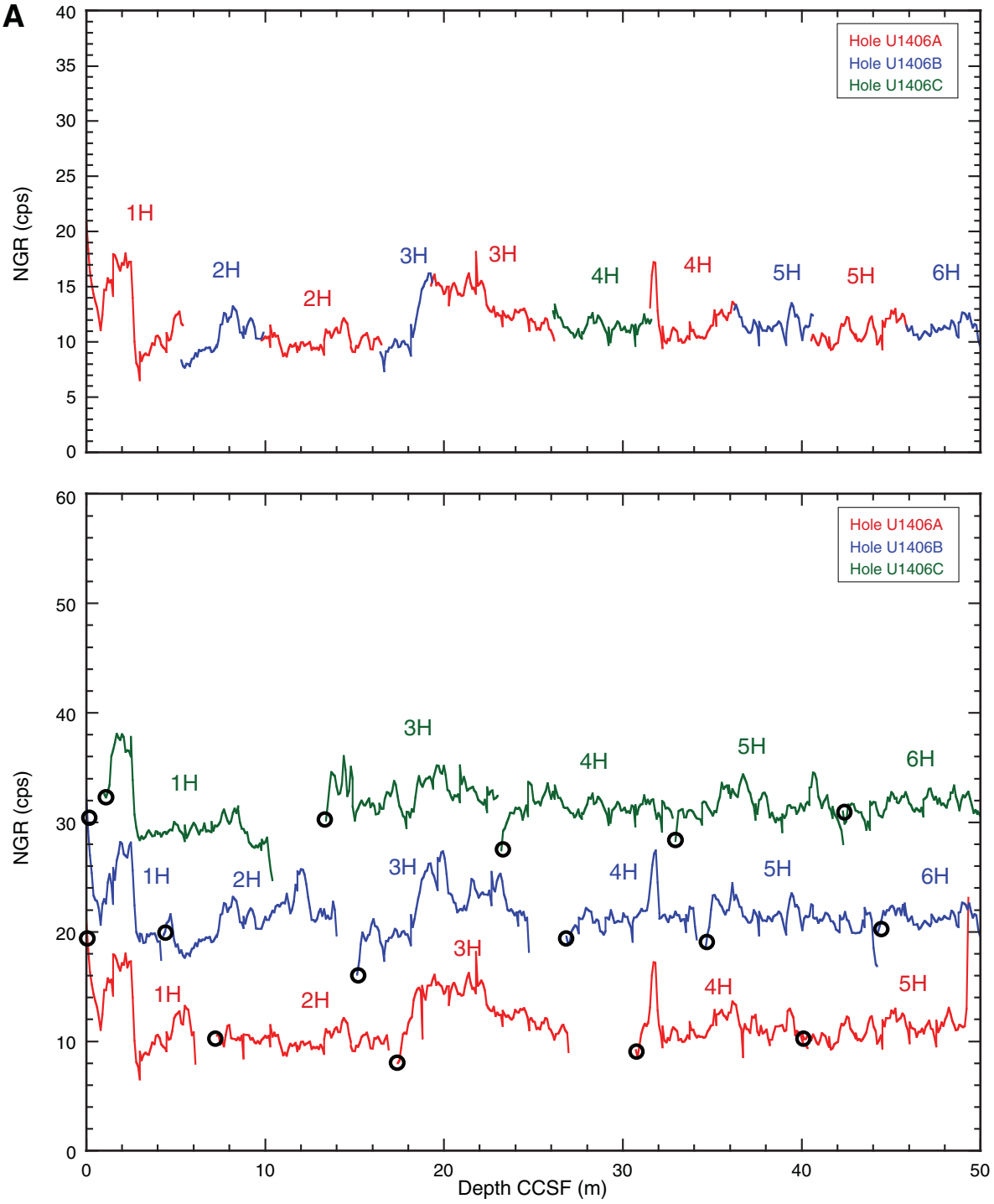

Figure F31 (continued). B. 50–100 m CCSF. (Continued on next page.)

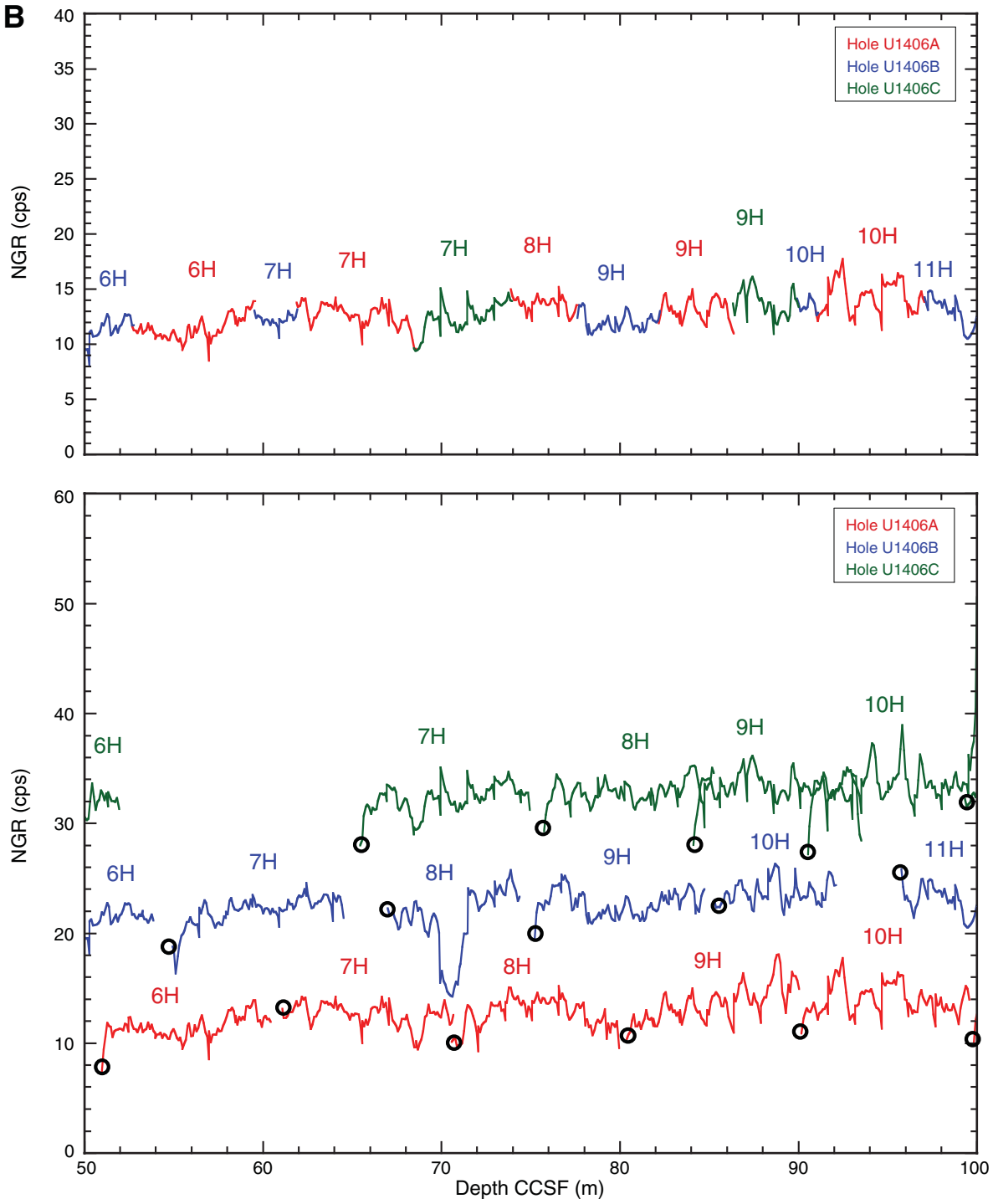

Figure F31 (continued). C. 100–150 m CCSF. (Continued on next page.)

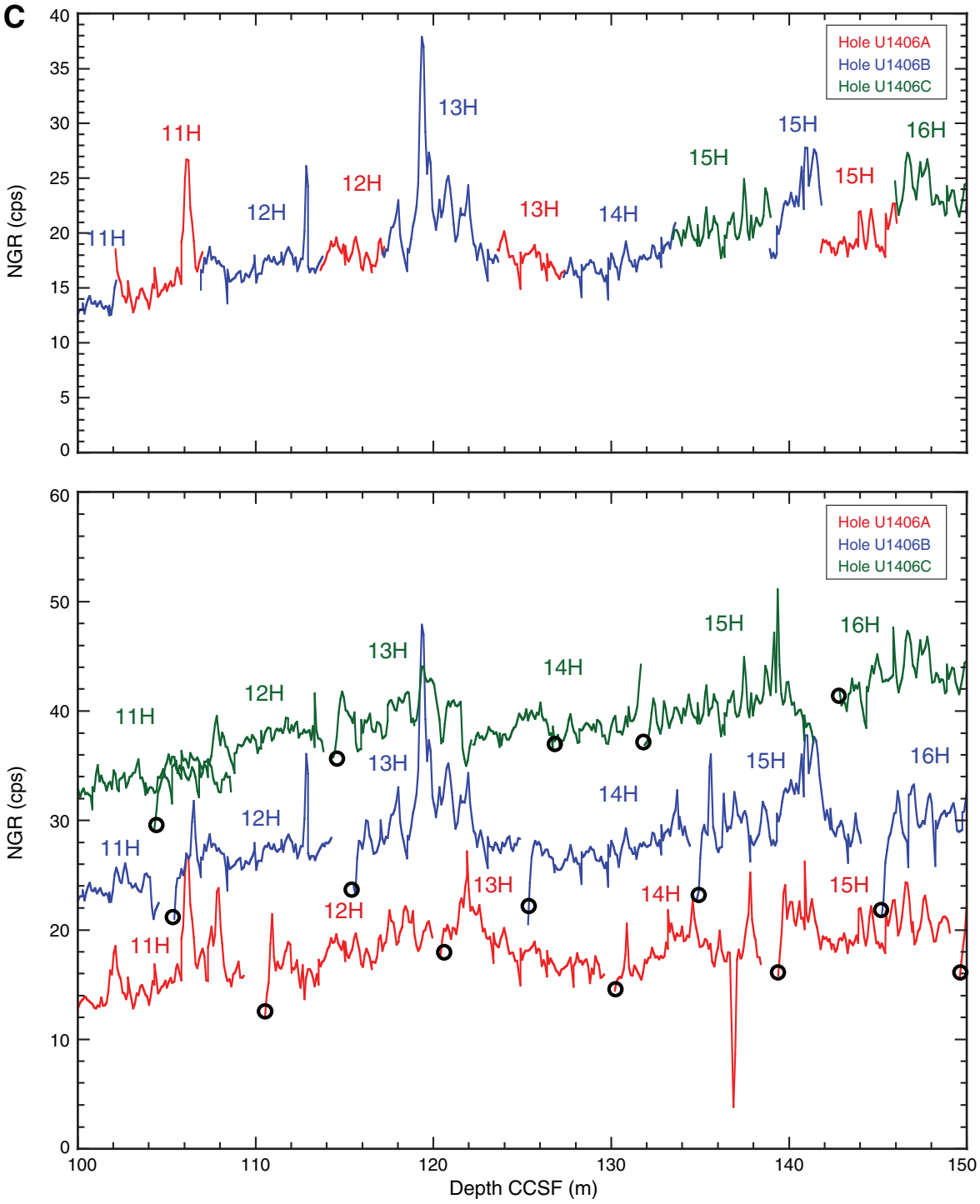

Figure F31 (continued). D. 150–200 m CCSF. (Continued on next page.)

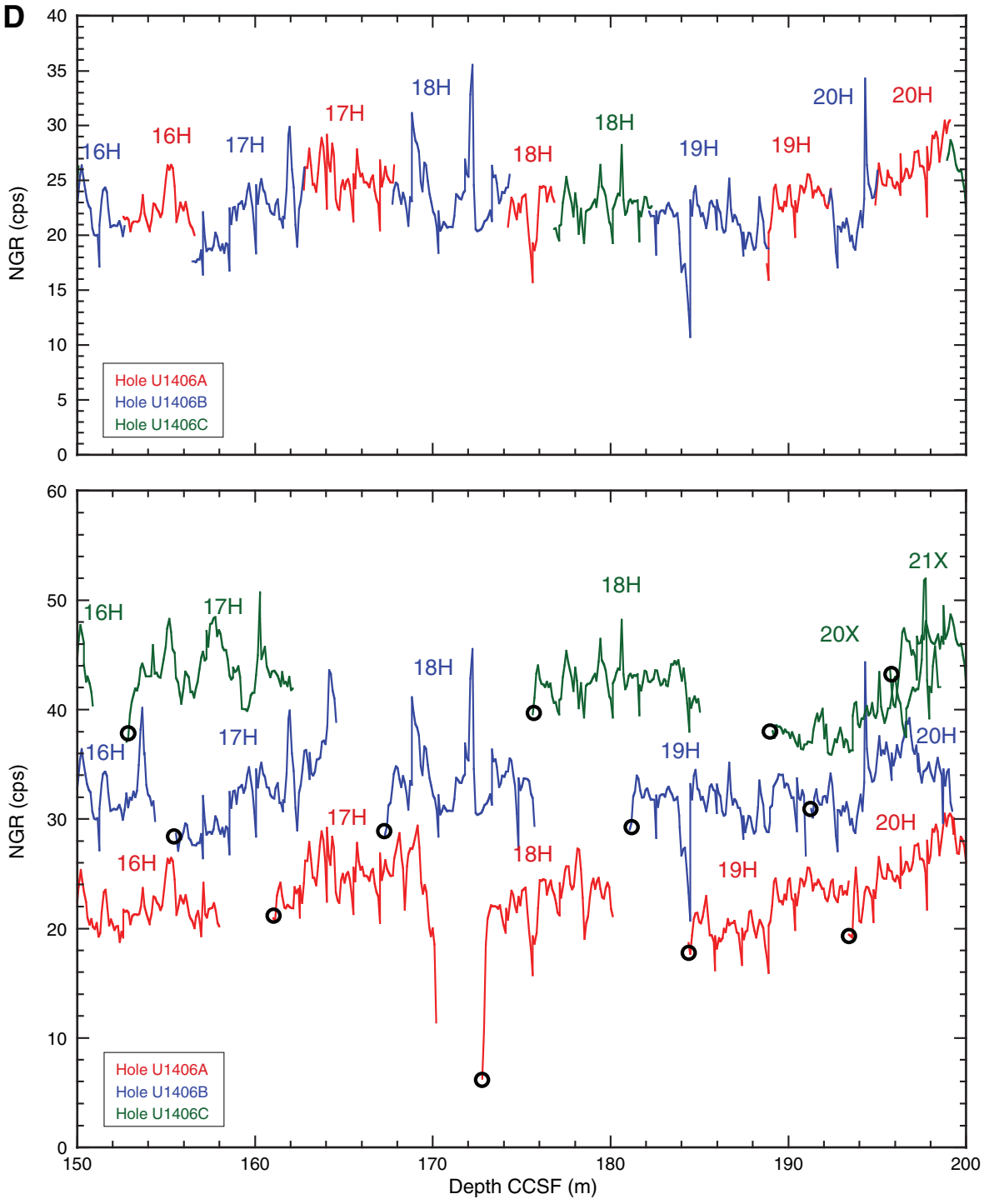

Figure F31 (continued). E. 200–250 m CCSF. (Continued on next page.)

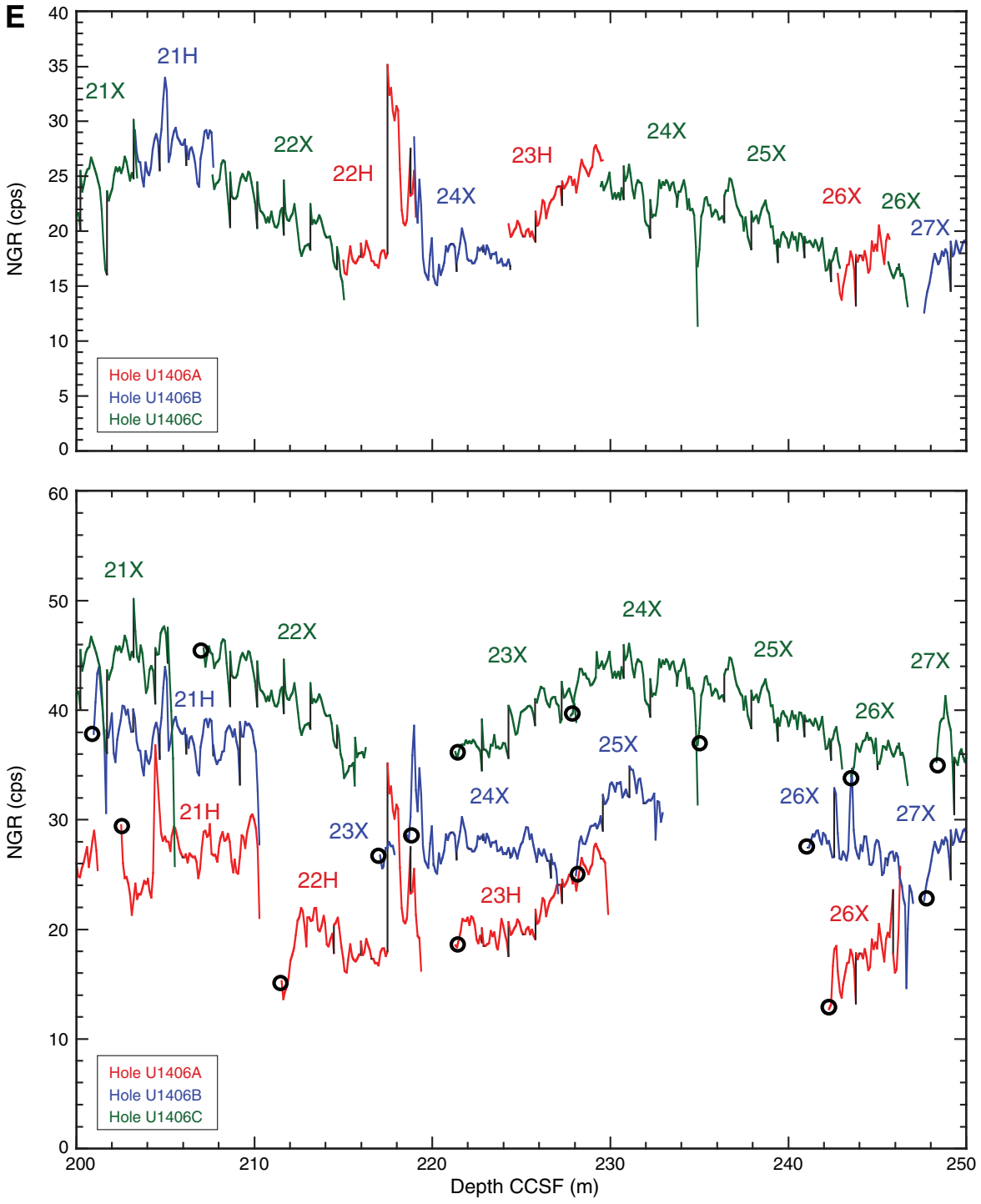

Figure F31 (continued). F. 250–300 m CCSF. (Continued on next page.)

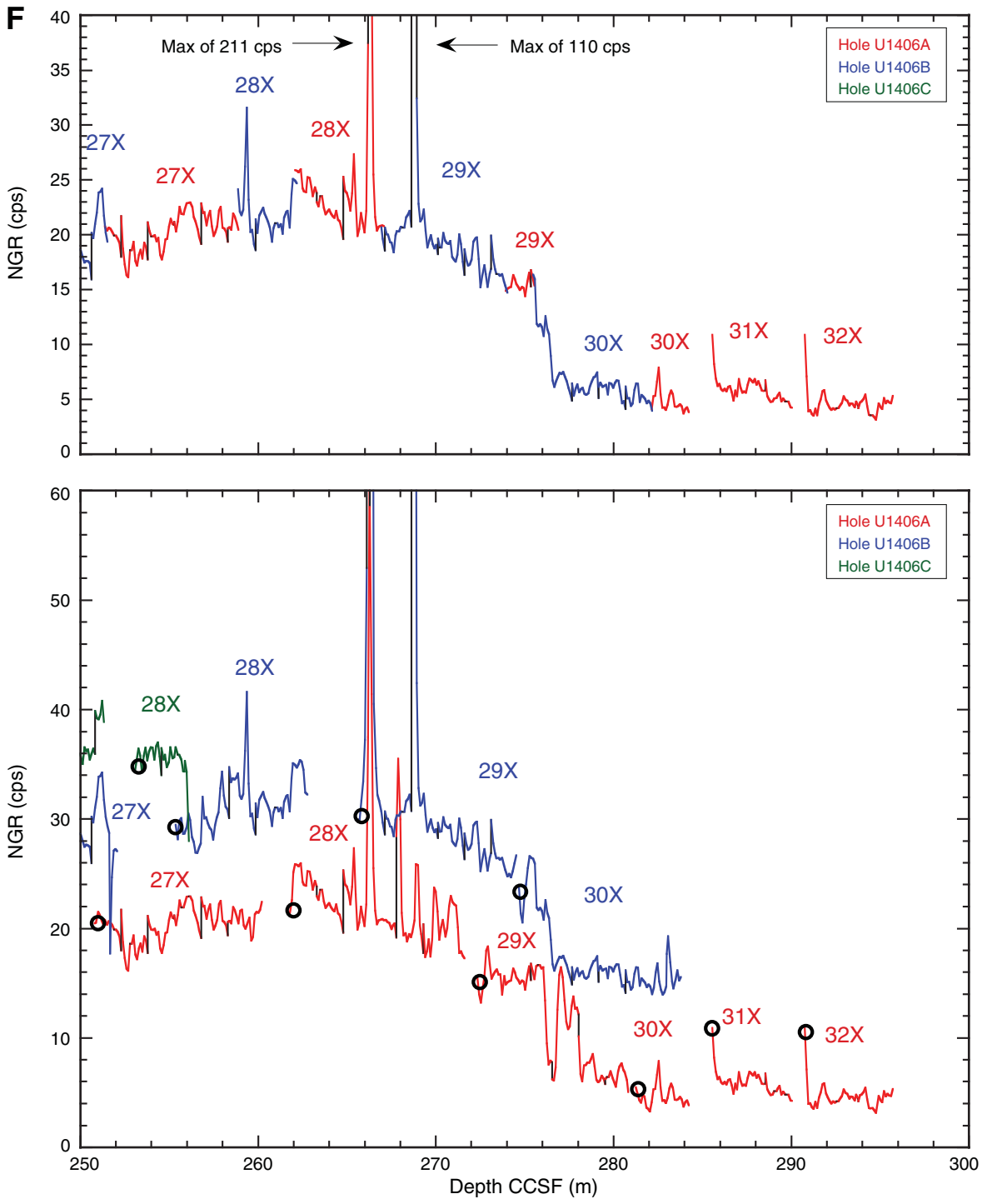

Figure F31 (continued). G. 300–350 m CCSF.

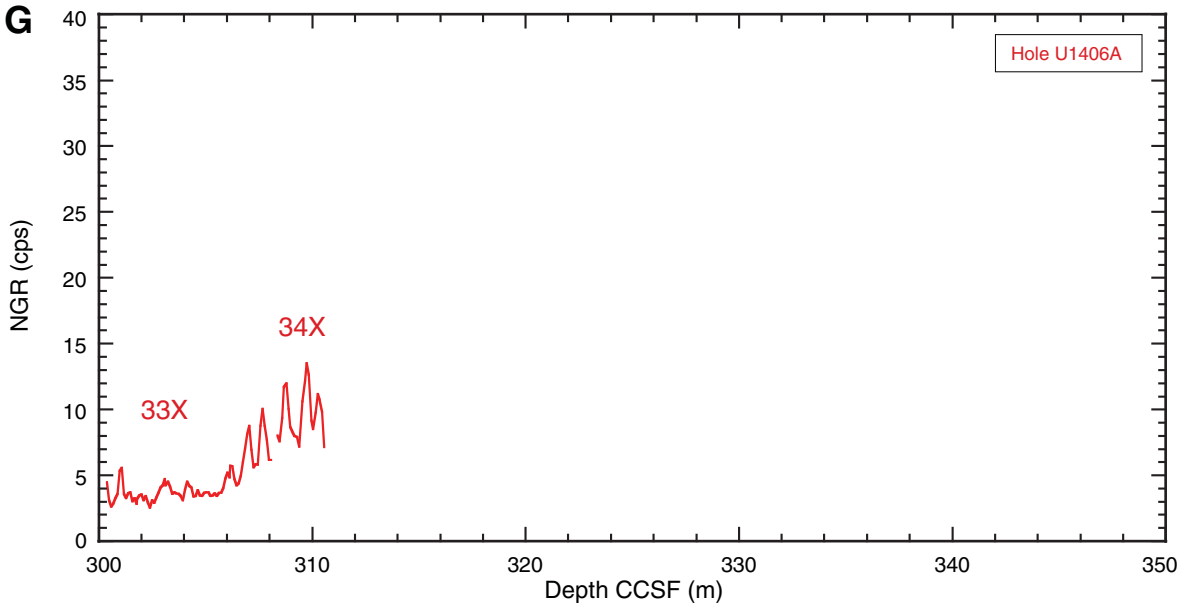

Figure F32. Plots of X-ray fluorescence scanning data for intervals where Ca/Fe data better reflects the correlation between holes, Site U1406. Top panels are the spliced section for each interval of the splice, and bottom panels Ca/Fe are records from all three holes. Data from Holes U1406B and U1406C are offset by 10 and 20, respectively, to aid visualization. Open circles indicate core tops. **A.** 50–100 m CCSF. (Continued on next two pages.)

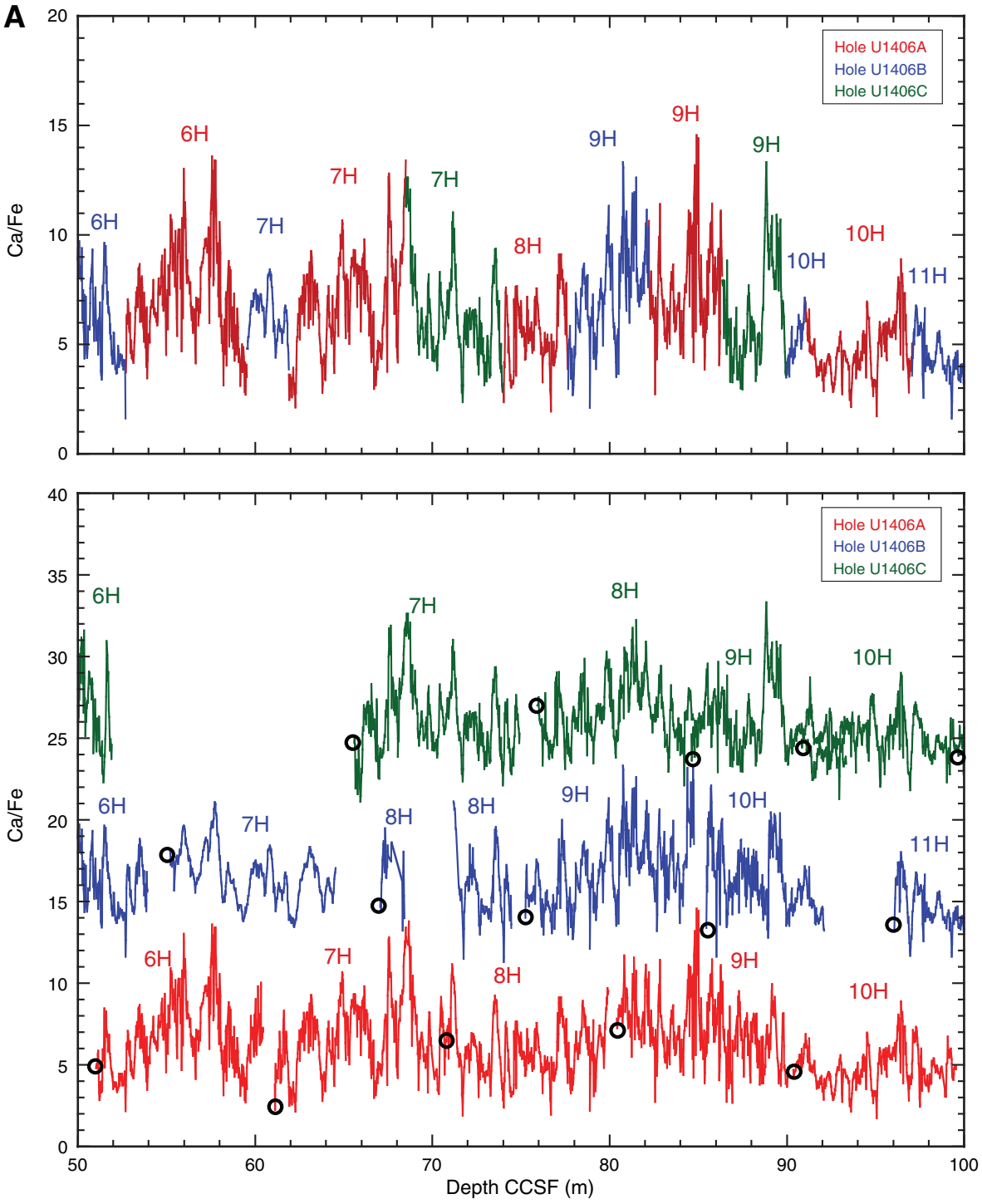

Figure F32 (continued). B. 100–150 m CCSF. (Continued on next page.)

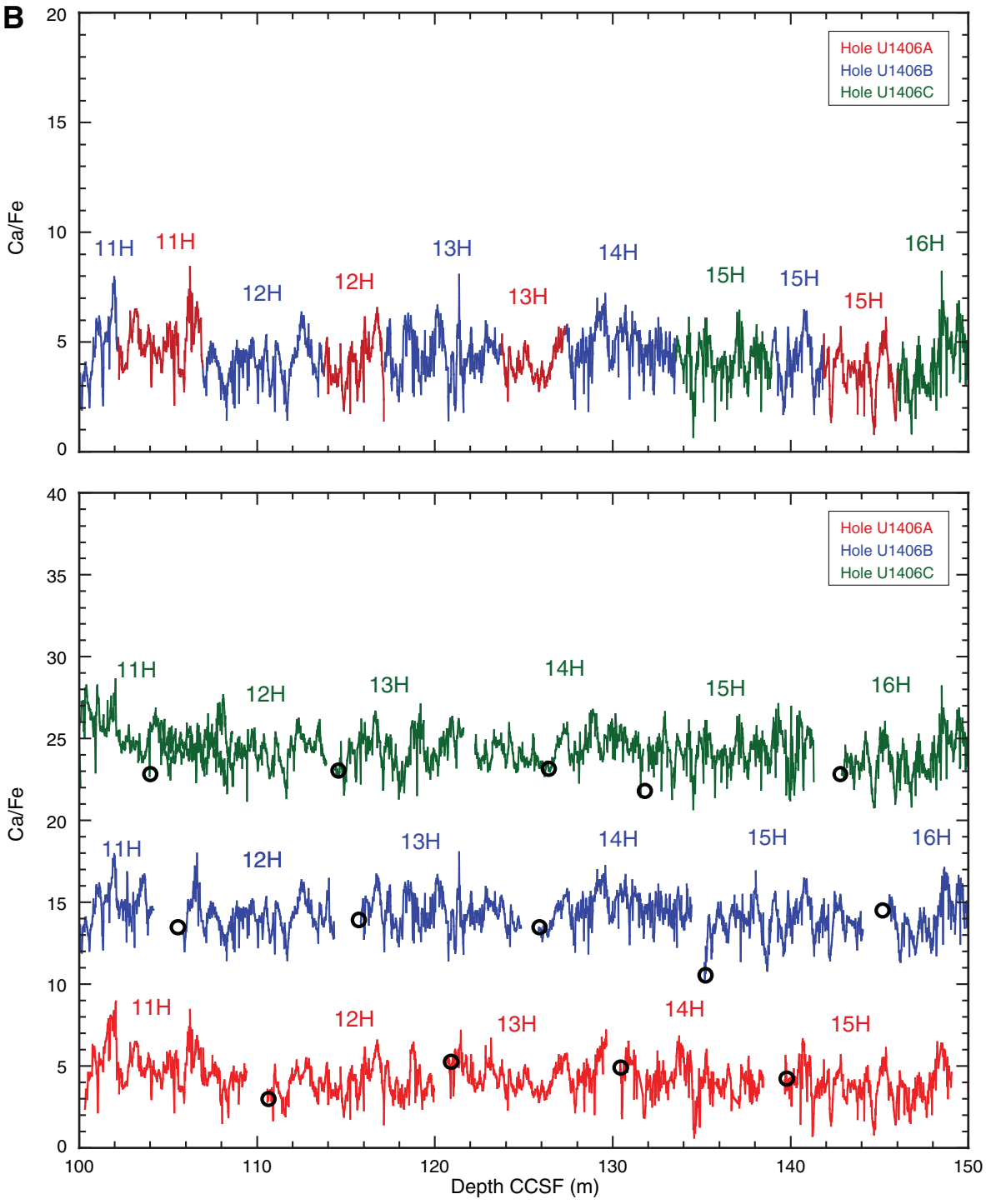

Figure F32 (continued). C. 150–200 m CCSF.

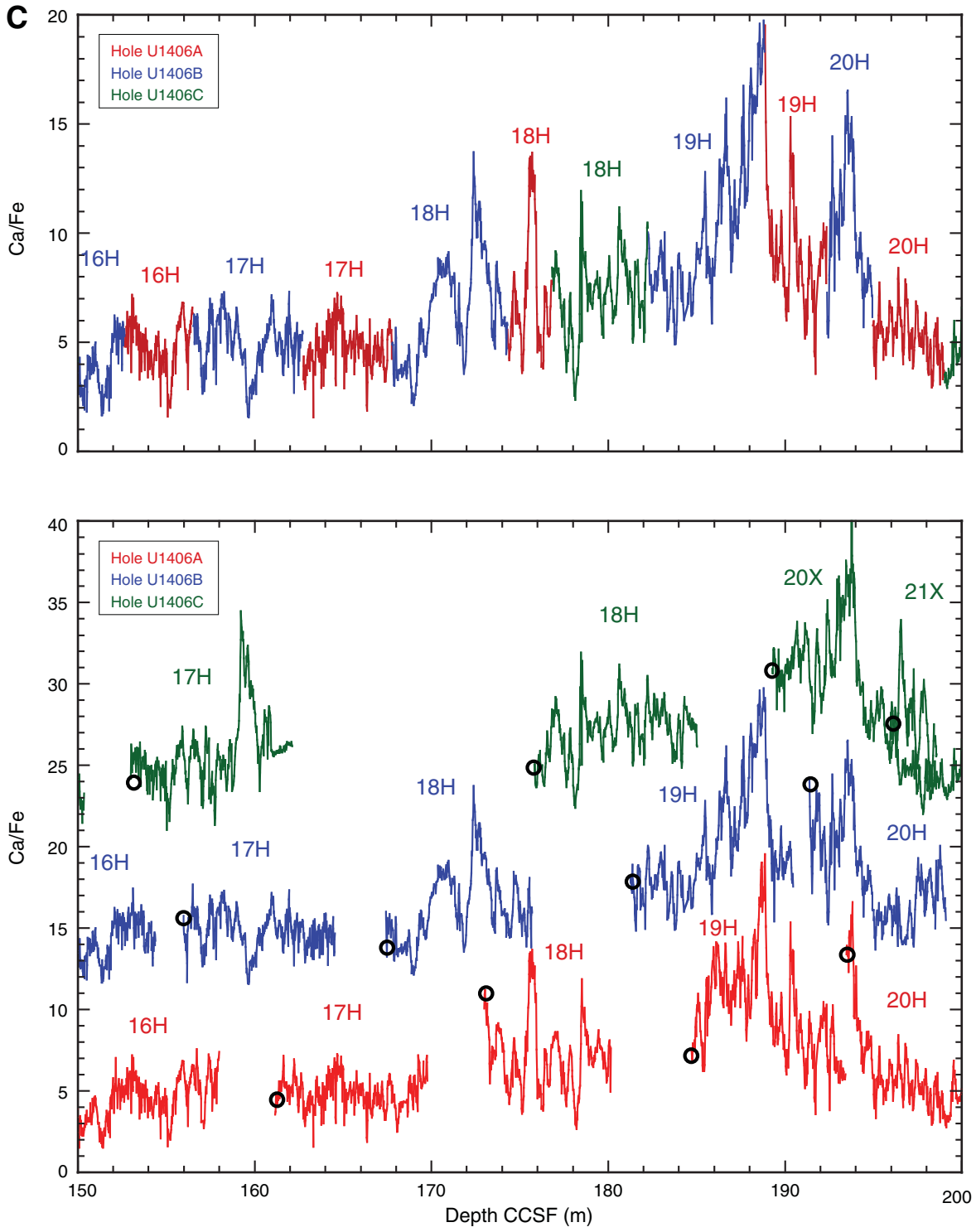

Figure F33. Plot of mbsf depth vs. CCSF depth, Site U1406. The growth factor is equal to the slope of the regression line.

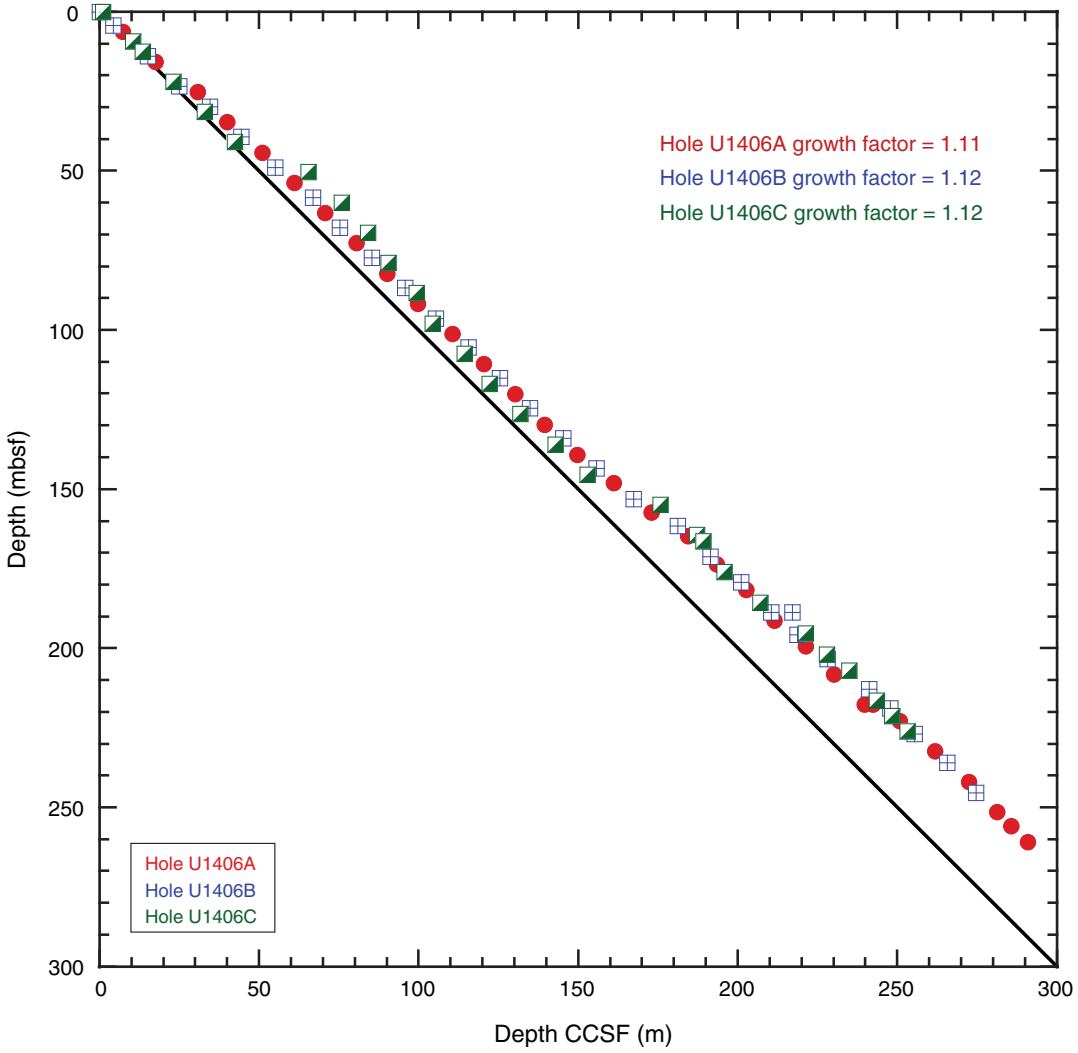

Table T1. Coring summary, Site U1406.(Continued on next page.)

Core	Date (2012)	Time UTC (h)	Depth DSF (m) Top of cored interval	Depth DSF (m) Bottom of cored interval	Interval cored (m)	Curated length (m)	Depth CSF-A (m) Top of core	Depth CSF-A (m) Bottom of core	Recovery (%)	Sections (*N*)
342-U1406A-										
1H	30 Jun	2320	0.0	6.2	6.2	6.25	43.06	43.06	101	6
2H	1 Jul	0035	6.2	15.7	9.5	9.86	52.89	52.89	104	8
3H	1 Jul	0130	15.7	25.2	9.5	9.81	62.26	62.26	103	8
4H	1 Jul	0220	25.2	34.7	9.5	9.89	71.62	71.62	104	8
5H	1 Jul	0310	34.7	44.2	9.5	9.77	80.95	80.95	103	8
6H	1 Jul	0400	44.2	53.7	9.5	9.76	90.84	90.84	103	8
7H	1 Jul	0450	53.7	63.2	9.5	9.99	99.86	99.86	105	8
8H	1 Jul	0550	63.2	72.7	9.5	9.47	109.93	109.93	100	7
9H	1 Jul	0635	72.7	82.2	9.5	9.98	118.97	118.97	105	8
10H	1 Jul	0725	82.2	91.7	9.5	9.48	128.50	128.50	100	7
11H	1 Jul	0820	91.7	101.2	9.5	9.84	136.83	136.83	104	8
12H	1 Jul	0910	101.2	110.7	9.5	9.53	147.13	147.13	100	7
13H	1 Jul	1005	110.7	120.2	9.5	9.43	156.81	156.81	99	7
14H	1 Jul	1100	120.2	129.7	9.5	8.38	166.34	166.34	88	8
15H	1 Jul	1155	129.7	139.2	9.5	10.01	176.13	176.13	105	8
16H	1 Jul	1245	139.2	148.1	8.9	8.90	185.80	185.80	100	7
17H	1 Jul	1400	148.1	157.3	9.2	9.20	195.43	195.43	100	7
18H	1 Jul	1525	157.3	164.7	7.4	7.43	204.09	204.09	100	6
19H	1 Jul	1645	164.7	173.7	9.0	9.09	214.46	214.46	101	6
20H	1 Jul	1755	173.7	181.7	8.0	8.06	223.33	223.33	101	7
21H	1 Jul	1905	181.7	191.2	9.5	9.83	43.06	43.06	103	8
22H	1 Jul	2050	191.2	199.3	8.1	8.11	52.89	52.89	100	7
23H	1 Jul	2200	199.3	208.1	8.8	8.86	62.26	62.26	101	6
24H	1 Jul	2300	208.1	217.6	9.5	0.00	71.62	71.62	0	0
25H	2 Jul	0015	217.6	217.7	0.1	0.15	80.95	80.95	150	1
26X	2 Jul	0200	217.7	222.8	5.1	4.09	90.84	90.84	80	4
27X	2 Jul	0415	222.8	232.4	9.6	9.55	99.86	99.86	99	8
28X	2 Jul	0625	232.4	241.9	9.5	9.93	109.93	109.93	105	8
29X	2 Jul	0805	241.9	251.5	9.6	8.93	118.97	118.97	93	7
30X	2 Jul	1025	251.5	255.8	4.3	3.34	128.50	128.50	78	3
31X	2 Jul	1240	255.8	261.0	5.2	4.67	136.83	136.83	90	4
32X	2 Jul	1500	261.0	270.6	9.6	5.21	147.13	147.13	54	5
33X	2 Jul	1720	270.6	278.6	8.0	8.05	156.81	156.81	101	7
34X	2 Jul	1955	278.6	283.3	4.7	2.45	166.34	166.34	52	3
				Totals:	283.3	267.3			95	218
342-U1406B-										
1H	3 Jul	2345	0.0	4.3	4.3	4.31	0.00	4.31	100	4
2H	3 Jul	0055	4.3	13.8	9.5	9.95	4.30	14.25	105	8
3H	3 Jul	0145	13.8	23.3	9.5	9.83	13.80	23.63	103	8
4H	3 Jul	0300	23.3	29.8	6.5	9.56	23.30	32.86	147	8
5H	3 Jul	0350	29.8	39.3	9.5	9.85	29.80	39.65	104	8
6H	3 Jul	0445	39.3	48.8	9.5	10.04	39.30	49.34	106	8
7H	3 Jul	0530	48.8	58.3	9.5	9.86	48.80	58.66	104	8
8H	3 Jul	0615	58.3	67.8	9.5	7.95	58.30	66.25	84	8
9H	3 Jul	0715	67.8	77.3	9.5	9.85	67.80	77.65	104	8
10H	3 Jul	0810	77.3	86.8	9.5	7.23	77.30	84.53	76	7
11H	3 Jul	0900	86.8	96.3	9.5	8.92	86.80	95.72	94	7
12H	3 Jul	0955	96.3	105.5	9.2	9.21	96.30	105.51	100	7
13H	3 Jul	1055	105.5	115.0	9.5	9.64	105.50	115.14	101	8
14H	3 Jul	1140	115.0	124.5	9.5	9.41	115.00	124.41	99	8
15H	3 Jul	1230	124.5	134.0	9.5	9.53	124.50	134.03	100	8
16H	3 Jul	1325	134.0	143.5	9.5	9.47	134.00	143.47	100	8
17H	3 Jul	1420	143.5	153.0	9.5	9.25	143.50	152.75	97	7
18H	3 Jul	1525	153.0	161.6	8.6	8.65	153.00	161.65	101	7
19H	3 Jul	1630	161.6	171.1	9.5	9.99	161.60	171.59	105	8
20H	3 Jul	1800	171.1	179.2	8.1	8.10	171.10	179.20	100	7
21H	3 Jul	1900	179.2	188.7	9.5	9.55	179.20	188.75	101	8
22H	3 Jul	2000	188.7	188.8	0.1	0.09	188.70	188.79	90	1
23X	3 Jul	2225	188.8	195.8	7.0	0.91	188.80	189.71	13	2
24X	4 Jul	0010	195.8	203.3	7.5	8.56	195.80	204.36	114	7
25X	4 Jul	0220	203.3	212.9	9.6	4.87	203.30	208.17	51	4
26X	4 Jul	0445	212.9	218.9	6.0	6.00	212.90	218.90	100	5
27X	4 Jul	0740	218.9	226.9	8.0	4.45	218.90	223.35	56	4
28X	4 Jul	1010	226.9	235.9	9.0	7.56	226.90	234.46	84	6
29X	4 Jul	1235	235.9	245.4	9.5	9.32	235.90	245.22	98	7

Table T1 (continued).

Core	Date (2012)	Time UTC (h)	Depth DSF (m) Top of cored interval	Depth DSF (m) Bottom of cored interval	Interval cored (m)	Curated length (m)	Depth CSF-A (m) Top of core	Depth CSF-A (m) Bottom of core	Recovery (%)	Sections (*N*)
30X	4 Jul	1520	245.4	253.6	8.2	9.43	245.40	254.83	115	8
				Totals:	253.6	241.34			95	202
342-U1406C-										
1H	4 Jul	1910	0.0	9.4	9.4	9.46	0.00	9.46	101	8
21	4 Jul	1950			****Drilled from 9.4 to 12.4 m DSF****					
3H	4 Jul	2025	12.4	21.9	9.5	9.94	12.40	22.34	105	8
4H	4 Jul	2110	21.9	31.4	9.5	9.83	21.90	31.73	103	8
5H	4 Jul	2150	31.4	40.9	9.5	9.49	31.40	40.89	100	8
6H	4 Jul	2240	40.9	50.4	9.5	9.87	40.90	50.77	104	8
7H	4 Jul	2330	50.4	59.9	9.5	9.57	50.40	59.97	101	7
8H	5 Jul	0015	59.9	69.4	9.5	9.76	59.90	69.66	103	8
9H	5 Jul	0100	69.4	78.9	9.5	9.47	69.40	78.87	100	8
10H	5 Jul	0150	78.9	88.4	9.5	9.60	78.90	88.50	101	7
11H	5 Jul	0230	88.4	97.9	9.5	9.55	88.40	97.95	101	8
12H	5 Jul	0315	97.9	107.4	9.5	9.86	97.90	107.76	104	8
13H	5 Jul	0400	107.4	116.9	9.5	7.89	107.40	115.29	83	7
14H	5 Jul	0510	116.9	126.4	9.5	9.60	116.90	126.50	101	8
15H	5 Jul	0605	126.4	135.9	9.5	9.61	126.40	136.01	101	8
16H	5 Jul	0645	135.9	145.4	9.5	8.28	135.90	144.18	87	7
17H	5 Jul	0735	145.4	154.9	9.5	9.64	145.40	155.04	101	8
18H	5 Jul	0835	154.9	164.4	9.5	9.57	154.90	164.47	101	8
191	5 Jul	0925			****Drilled from 164.4 to 166.4 m DSF****					
20X	5 Jul	1050	166.4	176.0	9.6	9.82	166.40	176.22	102	8
21X	5 Jul	1240	176.0	185.6	9.6	9.81	176.00	185.81	102	8
22X	5 Jul	1415	185.6	195.2	9.6	9.75	185.60	195.35	102	9
23X	5 Jul	1630	195.2	201.9	6.7	7.14	195.20	202.34	107	6
24X	5 Jul	1755	201.9	206.9	5.0	7.12	201.90	209.02	142	6
25X	5 Jul	2000	206.9	216.5	9.6	8.53	206.90	215.43	89	7
26X	5 Jul	2220	216.5	221.3	4.8	3.49	216.50	219.99	73	4
27X	6 Jul	0020	221.3	226.1	4.8	3.28	221.30	224.58	68	4
28X	6 Jul	0240	226.1	231.8	5.7	3.09	226.10	229.19	54	3
29X	6 Jul	0545	231.8	241.4	9.6	3.09	231.80	234.89	NA	0
				Totals:	241.4	226.11			91	187
				Site U1406 totals:	778.3	734.75			94	607

DSF = drilling depth below seafloor, CSF-A = core depth below seafloor, method A. H = advanced piston core, X = extended core barrel core, numeric core type = drilled interval. NA = not available.

Table T2. Lithostratigraphic unit intervals, Site U1406.

Lith. unit	Core, section, interval (cm) Top	Core, section, interval (cm) Bottom	Depth (mbsf) Top	Depth (mbsf) Bottom
	342-U1406A-	342-U1406A-		
I	1H-1, 0	1H-2, 111	0.00	2.61
II	1H-2, 111	21H-3, 91	2.61	184.86
III	21H-3, 91	29X-2, 0	184.86	243.40
IV	29X-2, 0	34X-CC, 28	243.40	281.05
	342-U1406B-	342-U1406B-		
I	1H-1, 0	1H-2, 112	0.00	2.62
II	1H-2, 112	21H-2, 120	2.62	181.12
III	21H-2, 120	29X-6, 10	181.12	243.50
IV	29X-6, 10	30X-CC, 25	243.50	254.83
	342-U1406C-	342-U1406C-		
I	1H-1, 0	1H-2, 10	0.00	1.60
II	1H-2, 10	21X-6, 107	1.60	184.57
III	21X-6, 107	28X-CC, 27	184.57	229.19
IV	Not drilled			

Table T3. Calcareous nannofossil datums, Site U1406. (Continued on next page.)

Hole, core, section, interval (cm)		Age	Zone/ Subzone	Marker species	Age (Ma)	Depth (mbsf)			
Top	Bottom					Top	Bottom	Mid-point	±
342-	342-								
		Pleistocene							
U1406A-1H-1, 75	U1406A-1H-1, 75		NN20	T *Pseudoemiliania lacunosa*	0.44	0.00	0.75	0.38	0.38
U1406A-1H-1, 75	U1406A-1H-2, 75		NN19	T *Discoaster brouweri*	1.93	0.75	2.26	1.51	0.76
		Miocene							
U1406A-1H-2, 75	U1406A-1H-3, 75		NN6	T *Sphenolithus heteromorphus*	13.53	2.26	3.76	3.01	0.75
U1406A-1H-2, 75	U1406A-1H-3, 75		NN5	T *Helicosphaera ampliaperta*	14.91	2.26	3.76	3.01	0.75
U1406A-1H-CC	U1406A-2H-2, 100			B *Sphenolithus heteromorphus*	17.71	6.23	8.71	7.47	1.24
U1406A-2H-2, 100	U1406A-2H-4, 100		NN4	T *Sphenolithus belemnos*	17.95	8.71	11.70	10.21	1.50
U1406A-1H-2, 75	U1406A-2H-6, 75		NN3	Tc *Triquetrorhabdulus carinatus*	18.28	11.70	14.45	13.08	1.38
U1406A-1H-2, 75	U1406A-5H-2, 100			B *Sphenolithus belemnos*	19.03	35.07	37.21	36.14	1.07
U1406A-8H-7 (CC)	U1406A-9H-2, 100			B *Sphenolithus disbelemnos*	22.76	72.63	75.21	73.92	1.29
U1406A-9H-5, 88	U1406A-9H-6, 88			T *Sphenolithus capricornutus*	22.97	79.72	81.12	80.42	0.70
		Oligocene/Miocene boundary							
U1406A-9H-5, 88	U1406A-9H-6, 88			T *Sphenolithus delphix*	23.11	79.72	81.12	80.42	0.70
U1406A-10H-1,100	U1406A-10H-2,100			B *Sphenolithus delphix*	23.21	83.20	84.70	83.95	0.75
U1406A-11H-5,100	U1406A-11H-6,100		NN1	T *Sphenolithus ciperoensis*	24.43	98.70	100.22	99.46	0.76
U1406A-16H-5, 75	U1406A-16H-CC		NP25	T *Sphenolithus distentus*	26.44	145.95	148.04	146.99	1.04
U1406A-16H-5, 75	U1406A-16H-CC			Bc *Triquetrorhabdulus carinatus*	26.57	145.95	148.04	146.99	1.04
U1406A-18H-1, 75	U1406A-18H-3, 75		NP24	B *Sphenolithus ciperoensis*	29.62	158.05	160.89	159.47	1.42
U1406A-19H-2, 75	U1406A-19H-3, 75			B *Sphenolithus distentus*	30.00	166.95	168.45	167.70	0.75
U1406A-19H-6, 154 (CC)	U1406A-20H-CC		NP23	T *Reticulofenestra umbilicus* (>14 µm)	32.02	173.77	181.70	177.74	3.96
U1406A-20H-CC	U1406A-21H-4, 75			T *Isthmolithus recurvus*	32.49	181.73	186.08	183.91	2.18
U1406A-21H-CC	U1406A-22H-2, 150		NP22	T *Coccolithus formosus*	32.92	191.51	194.16	192.84	1.33
		Eocene/Oligocene boundary							
U1406A-22H-CC	U1406A-23H-1, 7		NP21	T *Discoaster saipanensis*	34.44	199.29	199.37	199.33	0.04
U1406A-23H-2, 30	U1406A-23H-3, 47			T *Discoaster barbadiensis*	34.76	201.10	202.77	201.94	0.84
U1406A-26H-3, 50	U1406A-26X-CC		NP19/NP20	B *Isthmolithus recurvus*	36.97	221.20	221.77	221.49	0.29
U1406A-26X-CC	U1406A-27X-2,100		NP18	Bc *Chiasmolithus oamaruensis*	38.09	221.77	225.30	223.53	1.77
U1406A-26X-CC	U1406A-27X-2,100			T *Chiasmolithus grandis*	37.98	221.77	225.30	223.53	1.77
U1406A-28X-1, 100	U1406A-28X-2, 100			B *Dictyococcites bisectus* (>10 µm)*	40.36	233.41	234.91	234.16	0.75
U1406A-28X-2, 100	U1406A-28X-4, 100		NP17	T *Chiasmolithus solitus*	40.40	234.91	239.90	237.41	2.50
U1406A-28X-6, 63	U1406A-28X-CC			B *Reticulofenestra reticulata*	41.66	240.53	242.30	241.42	0.89
U1406A-28X-6, 63	U1406A-28X-CC			T *Nannotetrina* spp.	41.85	240.53	242.30	241.42	0.89
U1406A-28X-CC	U1406A-29X-1, 57			B *Reticulofenestra umbilicus* (>14 µm)	41.94	242.30	242.47	242.39	0.08
U1406A-28X-CC	U1406A-29X-1, 57			T *Nannotetrina fulgens*	42.87	242.30	242.47	242.39	0.08
U1406A-29X-1, 57	U1406A-29X-3, 20		NP15c	T *Chiasmolithus gigas*	44.12	242.47	245.11	243.79	1.32
U1406A-29X-4, base	U1406A-29X-5, base		NP15b	B *Chiasmolithus gigas*	45.49	247.60	249.10	248.35	0.75
U1406A-29X-6, base	U1406A-29X-CC		NP15a	B *Nannotetrina fulgens*	46.29	250.45	250.79	250.62	0.17
U1406A-29X-CC	U1406A-30X-CC			B *Nannotetrina cristata*	47.73	250.79	254.68	252.73	1.94
		Paleocene							
U1406A-30X-CC	U1406A-31X-1, 8			*Fasciculithus* div. decline†	56.00	254.68	255.88	255.28	0.60
U1406A-30X-CC	U1406A-31X-1, 8			T *Fasciculithus alanii*†	56.00	254.68	255.88	255.28	0.60
U1406A-31X-CC	U1406A-32X-2, 34			T *Ericsonia robusta* (>9 µm)†	57.10	260.44	262.84	261.64	1.20
U1406A-32X-2, 34	U1406A-32X-3, 74		NP9	B *Discoaster multiradiatus*	57.21	262.84	264.75	263.80	0.95
U1406A-32X-2, 34	U1406A-32X-3, 74			Tc *Sphenolithus anarrhopus*		262.84	264.75	263.80	0.95
U1406A-32X-3, 74	U1406A-32X-4, 75			B *Discoaster delicatus*†	57.45	264.75	265.90	265.33	0.57
U1406A-32X-3, 74	U1406A-32X-4, 75			B *Ericsonia robusta* (>9 µm)†	57.54	264.75	265.90	265.33	0.57
U1406A-32X-3, 74	U1406A-32X-4, 75			Tc *Discoaster backmanii*†	57.57	264.75	265.90	265.33	0.57
U1406A-32X-CC	U1406A-33X-3, 58			B *Discoaster backmanii*†	58.28	267.19	273.94	270.56	3.38

Table T3 (continued).

Hole, core, section, interval (cm)		Age	Zone/ Subzone	Marker species	Age (Ma)	Depth (mbsf)			
Top	Bottom					Top	Bottom	Mid-point	±
		Paleocene							
U1406A-32X-CC	U1406A-33X-3, 58		NP8	B *Heliolithus riedellii*	58.70	267.19	273.94	270.56	3.38
U1406A-33X-CC	U1406A-34X-1, 83		NP7	B *Discoaster mohleri*	58.97	278.63	279.43	279.03	0.40
U1406A-33X-CC	U1406A-34X-1, 83			B *Sphenolithus anarrhopus*†	59.40	278.63	279.43	279.03	0.40
U1406A-34X-1, 83	U1406A-34X-2, 60		NP6	B *Heliolithus kleinpellii*	59.54	279.43	280.37	279.90	0.47
U1406A-34X-2, 60	U1406A-34X-CC			B *Heliolithus cantabriae*	59.60	280.37	281.03	280.70	0.33
U1406A-34X-CC	U1406A-34X-CC		NP5	B *Fasciculithus tympaniformis*	61.51	281.03	281.03	281.03	0.00

* = from Fornaciari et al. (2010) recalibrated to GTS2012. † = from Agnini et al. (2007) recalibrated to GTS2012. B = base, Bc = Base common, T = top, Tc = Top common.

Table T4. Calcareous nannofossil distribution, Site U1406. This table is available in an **oversized format.**

Table T5. Radiolarian datums, Site U1406.

Core, section, interval (cm)		Age	Zone/ Subzone	Marker species	Age (Ma)	Depth (mbsf)			
Top	Bottom					Top	Bottom	Mid-point	±
342-U1406A-	342-U1406A-								
		Miocene							
	2H-CC			T *Lychnocanoma elongata*	17.59		16.04	16.04	
3H-CC	4H-CC		RN3	B *Dorcadospyris dentata*	18.22	25.49	35.07	30.28	4.79
3H-CC	4H-CC			T *Dorcadospyris ateuchus*	18.64	25.49	35.07	30.28	4.79
4H-CC	5H-CC		RN2	T *Theocyrtis annosa*	20.05	35.07	44.43	39.75	4.68
8H-7	9H-CC			B *Cyrtocapsa tetrapera*	21.82	72.63	82.64	77.63	5.00
8H-7	9H-CC			T *Artophormis gracilis*	22.41	72.63	82.64	77.63	5.00
10H-7	11H-CC		RP22	B *Lychnocanoma elongata*	24.18	91.65	101.52	96.59	4.94
13H-7	14H-CC		RP21b	B *Lychnocanoma apadora*	26.50	120.06	128.55	124.30	4.25
15H-CC	29X-3, 20–22		RP21a	B *Dorcadospyris ateuchus*	28.64	139.68		139.68	
		Eocene							
15H-CC	29X-3, 20–22			T *Theocotyle conica*	45.63		245.11	245.11	0.00
29X-3, 98–100	29X-4, 16–18		RP12	B *Eusyringium lagena*	46.21	245.89	246.57	246.23	0.34
29X-4, 16–18	31X-1, 15–17		RP11	B *Dictyoprora mongolfieri*	47.98	246.57	255.96	251.27	4.70
		Paleocene							
29X-3, 98–101	31X-1, 15–17			T *Amphisphaera goruna*	55.50	246.57	255.96	251.27	4.70
31X-1, 15–17	31X-CC			T *Lamptonium pennatum*	55.90	255.96	260.44	258.20	2.24
31X-CC	32X-CC			T *Bekoma campechensis*	57.83	260.44	266.19	263.32	2.88
32X-CC	33X-4, 102–103			B *Podocyrtis papalis*	55.96	266.19	275.89	271.04	4.85
32X-CC	33X-4, 102–103		RP7	B *Bekoma bidartensis*	58.35	266.19	275.89	271.04	4.85
33X-4, 102–103			RP6	T *Buryella pentadica*	59.71	275.89			

B = base, T = top.

Table T6. Radiolarian distribution, Site U1406. (Continued on next two pages.)

Core, section, interval (cm)	Depth (mbsf)	Zone/ Subzone	Event	Age (Ma)	Preservation	Abundance	Diatoms	Miocene–Oligocene																														
								Collosphaerids undet.	Orosphaerids undet.	*Anthocyrtidium mariae*	*Artophormis gracilis*	*Axoprunum bispiculum*	*Calocycletta robusta*	*Calocycletta serrata*	*Calocycletta virginis*	*Carpocanopsis favosa*	*Cryptocarpium?* sp.	*Cryptocarpium ornatum*	*Cyrtocapsella cornuta*	*Cyrtocapsella japonica*	*Cyrtocapsella tetrapera*	*Dictyophimus crisae*	*Didymocyrtis prismatica*	*Didymocyrtis tubaria*	*Didymocyrtis violina*	*Dorcadospyris ateuchus*	*Dorcadospyris dentata*	*Dorcadospyris forcipata*	*Dorcadospyris riedeli*	*Eucyrtidium diaphanes*	*Heliodiscus asteriscus*	*Lamprocylcas particollis*	*Lophocyrtis galenum*	*Lophocyrtis leptetrum*	*Lophocyrtis pegetrum*
342-U1406A-																																						
2H-CC	16.04	RN3	T *Lychnocanoma elongata*	17.59	M	A	R	x	x				?		x		x			x	x	x	x		x		x		x	x			x		x		
3H-CC	25.49	RN3	B *Dorcadospyris dentata*	18.22	M	A	R		x				?		x						x			x			x										
4H-CC	35.07	RN2	T *Dorcadospyris ateuchus*	18.64	M	A	R		x	x				x			x			?	x	x	x				x			x	x			x			
5H-CC	44.43	RN2	T *Theocyrtis annosa*	20.05	G	A	R		x	x			x	x				x			x	x	x	x	x	x		x			x			x			
6H-CC	53.93	RN1		—	G	A	R		x				x		x				x		x		x	x		x					x			x			
7H-CC	63.65	RN1		—	G	A	R		x	x				x	x			x	x		x		x		x	x				x			x			
8H-7	72.63	RN1	B *Cyrtocapsella tetrapera*	21.82	M	A	R		x	x				x	x						x	x	x		x	x				x			x			
9H-CC	82.64	RP22	T *Artophormis gracilis*	22.41	G	A	R		x		x		x	x	x						x				x					x			x			
10H-7	91.65	RP22	B *Lychnocanoma elongata*	24.18	G	A	R		x		x				x	x					x			x	x							x					
11H-CC	101.52	RP21b		—	M	C	R		x		x																										
12H-7	110.70	RP21b		—	M	F	B		x				x				x				x					x											
13H-7	120.06	RP21b	B *Lychnocanoma apadora*	26.50	M	C	B		x		x	x														x					x	x					
14H-CC	128.55	RP21a		—	M	C	B		x		x	x									x					x					x						x
15H-CC	139.68	RP21a	B *Dorcadospyris ateuchus*	28.64	M	C	B		x												x					x											
29X-3, 20–22	245.11	RP12	T *Theocotyle conica*	45.63	P	C	B																														
29X-3, 98–100	245.89	RP12	B *Eusyringium lagena*	46.21	P	F	B																														
29X-4, 16–18	246.57	RP11	B *Dictyoprora mongolfieri*	47.98	M	C	B																														
31X-1, 15–17	255.96	RP7?	T *Amphisphaera goruna*	55.5	P	F	B																														
31X-2, 99–101	258.30	RP7		—	M	A	B																														
31X-3, 97–99	259.78	—		—	G	A	B																														
31X-CC	260.44	RP7	T *Lamptonium pennatum*	55.90	G	A	B																														
32X-CC	266.19	RP7	B *Bekoma bidartensis*, T *Bekoma campechensis*	58.35, 57.83	M	C	B																														
33X-4, 102–103	275.89	RP6	B *Buryella pentadica*	59.71	G	A	B																														

Preservation: G = good, M = moderate, P = poor. Abundance: A = abundant, C = common, F = few, R = rare, B = barren. ? = undetermined, Rew = reworked. — = not assigned. See **"Biostratigraphy"** in the "Methods" chapter (Norris et al., 2014a) for preservation and abundance definitions.

Table T6 (continued). (Continued on next page.)

Core, section, interval (cm)	Depth (mbsf)	Zone/ Subzone	Event	Age (Ma)	Preservation	Abundance	Diatoms	Miocene–Oligocene														Eocene–Paleocene										
								Lychnocanoma apodora	*Lychnocanoma elongata*	*Lychnocanoma grande*	*Lychnocanoma klausi*	*Lychnocanoma tripodium*	*Lychnodictyum audax*	*Periphaena decora*	*Phormocyrtis alexandarae*	*Pterocanium trilobum*	*Stichocorys delmontensis*	*Stichocorys subligata gr.*	*Stichocorys wolffii*	*Theocorys redondoensis*	*Theocorys spongoconum*	*Theocyrtis annosa*	*Zygocircus* spp.	*Amphicraspedum murrayanum*	*Amphisphaera coronata*	*Amphisphaera goruna*	*Anthocyrtoma frizzelli*	*Axoprunum pierinae*	*Bekoma bidartensis*	*Bekoma campechensis*	*Buryella pentadica*	*Buryella tetradica*	*Calocyclomma ampulla*
342-U1406A-																																
2H-CC	16.04	RN3	T *Lychnocanoma elongata*	17.59	M	A	R		x							x			x			x		x							
3H-CC	25.49	RN3	B *Dorcadospyris dentata*	18.22	M	A	R												x			x										
4H-CC	35.07	RN2	T *Dorcadospyris ateuchus*	18.64	M	A	R									x	x					x										
5H-CC	44.43	RN2	T *Theocyrtis annosa*	20.05	G	A	R								x		x				x	x	x									
6H-CC	53.93	RN1		—	G	A	R		x	x						x	x				x		x									
7H-CC	63.65	RN1		—	G	A	R						x			x	x		x			x	x									
8H-7	72.63	RN1	B *Cyrtocapsella tetrapera*	21.82	M	A	R						x		x		x	x		x	x		x									
9H-CC	82.64	RP22	T *Artophormis gracilis*	22.41	G	A	R	x	x			x		x	x		x	x		x	x	x	x									
10H-7	91.65	RP22	B *Lychnocanoma elongata*	24.18	G	A	R	x	x							x					x		x									
11H-CC	101.52	RP21b		—	M	C	R										?						x									
12H-7	110.70	RP21b		—	M	F	B													x			x									
13H-7	120.06	RP21b	B *Lychnocanoma apadora*	26.50	M	C	B	x												x			x									
14H-CC	128.55	RP21a		—	M	C	B				x												x									
15H-CC	139.68	RP21a	B *Dorcadospyris ateuchus*	28.64	M	C	B							x									x									
29X-3, 20–22	245.11	RP12	T *Theocotyle conica*	45.63	P	C	B																		x	Rew			x		x	x
29X-3, 98–100	245.89	RP12	B *Eusyringium lagena*	46.21	P	F	B																		x							x
29X-4, 16–18	246.57	RP11	B *Dictyoprora mongolfieri*	47.98	M	C	B																		x							x
31X-1, 15–17	255.96	RP7?	T *Amphisphaera goruna*	55.5	P	F	B																			x					x	
31X-2, 99–101	258.30	RP7		—	M	A	B																		x	x		x	x	?		x	x
31X-3, 97–99	259.78	—		—	G	A	B																		x	x	x	x	x	?		x	x
31X-CC	260.44	RP7	T *Lamptonium pennatum*	55.90	G	A	B																		x	x		x	x			x	
32X-CC	266.19	RP7	B *Bekoma bidartensis*, T *Bekoma campechensis*	58.35, 57.83	M	C	B																	x	x	x		x	x	x		x	
33X-4, 102–103	275.89	RP6	B *Buryella pentadica*	59.71	G	A	B																		x	x				x	x	x	

Table T6 (continued).

								Eocene–Paleocene																									
Core, section, interval (cm)	Depth (mbsf)	Zone/ Subzone	Event	Age (Ma)	Preservation	Abundance	Diatoms	*Clathrocyclas universa*	*Dictyoprora amphora*	*Dictyoprora mongolfieri*	*Diplocyclas bicorona bicorona*	*Dorcadospyris platyacantha*	*Eusyringium lagena*	*Heliodiscus asteriscus*	*Lamptonium pennatum*	*Lithochytris vespertilio*	*Lychnocanoma amphitrite*	*Lychnocanoma bellum*	*Lychnocanoma carinatum*	*Middourium regularis*	*Phormocyrtis striata exquisita*	*Phormocyrtis striata striata*	*Phormocyrtic turgida*	*Podocyrtis papalis*	*Podocyrtis sinuosa*	*Pterocodon poculum*	*Pterocodon tenellus*	*Sethochytris bablylonis*	*Theocorys phyzella*	*Theocorys* aff. *phyzella*	*Theocotyle conica*	*Theocotyle cryptocephala*	*Thyrsocyrtis rhizodon*
342-U1406A-																																	
2H-CC	16.04	RN3	T *Lychnocanoma elongata*	17.59	M	A	R																										
3H-CC	25.49	RN3	B *Dorcadospyris dentata*	18.22	M	A	R																										
4H-CC	35.07	RN2	T *Dorcadospyris ateuchus*	18.64	M	A	R																										
5H-CC	44.43	RN2	T *Theocyrtis annosa*	20.05	G	A	R																										
6H-CC	53.93	RN1		—	G	A	R																										
7H-CC	63.65	RN1		—	G	A	R																										
8H-7	72.63	RN1	B *Cyrtocapsella tetrapera*	21.82	M	A	R																										
9H-CC	82.64	RP22	T *Artophormis gracilis*	22.41	G	A	R																										
10H-7	91.65	RP22	B *Lychnocanoma elongata*	24.18	G	A	R																										
11H-CC	101.52	RP21b		—	M	C	R																										
12H-7	110.70	RP21b		—	M	F	B																										
13H-7	120.06	RP21b	B *Lychnocanoma apadora*	26.50	M	C	B																										
14H-CC	128.55	RP21a		—	M	C	B																										
15H-CC	139.68	RP21a	B *Dorcadospyris ateuchus*	28.64	M	C	B																										
29X-3, 20–22	245.11	RP12	T *Theocotyle conica*	45.63	P	C	B	x	x	x			x					x	x			x	Rew	x	x			x	Rew		x	x	x
29X-3, 98–100	245.89	RP12	B *Eusyringium lagena*	46.21	P	F	B			x			x	x		x	x	x				x		x				x					
29X-4, 16–18	246.57	RP11	B *Dictyoprora mongolfieri*	47.98	M	C	B			x						x	x					x		x	x			x					x
31X-1, 15–17	255.96	RP7?	T *Amphisphaera goruna*	55.5	P	F	B																					x					
31X-2, 99–101	258.30	RP7		—	M	A	B					x							x		x	x		x			x	x	x	x			
31X-3, 97–99	259.78	—		—	G	A	B					x									x	x		x				x	x	x			
31X-CC	260.44	RP7	T *Lamptonium pennatum*	55.90	G	A	B				x	x			x				x		x	x	x	x		x		x	x	x			
32X-CC	266.19	RP7	B *Bekoma bidartensis*, T *Bekoma campechensis*	58.35, 57.83	M	C	B				x	x			x				x	x	x	x		x		x		x	x	x			
33X-4, 102–103	275.89	RP6	B *Buryella pentadica*	59.71	G	A	B				x	x			x				x		x	x				?		x	x	x			

Table T7. Planktonic foraminifer datums, Site U1406.

Core, section, interval (cm)		Age	Zone/ Subzone	Marker event	Age (Ma)	Depth (mbsf)			
Top	Bottom					Top	Bottom	Mid-point	±
342-U1406A-	342-U1406A-								
2H-CC	3H-2, 100–102	early Miocene	M4/M5	B *Praeorbulina sicana*	16.38	16.01	18.08	17.05	1.03
3H-6, 100–102	3H-CC	early Miocene	M3/M4	T *Catapsydrax dissimilis*	17.54	24.08	25.46	24.77	0.69
5H-4, 100–102	5H-6, 100–102	early Miocene	M1b/M2	T *Paragloborotalia kugleri*	21.12	40.20	43.20	41.70	1.50
8H-4, 100–102	8H-6, 100–102	early Miocene	M1a/M1b	T *Globoquadrina dehiscens*	22.44	68.70	71.70	70.20	1.50
9H-4, 100–102	9H-6, 88–90	early Miocene	O7/M1a	B *Paragloborotalia kugleri*	22.96	78.21	81.11	79.66	1.45
13H-6, 75–77	13H-CC	late Oligocene	O6/O7	B *Paragloborotalia pseudokugleri*	25.21	118.96	119.98	119.47	0.51
17H-3, 46–48	17H-5, 41–43	early Oligocene	O3/O4	B *Globoturborotalita angulisuturalis*	29.18	151.56	155.01	153.29	1.72
18H-2, 45–47	18H-4, 60–62	early Oligocene	O2/O3	T *Turborotalia ampliapertura*	30.28	159.09	162.24	160.67	1.58
19H-6, 154–159	20H-2, 100–102	early Oligocene	O1/O2	T *Pseudohastigernia naguewichiensis*	32.10	173.74	176.11	174.93	1.19
23H-1, 100–102	23H-2, 100–102	late Eocene	E15/E16	T *Globigerinatheka index*	34.61	200.30	201.80	201.05	0.75
26X-1, 100–102	26X-2, 100–102	late Eocene	E14/E15	T *Globigerinatheka semiinvoluta*	36.18	218.70	220.20	219.45	0.75
26X-CC	27X-2, 100–102	middle Eocene	lower E14	T *Acarinina* spp.	37.75	221.74	225.30	223.52	1.78
27X-4, 100–102	27X-6, 100–102	middle Eocene	E13/E14	T *Morozovelloides crassatus*	38.25	228.30	231.30	229.80	1.50
28X-3, 100–102	28X-4, 100–102	middle Eocene	E10/E11	T *Guembelitrioides nuttalli*	42.07	236.40	237.90	237.15	0.75
29X-1, 45–47	29X-2, 50–52	middle Eocene	E7/E8	B *Guembelitrioides nuttalli*	45.72	242.35	243.90	243.13	0.78
31X-2, 14–16	31X-3, 10–11	late Paleocene	P4/P5	T *Globanomalina pseudomenardii*	57.10	257.44	258.90	258.17	0.73

T = top, B = base.

Table T8. Planktonic foraminifer distribution, Site U1406. This table is available in an **oversized format.**

Table T9. Benthic foraminifer distribution, Site U1406. (Continued on next page.)

Core, section	Depth (mbsf)	Preservation	Abundance	*Abyssamina poagi*	*Abyssamina quadrata*	*Alabamina* sp.	*Anomalina* sp.	*Anomalinoides semicribratus*	*Anomalinoides* sp.	*Aragonia aragonensis*	*Aragonia velascoensis*	*Astacolus parallelus*	*Astacolus* sp.	*Bathysiphon* sp.	*Bolivina* sp.	*Bulbobaculites?*	*Bulimina aculeata*	*Bulimina* sp.	*Buliminella* sp.	*Cassidulina* sp.	*Cassidulina subglobosa*	*Chrysalogonium* sp.	*Cibicidoides* aff. *laurisae*	*Cibicidoides* cf. *havanensis*	*Cibicidoides eocaenus*	*Cibicidoides grimsdalei*	*Cibicidoides havanensis*	*Cibicidoides incrassatus*	*Cibicidoides kullenbergi*	*Cibicidoides mundulus*	*Cibicidoides pseudoperlucidus*	*Cibicidoides* sp.	*Cibicidoides subspiratus*	*Dentalina* sp.	*Dorothia trochoides*	*Eggerella bradyi*	*Ellipsodimorphina* spp.	*Ellipsoidella* sp.	*Epistominella* sp.	*Epistominella umbonifera?*	*Eponides* sp.	*Fissurina* sp.	*Gaudryina pyramidata*	*Gavelinella beccariiformis*	*Gavelinella hyphalus*	*Gavelinella* sp.	*Glomospira* sp.	*Guttulina* sp.	*Gyroidina* sp.	*Gyroidinoides globosus*	*Gyroidinoides* spp.
342-U1406A-																																																		
1H-CC	6.23	VG	P				F		F				P					F			A	F					F			P			F	F			F	F		P				F		F
2H-CC	16.04	VG	P				A		F				P	P							A						F					F	F				F	F						F		F
3H-CC	25.49	VG	R			P	F	F	F					P	F			F			A						F	P		P			F		F	D		F					P		P
4H-CC	35.07	VG	P				F	P	F					F							F						P	P		F			F				F						F		F
5H-CC	44.43	VG	P				F	F	F					P				F			D	F					F						F			P		F					P		P
6H-CC	53.93	VG	P				F		F									F			A	F	P	P			F	F		F			F	F	P		P					F		F
7H-CC	63.65	VG	P			P	F		F												D					P			F	F			F				P									F
8H-CC	72.63	VG	P				F	P	A												A	F					F	P					P	F		F		P								F
9H-CC	82.64	VG	P			F	F		P					F				P			A	F					F	A		F			P	A		P		F	F				F		F
10H-CC	91.65	VG	P			P	A		P					F				F			F	P								P			F	F		F		P							F
11H-CC	101.52	VG	P				F		F					P				A			A	P					F	F		F			F	F				P					F		F
12H-CC	110.70	VG	P				A	F	F					F				D			D	F				P				F			F	F		P		P					F		F
13H-CC	120.06	VG	P			P	F		F				P	F		P				A	A					F		P	P	F			F	F	F	P		F					F		A
14H-CC	128.55	VG	P				F		F												F	A	F					F		F			F	F	F	F		P					P		F
15H-CC	139.68	VG	P				A		F												A	F		F	P		P			F			F	F		F						F		A
16H-CC	148.04	VG	P			P	A	F	F				P									F	F			P			P	P		P		F			F					F		F
17H-CC	157.27	G	D			F	P	P	P												F	A			A		P			F			P	F			F					P		F
18H-CC	164.71	VG	P			F	F	F	A					F				F			F	A	F				F			F			F	P	P	P		F					F		F
19H-CC	173.77	G	A			F	F	F	F					F				F			P	A	P			F	F			P		F	P	F		F		F					F		F
20H-CC	181.73	G	F			F	F		A					F				P			P	D	P			A				F		F	P	F	P	F		P		F	P	P			F		F
21H-CC	191.51	VG	R			P		F	F				P					F				A	F			P				F		A	F			P		F					F		F
22H-CC	199.29	VG	F			F	A		A					F				F			F	A	F			P	F			F		F	F	F		P		F					F		F
23H-CC	208.05	VG	A			F	F		F					F				F				A	F			F	F			F		F	F	F	P	F		F					F		F
25H-CC	217.68	G	F				A		F					F	P	F	P	P	F			F	A		F					P		F	A	F	F		P					F		F
26X-CC	221.77	G	R				F		F					F			F	P					F	P					F		F		F	P		F		P	F				F		F
27X-CC	232.31	M	R			F	F	F	A					F				F					F			P	F					F		F		F					F		F
28X-CC	242.30	G	P	F		F	F		F	A		P	P		P			F				P	F	P		F	P	P			F		A				F							F		F
29X-CC	250.79	M	P						P	F								P											P			F	A	P										F		
30X-CC	254.68	VG	P	P						P													P	P								F	A	A										F		
31X-CC	260.44	G	P				F		F	P			P					F															F	F				P			A	A	A			F		P
32X-CC	266.19	G	P		P	P	F		F		F							A															A	P			F		P		F	A		A	F	F		
33X-CC	278.63	M	P				F	P	F		F							F															F	F					P		F	A	F	A	F	F	P	F
34X-CC	281.03	M	A			P	P		F		F						F															F	F			F					A		A	F	P	P	P

Preservation: VG = very good, G = good, M = moderate. Abundance: D = dominant, A = abundant, F = few, R = rare, P = present. See **"Biostratigraphy"** in the "Methods" chapter (Norris et al., 2014a) for preservation and abundance definitions.

Table T9 (continued).

Core, section	Depth (mbsf)	Preservation	Abundance	*Hanzawaia* sp.	*Karreriella* sp.	*Laevidentalina* sp.	*Lagena* sp.	*Laticarinina pauperata*	*Lenticulina* cf. *adenalensis*	*Lenticulina* sp.	*Lenticulina whitei*	*Neoeponides* sp.	*Nodosarella* sp.	*Nodosaria aspera*	*Nodosaria* sp.	*Nonion* spp.	*Nuttallides truempyi*	*Oridorsalis* sp.	*Oridorsalis umbonatus*	*Osangularia* sp.	*Paralabamina hillebrandti*	*Pleurostomella acuta*	*Pleurostomella tenuis*	*Pleurostomella* sp.	*Polymorphina* sp.	*Pullenia bulloides*	*Pullenia* cf. *jarvisis*	*Pullenia coryelli*	*Pullenia jarvisi*	*Pullenia quinqueloba*	*Pyramidina* sp.	*Pyrgo* sp.	*Quinqueloculina* sp.	*Rectuvigerina* sp.	*Reophax* sp.	*Saracenaria* sp.	*Spiroplectammina spectabilis*	*Spiroplectammina* sp.	*Stilostomella gracillima*	*Stilostomella lepidula*	*Stilostomella paleocenica*	*Stilostomella* sp.	*Stilostomella subspinosa*	*Strictocostella scharbergana*	*Tritaxia* sp.	*Trochammina* sp.	*Turrilina* sp.	*Uvigerina elongata*	*Valvulina spinosa*?	Others
342-U1406A-																																																	
1H-CC	6.23	VG	P				P	F						P		F						F	F			F				P		P						F	F		F	A				P		P	F
2H-CC	16.04	VG	P				P	P		P						F			F				F			F				F			F					F			F	F				P	P	P	F
3H-CC	25.49	VG	R		P		F	F		P						F			F							P	P			F		F	P					F	P		F	F				F		P	P
4H-CC	35.07	VG	P				F						P					P	P							F	F			P		P						P	A		F	A						P	F
5H-CC	44.43	VG	P		F		F			P						P		P	F							F				F			F						P			P	F							F
6H-CC	53.93	VG	P				P											P	F							F	F			F		P						P	F		F	A						F	P
7H-CC	63.65	VG	P					P										P	F			P	P	P		F	P					F	F						F		P	F		A					F
8H-CC	72.63	VG	P		P			F								F			F				F			A				F			P					P	F		F	F			P				F
9H-CC	82.64	VG	P							P		P						F	P			F	P			P	P			P												F	A			P				F
10H-CC	91.65	VG	P		F											F			A				P	P		F	P			F								F	F		F	F			P	F			F
11H-CC	101.52	VG	P											P		F		F	F				F			F	F			P	P							P	F			A							F
12H-CC	110.70	VG	P		F									F				F	F				P				F			F								P	F			A							P
13H-CC	120.06	VG	P		F		F											F	F				P			F	F															P		F		P				
14H-CC	128.55	VG	P				P											P	F				F			P	P								P					P	F			P	F				F
15H-CC	139.68	VG	P		F	F										F		F	F				F			P	P			F										P	F			F	A		P		F			F
16H-CC	148.04	VG	P				F							P	P	P		P	F			A	F	F		F				A				F			P	F	P			F	P				F			F	F
17H-CC	157.27	G	D				F								F			P	F				P	F		F									P			F	A			F	F	P			F		F
18H-CC	164.71	VG	P				P							P	F	P		F					F		F	A									P			P	P			P	F		P		F			P
19H-CC	173.77	G	A		P										F			F	F						P	P	P			P									A			F	F			A	P	F		F
20H-CC	181.73	G	F		P									P	P	P		F	F				F		P	P	F			F				F								F				F	P		F	P
21H-CC	191.51	VG	R	P	P									P	F			P	F				P		F					F			F					F	A			F	P				P			F	F
22H-CC	199.29	VG	F							F						P		F	F				F	F		F				F									F			F								F	F
23H-CC	208.05	VG	A		F		F								P	P	F	F	F				P			F				F					P			P	P		F	F								F
25H-CC	217.68	G	F		P												F	P	A							F	P								P			P	F		F	P		F						
26X-CC	221.77	G	R		F		F								P		D		A				F		F	P	P								P				F		F	F						F	F
27X-CC	232.31	M	R		F				P								A	P	F						P	P									P			F	A		F	F		P				F	P
28X-CC	242.30	G	P		F										P		F	F	F				F	P	F													F	A		F	F		P					P
29X-CC	250.79	M	P														D		A																P			P			F									
30X-CC	254.68	VG	P														P	P	A						P																P									
31X-CC	260.44	G	P						P		A				P		A	P	F		F				P			F							F															P
32X-CC	266.19	G	P																P	F					P			P	F												F									P
33X-CC	278.63	M	P						F		P						A	P	F	P					F			F	F																					F
34X-CC	281.03	M	A														A			F		F						F	F																						F

Table T10. Benthic foraminifer morphotype distribution, Site U1406. (Continued on next page.)

Core, section, interval (cm)	Depth (mbsf)	Preservation	Group abundance	Agglutinated	Elongated	Planispiral	Tapered	Trochospiral
342-U1406A-								
2H-2, 100–102	8.71	VG	P	R	R	A	P	A
2H-4, 100–102	11.71	VG	P	P	R	A	P	A
2H-5, 100–102	13.21	VG	P	F	A	A	A	A
3H-4, 100–102	21.09	VG	P	A	A	F	A	D
3H-6, 100–102	24.09	VG	P	F	A	F	A	D
4H-2, 100–102	27.71	VG	A	A	A	A	A	D
4H-4, 100–102	30.71	VG	P	A	D	R	F	A
5H-2, 100–102	37.21	VG	A	A	A	F	A	D
5H-4, 100–102	40.21	VG	P	R	D	F	F	D
6H-2, 100–102	46.71	VG	R	A	A	F	A	A
6H-4, 100–102	49.71	VG	R	F	A	F	A	D
7H-2, 110–112	56.31	G	R	A	A	R	A	D
7H-4, 110–112	59.31	VG	R	F	A	F	A	D
8H-2, 100–102	65.71	G	D	F	A	R	D	D
8H-4, 100–102	68.71	G	P	A	A	R	D	A
8H-6, 100–102	71.71	G	P	F	A	A	D	A
9H-2, 100–102	75.21	VG	P	R	A	A	A	D
9H-4, 100–102	78.22	VG	R	A	D	B	A	D
9H-6, 88–90	81.12	VG	R	A	F	F	A	D
10H-4, 100–102	87.71	VG	R	A	A	R	A	D
10H-6, 100–102	90.71	VG	R	A	A	A	A	D
11H-4, 100–102	97.21	VG	A	R	A	F	A	D
11H-6, 100–102	100.22	M	R	B	A	B	A	D
12H-2, 90–92	103.61	G	R	A	F	R	D	D
12H-4, 100–102	106.71	VG	R	F	A	A	A	D
13H-2, 100–102	113.21	VG	A	A	F	R	A	D
13H-4, 100–102	116.22	VG	A	A	D	F	A	D
14H-2, 100–102	122.71	VG	A	A	F	R	A	D
14H-4, 100–102	125.71	G	A	A	A	A	F	D
15H-2, 100–102	132.21	VG	A	A	A	F	A	D
15H-4, 100–102	135.24	VG	A	A	A	F	A	D
16H-2, 100–102	141.71	G	R	R	A	F	D	D
16H-4, 100–102	144.71	G	D	F	A	R	D	A
16H-6, 80–82	147.51	VG	A	F	A	A	A	D
17H-3, 46–48	151.57	M	P	A	A	F	A	D
17H-5, 91–93	155.02	VG	P	A	F	F	D	A
18H-2, 45–47	159.10	VG	A	R	A	P	D	D
18H-4, 60–62	162.25	G	A	F	D	F	F	D
19H-1, 97–99	165.68	VG	R	A	F	F	D	A
19H-4, 86–88	170.07	G	A	F	A	P	D	D
20H-2, 100–102	176.12	VG	D	F	A	R	A	D
20H-4, 90–92	179.02	G	A	A	D	B	A	A
21H-3, 51–53	184.47	VG	A	R	D	F	A	D
21H-5, 95–97	187.65	VG	D	F	A	F	A	A
22H-1, 100–102	192.21	VG	A	R	A	F	D	D
22H-3, 100–102	195.17	VG	A	F	D	R	A	D
22H-5, 100–102	198.17	VG	D	R	A	R	D	D
22H-6, 50–52	198.97	VG	A	F	A	R	A	D
23H-1, 100–102	200.31	VG	D	P	A	B	A	D
23H-3, 100–102	203.31	VG	R	R	A	A	A	D
23H-5, 100–102	206.24	VG	R	R	A	F	A	D
26X-1, 100–102	218.71	VG	R	R	A	R	F	D
26X-2, 100–102	220.21	VG	R	R	A	A	A	D
27X-2, 100–102	225.31	VG	P	A	A	R	F	D
27X-4, 100–102	228.31	M	P	A	A	B	B	D
27X-6, 100–102	231.31	G	P	R	A	R	A	D
28X-2, 100–102	234.91	VG	R	A	A	B	R	D
28X-4, 100–102	237.91	G	P	R	D	B	A	A
28X-6, 100–102	240.91	VG	P	B	D	R	A	D
29X-2, 50–52	243.91	VG	P	F	A	B	F	D
29X-4, 100–102	247.11	G	P	A	A	A	F	D
30X-1, 75–77	252.26	VG	P	A	R	F	R	D
30X-2, 53–53	253.54	P	P	F	A	B	A	D

Table T10 (continued).

Core, section, interval (cm)	Depth (mbsf)	Preservation	Group abundance	Agglutinated	Elongated	Planispiral	Tapered	Trochospiral
31X-2, 14–16	257.45	VG	P	F	A	B	A	D
31X-3, 10–11	258.91	M	P	B	A	R	A	D
32X-3, 74–76	264.75	G	P	B	D	B	A	D
33X-2, 100–102	273.03	VG	P	A	D	B	A	D
33X-4, 100–102	275.87	VG	P	R	A	F	A	D
34X-1, 82–84	279.43	M	D	F	A	R	F	D

Preservation: VG = very good, G = good, M = moderate, P = poor. Abundance: D = dominant, A = abundant, F = few, R = rare, P = present, B = barren.

Table T11. Core orientation data, Site U1406.

Hole U1406A		Hole U1406B	
Core	MTF (°)	Core	MTF (°)
324-U1406A-		324-U1406B-	
1H	317	1H	259
2H	229	2H	232
3H	171	3H	190
4H	32	4H	101
5H	26	5H	87
6H	84	6H	42
7H	352	7H	337
8H	338	8H	64
9H	297	9H	185
10H	347	10H	59
11H	307	11H	170
12H	14	12H	6
13H	324	13H	200
14H	55	14H	355
15H	27	15H	262
16H	360	16H	291
17H	272	17H	238
		18H	283

MTF = magnetic tool face orientation from geomagnetic north.

Table T12. Summary of AF demagnetization results for discrete samples, Hole U1406A. (Continued on next two pages.)

Core, section, interval (cm)	Depth (mbsf)	Declination 20 mT or PCA (°)	Inclination 20 mT or PCA (°)	PCA MAD (°)	PCA range (mT)	NRM 20 mT (A/m)	Measurement error (%)
342-U1406A-							
1H-2-W, 75–77	2.26	131.7	–60.9			1.93E–03	4.9
1H-4-W, 45–77	5.11	–43.0	34.3			3.68E–05	22.1
2H-3-W, 75–77	9.96	157.0	–64.4			9.67E–05	11.8
2H-4-W, 75–77	11.46	161.8	–59.6			1.32E–04	12.4
2H-5-W, 75–77	12.96	268.3	67.0			6.50E–05	16.6
3H-3-W, 75–77	19.34	–0.9	54.7			2.46E–05	40.3
3H-5-W, 75–77	22.34	–30.1	33.9			2.51E–05	38.5
4H-4-W, 75–77	30.46	–21.2	24.6			6.65E–05	26.3
4H-5-W 75–77	31.96	161.8	–37.9			2.75E–05	42.4
5H-3-W 75–77	38.46	149.6	–54.6			2.47E–05	43.8
5H-5-W 75–77	41.46	126.3	–20.1			3.98E–05	22.6
6H-3-W, 75–77	47.96	4.7	33.2			3.16E–05	51.7
6H-6-W, 75–77	52.46	–26.6	–9.8			1.65E–05	80.8

Table T12 (continued). (Continued on next page.)

Core, section, interval (cm)	Depth (mbsf)	Declination 20 mT or PCA (°)	Inclination 20 mT or PCA (°)	PCA MAD (°)	PCA range (mT)	NRM 20 mT (A/m)	Measurement error (%)
7H-3-W, 75–77	57.46	–40.8	44.9			4.07E–05	32.3
7H-5-W, 75–77	60.46	–14.1	–82.9			2.29E–05	35.7
8H-3-W, 74–76	66.95	121.7	–26.3			1.72E–05	46.9
8H-5-W, 74–76	69.95	–32.0	5.0			1.27E–05	96.0
9H-3-W, 74–76	76.45	193.2	–45.3			2.81E–05	38.1
9H-4-W, 74–76	77.96	222.4	–31.6			3.13E–05	39.3
10H-3-W, 74–76	85.95	62.9	–76.0			5.75E–05	17.2
10H-5-W, 74–76	88.95	–18.3	1.3			4.32E–06	261.0
11H-2-W, 74–76	93.95	226.4	–56.6			3.13E–05	41.9
11H-3-W, 74–76	95.45	–48.6	44.7			5.13E–05	26.2
11H-4-W, 74–76	96.95	234.8	–70.0			7.97E–05	16.1
12H-1-W, 74–76	101.95	79.5	–57.3			2.09E–05	49.3
12H-2-W, 101–103	103.72	92.3	–69.8			5.30E–05	24.0
12H-3-W, 74–76	104.95	102.9	–55.5			1.82E–05	49.8
12H-5-W, 74–76	107.95	–31.0	36.2			1.10E–04	15.0
12H-6-W, 57–59	109.28	19.4	–85.4			4.00E–05	20.7
12H-7-W, 36–38	110.28	106.2	–61.3			2.71E–05	25.7
13H-1-W, 74–76	111.45	200.8	–65.0			2.29E–05	56.1
13H-2-W, 74–76	112.95	–24.7	14.2			4.05E–05	31.7
13H-4-W, 74–76	115.96	–12.7	45.9			3.88E–05	28.3
13H-5-W, 74–76	117.46	–16.1	26.3			6.78E–05	17.6
13H-6-W, 42–44	118.64	–54.9	51.9			6.32E–05	16.8
13H-7-W, 37–39	119.60	–10.3	45.5			4.15E–05	23.1
14H-1-W, 64–66	120.85	173.9	–21.3			4.07E–04	4.7
14H-2-W, 74–76	122.45	55.0	–79.6			4.86E–05	23.8
14H-4-W, 55–57	125.26	–12.3	0.9			3.30E–05	36.9
14H-5-W, 27–29	126.09	33.7	25.5			5.94E–05	26.5
14H-6-W, 23–25	126.63	101.5	–12.4			3.30E–05	27.4
14H-7-W, 59–61	127.94	–51.4	34.7			1.50E–04	12.7
15H-3-W, 74–76	133.46	128.3	–44.7			5.46E–05	4.3
15H-5-W, 74–76	136.51	148.3	–24.9			5.66E–05	5.2
15H-7-W, 29–31	139.07	44.3	18.1			3.32E–05	20.7
16H-1-W, 75–77	139.96	104.3	–32.7			2.17E–05	18.1
16H-4-W, 75–77	144.46	–15.3	48.2	16.3	10–60	9.29E–05	10.6
17H-3-W, 75–77	151.86	–58.7	70.3			3.58E–05	15.7
17H-4-W, 75–77	153.36	–71.7	27.6			2.25E–05	14.5
17H-5-W, 75–77	154.86	217.6	56.4			1.18E–05	43.8
17H-6-W, 75–77	156.36	182.0	2.5			2.04E–05	23.0
18H-1-W, 75–77	158.06	–51.2	–37.6			3.06E–05	14.9
18H-2-W, 75–77	159.40	–76.0	45.3			3.77E–05	9.4
18H-3-W, 75–77	160.90	2.3	60.7			1.02E–04	8.7
18H-4-W, 75–77	162.40	–14.2	72.2			6.93E–05	5.8
18H-5-W, 75–77	163.90	31.3	–84.9			6.07E–05	10.6
19H-2-W, 75–77	166.96	18.1	52.5			5.55E–05	8.8
19H-3-W, 75–77	168.46	245.4	–42.9	3.3	10–30	1.74E–04	6.2
19H-5-W, 75–77	171.46	222.6	–20.9			7.50E–05	10.1
20H-2-W, 75–77	175.87	40.0	44.7			6.32E–05	4.8
20H-3-W, 75–77	177.37	215.1	–35.4			2.62E–05	28.5
20H-4-W, 75–77	178.87	–86.0	–18.4			3.77E–05	16.2
20H-5-W, 75–77	180.37	256.2	–37.2			3.32E–05	16.2
20H-6-W, 35–37	181.28	254.1	–28.9			1.03E–04	8.6
21H-1-W, 100–102	182.71	41.9	–19.6			2.89E–04	3.6
21H-3-W, 75–77	184.71	–49.2	–19.6	6.3	10–60	4.73E–04	9.5
21H-5-W, 75–77	187.45	–51.4	–12.8			2.53E–04	10.0
21H-6-W, 35–37	188.43	105.6	–33.0			2.13E–04	2.7
22H-1-W, 75–77	191.96	116.0	–44.9			7.02E–05	10.3
22H-2-W, 75–77	193.42	126.3	–28.1			6.03E–05	11.8
22H-3-W, 75–77	194.92	–23.3	27.6			3.11E–05	27.0
22H-4-W, 75–77	196.42	–48.1	29.2			4.10E–05	12.4
22H-5-W, 75–77	197.92	–28.3	30.4			3.30E–05	10.7
23H-2-W, 74–76	201.55	97.8	–20.3			4.79E–05	16.4
23H-3-W, 74–76	203.05	–31.1	–19.0	6.7	20–60	3.30E–04	8.7
23H-4-W, 80–82	204.61	139.7	55.0			1.20E–04	5.1
26X-1-W, 76–78	218.47	248.4	60.7			6.01E–04	4.8
26X-2-W, 74–76	219.95	–89.8	42.0			1.32E–04	13.4
26X-3-W, 24–26	220.95	195.0	37.0	2.3	10–30	1.41E–03	4.5
27X-1-W, 73–75	223.54	157.5	60.7	9.8	10–60	9.18E–05	8.6
27X-7-W, 39–41	231.92	205.8	25.8			1.62E–04	7.2

Table T12 (continued).

Core, section, interval (cm)	Depth (mbsf)	Declination 20 mT or PCA (°)	Inclination 20 mT or PCA (°)	PCA MAD (°)	PCA range (mT)	NRM 20 mT (A/m)	Measurement error (%)
28X-2-W, 68–70	234.59	–4.4	4.8	3.4	20–60	5.12E–04	6.7
28X-6-W, 50–52	240.41	–23.0	17.3			5.58E–05	24.5
29X-1-W, 73–75	242.64	165.7	26.5			1.81E–04	4.9
29X-2-W, 82–84	244.23	21.4	17.2			1.25E–03	4.2
29X-3-W, 47–49	245.38	–81.6	12.2			2.12E–03	8.7
29X-5-W, 95–97	248.56	53.9	–3.5			4.12E–04	2.5
31X-1-W, 64–66	256.45	–28.7	–9.9			1.63E–03	8.3
31X-3-W, 57–59	259.38	94.8	–33.2			4.03E–04	2.6
32X-2-W, 47–49	262.98	13.7	–8.3			1.43E–03	4.7
32X-3-W, 59–61	264.60	86.9	16.4			5.84E–04	2.6
33X-1-W, 53–55	271.14	–87.9	–54.3			1.05E–03	6.7
33X-2-W, 30–32	272.33	–45.5	–42.9			5.39E–04	10.3
33X-3-W, 75–77	274.12	133.5	–21.8			4.32E–04	5.3
33X-4-W, 36–38	275.23	49.4	–10.6			7.92E–04	2.6
33X-5-W, 66–68	277.05	–0.2	–6.0			1.52E–03	6.1
33X-6-W, 22–24	278.04	68.6	–60.8			1.06E–03	4.3
34X-1-W, 37–39	278.98	51.7	12.5			4.38E–03	2.3
34X-2-W, 20–22	279.98	–5.6	58.4			8.81E–04	17.1

Declinations for Cores 1H to 17H are corrected into geographical coordinates using FlexIT orientation data. PCA = principal component analysis, MAD = maximum angle of deviation, NRM = natural remanent magnetism.

Table T13. Magnetostratigraphic tie points, Site U1406. (Continued on next two pages.)

Chron boundary	Age (Ma)	Hole U1406A Top Core, section, interval (cm)	Top Depth (mbsf)	Bottom Core, section, interval (cm)	Bottom Depth (mbsf)	Mid-point (mbsf)
		342-U1406A-		342-U1406A-		
C5Dn/C5Dr.1r	17.533	2H-3, 75.0	9.95	2H-3, 82.5	10.03	9.99
C5Dr.1r/C5Dr.1n	17.717	2H-3, 115.0	10.35	2H-3, 122.5	10.43	10.39
C5Dr.1n/C5Dr.2r	17.740	2H-3, 140.0	10.60	2H-4, 30.0	11.00	10.80
C5Dr.2r/C5En	18.056	2H-5, 32.5	12.53	2H-5, 40.0	12.60	12.57
C5En/C5Er	18.524	NI	NI	NI	NI	NI
C5Er/C6n	18.748	NI	NI	NI	NI	NI
C6n/C6r	19.722	4H-1, 107.5	26.28	4H-1, 120.0	26.40	26.34
C6r/C6An.1n	20.040	4H-2, 140.0	28.10	4H-3, 87.5	29.08	28.59
C6An.1n/C6An.1r	20.213	4H-4, 130.0	31.00	4H-5, 10.0	31.30	31.15
C6An.1r/C6An.2n	20.439	NI	NI	NI	NI	NI
C6An.2n/C6Ar	20.709	NI	NI	NI	NI	NI
C6Ar/C6AAn	21.083	NI	NI	NI	NI	NI
C6AAn/C6AAr.1r	21.159	NI	NI	NI	NI	NI
C6AAr.1r/C6AAr.1n	21.403	NI	NI	NI	NI	NI
C6AAr.1n/A6AAr.2r	21.483	NI	NI	NI	NI	NI
C6AAr.2r/C6AAr.2n	21.659	NI	NI	NI	NI	NI
C6AAr.2n/C6AAr.3r	21.688	NI	NI	NI	NI	NI
C6AAr.3r/C6Bn.1n	21.767	6H-2, 22.5	45.93	6H-2, 50.0	46.20	46.07
C6Bn.1n/C6Bn.1r	21.936	6H-5, 47.5	50.68	6H-5, 57.5	50.78	50.73
C6Bn.1r/C6Bn.2n	21.992	6H-6, 105.0	52.75	6H-7, 10.0	53.06	52.91
C6Bn.2n/C6Br	22.268	7H-4, 137.5	59.58	7H-5, 42.5	60.13	59.86
C6Br/C6Cn.1n	22.564	8H-4, 100.0	68.70	8H-5, 15.0	69.53	69.12
C6Cn.1n/C6Cn.1r	22.754	9H-1, 115.0	73.85	9H-2, 10.0	74.30	74.08
C6Cn.1r/C6Cn.2n	22.902	9H-5, 55.0	79.27	9H-5, 90.0	79.62	79.45
C6Cn.2n/C6Cn.2r	23.030	9H-6, 87.5	81.11	9H-6, 97.5	81.21	81.16
C6Cn.2r/C6Cn.3n	23.233	NI	NI	NI	NI	NI
C6Cn.3n/C6Cr	23.295	NI	NI	NI	NI	NI
C6Cr/C7n.1n	23.962	11H-2, 140.0	94.60	11H-3, 12.5	94.83	94.72
C7n.1n/C7n.1r	24.000	11H-3, 97.5	95.68	11H-3, 112.5	95.83	95.76
C7n.1r/C7n.2n	24.109	11H-4, 132.5	97.53	11H-5, 25.0	97.95	97.74
C7n.2n/C7r	24.474	NI	NI	NI	NI	NI
C7r/C7An	24.761	12H-3, 137.5	105.58	12H-4, 12.5	105.83	105.71
C7An/C7Ar	24.984	12H-5, 137.5	108.58	12H-6, 20.0	108.90	108.74
C7Ar/C8n.1n	25.099	NI	NI	NI	NI	NI
C8n.1n/C8n.1r	25.264	NI	NI	NI	NI	NI
C8n.1r/C8n.2n	25.304	NI	NI	NI	NI	NI
C8n.2n/C8r	25.987	NI	NI	NI	NI	NI
C8r/C9n	26.420	16H-1, 117.5	140.38	16H-2, 10.0	140.80	140.59
C9n/C9r	27.439	NI	NI	NI	NI	NI
C9r/C10n.1n	27.859	NI	NI	NI	NI	NI
C10n.1n/C10n.1r	28.087	NI	NI	NI	NI	NI
C10n.1r/C10n.2n	28.141	NI	NI	NI	NI	NI
C10n.2n/C10r	28.278	NI	NI	NI	NI	NI
C10r/C11n.1n	29.183	18H-2, 30.0	158.94	18H-2, 40.0	159.04	158.99
C11n.1n/C11n.1r	29.477	18H-4, 110.0	162.74	18H-4, 120.0	162.84	162.79
C11n.1r/C11n.2n	29.527	18H-5, 107.5	164.22	18H-5, 117.5	164.32	164.27
C11n.2n/C11r	29.970	19H-2, 100.0	167.30	19H-3, 20.0	167.90	167.60
C11r/C12n	30.591	NI	NI	NI	NI	NI
C12n/C12r	31.034	20H-2, 125.0	176.36	20H-3, 17.5	176.79	176.58
C12r/C13n	33.157	22H-2, 140.0	194.06	22H-4, 12.5	195.79	194.93
C13n/C13r	33.705	NI	NI	NI	NI	NI
C13r/C15n	34.999	23H-3, 120.0	203.50	23H-4, 37.5	204.18	203.84
C15n/C15r	35.294	NI	NI	NI	NI	NI

Ages from Gradstein et al. (2012). NI = not identified.

Table T13 (continued). (Continued on next page.)

Chron boundary	Age (Ma)	Hole U1406B Top Core, section, interval (cm)	Top Depth (mbsf)	Bottom Core, section, interval (cm)	Bottom Depth (mbsf)	Mid-point (mbsf)
		342-U1406B-		342-U1406B-		
C5Dn/C5Dr.1r	17.533	NI	NI	NI	NI	NI
C5Dr.1r/C5Dr.1n	17.717	NI	NI	NI	NI	NI
C5Dr.1n/C5Dr.2r	17.740	NI	NI	NI	NI	NI
C5Dr.2r/C5En	18.056	NI	NI	NI	NI	NI
C5En/C5Er	18.524	NI	NI	NI	NI	NI
C5Er/C6n	18.748	NI	NI	NI	NI	NI
C6n/C6r	19.722	4H-6, 140.0	31.86	5H-1, 10.0	29.90	30.88
C6r/C6An.1n	20.040	NI	NI	NI	NI	NI
C6An.1n/C6An.1r	20.213	5H-2, 47.5	31.78	5H-3, 12.5	32.93	32.35
C6An.1r/C6An.2n	20.439	5H-7, 45.0	39.15	6H-1, 10.0	39.40	39.28
C6An.2n/C6Ar	20.709	6H-1, 127.5	40.58	6H-2, 17.5	40.98	40.78
C6Ar/C6AAn	21.083	6H-5, 57.5	45.88	6H-5, 80.0	46.10	45.99
C6AAn/C6AAr.1r	21.159	6H-5, 137.5	46.68	6H-6, 37.5	47.18	46.93
C6AAr.1r/C6AAr.1n	21.403	6H-6, 80.0	47.60	6H-7, 12.5	48.43	48.01
C6AAr.1n/A6AAr.2r	21.483	NI	NI	NI	NI	NI
C6AAr.2r/C6AAr.2n	21.659	NI	NI	NI	NI	NI
C6AAr.2n/C6AAr.3r	21.688	NI	NI	NI	NI	NI
C6AAr.3r/C6Bn.1n	21.767	NI	NI	NI	NI	NI
C6Bn.1n/C6Bn.1r	21.936	NI	NI	NI	NI	NI
C6Bn.1r/C6Bn.2n	21.992	NI	NI	NI	NI	NI
C6Bn.2n/C6Br	22.268	NI	NI	NI	NI	NI
C6Br/C6Cn.1n	22.564	9H-1, 100.0	68.80	9H-1, 132.5	69.13	68.96
C6Cn.1n/C6Cn.1r	22.754	9H-5, 22.5	74.06	9H-5, 35.0	74.18	74.12
C6Cn.1r/C6Cn.2n	22.902	10H-1, 135.0	78.65	10H-2, 40.0	79.20	78.93
C6Cn.2n/C6Cn.2r	23.030	10H-4, 52.5	82.35	10H-4, 80.0	82.62	82.48
C6Cn.2r/C6Cn.3n	23.233	NI	NI	NI	NI	NI
C6Cn.3n/C6Cr	23.295	NI	NI	NI	NI	NI
C6Cr/C7n.1n	23.962	11H-5, 137.5	94.18	11H-6, 25.0	94.55	94.36
C7n.1n/C7n.1r	24.000	NI	NI	NI	NI	NI
C7n.1r/C7n.2n	24.109	NI	NI	NI	NI	NI
C7n.2n/C7r	24.474	12H-3, 95.0	100.26	12H-4, 25.0	101.07	100.67
C7r/C7An	24.761	12H-6, 130.0	105.14	13H-1, 30.0	105.80	105.47
C7An/C7Ar	24.984	13H-2, 62.5	107.64	13H-2, 90.0	107.91	107.77
C7Ar/C8n.1n	25.099	13H-3, 37.5	108.90	13H-3, 52.5	109.05	108.97
C8n.1n/C8n.1r	25.264	13H-6, 25.0	113.30	13H-6, 32.5	113.38	113.34
C8n.1r/C8n.2n	25.304	13H-6, 87.5	113.93	13H-6, 87.5	113.93	113.93
C8n.2n/C8r	25.987	15H-2, 112.5	127.13	15H-3, 25.0	127.75	127.44
C8r/C9n	26.420	16H-4, 27.5	138.81	16H-5, 10.0	140.14	139.47
C9n/C9r	27.439	NI	NI	NI	NI	NI
C9r/C10n.1n	27.859	NI	NI	NI	NI	NI
C10n.1n/C10n.1r	28.087	NI	NI	NI	NI	NI
C10n.1r/C10n.2n	28.141	NI	NI	NI	NI	NI
C10n.2n/C10r	28.278	NI	NI	NI	NI	NI
C10r/C11n.1n	29.183	NI	NI	NI	NI	NI
C11n.1n/C11n.1r	29.477	18H-3, 132.5	157.33	18H-4, 10.0	157.60	157.47
C11n.1r/C11n.2n	29.527	18H-5, 15.0	159.15	18H-5, 52.5	159.525	159.34
C11n.2n/C11r	29.970	19H-4, 112.5	166.135	19H-5, 60.0	167.11	166.62
C11r/C12n	30.591	19H-7, 97.5	170.485	20H-1, 115.0	172.25	171.37
C12n/C12r	31.034	20H-5, 102.5	178.165	20H-5, 110.0	178.24	178.20
C12r/C13n	33.157	NI	NI	NI	NI	NI
C13n/C13r	33.705	NI	NI	NI	NI	NI
C13r/C15n	34.999	NI	NI	NI	NI	NI
C15n/C15r	35.294	NI	NI	NI	NI	NI

Table T13 (continued).

Chron boundary	Age (Ma)	Hole U1406C Top Core, section, interval (cm)	Top Depth (mbsf)	Bottom Core, section, interval (cm)	Bottom Depth (mbsf)	Mid-point (mbsf)
		342-U1406C-		342-U1406C-		
C5Dn/C5Dr.1r	17.533	NI	NI	NI	NI	NI
C5Dr.1r/C5Dr.1n	17.717	NI	NI	NI	NI	NI
C5Dr.1n/C5Dr.2r	17.740	NI	NI	NI	NI	NI
C5Dr.2r/C5En	18.056	NI	NI	NI	NI	NI
C5En/C5Er	18.524	NI	NI	NI	NI	NI
C5Er/C6n	18.748	NI	NI	NI	NI	NI
C6n/C6r	19.722	NI	NI	NI	NI	NI
C6r/C6An.1n	20.040	NI	NI	NI	NI	NI
C6An.1n/C6An.1r	20.213	NI	NI	NI	NI	NI
C6An.1r/C6An.2n	20.439	NI	NI	NI	NI	NI
C6An.2n/C6Ar	20.709	NI	NI	NI	NI	NI
C6Ar/C6AAn	21.083	NI	NI	NI	NI	NI
C6AAn/C6AAr.1r	21.159	NI	NI	NI	NI	NI
C6AAr.1r/C6AAr.1n	21.403	NI	NI	NI	NI	NI
C6AAr.1n/A6AAr.2r	21.483	NI	NI	NI	NI	NI
C6AAr.2r/C6AAr.2n	21.659	NI	NI	NI	NI	NI
C6AAr.2n/C6AAr.3r	21.688	NI	NI	NI	NI	NI
C6AAr.3r/C6Bn.1n	21.767	NI	NI	NI	NI	NI
C6Bn.1n/C6Bn.1r	21.936	NI	NI	NI	NI	NI
C6Bn.1r/C6Bn.2n	21.992	NI	NI	NI	NI	NI
C6Bn.2n/C6Br	22.268	8H-4, 140.0	65.80	8H-5, 32.5	66.23	66.01
C6Br/C6Cn.1n	22.564	9H-1, 125.0	70.65	9H-2, 25.0	71.15	70.90
C6Cn.1n/C6Cn.1r	22.754	9H-2, 140.0	72.30	9H-3, 32.5	72.73	72.51
C6Cn.1r/C6Cn.2n	22.902	9H-4, 85.0	74.75	9H-4, 107.5	74.98	74.86
C6Cn.2n/C6Cn.2r	23.030	9H-5, 17.5	75.58	9H-5, 45.0	75.85	75.71
C6Cn.2r/C6Cn.3n	23.233	NI	NI	NI	NI	NI
C6Cn.3n/C6Cr	23.295	10H-1, 100.0	79.90	10H-1, 135.0	80.25	80.08
C6Cr/C7n.1n	23.962	11H-3, 140.0	92.80	11H-4, 12.5	93.03	92.91
C7n.1n/C7n.1r	24.000	11H-4, 135.0	94.25	11H-5, 10.0	94.50	94.38
C7n.1r/C7n.2n	24.109	11H-5, 110.0	95.50	11H-6, 17.5	96.08	95.79
C7n.2n/C7r	24.474	12H-4, 92.5	103.33	12H-4, 102.5	103.43	103.38
C7r/C7An	24.761	13H-2, 10.0	108.76	13H-3, 20.0	109.17	108.97
C7An/C7Ar	24.984	13H-4, 47.5	110.95	13H-4, 62.5	111.10	111.02
C7Ar/C8n.1n	25.099	NI	NI	NI	NI	NI
C8n.1n/C8n.1r	25.264	NI	NI	NI	NI	NI
C8n.1r/C8n.2n	25.304	NI	NI	NI	NI	NI
C8n.2n/C8r	25.987	15H-5, 85.0	133.50	15H-5, 25.0	134.15	133.83
C8r/C9n	26.420	NI	NI	NI	NI	NI
C9n/C9r	27.439	17H-3, 130.0	149.70	17H-4, 60.0	150.50	150.10
C9r/C10n.1n	27.859	NI	NI	NI	NI	NI
C10n.1n/C10n.1r	28.087	NI	NI	NI	NI	NI
C10n.1r/C10n.2n	28.141	NI	NI	NI	NI	NI
C10n.2n/C10r	28.278	NI	NI	NI	NI	NI
C10r/C11n.1n	29.183	NI	NI	NI	NI	NI
C11n.1n/C11n.1r	29.477	18H-2, 95.0	157.35	18H-2, 125.0	157.65	157.50
C11n.1r/C11n.2n	29.527	18H-3, 82.5	158.73	18H-3, 92.5	158.83	158.78
C11n.2n/C11r	29.970	NI	NI	NI	NI	NI
C11r/C12n	30.591	NI	NI	NI	NI	NI
C12n/C12r	31.034	NI	NI	NI	NI	NI
C12r/C13n	33.157	22X-6, 105.0	192.82	22X-7, 10.0	193.37	193.10
C13n/C13r	33.705	NI	NI	NI	NI	NI
C13r/C15n	34.999	23X-2, 85.0	197.55	23X-2, 110.0	197.8	197.68
C15n/C15r	35.294	23X-4, 137.5	201.08	23X-5, 27.5	201.48	201.28

Table T14. Summary of anisotropy of magnetic susceptibility of discrete samples, Hole U1406A. (Continued on next two pages.)

Core, section, interval (cm)	Depth (mbsf)	τ_3	V_3 (°)		τ_2	V_2 (°)		τ_1	V_1 (°)		Bulk susceptibility (SI)	Anisotropy (%)	*P*	L	F
			Declination	Inclination		Declination	Inclination		Declination	Inclination					
342-U1406A-															
1H-2W, 75–77	2.26	0.3329	111.4	62.1	0.3333	340.7	19.0	0.3337	243.7	19.6	2.31E–04	0.1	1.002	1.001	1.001
1H-4W, 45–47	5.11	0.3244	278.2	35.2	0.3358	172.7	20.7	0.3398	58.4	47.5	3.37E–05	1.5	1.048	1.012	1.035
2H-1W, 75–77	6.96	0.3193	99.3	6.3	0.3329	269.8	83.7	0.3478	9.2	1.0	2.66E–05	2.8	1.089	1.044	1.043
2H-3W, 75–77	9.96	0.3206	22.7	5.9	0.3343	119.8	49.8	0.3451	287.8	39.6	2.10E–05	2.5	1.076	1.032	1.043
2H-5W, 75–77	12.96	0.3279	122.7	45.1	0.3327	3.1	26.2	0.3394	254.1	33.4	3.08E–05	1.1	1.035	1.020	1.015
2H-7W, 35–37	15.56	0.3247	254.6	4.3	0.3332	163.5	14.4	0.3421	0.7	75.0	2.33E–05	1.7	1.054	1.026	1.026
3H-1W, 75–77	16.46	0.3267	264.3	0.3	0.3331	173.9	48.7	0.3402	354.6	41.3	2.96E–05	1.4	1.041	1.021	1.020
3H-3W, 75–77	19.34	0.3271	41.6	25.8	0.3324	304.1	15.1	0.3405	187.0	59.5	2.98E–05	1.3	1.041	1.025	1.016
3H-5W, 75–77	22.34	0.3258	168.7	66.4	0.3337	288.4	12.2	0.3405	22.9	19.9	3.00E–05	1.5	1.045	1.020	1.024
3H-7W, 30–32	24.89	0.3187	290.3	46.7	0.3370	171.6	24.4	0.3443	64.3	33.3	2.59E–05	2.6	1.080	1.022	1.057
4H-1W, 75–77	25.96	0.3231	98.5	43.8	0.3359	206.5	17.8	0.3410	312.6	40.8	3.36E–05	1.8	1.055	1.015	1.040
4H-3W, 75–77	28.96	0.3269	253.0	20.1	0.3354	60.0	69.4	0.3377	161.4	4.3	2.18E–05	1.1	1.033	1.007	1.026
4H-5W, 75–77	31.96	0.3149	272.4	32.4	0.3404	63.4	54.0	0.3447	173.3	13.9	2.34E–05	3.0	1.095	1.013	1.081
4H-7W, 30–32	34.51	0.3304	330.3	14.6	0.3326	60.5	1.0	0.3370	154.2	75.4	2.18E–05	0.7	1.020	1.013	1.007
5H-1W, 65–67	35.36	0.3219	353.4	42.5	0.3315	125.5	36.2	0.3466	236.7	26.2	2.58E–05	2.5	1.077	1.045	1.030
5H-3W, 75–77	38.46	0.3104	278.4	27.5	0.3369	151.6	49.0	0.3527	24.3	27.8	2.83E–05	4.2	1.136	1.047	1.086
5H-5W, 75–77	41.46	0.3177	183.7	39.1	0.3339	64.2	31.3	0.3484	308.7	35.3	2.75E–05	3.1	1.097	1.044	1.051
5H-7W, 25–27	43.96	0.3236	231.0	7.5	0.3345	127.1	61.5	0.3419	324.9	27.3	2.48E–05	1.8	1.056	1.022	1.034
6H-1W, 75–77	44.96	0.3166	63.8	20.7	0.3379	192.3	58.7	0.3455	324.8	22.3	2.26E–05	2.9	1.091	1.022	1.067
6H-3W, 75–77	47.96	0.3253	246.1	57.1	0.3330	48.3	31.7	0.3417	143.3	8.2	1.99E–05	1.6	1.050	1.026	1.024
6H-5W, 75–77	50.96	0.3250	47.0	25.5	0.3315	305.2	23.1	0.3434	178.6	54.4	1.81E–05	1.8	1.057	1.036	1.020
6H-7W, 30–32	53.27	0.3179	120.0	81.1	0.3307	9.4	3.1	0.3514	279.0	8.3	1.68E–05	3.4	1.106	1.062	1.041
7H-1W, 75–77	54.46	0.3237	0.1	72.9	0.3341	226.7	12.0	0.3422	134.1	12.1	2.77E–05	1.9	1.057	1.024	1.032
7H-3W, 75–77	57.46	0.3175	116.3	38.9	0.3331	1.2	27.7	0.3494	246.4	38.6	2.26E–05	3.2	1.100	1.049	1.049
7H-5W, 75–77	60.46	0.3183	44.2	14.8	0.3343	173.2	67.2	0.3474	309.6	16.9	2.87E–05	2.9	1.092	1.039	1.050
7H-7W, 30–32	63.01	0.3243	136.5	18.3	0.3301	6.8	62.7	0.3456	233.2	19.6	4.54E–05	2.1	1.066	1.047	1.018
8H-1W, 74–76	63.95	0.3247	222.2	35.4	0.3322	343.4	36.0	0.3431	103.2	34.3	3.16E–05	1.8	1.057	1.033	1.023
8H-3W, 74–76	66.95	0.3230	254.8	34.6	0.3321	13.1	34.4	0.3449	133.9	36.7	3.38E–05	2.2	1.068	1.038	1.028
8H-5W, 74–76	69.95	0.3235	248.9	45.4	0.3336	69.0	44.6	0.3429	339.0	0.1	2.52E–05	1.9	1.060	1.028	1.031
8H-7W, 29–31	72.27	0.3268	208.3	5.8	0.3334	302.9	38.4	0.3398	111.1	51.0	2.61E–05	1.3	1.040	1.019	1.020
9H-1W, 74–76	73.45	0.3182	12.5	17.4	0.3352	246.7	61.9	0.3465	109.5	21.4	2.94E–05	2.8	1.089	1.034	1.053
9H-3W, 74–76	76.45	0.3270	111.9	1.6	0.3321	306.6	88.4	0.3409	201.9	0.4	3.33E–05	1.4	1.042	1.026	1.015
9H-7W, 30–32	82.07	0.3284	198.0	30.7	0.3302	107.0	1.7	0.3414	14.1	59.2	4.04E–05	1.3	1.040	1.034	1.005
10H-1W, 74–76	82.95	0.3244	24.4	16.3	0.3314	145.3	60.4	0.3442	286.9	24.0	3.55E–05	2.0	1.061	1.039	1.021
10H-3W, 74–76	85.95	0.3305	137.8	31.9	0.3325	266.9	45.4	0.3370	28.9	27.6	4.62E–05	0.6	1.020	1.014	1.006
10H-5W, 74–76	88.95	0.3286	133.3	11.3	0.3325	33.3	41.0	0.3389	235.6	46.8	4.45E–05	1.0	1.031	1.019	1.012
10H-7W, 34–36	91.25	0.3276	297.3	40.9	0.3300	149.1	44.5	0.3423	42.2	16.5	2.73E–05	1.5	1.045	1.037	1.007
11H-1W, 74–76	92.45	0.3250	359.4	27.4	0.3342	252.4	29.4	0.3408	124.2	47.7	2.98E–05	1.6	1.049	1.020	1.029
11H-3W, 74–76	95.45	0.3282	204.5	3.1	0.3341	295.2	12.3	0.3377	100.8	77.3	3.32E–05	0.9	1.029	1.011	1.018
11H-5W, 74–76	98.45	0.3301	137.2	35.3	0.3340	288.5	51.1	0.3359	36.9	14.3	3.85E–05	0.6	1.018	1.006	1.012
11H-7W, 43–45	100.86	0.3292	297.2	1.9	0.3344	203.9	60.3	0.3364	28.3	29.6	4.50E–05	0.7	1.022	1.006	1.016
12H-1W, 74–76	101.95	0.3277	325.3	68.6	0.3357	223.6	4.5	0.3366	131.9	20.8	4.72E–05	0.9	1.027	1.003	1.024
12H-3W, 74–76	104.95	0.3302	260.3	8.0	0.3337	154.9	62.1	0.3361	354.3	26.6	4.95E–05	0.6	1.018	1.007	1.011
12H-5W, 74–76	107.95	0.3301	281.6	5.1	0.3332	190.3	14.2	0.3367	31.0	74.9	4.78E–05	0.7	1.020	1.011	1.009
12H-7W, 36–38	110.28	0.3302	240.7	28.1	0.3321	20.8	55.1	0.3376	140.2	18.9	4.87E–05	0.7	1.022	1.017	1.006

Table T14 (continued). (Continued on next page.)

Core, section, interval (cm)	Depth (mbsf)	τ_3	V_3 (°)		τ_2	V_2 (°)		τ_1	V_1 (°)		Bulk susceptibility (SI)	Anisotropy (%)	*P*	L	F
			Declination	Inclination		Declination	Inclination		Declination	Inclination					
13H-1W, 74–76	111.45	0.3317	194.7	64.1	0.3329	329.8	19.0	0.3354	65.8	17.0	4.03E–05	0.4	1.011	1.008	1.003
13H-3W, 74–76	114.45	0.3302	204.9	35.0	0.3320	359.1	52.1	0.3378	105.8	12.6	4.86E–05	0.8	1.023	1.017	1.006
13H-5W, 74–76	117.46	0.3302	264.3	4.4	0.3317	354.3	0.5	0.3381	90.7	85.6	4.75E–05	0.8	1.024	1.019	1.004
13H-7W, 37–39	119.60	0.3302	55.9	11.5	0.3310	316.5	38.9	0.3388	159.3	48.8	3.76E–05	0.9	1.026	1.023	1.003
14H-1W, 64–66	120.85	0.3307	89.1	39.1	0.3334	249.5	49.2	0.3359	351.0	9.8	3.92E–05	0.5	1.016	1.007	1.008
14H-3W, 74–76	123.95	0.3292	239.6	0.8	0.3330	147.3	69.9	0.3378	329.9	20.1	4.55E–05	0.9	1.026	1.015	1.011
14H-5W, 27–29	126.09	0.3313	113.3	8.1	0.3321	218.0	60.8	0.3366	19.0	27.9	5.07E–05	0.5	1.016	1.014	1.003
14H-7W, 59–61	127.94	0.3271	45.5	20.3	0.3353	250.0	67.9	0.3376	138.6	8.4	4.90E–05	1.1	1.032	1.007	1.025
15H-1W, 74–76	130.45	0.3310	264.7	20.7	0.3335	170.5	11.1	0.3355	54.0	66.3	4.92E–05	0.4	1.013	1.006	1.007
15H-3W, 74–76	133.46	0.3254	38.4	43.7	0.3343	298.1	10.6	0.3403	197.6	44.4	5.16E–05	1.5	1.046	1.018	1.028
15H-5W, 74–76	136.51	0.3290	65.6	30.4	0.3323	219.2	56.8	0.3387	328.4	12.1	4.68E–05	1.0	1.029	1.019	1.010
15H-7W, 29–31	139.07	0.3276	79.5	66.4	0.3339	215.0	17.3	0.3385	310.0	15.5	5.36E–05	1.1	1.033	1.014	1.019
16H-1W, 75–77	139.96	0.3302	253.5	49.5	0.3328	21.2	27.5	0.3370	126.7	27.1	6.49E–05	0.7	1.021	1.012	1.008
16H-3W, 75–77	142.96	0.3283	313.7	35.4	0.3339	150.3	53.4	0.3379	49.4	8.0	4.82E–05	1.0	1.029	1.012	1.017
16H-5W, 75–77	145.96	0.3262	42.3	32.7	0.3320	263.7	49.4	0.3418	146.7	21.2	4.73E–05	1.6	1.048	1.029	1.018
17H-1W, 75–77	148.86	0.3287	266.1	37.5	0.3332	85.1	52.5	0.3381	175.7	0.5	6.25E–05	0.9	1.028	1.015	1.014
17H-3W, 75–77	151.86	0.3294	293.3	44.5	0.3324	124.0	45.0	0.3382	28.6	5.4	5.61E–05	0.9	1.026	1.017	1.009
17H-5W, 75–77	154.86	0.3313	64.1	64.0	0.3337	202.6	20.0	0.3350	298.5	15.8	6.80E–05	0.4	1.011	1.004	1.007
18H-1W, 75–77	158.06	0.3278	219.9	69.0	0.3344	11.4	18.6	0.3378	104.5	9.3	6.31E–05	1.0	1.031	1.010	1.020
18H-3W, 75–77	160.90	0.3298	158.7	12.5	0.3341	251.4	11.7	0.3361	23.1	72.7	8.00E–05	0.6	1.019	1.006	1.013
18H-5W, 75–77	163.90	0.3293	199.0	73.0	0.3341	307.3	5.5	0.3366	38.9	16.1	6.95E–05	0.7	1.022	1.008	1.015
19H-1W, 75–77	165.46	0.3291	226.8	44.1	0.3339	55.4	45.6	0.3369	321.0	4.3	6.44E–05	0.8	1.024	1.009	1.015
19H-3W, 75–77	168.46	0.3268	285.9	52.5	0.3359	98.3	37.3	0.3373	191.1	3.7	5.98E–05	1.1	1.032	1.004	1.028
19H-5W, 75–77	171.46	0.3298	31.6	56.4	0.3346	294.5	4.7	0.3356	201.5	33.2	8.86E–05	0.6	1.018	1.003	1.015
20H-1W, 75–77	174.46	0.3304	63.0	3.5	0.3344	326.3	62.1	0.3353	154.8	27.7	6.27E–05	0.5	1.015	1.003	1.012
20H-3W, 75–77	177.37	0.3295	139.3	57.2	0.3331	255.2	15.7	0.3373	353.8	28.0	8.15E–05	0.8	1.024	1.013	1.011
20H-5W, 75–77	180.37	0.3305	125.1	34.9	0.3328	24.4	15.0	0.3368	275.0	51.1	8.22E–05	0.6	1.019	1.012	1.007
21H-1W, 100–102	182.71	0.3314	324.4	3.5	0.3327	60.2	58.4	0.3359	232.3	31.4	9.57E–05	0.4	1.013	1.009	1.004
21H-3W, 75–77	186.09	0.3298	169.5	65.9	0.3339	64.0	6.8	0.3363	331.1	23.1	1.02E–04	0.6	1.020	1.007	1.012
21H-5W, 75–77	187.45	0.3281	149.1	66.9	0.3346	309.7	22.0	0.3373	42.5	7.0	1.02E–04	0.9	1.028	1.008	1.020
22H-1W, 75–77	191.96	0.3306	106.7	46.6	0.3342	316.3	39.4	0.3352	213.4	15.2	5.97E–05	0.5	1.014	1.003	1.011
22H-3W, 75–77	194.92	0.3282	46.8	38.0	0.3341	305.1	14.6	0.3377	198.1	48.3	3.89E–05	0.9	1.029	1.011	1.018
22H-5W, 75–77	197.92	0.3242	83.4	24.5	0.3315	330.1	41.0	0.3443	195.2	39.1	3.51E–05	2.0	1.062	1.039	1.022
23H-1W, 76–78	200.07	0.3281	138.5	59.9	0.3325	42.8	3.3	0.3393	310.8	29.9	6.99E–05	1.1	1.034	1.020	1.013
23H-3W, 74–76	203.05	0.3251	110.4	61.3	0.3363	226.4	13.5	0.3387	322.8	24.8	6.91E–05	1.4	1.042	1.007	1.035
23H-5W, 74–76	206.05	0.3301	68.8	56.2	0.3335	252.1	33.7	0.3364	161.1	1.5	8.92E–05	0.6	1.019	1.009	1.010
26X-1W, 76–78	218.47	0.3276	16.6	54.9	0.3338	183.6	34.4	0.3386	277.8	6.1	6.87E–05	1.1	1.034	1.015	1.019
26X-3W, 24–26	220.95	0.3313	55.4	24.9	0.3316	208.9	62.6	0.3371	320.3	10.7	1.14E–04	0.6	1.017	1.016	1.001
27X-1W, 73–75	223.54	0.3278	96.8	57.3	0.3327	325.5	23.0	0.3395	225.6	21.9	7.00E–05	1.2	1.036	1.020	1.015
27X-3W, 74–76	226.55	0.3287	253.8	37.9	0.3334	125.5	38.6	0.3379	9.3	29.0	5.53E–05	0.9	1.028	1.014	1.014
27X-5W, 84–86	229.65	0.3284	131.3	20.4	0.3301	7.6	56.2	0.3415	231.6	25.7	5.55E–05	1.3	1.040	1.035	1.005
27X-7W, 39–41	231.92	0.3303	59.5	86.5	0.3315	225.2	3.4	0.3382	315.2	0.9	7.98E–05	0.8	1.024	1.020	1.004
28X-1W, 60–62	233.01	0.3282	250.1	54.6	0.3342	359.0	13.0	0.3376	97.4	32.3	9.37E–05	0.9	1.029	1.010	1.018
28X-3W, 80–82	236.21	0.3284	265.6	45.1	0.3344	26.5	27.1	0.3372	135.6	32.6	5.06E–05	0.9	1.027	1.008	1.018
28X-5W, 65–67	239.06	0.3282	271.7	52.1	0.3320	178.7	2.4	0.3398	86.8	37.8	5.91E–05	1.2	1.035	1.024	1.011
29X-1W, 73–75	242.64	0.3281	115.2	38.7	0.3303	208.3	3.9	0.3416	303.1	51.0	5.08E–05	1.4	1.041	1.034	1.007
29X-3W, 47–49	245.38	0.3283	253.0	68.8	0.3355	32.2	16.4	0.3361	126.1	13.1	9.85E–05	0.8	1.024	1.002	1.022

Table T14 (continued).

Core, section, interval (cm)	Depth (mbsf)	τ_3	V_3 (°)		τ_2	V_2 (°)		τ_1	V_1 (°)		Bulk susceptibility (SI)	Anisotropy (%)	*P*	L	F
			Declination	Inclination		Declination	Inclination		Declination	Inclination					
29X-5W, 95–97	248.56	0.3215	215.0	42.1	0.3349	315.0	10.9	0.3436	56.4	45.8	3.36E–05	2.2	1.069	1.026	1.042
31X-1W, 64–66	256.45	0.3242	245.9	60.5	0.3361	355.3	10.7	0.3397	90.8	27.2	5.65E–05	1.6	1.048	1.011	1.037
31X-3W, 57–59	259.38	0.3182	62.5	53.7	0.3372	207.3	31.0	0.3446	307.9	17.0	3.01E–05	2.6	1.083	1.022	1.059
32X-1W, 83–85	261.84	0.3307	31.2	56.3	0.3326	129.3	5.4	0.3367	222.8	33.1	4.72E–05	0.6	1.018	1.013	1.006
32X-3W, 59–61	264.60	0.3279	327.4	9.2	0.3346	235.3	12.9	0.3375	92.0	74.1	3.67E–05	1.0	1.029	1.009	1.020
33X-1W, 53–55	271.14	0.3301	187.2	0.8	0.3317	95.2	67.7	0.3382	277.5	22.3	3.91E–05	0.8	1.024	1.020	1.005
33X-5W, 66–68	277.05	0.3309	296.1	54.6	0.3326	55.2	19.0	0.3366	156.1	28.6	4.62E–05	0.6	1.017	1.012	1.005
34X-1W, 37–39	278.98	0.3287	69.7	81.5	0.3354	229.8	8.0	0.3360	320.2	2.9	1.75E–04	0.7	1.022	1.002	1.020
34X-2W, 20–22	279.98	0.3292	207.8	73.0	0.3347	91.1	7.8	0.3361	358.9	15.0	2.23E–04	0.7	1.021	1.004	1.017

τ_1, τ_2, and τ_3 are eigenvalues, and V_3, V_2, and V_1 are eigenvectors associated with minimum, intermediate, and maximum susceptibility, respectively. Measurement field = 300 A/m, sample volume = 7 cm^3. *P* = anisotropy degree, L = lineation, F = foliation.

Table T15. Biostratigraphic and magnetostratigraphic datums, Hole U1406A. (Continued on next page.)

Datum tie point	Datum	Datum type	Zone/Subzone	Age (Ma)	Depth (mbsf)		
					Top	Bottom	Mid-point
D01	T *Pseudoemiliania lacunosa*	Calcareous nannofossil	NN20	0.44	0.00	0.75	0.38
	T *Discoaster brouweri*	Calcareous nannofossil	NN19	1.93	0.75	2.26	1.51
	T *Sphenolithus heteromorphus*	Calcareous nannofossil	NN6	13.53	2.26	3.76	3.01
	T *Helicosphaera ampliaperta*	Calcareous nannofossil	NN5	14.91	2.26	3.76	3.01
	B *Sphenolithus heteromorphus*	Calcareous nannofossil		17.71	6.23	8.71	7.47
	T *Sphenolithus belemnos*	Calcareous nannofossil	NN4	17.95	8.71	11.70	10.21
	Tc *Triquetrorhabdulus carinatus*	Calcareous nannofossil	NN3	18.28	11.70	14.45	13.08
	B *Sphenolithus belemnos*	Calcareous nannofossil		19.03	35.07	37.21	36.14
	B *Sphenolithus disbelemnos*	Calcareous nannofossil		22.76	72.63	75.21	73.92
	T *Sphenolithus capricornutus*	Calcareous nannofossil		22.97	79.72	81.12	80.42
	T *Sphenolithus delphix*	Calcareous nannofossil		23.11	79.72	81.12	80.42
	B *Sphenolithus delphix*	Calcareous nannofossil		23.21	83.20	84.70	83.95
	T *Sphenolithus ciperoensis*	Calcareous nannofossil	NN1	24.43	98.70	100.22	99.46
	T *Sphenolithus distentus*	Calcareous nannofossil	NP25	26.44	145.95	148.04	146.99
D09	Bc *Triquetrorhabdulus carinatus*	Calcareous nannofossil		26.57	145.95	148.04	146.99
	B *Sphenolithus ciperoensis*	Calcareous nannofossil	NP24	29.62	158.05	160.89	159.47
	B *Sphenolithus distentus*	Calcareous nannofossil		30.00	166.95	168.45	167.70
	T *Reticulofenestra umbilicus* (>14 µm)	Calcareous nannofossil	NP23	32.02	173.77	181.70	177.74
	T *Isthmolithus recurvus*	Calcareous nannofossil		32.49	181.73	186.08	183.91
	T *Coccolithus formosus*	Calcareous nannofossil	NP22	32.92	191.51	194.16	192.84
	T *Discoaster saipanensis*	Calcareous nannofossil	NP21	34.44	199.29	199.37	199.33
	T *Discoaster barbadiensis*	Calcareous nannofossil		34.76	201.10	202.77	201.94
	B *Isthmolithus recurvus*	Calcareous nannofossil	NP19/NP20	36.97	221.20	221.77	221.49
	Bc *Chiasmolithus oamaruensis*	Calcareous nannofossil	NP18	38.09	221.77	225.30	223.53
	T *Chiasmolithus grandis*	Calcareous nannofossil		37.98	221.77	225.30	223.53
	B *Dictyococcites bisectus* (>10 µm)*	Calcareous nannofossil		40.36	233.41	234.91	234.16
D13	T *Chiasmolithus solitus*	Calcareous nannofossil	NP17	40.40	234.91	239.90	237.41
	B *Reticulofenestra reticulata*	Calcareous nannofossil		41.66	240.53	242.30	241.42
	T *Nannotetrina* spp.	Calcareous nannofossil		41.85	240.53	242.30	241.42
	B *Reticulofenestra umbilicus* (>14 µm)	Calcareous nannofossil		41.94	242.30	242.47	242.39
	T *Nannotetrina fulgens*	Calcareous nannofossil		42.87	242.30	242.47	242.39
	T *Chiasmolithus gigas*	Calcareous nannofossil	NP15c	44.12	242.47	245.11	243.79
	B *Chiasmolithus gigas*	Calcareous nannofossil	NP15b	45.49	247.60	249.10	248.35
	B *Nannotetrina fulgens*	Calcareous nannofossil	NP15a	46.29	250.45	250.79	250.62
	B *Nannotetrina cristata*	Calcareous nannofossil		47.73	250.79	254.80	252.73
	Fasciculithus division decline†	Calcareous nannofossil		56.00	254.68	255.88	255.28
	T *Fasciculithus alanii*†	Calcareous nannofossil		56.00	254.68	255.88	255.28
	T *Ericsonia robusta* (>9 µm)†	Calcareous nannofossil		57.10	260.44	262.84	261.64
	B *Discoaster multiradiatus*	Calcareous nannofossil	NP9	57.21	262.84	264.75	263.80
	Tc *Sphenolithus anarrhopus*	Calcareous nannofossil			262.84	264.75	263.80
	B *Discoaster delicatus*†	Calcareous nannofossil		57.45	264.75	265.90	265.33
	B *Ericsonia robusta* (>9 µm)†	Calcareous nannofossil		57.54	264.75	265.90	265.33
	Tc *Discoaster backmanii*†	Calcareous nannofossil		57.57	264.75	265.90	265.33
	B *Discoaster backmanii*†	Calcareous nannofossil		58.28	267.19	273.94	270.56
	B *Heliolithus riedellii*	Calcareous nannofossil	NP8	58.70	267.19	273.94	270.56
	B *Discoaster mohleri*	Calcareous nannofossil	NP7	58.97	278.63	279.43	279.03
	B *Sphenolithus anarrhopus*†	Calcareous nannofossil		59.40	278.63	279.43	279.03
	B *Heliolithus kleinpellii*	Calcareous nannofossil	NP6	59.54	279.43	280.37	279.90
D16	B *Heliolithus cantabriae*	Calcareous nannofossil		59.60	280.37	281.03	280.70
D17	B *Fasciculithus tympaniformis*	Calcareous nannofossil	NP5	61.51	281.03	281.03	281.03
	T *Didymocyrtis prismatica*	Radiolarian		16.73		16.04	16.04
	B *Dorcadospyris dentata*	Radiolarian		18.22	25.49	35.07	30.28
	T *Dorcadospyris ateuchus*	Radiolarian		18.64	25.49	35.07	30.28
	T *Theocotylissa annosa*	Radiolarian		20.05	35.07	44.43	39.75
	B *Cyrtocapsella tetrapera*	Radiolarian		21.82	72.63	82.64	77.63
	T *Lychnocanoma elongata*	Radiolarian		17.59		16.04	16.04
	B *Dorcadospyris dentata*	Radiolarian	RN3	18.22	25.49	35.07	30.28
	T *Dorcadospyris ateuchus*	Radiolarian		18.64	25.49	35.07	30.28
	T *Theocyrtis annosa*	Radiolarian	RN02	20.05	35.07	44.43	39.75
	B *Cyrtocapsa tetrapera*	Radiolarian		21.82	72.63	82.64	77.63
	T *Artophormis gracilis*	Radiolarian		22.41	72.63	82.64	77.63
	B *Lychnocanoma elongata*	Radiolarian	RP22	24.18	91.65	101.62	96.59
	B *Lychnocanoma apadora*	Radiolarian	RP21b	26.50	120.06	128.55	124.30
	B *Dorcadospyris ateuchus*	Radiolarian	RP21a	28.64	139.68		139.68
	T *Theocotyle conica*	Radiolarian		45.63		245.11	245.11
	B *Eusyringium lagena*	Radiolarian	RP12	46.21	245.90	246.57	246.23
D14	B *Dictyoprora mongolfieri*	Radiolarian	RP11	47.98	246.57	255.96	251.27
D15	T *Amphisphaera goruna*	Radiolarian		55.50	246.57	255.96	251.27

Table T15 (continued).

Datum tie point	Datum	Datum type	Zone/Subzone	Age (Ma)	Depth (mbsf)		
					Top	Bottom	Mid-point
	T *Lamptonium pennatum*	Radiolarian		55.90	255.96	260.44	258.20
	T *Bekoma campechensis*	Radiolarian		57.83	260.44	266.19	263.32
	B *Podocyrtis papalis*	Radiolarian		55.96	266.19	275.89	271.04
	B *Bekoma bidartensis*	Radiolarian	RP7	58.35	266.19	275.89	271.04
	T *Buryella pentadica*	Radiolarian	RP6	59.71	275.89		275.89
	B *Praeorbulina sicana*	Planktonic foraminifer	M4/M5	16.38	16.01	18.08	17.05
	T *Catapsydrax dissimilis*	Planktonic foraminifer	M3/M4	17.54	24.08	25.46	24.77
	T *Paragloborotalia kugleri*	Planktonic foraminifer	M1b/M2	21.12	40.20	43.20	41.70
	T *Globoquadrina dehiscens*	Planktonic foraminifer	M1a/M1b	22.44	68.70	71.70	70.20
	B *Paragloborotalia kugleri*	Planktonic foraminifer	O7/M1a	22.96	78.21	81.11	79.66
	B *Paragloborotalia pseudokugleri*	Planktonic foraminifer	O6/O7	25.21	118.96	119.98	119.47
	B *Globoturborotalita angulisuturalis*	Planktonic foraminifer	O3/O4	29.18	151.56	155.01	153.29
	T *Turborotalia ampliapertura*	Planktonic foraminifer	O2/O3	30.28	159.09	162.24	160.67
	T *Pseudohastigernia naguewichiensis*	Planktonic foraminifer	O1/O2	32.10	173.74	176.11	174.93
	T *Globigerinatheka index*	Planktonic foraminifer	E15/E16	34.61	200.30	201.80	201.05
	T *Globigerinatheka semiinvoluta*	Planktonic foraminifer	E14/E15	36.18	218.70	220.20	219.45
	T *Acarinina* spp.	Planktonic foraminifer	Lower E14	37.75	221.74	225.30	223.52
	T *Morozovelloides crassatus*	Planktonic foraminifer	E13/E14	38.25	228.30	231.30	229.80
	T *Guembelitrioides nuttalli*	Planktonic foraminifer	E10/E11	42.07	236.40	237.90	237.15
	B *Guembelitrioides nuttalli*	Planktonic foraminifer	E7/E8	45.72	242.35	243.90	243.13
	T *Globanomalina pseudomenardii*	Planktonic foraminifer	P4/P5	57.10	257.44	258.90	258.17
D02	C5Dn/C5Dr.1r	Chron boundary		17.53			9.99
	C5Dr.1r/C5Dr.1n	Chron boundary		17.72			10.39
	C5Dr.1n/C5Dr.2r	Chron boundary		17.74			10.80
	C5Dr.2r/C5En	Chron boundary		18.06			12.57
D03	C6n/C6r	Chron boundary		19.72			26.34
	C6r/C6An.1n	Chron boundary		20.04			28.59
	C6An.1n/C6An.1r	Chron boundary		20.21			31.15
D04	C6AAr.3r/C6Bn.1n	Chron boundary		21.77			46.07
	C6Bn.1n/C6Bn.1r	Chron boundary		21.94			50.73
	C6Bn.1r/C6Bn.2n	Chron boundary		21.99			52.91
	C6Bn.2n/C6Br	Chron boundary		22.27			59.86
	C6Br/C6Cn.1n	Chron boundary		22.56			69.12
	C6Cn.1n/C6Cn.1r	Chron boundary		22.75			74.08
	C6Cn.1r/C6Cn.2n	Chron boundary		22.90			79.45
D05	C6Cn.2n/C6Cn.2r	Chron boundary		23.03			81.16
D06	C6Cr/C7n.1n	Chron boundary		23.96			94.72
	C7n.1n/C7n.1r	Chron boundary		24.00			95.76
	C7n.1r/C7n.2n	Chron boundary		24.11			97.74
	C7r/C7An	Chron boundary		24.76			105.71
D07	C7An/C7Ar	Chron boundary		24.98			108.74
D08	C8r/C9n	Chron boundary		26.42			140.59
D11	C10r/C11n.1n	Chron boundary		29.18			158.99
	C11n.1n/C11n.1r	Chron boundary		29.48			162.79
	C11n.1r/C11n.2n	Chron boundary		29.53			164.27
	C11n.2n/C11r	Chron boundary		29.97			167.60
	C12n/C12r	Chron boundary		31.03			176.58
D12	C12r/C13n	Chron boundary		33.16			194.93
	C13r/C15n	Chron boundary		35.00			203.84

* = from Fornacini et al. (2010) recalibrated to GTS2012, † = from Agnini et al. (2007) recalibrated to GTS2012. T = top, Tc = top common, B = base, Bc = base common.

Table T16. Datum tie points, Hole U1406A.

Datum tie point	Datum	Datum type	Zone	Age (Ma)	Mid-point depth (mbsf)	Length (m)	Duration (Ma)	LSR (cm/k.y.)	Notes
D01	T *Pseudoemiliania lacunosa*	Calcareous nannofossil		0.44	0.38				
D02	C5Dn/C5Dr.1r	Chron boundary		17.53	9.99	9.62	17.09	0.06	0.06
D03	C6n/C6r	Chron boundary		19.72	26.34	16.35	2.19	0.75	Average rate = 0.85 cm/k.y.
D04	C6AAr.3r/C6Bn.1n	Chron boundary		21.77	46.07	19.73	2.04	0.96	
D05	C6Cn.2n/C6Cn.2r	Chron boundary		23.03	81.16	35.10	1.26	2.78	2.78
D06	C6Cr/C7n.1n	Chron boundary		23.96	94.72	13.56	0.93	1.45	Average rate = 1.41 cm/k.y.
D07	C7An/C7Ar	Chron boundary		24.98	108.74	14.03	1.02	1.37	
D08	C8r/C9n	Chron boundary		26.42	140.59	31.85	1.44	2.22	Average rate = 2.41 cm/k.y.
D09	Bc *Triquetrorhabdulus carinatus*	Calcareous nannofossil		26.57	146.99	6.40	0.15	4.27	
D10	Inferred hiatus			27.70	146.99	–0.00	1.13	–0.00	Hiatus
D11	C10r/C11n.1n	Chron boundary		29.18	158.99	12.00	1.48	0.81	Average rate = 0.88 cm/k.y.
D12	C12r/C13n	Chron boundary		33.16	194.93	35.94	3.97	0.90	
D13	T *Chiasmolithus solitus*	Calcareous nannofossil		40.40	237.41	42.48	7.24	0.59	0.59
D14	B *Dictyoprora mongolfieri*	Radiolarian		47.98	251.27	13.86	7.58	0.18	0.18
D15	T *Amphisphaera goruna*	Radiolarian		55.50	251.27	0.00	7.52	0.00	Hiatus
D16	B *Heliolithus cantabriae*	Calcareous nannofossil		59.60	280.70	29.43	4.10	0.72	0.72
D17	B *Fasciculithus tympaniformis*	Calcareous nannofossil		61.51	281.03	0.33	1.91	0.02	0.02

LSR = linear sedimentation rate. T = top, B = base, Bc = base common.

Table T17. Carbonate content and accumulation rates, Site U1406. (Continued on next four pages.)

Age (Ma)	LSR (cm/k.y.)	Dry density (g/cm^3)	$CaCO_3$ (wt%)	MAR (g/cm^2/k.y.)	CAR (g/cm^2/k.y.)	nCAR (g/cm^2/k.y.)
0.6	0.06	0.80	58.16	0.05	0.03	0.02
0.8	0.06	0.80	57.61	0.04	0.03	0.02
1.0	0.06	0.79	57.06	0.04	0.03	0.02
1.2	0.06	0.79	56.50	0.04	0.03	0.02
1.4	0.06	0.79	55.95	0.04	0.02	0.02
1.6	0.06	0.78	55.39	0.04	0.02	0.02
1.8	0.06	0.78	54.84	0.04	0.02	0.02
2.0	0.06	0.77	54.28	0.04	0.02	0.02
2.2	0.06	0.77	53.73	0.04	0.02	0.02
2.4	0.06	0.76	53.18	0.04	0.02	0.02
2.6	0.06	0.76	52.62	0.04	0.02	0.02
2.8	0.06	0.75	52.07	0.04	0.02	0.02
3.0	0.06	0.75	51.51	0.04	0.02	0.02
3.2	0.06	0.74	51.29	0.04	0.02	0.02
3.4	0.06	0.72	51.55	0.04	0.02	0.02
3.6	0.06	0.71	51.81	0.04	0.02	0.02
3.8	0.06	0.69	52.07	0.04	0.02	0.02
4.0	0.06	0.68	52.33	0.04	0.02	0.02
4.2	0.06	0.66	52.60	0.04	0.02	0.02
4.4	0.06	0.64	52.86	0.04	0.02	0.02
4.6	0.06	0.63	53.12	0.04	0.02	0.02
4.8	0.06	0.61	53.38	0.03	0.02	0.02
5.0	0.06	0.59	53.65	0.03	0.02	0.02
5.2	0.06	0.58	53.91	0.03	0.02	0.01
5.4	0.06	0.56	54.17	0.03	0.02	0.01
5.6	0.06	0.55	54.43	0.03	0.02	0.01
5.8	0.06	0.53	54.58	0.03	0.02	0.01
6.0	0.06	0.53	54.23	0.03	0.02	0.01
6.2	0.06	0.54	53.83	0.03	0.02	0.01
6.4	0.06	0.54	53.43	0.03	0.02	0.01
6.6	0.06	0.54	53.03	0.03	0.02	0.01
6.8	0.06	0.55	52.63	0.03	0.02	0.01
7.0	0.06	0.55	52.23	0.03	0.02	0.01
7.2	0.06	0.55	51.83	0.03	0.02	0.02
7.4	0.06	0.56	51.43	0.03	0.02	0.02
7.6	0.06	0.56	51.03	0.03	0.02	0.02
7.8	0.06	0.56	50.63	0.03	0.02	0.02
8.0	0.06	0.57	50.23	0.03	0.02	0.02
8.2	0.06	0.57	49.40	0.03	0.02	0.02
8.4	0.06	0.57	47.30	0.03	0.02	0.02
8.6	0.06	0.57	45.13	0.03	0.01	0.02
8.8	0.06	0.57	42.95	0.03	0.01	0.02
9.0	0.06	0.57	40.78	0.03	0.01	0.02
9.2	0.06	0.57	38.60	0.03	0.01	0.02
9.4	0.06	0.57	36.43	0.03	0.01	0.02
9.6	0.06	0.57	34.25	0.03	0.01	0.02
9.8	0.06	0.57	32.29	0.03	0.01	0.02
10.0	0.06	0.56	32.28	0.03	0.01	0.02
10.2	0.06	0.55	32.74	0.03	0.01	0.02
10.4	0.06	0.54	33.21	0.03	0.01	0.02
10.6	0.06	0.53	33.67	0.03	0.01	0.02
10.8	0.06	0.53	34.14	0.03	0.01	0.02
11.0	0.06	0.52	34.60	0.03	0.01	0.02
11.2	0.06	0.51	35.07	0.03	0.01	0.02
11.4	0.06	0.50	35.53	0.03	0.01	0.02
11.6	0.06	0.49	36.00	0.03	0.01	0.02
11.8	0.06	0.48	36.46	0.03	0.01	0.02
12.0	0.06	0.48	36.93	0.03	0.01	0.02
12.2	0.06	0.47	37.37	0.03	0.01	0.02
12.4	0.06	0.46	37.54	0.03	0.01	0.02
12.6	0.06	0.45	37.65	0.03	0.01	0.02
12.8	0.06	0.44	37.77	0.02	0.01	0.02
13.0	0.06	0.43	37.88	0.02	0.01	0.02
13.2	0.06	0.43	37.99	0.02	0.01	0.01
13.4	0.06	0.42	38.10	0.02	0.01	0.01
13.6	0.06	0.41	38.22	0.02	0.01	0.01
13.8	0.06	0.40	38.33	0.02	0.01	0.01
14.0	0.06	0.39	38.44	0.02	0.01	0.01
14.2	0.06	0.39	38.56	0.02	0.01	0.01

Table T17 (continued). (Continued on next page.)

Age (Ma)	LSR (cm/k.y.)	Dry density (g/cm^3)	$CaCO_3$ (wt%)	MAR (g/cm^2/k.y.)	CAR (g/cm^2/k.y.)	nCAR (g/cm^2/k.y.)
14.4	0.06	0.40	38.69	0.02	0.01	0.01
14.6	0.06	0.41	38.82	0.02	0.01	0.01
14.8	0.06	0.42	38.95	0.02	0.01	0.01
15.0	0.06	0.44	39.08	0.02	0.01	0.01
15.2	0.06	0.45	39.21	0.03	0.01	0.02
15.4	0.06	0.46	39.34	0.03	0.01	0.02
15.6	0.06	0.47	39.47	0.03	0.01	0.02
15.8	0.06	0.48	39.60	0.03	0.01	0.02
16.0	0.06	0.49	39.73	0.03	0.01	0.02
16.2	0.06	0.50	39.87	0.03	0.01	0.02
16.4	0.06	0.52	40.00	0.03	0.01	0.02
16.6	0.06	0.53	40.13	0.03	0.01	0.02
16.8	0.06	0.54	40.33	0.03	0.01	0.02
17.0	0.06	0.54	41.23	0.03	0.01	0.02
17.2	0.06	0.54	42.29	0.03	0.01	0.02
17.4	0.06	0.54	43.36	0.03	0.01	0.02
17.6	0.75	0.54	44.41	0.40	0.18	0.23
17.8	0.75	0.56	44.00	0.42	0.18	0.23
18.0	0.75	0.55	44.72	0.41	0.19	0.23
18.2	0.75	0.55	44.55	0.41	0.18	0.23
18.4	0.75	0.54	44.37	0.40	0.18	0.22
18.6	0.75	0.55	43.43	0.41	0.18	0.23
18.8	0.75	0.57	43.49	0.42	0.18	0.24
19.0	0.75	0.60	45.81	0.45	0.21	0.24
19.2	0.75	0.57	46.49	0.42	0.20	0.23
19.4	0.75	0.58	48.45	0.43	0.21	0.22
19.6	0.75	0.59	46.31	0.44	0.20	0.24
19.8	0.96	0.56	46.95	0.54	0.25	0.29
20.0	0.96	0.55	45.59	0.53	0.24	0.29
20.2	0.96	0.54	47.19	0.52	0.25	0.28
20.4	0.96	0.54	43.72	0.52	0.23	0.29
20.6	0.96	0.57	42.00	0.55	0.23	0.32
20.8	0.96	0.56	47.22	0.54	0.26	0.29
21.0	0.96	0.56	45.13	0.54	0.24	0.30
21.2	0.96	0.56	44.79	0.54	0.24	0.30
21.4	0.96	0.54	38.46	0.52	0.20	0.32
21.6	0.96	0.52	36.18	0.51	0.18	0.32
21.8	2.78	0.57	46.42	1.57	0.73	0.84
22.0	2.78	0.59	44.92	1.63	0.73	0.90
22.2	2.78	0.60	44.93	1.68	0.76	0.93
22.4	2.78	0.61	44.44	1.68	0.75	0.94
22.6	2.78	0.59	39.08	1.64	0.64	1.00
22.8	2.78	0.65	47.72	1.80	0.86	0.94
23.0	2.78	0.71	45.37	1.96	0.89	1.07
23.2	1.45	0.59	35.77	0.86	0.31	0.55
23.4	1.45	0.61	31.68	0.89	0.28	0.61
23.6	1.45	0.66	40.82	0.96	0.39	0.57
23.8	1.45	0.62	39.59	0.91	0.36	0.55
24.0	1.37	0.66	42.46	0.90	0.38	0.52
24.2	1.37	0.83	39.28	1.13	0.45	0.69
24.4	1.37	0.66	35.62	0.91	0.32	0.59
24.6	1.37	0.73	37.44	1.00	0.37	0.63
24.8	1.37	0.80	38.46	1.10	0.42	0.67
25.0	2.22	0.82	35.59	1.83	0.65	1.18
25.2	2.22	0.82	36.44	1.82	0.66	1.16
25.4	2.22	0.74	37.29	1.65	0.61	1.03
25.6	2.22	0.74	37.43	1.63	0.61	1.02
25.8	2.22	0.74	35.21	1.64	0.58	1.07
26.0	2.22	0.75	30.36	1.66	0.50	1.16
26.2	2.22	0.79	30.40	1.75	0.53	1.22
26.4	2.22	0.85	34.72	1.89	0.66	1.24
26.6	–0.00	0.95	40.84	–0.00	–0.00	–0.00
26.8	–0.00	0.94	39.87	–0.00	–0.00	–0.00
27.0	–0.00	0.94	39.27	–0.00	–0.00	–0.00
27.2	–0.00	0.93	38.67	–0.00	–0.00	–0.00
27.4	–0.00	0.93	38.07	–0.00	–0.00	–0.00
27.6	–0.00	0.93	37.47	–0.00	–0.00	–0.00
27.8	0.81	0.92	36.87	0.75	0.28	0.47
28.0	0.81	0.96	34.50	0.78	0.27	0.51

Table T17 (continued). (Continued on next page.)

Age (Ma)	LSR (cm/k.y.)	Dry density (g/cm^3)	$CaCO_3$ (wt%)	MAR (g/cm^2/k.y.)	CAR (g/cm^2/k.y.)	nCAR (g/cm^2/k.y.)
28.2	0.81	0.96	39.53	0.78	0.31	0.47
28.4	0.81	0.97	40.28	0.79	0.32	0.47
28.6	0.81	0.99	33.57	0.80	0.27	0.53
28.8	0.81	1.08	36.72	0.87	0.32	0.55
29.0	0.81	1.10	49.59	0.89	0.44	0.45
29.2	0.90	1.08	43.78	0.97	0.43	0.55
29.4	0.90	1.13	42.22	1.02	0.43	0.59
29.6	0.90	1.17	46.16	1.06	0.49	0.57
29.8	0.90	1.15	48.82	1.04	0.51	0.53
30.0	0.90	1.16	55.33	1.05	0.58	0.47
30.2	0.90	1.20	52.57	1.08	0.57	0.51
30.4	0.90	1.22	52.19	1.10	0.57	0.53
30.6	0.90	1.25	51.28	1.13	0.58	0.55
30.8	0.90	1.17	57.17	1.06	0.60	0.45
31.0	0.90	1.16	43.03	1.05	0.45	0.60
31.2	0.90	1.17	37.74	1.05	0.40	0.66
31.4	0.90	1.18	36.31	1.06	0.39	0.68
31.6	0.90	1.19	39.74	1.07	0.43	0.65
31.8	0.90	1.19	46.39	1.08	0.50	0.58
32.0	0.90	1.21	38.65	1.09	0.42	0.67
32.2	0.90	1.24	42.40	1.12	0.48	0.65
32.4	0.90	1.23	40.29	1.11	0.45	0.66
32.6	0.90	1.24	49.97	1.12	0.56	0.56
32.8	0.90	1.23	59.02	1.11	0.66	0.46
33.0	0.90	1.23	53.26	1.11	0.59	0.52
33.2	0.59	1.25	61.62	0.73	0.45	0.28
33.4	0.59	1.26	69.48	0.74	0.51	0.23
33.6	0.59	1.23	77.97	0.72	0.56	0.16
33.8	0.59	1.24	70.15	0.73	0.51	0.22
34.0	0.59	1.24	54.04	0.73	0.39	0.34
34.2	0.59	1.25	56.38	0.73	0.41	0.32
34.4	0.59	1.29	56.48	0.76	0.43	0.33
34.6	0.59	1.32	58.06	0.77	0.45	0.32
34.8	0.59	1.35	51.64	0.79	0.41	0.38
35.0	0.59	1.39	51.76	0.82	0.42	0.39
35.2	0.59	1.38	48.07	0.81	0.39	0.42
35.4	0.59	1.37	48.28	0.80	0.39	0.42
35.6	0.59	1.37	48.81	0.80	0.39	0.41
35.8	0.59	1.37	49.33	0.80	0.40	0.41
36.0	0.59	1.36	49.85	0.80	0.40	0.40
36.2	0.59	1.36	50.37	0.80	0.40	0.40
36.4	0.59	1.36	50.90	0.80	0.41	0.39
36.6	0.59	1.36	51.42	0.80	0.41	0.39
36.8	0.59	1.36	51.94	0.80	0.41	0.38
37.0	0.59	1.36	52.46	0.80	0.42	0.38
37.2	0.59	1.37	55.51	0.81	0.45	0.36
37.4	0.59	1.41	61.19	0.82	0.50	0.32
37.6	0.59	1.41	63.53	0.83	0.53	0.30
37.8	0.59	1.39	58.52	0.82	0.48	0.34
38.0	0.59	1.38	56.35	0.81	0.46	0.35
38.2	0.59	1.42	64.83	0.83	0.54	0.29
38.4	0.59	1.41	59.64	0.83	0.49	0.33
38.6	0.59	1.39	53.54	0.82	0.44	0.38
38.8	0.59	1.38	51.18	0.81	0.42	0.40
39.0	0.59	1.37	50.62	0.80	0.41	0.40
39.2	0.59	1.34	49.30	0.79	0.39	0.40
39.4	0.59	1.28	51.96	0.75	0.39	0.36
39.6	0.59	1.29	45.22	0.76	0.34	0.41
39.8	0.59	1.25	37.05	0.73	0.27	0.46
40.0	0.59	1.28	43.37	0.75	0.32	0.42
40.2	0.59	1.31	50.95	0.77	0.39	0.38
40.4	0.18	1.32	52.56	0.24	0.13	0.11
40.6	0.18	1.31	52.51	0.24	0.13	0.11
40.8	0.18	1.30	52.31	0.24	0.12	0.11
41.0	0.18	1.29	52.12	0.24	0.12	0.11
41.2	0.18	1.29	52.15	0.24	0.12	0.11
41.4	0.18	1.29	52.46	0.24	0.12	0.11
41.6	0.18	1.29	52.77	0.24	0.12	0.11
41.8	0.18	1.29	53.08	0.24	0.13	0.11

Table T17 (continued). (Continued on next page.)

Age (Ma)	LSR (cm/k.y.)	Dry density (g/cm^3)	$CaCO_3$ (wt%)	MAR (g/cm^2/k.y.)	CAR (g/cm^2/k.y.)	nCAR (g/cm^2/k.y.)
42.0	0.18	1.30	53.71	0.24	0.13	0.11
42.2	0.18	1.31	54.74	0.24	0.13	0.11
42.4	0.18	1.33	55.76	0.24	0.14	0.11
42.6	0.18	1.34	56.79	0.25	0.14	0.11
42.8	0.18	1.33	57.82	0.24	0.14	0.10
43.0	0.18	1.32	58.83	0.24	0.14	0.10
43.2	0.18	1.31	59.01	0.24	0.14	0.10
43.4	0.18	1.31	58.71	0.24	0.14	0.10
43.6	0.18	1.31	58.41	0.24	0.14	0.10
43.8	0.18	1.31	58.10	0.24	0.14	0.10
44.0	0.18	1.30	57.25	0.24	0.14	0.10
44.2	0.18	1.27	55.93	0.23	0.13	0.10
44.4	0.18	1.25	54.61	0.23	0.12	0.10
44.6	0.18	1.22	53.29	0.22	0.12	0.10
44.8	0.18	1.19	51.30	0.22	0.11	0.11
45.0	0.18	1.14	48.49	0.21	0.10	0.11
45.2	0.18	1.09	45.68	0.20	0.09	0.11
45.4	0.18	1.08	46.24	0.20	0.09	0.11
45.6	0.18	1.13	55.07	0.21	0.11	0.09
45.8	0.18	1.19	64.26	0.22	0.14	0.08
46.0	0.18	1.26	73.46	0.23	0.17	0.06
46.2	0.18	1.31	80.77	0.24	0.19	0.05
46.4	0.18	1.33	82.59	0.24	0.20	0.04
46.6	0.18	1.35	84.07	0.25	0.21	0.04
46.8	0.18	1.38	85.55	0.25	0.22	0.04
47.0	0.18	1.40	86.74	0.26	0.22	0.03
47.2	0.18	1.40	86.94	0.26	0.22	0.03
47.4	0.18	1.40	87.05	0.26	0.22	0.03
47.6	0.18	1.40	87.16	0.26	0.22	0.03
47.8	0.18	1.39	87.27	0.26	0.22	0.03
48.0	0.00	1.39	87.39	0.00	0.00	0.00
48.2	0.00	1.39	87.50	0.00	0.00	0.00
48.4	0.00	1.39	87.61	0.00	0.00	0.00
48.6	0.00	1.39	87.72	0.00	0.00	0.00
48.8	0.00	1.39	87.83	0.00	0.00	0.00
49.0	0.00	1.39	87.95	0.00	0.00	0.00
49.2	0.00	1.39	88.06	0.00	0.00	0.00
49.4	0.00	1.39	88.17	0.00	0.00	0.00
49.6	0.00	1.39	88.28	0.00	0.00	0.00
49.8	0.00	1.39	88.39	0.00	0.00	0.00
50.0	0.00	1.39	88.50	0.00	0.00	0.00
50.2	0.00	1.39	88.62	0.00	0.00	0.00
50.4	0.00	1.39	88.73	0.00	0.00	0.00
50.6	0.00	1.39	88.84	0.00	0.00	0.00
50.8	0.00	1.39	88.95	0.00	0.00	0.00
51.0	0.00	1.39	89.06	0.00	0.00	0.00
51.2	0.00	1.39	89.18	0.00	0.00	0.00
51.4	0.00	1.39	89.29	0.00	0.00	0.00
51.6	0.00	1.39	89.40	0.00	0.00	0.00
51.8	0.00	1.38	89.51	0.00	0.00	0.00
52.0	0.00	1.38	89.62	0.00	0.00	0.00
52.2	0.00	1.38	89.73	0.00	0.00	0.00
52.4	0.00	1.38	89.85	0.00	0.00	0.00
52.6	0.00	1.38	89.96	0.00	0.00	0.00
52.8	0.00	1.38	90.07	0.00	0.00	0.00
53.0	0.00	1.38	90.18	0.00	0.00	0.00
53.2	0.00	1.38	90.29	0.00	0.00	0.00
53.4	0.00	1.38	90.41	0.00	0.00	0.00
53.6	0.00	1.38	90.52	0.00	0.00	0.00
53.8	0.00	1.38	90.63	0.00	0.00	0.00
54.0	0.00	1.38	90.74	0.00	0.00	0.00
54.2	0.00	1.38	90.85	0.00	0.00	0.00
54.4	0.00	1.38	90.96	0.00	0.00	0.00
54.6	0.00	1.38	91.08	0.00	0.00	0.00
54.8	0.00	1.38	91.19	0.00	0.00	0.00
55.0	0.00	1.38	91.30	0.00	0.00	0.00
55.2	0.00	1.38	91.41	0.00	0.00	0.00
55.4	0.00	1.38	91.52	0.00	0.00	0.00
55.6	0.72	1.37	91.45	0.98	0.90	0.08

Table T17 (continued).

Age (Ma)	LSR (cm/k.y.)	Dry density (g/cm^3)	$CaCO_3$ (wt%)	MAR (g/cm^2/k.y.)	CAR (g/cm^2/k.y.)	nCAR (g/cm^2/k.y.)
55.8	0.72	1.32	89.94	0.95	0.86	0.10
56.0	0.72	1.38	85.08	0.99	0.84	0.15
56.2	0.72	1.43	80.17	1.03	0.83	0.20
56.4	0.72	1.37	79.83	0.98	0.79	0.20
56.6	0.72	1.26	79.75	0.91	0.72	0.18
56.8	0.72	1.20	79.34	0.86	0.69	0.18
57.0	0.72	1.16	79.11	0.83	0.66	0.17
57.2	0.72	1.10	76.50	0.79	0.61	0.19
57.4	0.72	0.98	72.28	0.71	0.51	0.20
57.6	0.72	0.93	72.77	0.67	0.49	0.18
57.8	0.72	0.99	76.15	0.71	0.54	0.17
58.0	0.72	1.06	79.52	0.76	0.61	0.16
58.2	0.72	1.12	82.55	0.81	0.67	0.14
58.4	0.72	1.17	82.53	0.84	0.69	0.15
58.6	0.72	1.19	83.22	0.86	0.71	0.14
58.8	0.72	1.23	82.28	0.88	0.73	0.16
59.0	0.72	1.26	77.95	0.91	0.71	0.20
59.2	0.72	1.34	72.40	0.97	0.70	0.27

LSR = linear sedimentation rate, MAR = mass accumulation rate, CAR = carbonate accumulation rate, nCAR = noncarbonate accumulation rate.

Table T18. Geochemistry of headspace gas samples, Hole U1406A.

Core, section, interval (cm)	Depth (mbsf)	Methane (ppmv)
342-U1406A-		
1H-5, 0–5	5.50	1.48
2H-7, 0–5	15.20	1.96
3H-7, 0–5	24.58	1.84
4H-7, 0–5	34.20	1.95
5H-7, 0–5	43.70	2.39
6H-7, 0–5	52.96	2.02
7H-7, 0–5	62.70	2.35
8H-7, 0–5	71.97	2.07
9H-7, 0–5	81.76	2.46
10H-7, 0–5	90.90	2.8
11H-7, 0–5	100.42	2.84
12H-7, 0–5	109.91	2.81
13H-7, 0–5	119.22	2.39
14H-7, 0–5	127.34	2.49
15H-7, 0–5	138.77	2.95
16H-6, 0–5	146.70	2.69
17H-6, 0–5	155.60	2.43
18H-5, 0–5	163.14	2.64
19H-6, 0–5	172.20	2.35
20H-6, 0–5	180.92	2.24
21H-2, 0–5	183.20	2.52
22H-6, 0–5	198.46	2.57
23H-6, 0–5	206.80	2.00
26X-3, 0–5	220.70	1.92
27X-7, 0–5	231.52	2.24
28X-7, 0–5	241.16	2.21
29X-2, 0–5	243.40	1.85
30X-2, 0–5	253.00	1.84
31X-2, 0–5	257.30	1.99
32X-4, 0–5	265.15	1.49
33X-6, 0–5	277.81	1.78
34X-2, 0–5	279.77	1.58

Table T19. Interstitial water constituents, Hole U1406A.

Core, section, interval (cm)	Depth (mbsf)	pH	Alkalinity (mM)	NH_4 (μM)	Salinity	Cl^- (mM)	Na^+ (mM)	SO_4^{2-} (mM)	HPO_4^- (μM)	Mn^{2+} (μM)	Fe^{2+} (μM)	Ca^{2+} (mM)	Mg^{2+} (mM)	Sr^{2+} (μM)	K^+ (mM)	Sr/Ca	Mg/Ca
342-U1406A-																	
1H-4, 95–100	5.45	7.53	2.73	0	37	545.9	465.1	26.2	BDL	BDL	BDL	10.8	52.2	78.0	12.0	7.2	4.8
2H-6, 145–150	15.15	7.49	3.38	0	37	539.3	477.1	27.3	BDL	BDL	BDL	11.7	53.1	81.8	12.1	7.0	4.5
3H-6, 145–150	24.53	7.34	3.34	0	37	550.4	480.3	27.0	BDL	2.3	BDL	12.3	52.8	84.6	12.6	6.9	4.3
4H-6, 145–150	34.15	7.44	3.30	0	37	542.9	480.7	25.6	BDL	3.4	0.1	12.8	52.2	87.0	13.0	6.8	4.1
5H-6, 145–150	43.65	7.36	3.53	0	37	546.8	478.1	28.5	BDL	5.2	0.1	13.3	51.6	90.1	13.5	6.8	3.9
6H-6, 121–126	52.91	7.32	3.64	0	38	552.5	478.1	27.0	BDL	6.7	0.2	13.9	51.2	93.1	17.0	6.7	3.7
7H-6, 145–150	62.65	7.16	3.99	0	37	555.1	476.1	27.3	BDL	8.4	0.2	14.3	50.4	95.6	14.4	6.7	3.5
8H-6, 122–127	71.92	7.18	4.29	0	37	546.6	480.8	26.2	BDL	9.7	0.9	15.3	50.9	98.9	16.6	6.5	3.3
9H-6, 148–153	81.71	7.22	4.54	0	37	562.8	485.3	25.7	BDL	10.6	0.7	15.8	50.9	102.4	16.4	6.5	3.2
10H-6, 115–120	90.85	7.28	4.54	3	37	553.9	477.3	26.0	BDL	9.8	0.5	15.8	49.7	105.4	10.0	6.7	3.1
11H-6, 116–121	100.37	7.19	4.85	2	37	559.2	489.6	28.1	BDL	11.5	1.1	16.6	51.1	106.0	10.4	6.4	3.1
12H-6, 116–121	109.86	7.23	4.62	2	37	535.4	472.3	23.9	BDL	11.9	0.4	16.6	48.9	110.1	14.6	6.6	3.0
13H-6, 96–101	119.17	7.18	4.79	4	37	552.9	479.3	24.5	BDL	12.8	0.9	17.2	49.2	111.9	11.4	6.5	2.9
14H-4, 106–111	125.76	7.00	5.00	6	37	534.7	469.1	24.4	BDL	13.0	1.4	17.1	48.2	115.4	11.0	6.7	2.8
15H-6, 145–150	138.72	7.14	4.95	5	37	550.1	475.6	25.1	BDL	13.8	0.9	17.6	48.3	117.0	10.5	6.6	2.7
16H-5, 145–150	146.65	7.14	5.06	6	37	557.3	477.0	25.1	BDL	13.3	0.5	18.2	49.8	120.5	12.9	6.6	2.7
17H-5, 140–150	155.50	7.10	5.19	5	37	549.0	470.8	25.9	BDL	15.1	1.3	18.0	48.5	120.8	13.1	6.7	2.7
18H-4, 140–145	163.04	7.01	5.57	8	37	560.9	478.2	24.6	BDL	16.5	2.2	18.2	48.5	120.8	13.4	6.6	2.7
19H-5, 140–150	172.10	7.29	5.55	6	37	546.9	468.2	23.8	BDL	16.2	8.3	18.0	47.8	122.2	12.3	6.8	2.7
20H-5, 121–131	180.82	6.99	5.19	5	37	537.1	460.7	22.7	BDL	8.6	0.5	18.4	49.6	125.2	10.3	6.8	2.7
23H-5, 140–150	206.70	7.07	5.25	3	37	525.3	458.4	21.7	BDL	7.1	0.7	17.1	45.8	130.0	9.9	7.6	2.7
26X-2, 140–150	220.60	7.24	4.78	3	37	531.1	462.4	22.2	BDL	5.2	0.2	16.8	45.4	124.9	10.5	7.4	2.7
27X-6, 112–122	231.42	7.15	4.29	2	36	519.7	458.6	21.6	BDL	4.2	0.7	16.9	46.4	126.2	9.0	7.4	2.7
28X-6, 116–126	241.06	7.21	4.33	0	36	518.0	456.6	21.3	BDL	2.7	0.0	16.9	46.9	125.7	9.9	7.4	2.8
29X-1, 140–150	243.30	6.96	4.95	2	37	524.4	466.8	21.9	BDL	2.5	0.2	17.4	47.1	122.4	11.5	7.0	2.7
30X-1, 140–150	252.90	7.15	4.63	0	37	528.6	470.3	22.1	BDL	BDL	0.2	16.8	47.0	118.1	12.1	7.0	2.8
31X-1, 140–150	257.20	7.25	4.36	0	37	531.1	469.1	21.8	BDL	BDL	BDL	16.6	46.9	ND	12.7	0.0	2.8
32X-3, 105–115	265.05	7.25	4.33	0	37	525.4	471.7	22.2	BDL	BDL	BDL	16.6	47.7	112.7	11.4	6.8	2.9
33X-5, 133–143	277.71	7.22	3.99	2	37	532.0	472.3	22.7	BDL	BDL	BDL	16.0	48.2	106.9	12.8	6.7	3.0
34X-1, 107–117	279.67	7.22	3.85	2	37	537.7	480.5	21.1	BDL	0.4	BDL	16.1	49.0	104.5	13.5	6.5	3.0

BDL = below detection limit (HPO_4^- = 0.2 μM, Mn^{2+} = 0.1 μM, Fe^{2+} = 0.6 μM), calculated as two times the standard deviation of multiple measures of a blank. ND = not detected.

Table T20. Sedimentary sample and bulk elemental geochemistry, Site U1406. (Continued on next five pages.)

Core, section, interval (cm)	Depth (mbsf)	$CaCO_3$ (wt%)	IC (wt%)	TC (wt%)	TN (wt%)	TOC (wt%)	Corrected TC (wt%)	Corrected TOC (wt%)	TN (wt%)	TOC/TN
342-U1406A-										
1H-1, 38–39	0.38	58.58	7.02	7.36	0.36	0.34	8.15	1.13		0.94
1H-2, 38–39	1.88	51.18	6.14	5.88	0.04	BDL	6.82	0.68	0.04	
1H-3, 38–39	3.38	54.67	6.56	6.53	0.07	BDL	7.40	0.85	0.07	
1H-4, 22–23	4.72	49.91	5.98	5.92	0.04	BDL	6.85	0.87	0.04	
1H-5, 15–16	5.65	31.86	3.82	3.75	0.05	BDL	4.90	1.08	0.05	
2H-1, 80–81	7.00	37.44	4.49	4.72	0.03	0.23	5.77	1.28	0.03	7.67
2H-2, 38–39	8.08	38.52	4.62	4.77	0.21	0.15	5.82	1.20		0.71
2H-3, 39–40	9.59	40.27	4.83	4.95	0.04	0.12	5.98	1.15	0.04	3.00
2H-4, 39–40	11.09	44.85	5.38	5.19	0.05	BDL	6.20	0.82	0.05	
2H-5, 39–40	12.59	43.40	5.20	5.30	0.04	0.10	6.30	1.09	0.04	2.50
2H-6, 39–40	14.09	45.63	5.47	5.58	0.04	0.11	6.55	1.08	0.04	2.75
2H-7, 18–19	15.38	43.95	5.27	5.49	0.03	0.22	6.47	1.20	0.03	7.33
3H-1, 38–39	16.08	44.59	5.35	5.59	0.05	0.24	6.56	1.21	0.05	4.80
3H-2, 38–39	17.46	44.02	5.28	5.47	0.06	0.19	6.45	1.17	0.06	3.17
3H-3, 38–39	18.96	42.37	5.08	5.27	0.05	0.19	6.27	1.19	0.05	3.80
3H-4, 38–39	20.46	46.75	5.61	ND	ND	BDL	ND	ND	ND	ND
3H-4, 38–39	20.46	44.10	5.29	5.24	0.04	BDL	6.24	0.95	0.04	ND
3H-5, 38–39	21.96	46.63	5.59	5.86	0.40	0.27	6.80	1.21	ND	0.68
3H-6, 38–39	23.46	46.26	5.55	5.60	0.08	0.05	6.57	1.02	0.08	0.63
3H-7, 16–17	24.74	52.06	6.24	6.19	0.05	BDL	7.10	0.86	0.05	ND
4H-1, 38–39	25.58	42.86	5.14	5.28	0.06	0.14	6.28	1.14	0.06	2.33
4H-2, 38–39	27.08	48.14	5.77	5.88	0.04	0.11	6.82	1.05	0.04	2.75
4H-3, 38–39	28.58	45.39	5.44	5.78	0.05	0.34	6.73	1.29	0.05	6.80
4H-4, 38–39	30.08	45.63	5.47	5.64	0.06	0.17	6.60	1.13	0.06	2.83
4H-5, 38–39	31.58	48.66	5.83	5.92	0.07	0.09	6.85	1.02	0.07	1.29
4H-6, 38–39	33.08	41.54	4.98	4.85	0.10	BDL	5.89	0.91	0.1	
4H-7, 15–16	34.35	45.34	5.44	5.57	0.06	0.13	6.54	1.10	0.06	2.17
5H-1, 38–39	35.08	38.16	4.58	4.73	0.10	0.15	5.78	1.21	0.1	1.50
5H-2, 38–39	36.58	47.85	5.74	6.02	0.62	0.28	6.94	1.21		0.45
5H-3, 38–39	38.08	49.66	5.95	6.00	0.07	0.05	6.93	0.97	0.07	0.71
5H-4, 38–39	39.58	39.08	4.69	4.69	0.06	BDL	5.75	1.06	0.06	
5H-5, 38–39	41.08	48.56	5.82	5.93	0.06	0.11	6.86	1.04	0.06	1.83
5H-6, 38–39	42.58	37.49	4.50	4.54	0.06	0.05	5.61	1.12	0.06	0.83
5H-7, 13–14	43.83	30.25	3.63	3.70	0.09	0.07	4.85	1.23	0.09	0.78
6H-1, 39–40	44.59	37.95	4.55	4.41	0.10	BDL	5.49	0.94	0.1	
6H-2, 39–40	46.09	45.00	5.40	5.39	0.05	BDL	6.38	0.98	0.05	
6H-3, 39–40	47.59	42.90	5.14	5.41	0.68	0.27	6.39	1.25		0.40
6H-4, 39–40	49.09	55.31	6.63	6.61	0.10	BDL	7.48	0.84	0.1	
6H-5, 39–40	50.59	53.07	6.36	6.55	0.06	0.19	7.42	1.06	0.06	3.17
6H-6, 39–40	52.09	43.32	5.19	5.13	0.05	BDL	6.14	0.95	0.05	
6H-7, 15–16	53.11	42.70	5.12	5.16	0.09	0.04	6.17	1.05	0.09	0.44
7H-1, 39–40	54.09	36.97	4.43	4.97	0.06	0.54	6.00	1.57	0.06	9.00
7H-2, 39–40	55.59	47.56	5.70	5.65	0.05	BDL	6.61	0.91	0.05	
7H-3, 39–40	57.09	37.16	4.46			BDL				
7H-4, 39–40	58.59	44.94	5.39	5.48	0.08	0.09	6.46	1.07	0.08	1.13
7H-5, 39–40	60.09	51.46	6.17	6.25	0.05	0.08	7.15	0.98	0.05	1.60
7H-6, 39–40	61.59	49.62	5.95	6.14	0.05	0.19	7.05	1.10	0.05	3.80
7H-7, 16–17	62.86	37.23	4.46	4.72	0.05	0.26	5.77	1.31	0.05	5.20
8H-1, 38–39	63.58	51.98	6.23	6.17	0.07	BDL	7.08	0.85	0.07	
8H-2, 38–39	65.08	43.23	5.18	5.27	0.10	0.09	6.27	1.09	0.1	0.90
8H-3, 38–39	66.58	32.12	3.85	4.03	0.10	0.18	5.15	1.30	0.1	1.80
8H-4, 38–39	68.08	38.38	4.60	4.60	0.07	BDL	5.66	1.06	0.07	
8H-5, 38–39	69.58	37.11	4.45	4.65	0.04	0.20	5.71	1.26	0.04	5.00
8H-6, 28–29	70.98	44.19	5.30	5.41	0.08	0.11	6.39	1.10	0.08	1.38
8H-7, 14–15	72.11	45.96	5.51	5.58	0.06	0.07	6.55	1.04	0.06	1.17
9H-1, 38–39	73.08	53.53	6.42	6.34	0.06	BDL	7.23	0.81	0.06	
9H-2, 38–39	74.58	52.69	6.32	6.39	0.11	0.07	7.28	0.96	0.11	0.64
9H-3, 38–39	76.08	40.26	4.83	4.91	0.05	0.08	5.94	1.12	0.05	1.60
9H-4, 38–39	77.59	44.11	5.29	5.44	0.12	0.15	6.42	1.13	0.12	1.25
9H-5, 38–39	79.10	45.98	5.51	5.96	0.07	0.45	6.89	1.38	0.07	6.43
9H-6, 30–31	80.53	49.08	5.88	6.19	0.42	0.31	7.10	1.21		0.74
9H-7, 14–15	81.90	41.54	4.98	5.16	0.08	0.18	6.17	1.19	0.08	2.25
10H-1, 38–39	82.58	39.50	4.74	4.72	0.06	BDL	5.77	1.04	0.06	
10H-2, 38–39	84.08	34.07	4.08	4.08	0.10	BDL	5.20	1.11	0.1	
10H-3, 38–39	85.58	29.49	3.54	3.49	0.05	BDL	4.66	1.13	0.05	
10H-4, 38–39	87.08	30.25	3.63	3.80	0.42	0.17	4.94	1.32		0.40
10H-5, 38–39	88.58	48.55	5.82	5.84	0.09	0.02	6.78	0.96	0.09	0.22

Table T20 (continued). (Continued on next page.)

Core, section, interval (cm)	Depth (mbsf)	$CaCO_3$ (wt%)	IC (wt%)	TC (wt%)	TN (wt%)	TOC (wt%)	Corrected TC (wt%)	Corrected TOC (wt%)	TN (wt%)	TOC/TN
10H-6, 22–23	89.92	34.35	4.12	4.25	0.11	0.13	5.35	1.23	0.11	1.18
10H-7, 15–16	91.05	41.96	5.03	4.93	0.07	BDL	5.96	0.93	0.07	
11H-1, 38–39	92.08	33.56	4.02	4.26	0.06	0.24	5.36	1.33	0.06	4.00
11H-2, 38–39	93.58	45.48	5.45	5.69	0.05	0.24	6.65	1.19	0.05	4.80
11H-3, 38–39	95.08	44.43	5.33	5.32	0.08	BDL	6.31	0.99	0.08	
11H-4, 38–39	96.58	36.56	4.38	4.36	0.10	BDL	5.45	1.07	0.1	
11H-5, 38–39	98.08	41.61	4.99	5.13	0.13	0.14	6.14	1.15	0.13	1.08
11H-6, 22–23	99.43	36.95	4.43	4.57	0.12	0.14	5.64	1.21	0.12	1.17
11H-7, 20–21	100.62	34.90	4.18	4.32	0.10	0.14	5.41	1.23	0.1	1.40
12H-1, 38–39	101.58	35.26	4.23	4.30	0.07	0.07	5.39	1.17	0.07	1.00
12H-2, 38–39	103.08	36.81	4.41	4.38	0.06	BDL	5.47	1.05	0.06	
12H-3, 38–39	104.58	39.00	4.68	4.62	0.06	BDL	5.68	1.01	0.06	
12H-4, 38–39	106.08	36.79	4.41	4.42	0.07	0.01	5.50	1.09	0.07	0.14
12H-5, 38–39	107.58	41.38	4.96	4.95	0.08	BDL	5.98	1.02	0.08	
12H-6, 27–28	108.97	32.47	3.89	4.05	0.07	0.16	5.17	1.27	0.07	2.29
12H-7, 17–18	110.08	31.63	3.79	3.89	0.08	0.10	5.02	1.23	0.08	1.25
13H-1, 38–39	111.08	40.23	4.82	4.74	0.07	BDL	5.79	0.97	0.07	
13H-2, 38–39	112.58	31.57	3.79	3.89	0.06	0.11	5.02	1.24	0.06	1.83
13H-3, 38–39	114.08	40.12	4.81	4.78	0.06	BDL	5.83	1.02	0.06	
13H-4, 38–39	115.59	35.89	4.30	4.20	0.07	BDL	5.30	1.00	0.07	
13H-5, 38–39	117.09	37.99	4.55	4.55	0.05	BDL	5.62	1.07	0.05	
13H-6, 18–19	118.39	36.03	4.32	4.30	0.07	BDL	5.39	1.07	0.07	
13H-7, 18–19	119.40	38.38	4.60	4.53	0.06	BDL	5.60	1.00	0.06	
14H-1, 38–39	120.58	37.58	4.51	4.30	0.07	BDL	5.39	0.89	0.07	
14H-2, 38–39	122.08	34.71	4.16	4.22	0.07	0.06	5.32	1.16	0.07	0.86
14H-3, 38–39	123.58	40.72	4.88	4.67	0.07	BDL	5.73	0.85	0.07	
14H-4, 27–28	124.97	35.26	4.23	4.31	0.07	0.08	5.40	1.18	0.07	1.14
14H-5, 14–15	125.95	32.74	3.93	3.91	0.06	BDL	5.04	1.12	0.06	
14H-6, 10–11	126.49	36.18	4.34	4.56	0.06	0.22	5.63	1.29	0.06	3.67
14H-7, 27–28	127.61	35.52	4.26	4.16	0.08	BDL	5.27	1.01	0.08	
15H-1, 38–39	130.08	35.16	4.22	4.30	0.08	0.08	5.39	1.18	0.08	1.00
15H-2, 38–39	131.58	20.28	2.43	2.48	0.07	0.05	3.75	1.32	0.07	0.71
15H-2, 38–39	131.58	19.85	2.38			BDL				
15H-3, 38–39	133.09	35.39	4.24	4.57	0.07	0.33	5.64	1.39	0.07	4.71
15H-4, 38–39	134.61	36.94	4.43	4.40	0.07	BDL	5.48	1.06	0.07	
15H-5, 38–39	136.14	20.45	2.45	2.60	0.08	0.15	3.86	1.41	0.08	1.88
15H-5, 38–39	136.14	20.19	2.42			BDL				
15H-6, 35–36	137.62	34.21	4.10	4.15	0.08	0.05	5.26	1.16	0.08	0.63
15H-7, 14–15	138.91	40.92	4.91	5.13	0.07	0.22	6.14	1.24	0.07	3.14
16H-1, 39–40	139.59	33.56	4.02			BDL				
16H-2, 39–40	141.09	24.86	2.98			BDL				
16H-2, 39–40	141.09	24.43	2.93			BDL				
16H-3, 39–40	142.59	41.95	5.03	4.97	0.07	BDL	6.00	0.97	0.07	
16H-4, 39–40	144.09	39.38	4.72	4.85	0.07	0.13	5.89	1.17	0.07	1.86
16H-5, 39–40	145.59	43.58	5.23	5.26	0.07	0.03	6.26	1.03	0.07	0.43
16H-6, 24–25	146.94	40.56	4.86			BDL				
17H-1, 39–40	148.49	36.60	4.39	4.48	0.06	0.09	5.56	1.17	0.06	1.50
17H-2, 39–40	149.99	32.90	3.94	4.07	0.07	0.13	5.19	1.24	0.07	1.86
17H-3, 39–40	151.49	43.00	5.16	5.19	0.06	0.03	6.20	1.04	0.06	0.50
17H-4, 39–40	152.99	39.81	4.77	4.79	0.07	0.02	5.84	1.06	0.07	0.29
17H-5, 39–40	154.49	31.41	3.77	3.88	0.12	0.11	5.02	1.25		0.92
17H-6, 39–40	155.99	35.71	4.28	4.26	0.06	BDL	5.36	1.08	0.06	
18H-1, 39–40	157.69	55.22	6.62			BDL				
18H-1, 39–40	157.69	52.16	6.25	6.27	0.05	BDL	7.17	0.92	0.05	
18H-2, 39–40	159.03	42.85	5.14	5.03	0.29	BDL	6.05	0.91		
18H-3, 39–40	160.53	40.93	4.91	4.94	0.09	0.03	5.97	1.06	0.09	0.33
18H-4, 39–40	162.03	45.49	5.45	5.49	0.19	0.04	6.47	1.01		0.21
18H-4, 39–40	162.03	43.74	5.24			BDL				
18H-5, 39–40	163.53	47.90	5.74	5.66	0.08	BDL	6.62	0.88	0.08	
19H-1, 38–39	165.08	49.02	5.88	5.76	0.20	BDL	6.71	0.83		
19H-2, 38–39	166.58	57.96	6.95			BDL				
19H-3, 38–39	168.08	51.35	6.16	6.29	0.05	0.13	7.19	1.03	0.05	2.60
19H-4, 38–39	169.58	56.29	6.75			BDL				
19H-4, 38–39	169.58	51.01	6.12	6.14	0.10	BDL	7.05	0.94	0.1	
19H-5, 38–39	171.08	49.50	5.94			BDL				
19H-6, 36–37	172.56	53.39	6.40			BDL				
19H-6, 36–37	172.56	52.47	6.29	6.27	0.12	BDL	7.17	0.88		
20H-1, 39–40	174.09	60.53	7.26	5.41	0.05	BDL	6.39		0.05	

Table T20 (continued). (Continued on next page.)

Core, section, interval (cm)	Depth (mbsf)	$CaCO_3$ (wt%)	IC (wt%)	TC (wt%)	TN (wt%)	TOC (wt%)	Corrected TC (wt%)	Corrected TOC (wt%)	TN (wt%)	TOC/TN
20H-2, 39–40	175.50	38.96	4.67	4.76	0.05	0.09	5.81	1.14	0.05	1.80
20H-3, 39–40	177.00	38.90	4.66	4.74	0.06	0.08	5.79	1.13	0.06	1.33
20H-4, 39–40	178.50	34.20	4.10	4.25	0.06	0.15	5.35	1.25	0.06	2.50
20H-5, 39–40	180.00	39.52	4.74	4.88	0.06	0.14	5.92	1.18	0.06	2.33
20H-6, 19–20	181.11	37.98	4.55			BDL				
21H-1, 50–51	182.20	50.37	6.04			BDL				
21H-1, 50–51	182.20	49.67	5.96	5.91	0.37	BDL	6.84	0.89		
21H-2, 20–21	183.40	43.10	5.17			BDL				
21H-3, 39–40	184.34	36.12	4.33			BDL				
21H-4, 39–40	185.72	42.66	5.12			BDL				
21H-4, 39–40	185.72	41.91	5.03			BDL				
21H-5, 39–40	187.08	44.22	5.30			BDL				
21H-5, 39–40	187.08	41.71	5.00	5.03	0.15	BDL	6.05	1.05		
21H-6, 17–18	188.24	37.77	4.53			BDL				
21H-7, 98–99	190.44	54.03	6.48	5.91	0.07	BDL	6.84	0.37	0.07	
22H-1, 38–39	191.58	62.94	7.55	7.61	0.05	0.06	8.38	0.83	0.05	1.20
22H-2, 38–39	193.04	52.04	6.24			BDL				
22H-2, 38–39	193.04	47.01	5.64	5.67	0.05	BDL	6.63	0.99	0.05	
22H-3, 38–39	194.54	55.86	6.70			BDL				
22H-3, 38–39	194.54	61.43	7.37	7.29	0.04	BDL	8.09	0.72	0.04	
22H-4, 38–39	196.04	66.59	7.98	7.95	0.06	BDL	8.68	0.70	0.06	
22H-5, 38–39	197.54	80.34	9.63	9.67	0.04	0.04	10.23	0.60	0.04	1.00
22H-6, 16–17	198.62	72.74	8.72	8.68	0.02	BDL	9.34	0.62	0.02	
23H-1, 38–39	199.68	52.51	6.30			BDL				
23H-1, 76–77	200.06	51.94	6.23	6.21	0.06	BDL	7.12	0.89	0.06	
23H-2, 38–39	201.18	58.80	7.05			BDL				
23H-2, 74–75	201.54	54.24	6.50	6.36	0.04	BDL	7.25	0.75	0.04	
23H-3, 38–39	202.68	57.95	6.95	6.96	0.05	0.01	7.79	0.84	0.05	0.20
23H-3, 74–75	203.04	59.83	7.17			BDL				
23H-4, 38–39	204.18	54.69	6.56			BDL				
23H-4, 80–81	204.60	49.27	5.91	6.38	0.05	0.47	7.27	1.36	0.05	9.40
23H-5, 35–36	205.65	51.39	6.16	6.04	0.04	BDL	6.96	0.80	0.04	
23H-5, 74–75	206.04	53.55	6.42	6.47	0.05	0.05	7.35	0.93	0.05	1.00
23H-6, 35–36	207.15	45.77	5.49	5.54	0.06	0.05	6.51	1.02	0.06	0.83
23H-6, 74–75	207.54	48.05	5.76			BDL				
26X-1, 38–39	218.08	52.75	6.32	6.61	0.05	0.29	7.48	1.15	0.05	5.80
26X-2, 38–39	219.58	60.40	7.24	7.35	0.04	0.11	8.14	0.90	0.04	2.75
26X-3, 12–13	220.82	64.98	7.79	7.80	0.03	0.01	8.55	0.76	0.03	0.33
27X-1, 38–39	223.18	53.74	6.44			BDL				
27X-2, 38–39	224.68	67.68	8.11			BDL				
27X-3, 38–39	226.18	55.37	6.64	6.58	0.04	BDL	7.45	0.81	0.04	
27X-4, 38–39	227.68	51.21	6.14	6.13	0.04	BDL	7.04	0.90	0.04	
27X-5, 38–39	229.18	50.80	6.09	6.11	0.05	0.02	7.03	0.94	0.05	0.40
27X-6, 38–39	230.68	48.65	5.83	5.69	0.06	BDL	6.65	0.81	0.06	
27X-7, 24–25	231.76	53.79	6.45	6.34	0.05	BDL	7.23	0.78	0.05	
28X-1, 30–31	232.70	44.89	5.38	5.48	0.06	0.10	6.46	1.08	0.06	1.67
28X-2, 26–27	234.16	34.85	4.18			BDL				
28X-2, 26–27	234.16	33.73	4.04	4.09	0.06	BDL	5.20	1.16	0.06	
28X-3, 29–30	235.69	50.03	6.00	5.85	0.04	BDL	6.79	0.79	0.04	
28X-4, 31–32	237.21	52.73	6.32	6.25	0.04	BDL	7.15	0.83	0.04	
28X-5, 30–31	238.70	52.01	6.24	6.16	0.05	BDL	7.07	0.83	0.05	
28X-6, 27–28	240.17	53.25	6.38	6.45	0.05	0.07	7.33	0.95	0.05	1.40
29X-1, 38–39	242.28	59.20	7.10	7.10	0.03	BDL	7.92	0.82	0.03	
29X-2, 38–39	243.78	57.97	6.95	7.36	0.02	0.41	8.15	1.20	0.02	20.50
29X-3, 38–39	245.28	52.57	6.30	6.33	0.04	0.03	7.22	0.92	0.04	0.75
29X-4, 35–36	246.45	43.57	5.22	5.22	0.04	BDL	6.22	1.00	0.04	
29X-5, 34–35	247.94	80.82	9.69	9.82	0.02	0.13	10.37	0.68	0.02	6.50
29X-6, 32–33	249.42	86.81	10.41	10.88	0.01	0.47	11.32	0.92	0.01	47.00
30X-1, 39–40	251.89	91.63	10.99	11.07	0.02	0.08	11.49	0.51	0.02	4.00
30X-2, 39–40	253.39	90.48	10.85	10.81	0.01	BDL	11.26	0.41	0.01	
31X-1, 63–64	256.43	79.13	9.49	9.57	0.01	0.08	10.14	0.66	0.01	8.00
31X-2, 82–83	258.12	80.08	9.60	9.63	0.02	0.03	10.20	0.60	0.02	1.50
31X-3, 59–60	259.39	79.68	9.55	9.64	0.01	0.09	10.21	0.65	0.01	9.00
32X-1, 46–47	261.46	79.10	9.48	9.53	0.01	0.05	10.11	0.62	0.01	5.00
32X-2, 21–22	262.71	79.12	9.49	9.52	0.02	0.03	10.10	0.61	0.02	1.50
32X-3, 23–24	264.23	74.11	8.89	8.86	0.02	BDL	9.50	0.62	0.02	
32X-4, 38–39	265.53	70.75	8.48	8.66	0.03	0.18	9.32	0.84	0.03	6.00
33X-1, 22–23	270.82	83.23	9.98	10.22	0.01	0.24	10.73	0.75	0.01	24.00

Table T20 (continued). (Continued on next page.)

Core, section, interval (cm)	Depth (mbsf)	$CaCO_3$ (wt%)	IC (wt%)	TC (wt%)	TN (wt%)	TOC (wt%)	Corrected TC (wt%)	Corrected TOC (wt%)	TN (wt%)	TOC/TN
33X-2, 29–30	272.31	82.26	9.86	9.83	0.01	BDL	10.38	0.52	0.01	
33X-3, 74–75	274.10	83.69	10.03	10.01	0.01	BDL	10.54	0.51	0.01	
33X-4, 33–34	275.19	82.15	9.85	9.95	0.01	0.10	10.49	0.64	0.01	10.00
33X-5, 64–65	277.02	75.99	9.11	9.26	0.02	0.15	9.86	0.75	0.02	7.50
33X-6, 19–20	278.00	70.88	8.51	8.67	0.01	BDL	9.33	0.82	0.01	
34X-1, 22–23	278.82	72.32	8.67	8.56	0.01	BDL	9.23	0.56	0.01	
34X-2, 16–17	279.93	60.31	7.23	7.60	0.02	0.37	8.37	1.14	0.02	18.50
342-U1406B-										
23X-1, 15–16	188.95	57.11	6.85							
23X-1, 35–36	189.15	71.05	8.52							
23X-1, 35–36	189.15	70.82	8.49							
23X-1, 55–56	189.35	79.81	9.57							
23X-1, 75–76	189.55	73.42	8.80							
24X-1, 52–53	196.32	72.11	8.65							
24X-1, 97–98	196.77	71.03	8.52							
24X-1, 138–139	197.18	62.43	7.49							
24X-2, 20–21	197.50	69.96	8.39							
24X-2, 40–41	197.70	68.41	8.20							
24X-2, 60–61	197.90	59.18	7.10							
24X-2, 80–81	198.10	60.57	7.26							
24X-2, 100–101	198.30	57.54	6.90							
24X-2, 120–121	198.50	56.73	6.80							
24X-3, 20–21	198.80	53.55	6.42							
24X-3, 40–41	199.00	51.30	6.15							
24X-3, 60–61	199.20	54.02	6.48							
24X-3, 80–81	199.40	58.00	6.95							
24X-3, 80–81	199.40	57.97	6.95							
24X-3, 100–101	199.60	56.37	6.76							
24X-3, 120–121	199.80	51.49	6.17							
24X-3, 140–141	200.00	52.36	6.28							
24X-4, 20–21	200.30	50.51	6.06							
24X-4, 40–41	200.50	56.39	6.76							
24X-4, 60–61	200.70	55.16	6.61							
24X-4, 80–81	200.90	57.60	6.91							
24X-4, 100–101	201.10	57.82	6.93							
24X-4, 120–121	201.30	59.50	7.13							
24X-4, 140–141	201.50	53.98	6.47							
24X-5, 38–39	201.98	61.38	7.36							
25X-1, 18–19	203.48	53.00	6.36							
25X-1, 60–61	203.90	56.55	6.78							
25X-1, 110–111	204.40	54.72	6.56							
25X-2, 9–10	204.89	51.26	6.15							
25X-2, 61–62	205.41	46.46	5.57							
25X-2, 110–111	205.90	49.07	5.88							
25X-3, 10–11	206.40	43.92	5.27							
25X-3, 63–64	206.93	43.18	5.18							
25X-3, 113–114	207.43	50.21	6.02							
26X-1, 10–11	213.00	57.17	6.85							
26X-1, 60–61	213.50	56.02	6.72							
26X-1, 109–110	213.99	56.95	6.83							
26X-2, 10–11	214.50	70.61	8.47							
26X-2, 10–11	214.50	71.05	8.52							
26X-2, 50–51	214.90	66.33	7.95							
26X-2, 111–112	215.51	62.10	7.45							
26X-3, 10–11	216.00	65.66	7.87							
26X-3, 60–61	216.50	67.54	8.10							
26X-3, 100–101	216.90	63.44	7.61							
26X-3, 112–113	217.02	66.99	8.03							
26X-3, 120–121	217.10	61.42	7.36							
26X-3, 126–127	217.16	66.94	8.03							
26X-3, 140–141	217.30	76.06	9.12							
26X-3, 140–141	217.30	76.33	9.15							
26X-4, 10–11	217.50	57.76	6.93							
26X-4, 10–11	217.50	58.27	6.99							
26X-4, 59–60	217.99	71.64	8.59							
26X-4, 101–102	218.41	73.74	8.84							
27X-1, 11–12	219.01	58.96	7.07							
27X-1, 60–61	219.50	62.85	7.54							

Table T20 (continued). (Continued on next page.)

Core, section, interval (cm)	Depth (mbsf)	$CaCO_3$ (wt%)	IC (wt%)	TC (wt%)	TN (wt%)	TOC (wt%)	Corrected TC (wt%)	Corrected TOC (wt%)	TN (wt%)	TOC/TN
27X-1, 125–126	220.15	54.67	6.55							
27X-2, 10–11	220.50	62.39	7.48							
27X-2, 62–63	221.02	60.06	7.20							
27X-2, 113–114	221.53	60.98	7.31							
27X-3, 10–11	222.00	60.68	7.28							
27X-3, 104–105	222.94	58.87	7.06							
28X-1, 10–11	227.00	58.79	7.05							
28X-1, 60–61	227.50	59.17	7.09							
28X-1, 110–111	228.00	69.51	8.33							
28X-2, 10–11	228.50	55.07	6.60							
28X-2, 60–61	229.00	69.58	8.34							
28X-2, 110–111	229.50	61.77	7.41							
28X-3, 10–11	230.00	51.75	6.21							
28X-3, 60–61	230.50	65.65	7.87							
28X-3, 113–114	231.03	56.53	6.78							
28X-4, 10–11	231.50	60.50	7.25							
28X-4, 60–61	232.00	46.57	5.58							
28X-4, 110–111	232.50	51.22	6.14							
28X-5, 10–11	233.00	55.17	6.62							
28X-5, 60–61	233.50	34.69	4.16							
28X-5, 97–98	233.87	37.13	4.45							
29X-1, 10–11	236.00	58.47	7.01							
29X-1, 60–61	236.50	58.22	6.98							
29X-1, 110–111	237.00	49.51	5.94							
29X-2, 10–11	237.50	47.52	5.70							
29X-2, 60–61	238.00	50.55	6.06							
29X-2, 110–111	238.50	51.79	6.21							
29X-3, 51–52	239.41	53.96	6.47							
29X-3, 101–102	239.91	49.34	5.92							
29X-3, 146–147	240.36	47.30	5.67							
29X-4, 46–47	240.86	50.86	6.10							
29X-4, 97–98	241.37	54.92	6.58							
29X-4, 145–146	241.85	59.37	7.12							
29X-4, 145–146	241.85	59.51	7.14							
29X-5, 45–46	242.35	49.72	5.96							
29X-5, 90–91	242.80	67.61	8.11							
29X-5, 140–141	243.30	58.82	7.05							
29X-6, 31–32	243.71	60.20	7.22							
29X-6, 81–82	244.21	60.45	7.25							
29X-6, 129–130	244.69	59.88	7.18							
30X-1, 13–14	245.53	49.60	5.95							
30X-1, 20–21	245.60	78.98	9.47							
30X-1, 20–21	245.60	78.02	9.35							
30X-1, 70–71	246.10	48.66	5.84							
30X-1, 123–124	246.63	56.02	6.72							
30X-2, 7–8	246.97	68.95	8.27							
30X-2, 30–31	247.20	81.64	9.79							
30X-2, 85–86	247.75	83.98	10.07							
30X-2, 135–136	248.25	88.33	10.59							
30X-3, 9–10	248.49	87.76	10.52							
30X-3, 59–60	248.99	88.02	10.55							
30X-3, 109–110	249.49	88.13	10.57							
30X-4, 7–8	249.97	86.91	10.42							
30X-4, 57–58	250.47	87.11	10.44							
30X-4, 107–108	250.97	88.27	10.58							
30X-4, 145–146	251.35	90.48	10.85							
30X-5, 10–11	251.50	90.22	10.82							
30X-5, 59–60	251.99	90.55	10.86							
30X-5, 110–111	252.50	91.02	10.91							
30X-6, 8–9	252.98	92.22	11.06							
30X-6, 58–59	253.48	93.30	11.19							
30X-7, 15–16	253.86	80.48	9.65							
30X-7, 65–66	254.36	89.26	10.70							
342-U1406C-										
22X-1, 8–9	185.68	40.80	4.89							
22X-2, 27–28	186.04	30.73	3.68							
22X-2, 76–77	186.53	36.74	4.41							
22X-2, 122–123	186.99	32.32	3.88							

Table T20 (continued).

Core, section, interval (cm)	Depth (mbsf)	$CaCO_3$ (wt%)	IC (wt%)	TC (wt%)	TN (wt%)	TOC (wt%)	Corrected TC (wt%)	Corrected TOC (wt%)	TN (wt%)	TOC/TN
22X-3, 19–20	187.46	41.71	5.00							
22X-3, 67–68	187.94	43.62	5.23							
22X-3, 119–120	188.46	36.35	4.36							
22X-4, 11–12	188.88	47.06	5.64							
22X-4, 64–65	189.41	49.12	5.89							
22X-4, 114–115	189.91	47.61	5.71							
22X-5, 12–13	190.39	43.49	5.22							
22X-5, 112–113	191.39	59.14	7.09							
22X-5, 112–113	191.39	59.90	7.18							
22X-6, 12–13	191.89	51.70	6.20							
22X-6, 63–64	192.40	50.24	6.02							
22X-6, 114–115	192.91	52.21	6.26							
22X-7, 8–9	193.35	55.42	6.65							
22X-7, 70–71	193.97	63.17	7.57							
22X-8, 6–7	194.34	62.55	7.50							
22X-8, 32–33	194.60	63.69	7.64							
22X-8, 59–60	194.87	64.93	7.79							
22X-CC, 16–17	195.08	69.38	8.32							
24X-1, 23–24	202.13	50.51	6.06							
24X-1, 50–51	202.40	46.68	5.60							
24X-1, 75–76	202.65	47.15	5.65							
24X-1, 116–117	203.06	46.09	5.53							
24X-2, 26–27	203.62	45.29	5.43							
24X-2, 62–63	203.98	45.22	5.42							
24X-2, 112–113	204.48	48.63	5.83							
24X-3, 12–13	204.98	46.24	5.54							
24X-3, 62–63	205.48	48.42	5.81							
24X-3, 112–113	205.98	49.58	5.94							
24X-4, 12–13	206.48	49.60	5.95							
24X-4, 62–63	206.98	44.59	5.35							
24X-4, 116–117	207.52	44.53	5.34							
24X-5, 13–14	207.99	48.62	5.83							
24X-5, 53–54	208.39	41.77	5.01							
24X-CC, 12–13	208.64	49.43	5.93							

For corrected total carbon (TC) with high-carbonate La Luna shale calibration, if TC < 2.2/2.913, corrected TC = 2.913 × x; if TC > 2.2/2.913, corrected TC = 2.2 + (x – 2.2/2.913) × 0.901. Corrected total organic carbon (TOC) is corrected TC minus inorganic carbon (IC). Total nitrogen (TN) values are uncorrected with anomalous values (>0.25%) removed. BDL = below detection level (<0.03 wt%). ND = not detected.

Table T21. Core top and composite depth, Site U1406. (Continued on next page.)

Core	Depth (mbsf)	Depth (m CCSF)	Offset (m)	Cumulative offset (m)	Comment	Datasets used
342-U1406A-						
1H	0.00	0.00	0.00	0.00	Tentative	Physical properties
2H	6.20	7.30	1.10	1.10	Tentative	Physical properties
3H	15.70	17.40	0.60	1.70	Tentative	Physical properties
4H	25.20	30.73	3.83	5.53		XRF core scanning
5H	34.70	40.03	–0.20	5.33		XRF core scanning
6H	44.20	50.97	1.44	6.77		XRF core scanning
7H	53.70	61.07	0.60	7.37		XRF core scanning
8H	63.20	70.57	0.00	7.37		XRF core scanning
9H	72.70	80.37	0.30	7.67		XRF core scanning
10H	82.20	90.17	0.30	7.97		XRF core scanning
11H	91.70	99.82	0.15	8.12		XRF core scanning
12H	101.20	110.54	1.22	9.34		XRF core scanning
13H	110.70	120.39	0.35	9.69		XRF core scanning
14H	120.20	130.19	0.30	9.99		XRF core scanning
15H	129.70	139.39	–0.30	9.69		XRF core scanning
16H	139.20	149.59	0.70	10.39		XRF core scanning
17H	148.10	161.04	2.55	12.94		XRF core scanning
18H	157.30	172.79	2.55	15.49		XRF core scanning
19H	164.70	184.39	4.20	19.69		XRF core scanning
20H	173.70	193.39	0.00	19.69		XRF core scanning
21H	181.70	202.52	1.13	20.82		XRF core scanning
22H	191.20	211.52	–0.50	20.32		XRF core scanning
23H	199.30	221.29	1.67	21.99		XRF core scanning
24H	208.10	230.09	0.00	21.99		XRF core scanning
25H	217.60	239.59	0.00	21.99		XRF core scanning
26X	217.70	242.29	2.60	24.59	Tentative	XRF core scanning
27X	222.80	250.79	3.40	27.99	Tentative	XRF core scanning
28X	232.40	261.79	1.40	29.39	Tentative	XRF core scanning
29X	241.90	272.34	1.05	30.44		XRF core scanning
30X	251.50	281.24	–0.70	29.74		Physical properties
31X	255.80	285.55	0.01	29.75		Physical properties
32X	261.00	290.76	0.01	29.76		Physical properties
33X	270.60	300.37	0.01	29.77		Physical properties
34X	278.60	308.38	0.01	29.78		Physical properties
342-U1406B-						
1H	0.00	0.00	0.00	0.00	Tentative	Physical properties
2H	4.30	4.30	0.00	0.00	Tentative	Physical properties
3H	13.80	15.15	1.35	1.35	Tentative	Physical properties
4H	23.30	24.88	0.23	1.58		XRF core scanning
5H	29.80	34.63	3.25	4.83		XRF core scanning
6H	39.30	44.27	0.14	4.97		XRF core scanning
7H	48.80	54.92	1.15	6.12		XRF core scanning
8H	58.30	66.82	2.40	8.52		XRF core scanning
9H	67.80	75.22	–1.10	7.42		XRF core scanning
10H	77.30	85.29	0.57	7.99		XRF core scanning
11H	86.80	95.77	0.98	8.97		XRF core scanning
12H	96.30	105.42	0.15	9.12		XRF core scanning
13H	105.50	115.52	0.90	10.02		XRF core scanning
14H	115.00	125.32	0.30	10.32		XRF core scanning
15H	124.50	134.82	0.00	10.32		XRF core scanning
16H	134.00	145.22	0.90	11.22		XRF core scanning
17H	143.50	155.57	0.85	12.07		XRF core scanning
18H	153.00	167.32	2.25	14.32		XRF core scanning
19H	161.60	181.07	5.15	19.47		XRF core scanning
20H	171.10	191.27	0.70	20.17	Tentative	XRF core scanning
21H	179.20	200.97	1.60	21.77		XRF core scanning
22H	188.70	210.47	0.00	21.77		XRF core scanning
23X	188.80	217.07	6.50	28.27	Tentative	XRF core scanning
24X	195.80	218.57	–5.50	22.77	Tentative	XRF core scanning
25X	203.30	228.07	2.00	24.77		XRF core scanning
26X	212.90	241.07	3.40	28.17	Tentative	XRF core scanning
27X	218.90	247.62	0.55	28.72		XRF core scanning
28X	226.90	255.37	–0.25	28.47	Tentative	XRF core scanning
29X	235.90	265.62	1.25	29.72		XRF core scanning
30X	245.40	274.67	–0.45	29.27		XRF core scanning

Table T21 (continued).

Core	Depth (mbsf)	Depth (m CCSF)	Offset (m)	Cumulative offset (m)	Comment	Datasets used
342-U1406C-						
1H	0.00	1.00	1.00	1.00	Tentative	Physical properties
2H	9.40	10.40	0.00	1.00	Drilling advance	
3H	12.40	13.40	0.00	1.00	Tentative	Physical properties
4H	21.90	23.20	0.30	1.30		XRF core scanning
5H	31.40	32.93	0.23	1.53		XRF core scanning
6H	40.90	42.31	–0.12	1.41		XRF core scanning
7H	50.40	65.45	13.64	15.05	Unusually large offset	XRF core scanning
8H	59.90	75.75	0.80	15.85		XRF core scanning
9H	69.40	84.12	–1.13	14.72		XRF core scanning
10H	78.90	90.52	–3.10	11.62		XRF core scanning
11H	88.40	99.32	–0.70	10.92		XRF core scanning
12H	97.90	104.32	–4.50	6.42		XRF core scanning
13H	107.40	114.37	0.55	6.97		XRF core scanning
14H	116.90	122.22	–1.65	5.32		XRF core scanning
15H	126.40	131.87	0.15	5.47		XRF core scanning
16H	135.90	142.72	1.35	6.82		XRF core scanning
17H	145.40	152.77	0.55	7.37	Hiatus	XRF core scanning
18H	154.90	175.62	13.35	20.72	Hiatus	XRF core scanning
19H	164.40	187.12	2.00	22.72	Drilling advance	
20X	166.40	189.12	0.00	22.72		XRF core scanning
21X	176.00	195.72	–3.00	19.72		XRF core scanning
22X	185.60	206.98	1.66	21.38		XRF core scanning
23X	195.20	221.28	4.70	26.08		XRF core scanning
24X	201.90	227.78	–0.20	25.88		XRF core scanning
25X	206.90	234.91	2.13	28.01		XRF core scanning
26X	216.50	243.51	–1.00	27.01		XRF core scanning
27X	221.30	248.32	0.01	27.02		XRF core scanning
28X	226.10	253.07	–0.05	26.97	Tentative	XRF core scanning
29X	231.80	270.60	0.00		No recovery	Physical properties

Table T22. Splice tie points, Site U1406.

Hole, core, section, interval (cm)	Depth (mbsf)	Depth (m CCSF)		Hole, core, section, interval (cm)	Depth (mbsf)	Depth (m CCSF)	Comment	Data sets used
342-				342-				
				U1406A-1H-1, 0	0.00	0.00		
U1406A-1H-4, 85	5.35	5.35	Tie to	U1406B-2H-1, 105	5.35	5.35	Tentative	Physical properties
U1406B-2H-4, 106	9.86	9.86	Tie to	U1406A-2H-2, 106	8.76	9.86	Tentative	Physical properties
U1406A-2H-7, 20	15.40	16.50	Tie to	U1406B-3H-1, 135	15.15	16.50	Tentative	Physical properties
U1406B-3H-3, 116	17.96	19.31	Tie to	U1406A-3H-2, 53	17.61	19.31	Tentative	Physical properties
U1406A-3H-6, 138	24.46	26.16	Tie to	U1406C-4H-2, 146	24.86	26.16		XRF core scanning
U1406C-4H-6, 86	30.26	31.56	Tie to	U1406A-4H-1, 83	26.03	31.56		XRF core scanning
U1406A-4H-4, 102	30.72	36.25	Tie to	U1406B-5H-2, 12	31.42	36.25		XRF core scanning
U1406B-5H-4, 149	35.79	40.62	Tie to	U1406A-5H-1, 59	35.29	40.62		XRF core scanning
U1406A-5H-4, 137	40.57	45.90	Tie to	U1406B-6H-2, 13	40.93	45.90		XRF core scanning
U1406B-6H-6, 92	47.72	52.69	Tie to	U1406A-6H-2, 22	45.92	52.69		XRF core scanning
U1406A-6H-6, 106	52.76	59.53	Tie to	U1406B-7H-4, 11	53.41	59.53		XRF core scanning
U1406B-7H-5, 99	55.79	61.91	Tie to	U1406A-7H-1, 84	54.54	61.91		XRF core scanning
U1406A-7H-5, 142	61.12	68.49	Tie to	U1406C-7H-3, 4	53.44	68.49		XRF core scanning
U1406C-7H-6, 100	58.90	73.95	Tie to	U1406A-8H-3, 38	66.58	73.95		XRF core scanning
U1406A-8H-5, 108	70.28	77.65	Tie to	U1406B-9H-2, 93	70.23	77.65		XRF core scanning
U1406B-9H-5, 95	74.78	82.20	Tie to	U1406A-9H-2, 33	74.53	82.20		XRF core scanning
U1406A-9H-4, 147	78.68	86.35	Tie to	U1406C-9H-2, 73	71.63	86.35		XRF core scanning
U1406C-9H-4, 133	75.23	89.95	Tie to	U1406B-10H-4, 14	81.96	89.95		XRF core scanning
U1406B-10H-4, 124	83.06	91.05	Tie to	U1406A-10H-1, 88	83.08	91.05		XRF core scanning
U1406A-10H-5, 90	89.10	97.07	Tie to	U1406B-11H-1, 130	88.10	97.07		XRF core scanning
U1406B-11H-5, 37	93.17	102.14	Tie to	U1406A-11H-2, 82	94.02	102.14		XRF core scanning
U1406A-11H-5, 112	98.82	106.94	Tie to	U1406B-12H-2, 2	97.82	106.94		XRF core scanning
U1406B-12H-6, 76	104.60	113.72	Tie to	U1406A-12H-3, 18	104.38	113.72		XRF core scanning
U1406A-12H-5, 63	107.83	117.17	Tie to	U1406B-13H-2, 14	107.15	117.17		XRF core scanning
U1406B-13H-6, 60	113.65	123.67	Tie to	U1406A-13H-3, 28	113.98	123.67		XRF core scanning
U1406A-13H-5, 97	117.68	127.37	Tie to	U1406B-14H-2, 55	117.05	127.37		XRF core scanning
U1406B-14H-6, 72	123.22	133.54	Tie to	U1406C-15H-2, 17	128.07	133.54		XRF core scanning
U1406C-15H-5, 108	133.48	138.95	Tie to	U1406B-15H-3, 113	128.63	138.95		XRF core scanning
U1406B-15H-5, 99	131.49	141.81	Tie to	U1406A-15H-2, 92	132.12	141.81		XRF core scanning
U1406A-15H-5, 59	136.35	146.04	Tie to	U1406C-16H-4, 18	139.22	146.04		XRF core scanning
U1406C-16H-6, 114	143.20	150.02	Tie to	U1406B-16H-4, 27	138.80	150.02		XRF core scanning
U1406B-16H-5, 139	141.43	152.65	Tie to	U1406A-16H-3, 6	142.26	152.65		XRF core scanning
U1406A-16H-5, 92	146.12	156.51	Tie to	U1406B-17H-1, 94	144.44	156.51		XRF core scanning
U1406B-17H-5, 117	150.67	162.74	Tie to	U1406A-17H-2, 20	149.80	162.74		XRF core scanning
U1406A-17H-5, 73	154.83	167.77	Tie to	U1406B-18H-1, 45	153.45	167.77		XRF core scanning
U1406B-18H-5, 98	159.98	174.30	Tie to	U1406A-18H-2, 17	158.81	174.30		XRF core scanning
U1406A-18H-3, 119	161.33	176.82	Tie to	U1406C-18H-1, 120	156.10	176.82		XRF core scanning
U1406C-18H-5, 63	161.53	182.25	Tie to	U1406B-19H-1, 118	162.78	182.25		XRF core scanning
U1406B-19H-6, 136	169.37	188.84	Tie to	U1406A-19H-3, 145	169.15	188.84		XRF core scanning
U1406A-19H-6, 47	172.67	192.36	Tie to	U1406B-20H-1, 109	172.19	192.36	Tentative	XRF core scanning
U1406B-20H-3, 64	174.78	194.95	Tie to	U1406A-20H-2, 15	175.26	194.95		XRF core scanning
U1406A-20H-4, 121	179.32	199.01	Tie to	U1406C-21X-3, 29	179.29	199.01		XRF core scanning
U1406C-21X-6, 15	183.65	203.37	Tie to	U1406B-21H-3, 18	181.60	203.37		XRF core scanning
U1406B-21H-5, 148	185.90	207.67	Tie to	U1406C-22X-2, 52	186.29	207.67		XRF core scanning
U1406C-22X-7, 35	193.62	215.00	Tie to	U1406A-22H-3, 52	194.68	215.00		XRF core scanning
U1406A-22H-6, 21	198.67	218.99	Tie to	U1406B-24X-1, 42	196.22	218.99	Tentative	XRF core scanning
U1406B-24X-4, 147	201.57	224.34	Tie to	U1406A-23H-3, 5	202.35	224.34		XRF core scanning
U1406A-23H-6, 73	207.53	229.52	Tie to	U1406C-24X-2, 28	203.64	229.52		XRF core scanning
U1406C-24X-CC, 50	209.02	234.90	Append to	U1406C-25X-1, 0	206.90	234.91		XRF core scanning
U1406C-25X-6, 40	214.80	242.81	Tie to	U1406A-26X-1, 52	218.22	242.81	Tentative	XRF core scanning
U1406A-26X-3, 35	221.05	245.64	Tie to	U1406C-26X-2, 63	218.63	245.64	Tentative	XRF core scanning
U1406C-26X-CC, 20	219.96	246.97	Append to	U1406B-27X-1, 0	218.90	247.62		XRF core scanning
U1406B-27X-3, 85	222.75	251.47	Tie to	U1406A-27X-1, 68	223.48	251.47	Tentative	XRF core scanning
U1406A-27X-6, 58	230.88	258.87	Tie to	U1406B-28X-3, 50	230.40	258.87	Tentative	XRF core scanning
U1406B-28X-5, 77	233.67	262.14	Tie to	U1406A-28X-1, 35	232.75	262.14	Tentative	XRF core scanning
U1406A-28X-4, 72	237.62	267.01	Tie to	U1406B-29X-1, 139	237.29	267.01		XRF core scanning
U1406B-29X-6, 90	244.30	274.02	Tie to	U1406A-29X-2, 18	243.58	274.02		XRF core scanning
U1406A-29X-3, 18	245.08	275.52	Tie to	U1406B-30X-1, 85	246.25	275.52		XRF core scanning
U1406B-30X-5, 147	252.87	282.14	Tie to	U1406A-30X-1, 90	252.40	282.14		Physical properties
U1406A-30X-CC, 14	254.66	284.40	Append to	U1406A-31X-1, 23	256.03	285.78		Physical properties
U1406A-31X-3, 154	260.34	290.09	Append to	U1406A-32X-1, 0	261.00	290.76		Physical properties
U1406A-32X-4, 85	266.00	295.76	Append to	U1406A-33X-1, 10	270.70	300.47		Physical properties
U1406A-33X-CC, 59	278.60	308.37	Append to	U1406A-34X-1, 15	278.75	308.53		Physical properties
U1406A-34X-CC, 20	280.95	310.73						